DELOCALIZATION AND FUNCTIONAL GROUP FINGERPRINTING IN THE CORE EXCITATION SPECTROSCOPY OF MOLECULES AND POLYMERS

By

STEPHEN G. URQUHART, B.Sc.

A Thesis

Submitted to the School of Graduate Studies

in Partial Fulfilment of the Requirements

for the Degree of

Doctor of Philosophy

McMaster University

CORE EXCITATION SPECTROSCOPY

OF MOLECULES AND POLYMERS

DOCTOR OF PHILOSOPHY (1997)
(Chemistry)

McMaster University
Hamilton, Ontario

TITLE: Delocalization and Functional Group Fingerprinting in the Core Excitation Spectroscopy of Molecules and Polymers.

AUTHOR: Stephen G. Urquhart, B.Sc. (McMaster University)

SUPERVISOR: Professor A. P. Hitchcock

NUMBER OF PAGES: xx, 217

ABSTRACT

Core excitation spectroscopy is a sensitive probe of the local geometric and electronic structure of materials. Functional group "fingerprints" arise in core excitation spectroscopy from a balance between local structural sensitivity and electronic delocalization. Delocalization can add complexity and extended-structure sensitivity to core excitation spectroscopy.

In this thesis, Inner Shell Electron Energy Loss Spectroscopy (ISEELS) was used to acquire core excitation spectra of molecules that are structural analogues to polymers, and both ISEELS and Near Edge X-ray Absorption Fine Structure (NEXAFS) was used to acquire core excitation spectra of organosilane molecules. Core excitation spectra of structural analogues of polyurethane, polyurea and polyphthalate polymers were used to model and interpret the spectra of polymers. "Finger-printing" of polymer-relevant functional groups and the sensitivity to polyphthalate substitutional isomerism is demonstrated. Functional group fingerprinting is extended to organosilane molecules for the identification of bond-specific features and electronic delocalization. Molecular orbital calculations were performed to assist spectral interpretation and to examine structure-spectral relationships.

Developments in X-ray and electron spectromicroscopy techniques have improved the capability of core excitation for the chemical microanalysis of polymers. In spectromicroscopy of "real-world" materials, the core excitation spectra of these materials must be well understood for meaningful chemical analysis. This thesis provides some of the fundamental underpinnings for the application of core excitation spectroscopy to spatially resolved chemical analysis of organic and organosilane polymers.

ACKNOWLEDGMENTS

I wish to express my gratitude to my supervisor, Prof. Adam Hitchcock, for his support, guidance and faith in me. He gave me the opportunity to get involved in some great research projects and to develop some of my own research ideas.

I have learned much from Dr. Tolek Tyliszczak's approach to problem solving, best summed up in his own words: "*When you fix something, don't make it work as it used to work, make it work as it should work.*" I wish to thank him for his excellent technical advice and assistance that kept my spectrometer, my computer and my car running. He makes a mean cup of coffee.

A special appreciation is due to Dr. Ed Rightor, with whom I have worked in a rich and fruitful collaborative project for many years. I look forward to continuing in this collaboration!

Thanks to the lab folks, Alex Wen, Phillipe Aebi, James Francis, Cassia Turci, Jeff Aubry, Gabi Eustatu, Peter Brodersen and John Neville for their assistance and camaraderie in the lab!

I wish to thank my parents (Mom, Dad), their significant others (Pat and Joan, respectively), and to my partner Christine for their support and love. This thesis is dedicated to them.

A final mention is to my cats, Smokie, Marmalade and the late Zobot. Well, they didn't really help me - the truth is that they tried to distract me whenever they could. Um, thanks anyway...

> Greebo had spent an irritating two minutes in that box. Technically, a cat locked in a box may be alive or it may be dead. You never know until you look. In fact, the mere act of opening the box will determine the state of the cat, although in this case there were three determinate states the cat could be in: these being Alive, Dead, and Bloody Furious.
>
> Terry Pratchett, *Lords and Ladies*, 1992.

TABLE OF CONTENTS

LIST OF FIGURES

Chapter 3

Chapter 4A

Chapter 4C

Chapter 4D

Chapter 5A

LIST OF TABLES

List of Abbreviations

ALS	Advanced Light Source
B0, B2, BM	Identifiers for MDI-polyurethane polymers (See Figure 4.2.8)
BDO	Butane diol
CLS	Canadian Light Source
CSRF	Canadian Synchrotron Radiation Facility
DCM	Double Crystal Monochromator
EELS	Electron Energy Loss Spectroscopy
EHMO	Extended Hückel Molecular Orbital
EICVOM	Equivalent Ionic Core Virtual Orbital Model
EXAFS	Extended X-ray Absorption Fine Structure
FWHM	Full Width at Half Maximum
FY	Fluorescent Yield
HOMO	Highest Occupied Molecular Orbital
IP	Ionization Potential
ISEELS	Inner Shell Electron Energy Loss Spectroscopy
IVO	Improved Virtual Orbitals
LCAO	Linear Combination of Atomic Orbitals
LUMO	Lowest Unoccupied Molecular Orbital
MDI	4, 4'-methylene diphenyldiisocyanate
MO	Molecular Orbital

NEXAFS	Near Edge X-ray Absorption Fine Structure
NSLS	National Synchrotron Light Source
PEELS	Parallel Electron Energy Loss Spectroscopy
PPO	Poly(propylene oxide)
SRC	Synchrotron Radiation Center
STXM	Scanning Transmission X-ray Microscopy
TDI	Toluene diphenyldiisocyanate
TEM-EELS	Transmission Electron Microscopy - Electron Energy Loss Spectroscopy
TEY	Total Electron Yield
TIY	Total Ion Yield
TV	Term Value
XANES	X-ray Absorption Near Edge Structure
XAS	X-ray Absorption Spectroscopy

CHAPTER 1

INTRODUCTION

The principal forms of core excitation spectroscopy, Near Edge X-ray Absorption Fine Structure (NEXAFS) and Inner Shell Electron Energy Loss Spectroscopy (ISEELS) are presented. The interpretation of core excitation spectra within molecular orbital theory is discussed for organic and organosilane molecules and for polymers. The application of core excitation spectroscopy for the chemical microanalysis of materials, through x-ray and electron microscopy, is presented.

§1.1 Core Excitation Spectroscopy

Core excitation spectroscopy is a sensitive probe of the unoccupied electronic structure of materials. Its basis is in the excitation of inner shell (core) electrons to unoccupied orbitals or bands. In particular relevance to this thesis, core excitation spectroscopy is useful for identifying chemical functionalities in polymers. The chemical sensitivity of core excitation spectroscopy is based on how core excitation reflects both local geometry and the delocalized electronic structure.

Core excitation can be probed by two complementary techniques: Inner Shell Electron Energy Loss Spectroscopy (ISEELS) and Near Edge X-ray Absorption Fine Structure (NEXAFS). These spectroscopies measure core excitation by different physical probes: x-ray photoabsorption in NEXAFS and electron scattering in ISEELS.

§1.2 Near Edge X-ray Absorption Fine Structure (NEXAFS) Spectroscopy

Near Edge X-ray Absorption Fine Structure (NEXAFS) is a photoabsorption spectroscopy, in which an electron is excited from a core level to an unoccupied level or is ionized by the absorption of an x-ray photon. In NEXAFS spectroscopy, the attenuation of a monochromatic x-ray beam by a sample is measured as a function of the x-ray energy. This process is presented in **Figure 1.2.1** for the Si 1s NEXAFS spectrum of gaseous silylene Si[N^{t}BuCHCHN^{t}Bu] (from Chapter 5B) and is represented by equation 1.2.1:

$$h\upsilon(E) + M \rightarrow M^* \qquad (1.2.1)$$

where the excited state M^* is more energetic than the initial state M by an amount of energy equal to E. Discrete features in NEXAFS spectra result from *resonant* photoabsorption, where a transition only occurs when the photon energy ($h\upsilon$) is equal to the energy difference ($M^* - M$) between states. The resonant nature of electronic excitation in NEXAFS spectroscopy is important in contrast to the *non-resonant* nature of electron scattering, discussed below.

Experimental details of the NEXAFS techniques used for this thesis are presented in Chapter 2.

§1.3 Inner Shell Electron Energy Loss Spectroscopy (ISEELS)

Inner Shell Electron Energy Loss Spectroscopy (ISEELS) was also used to obtain core excitation spectra. ISEELS techniques once had a strong advantage over NEXAFS in the 250 - 1000 eV energy range because high resolution x-ray absorption experiments were difficult in this regime. In the past decade, the development and proliferation of

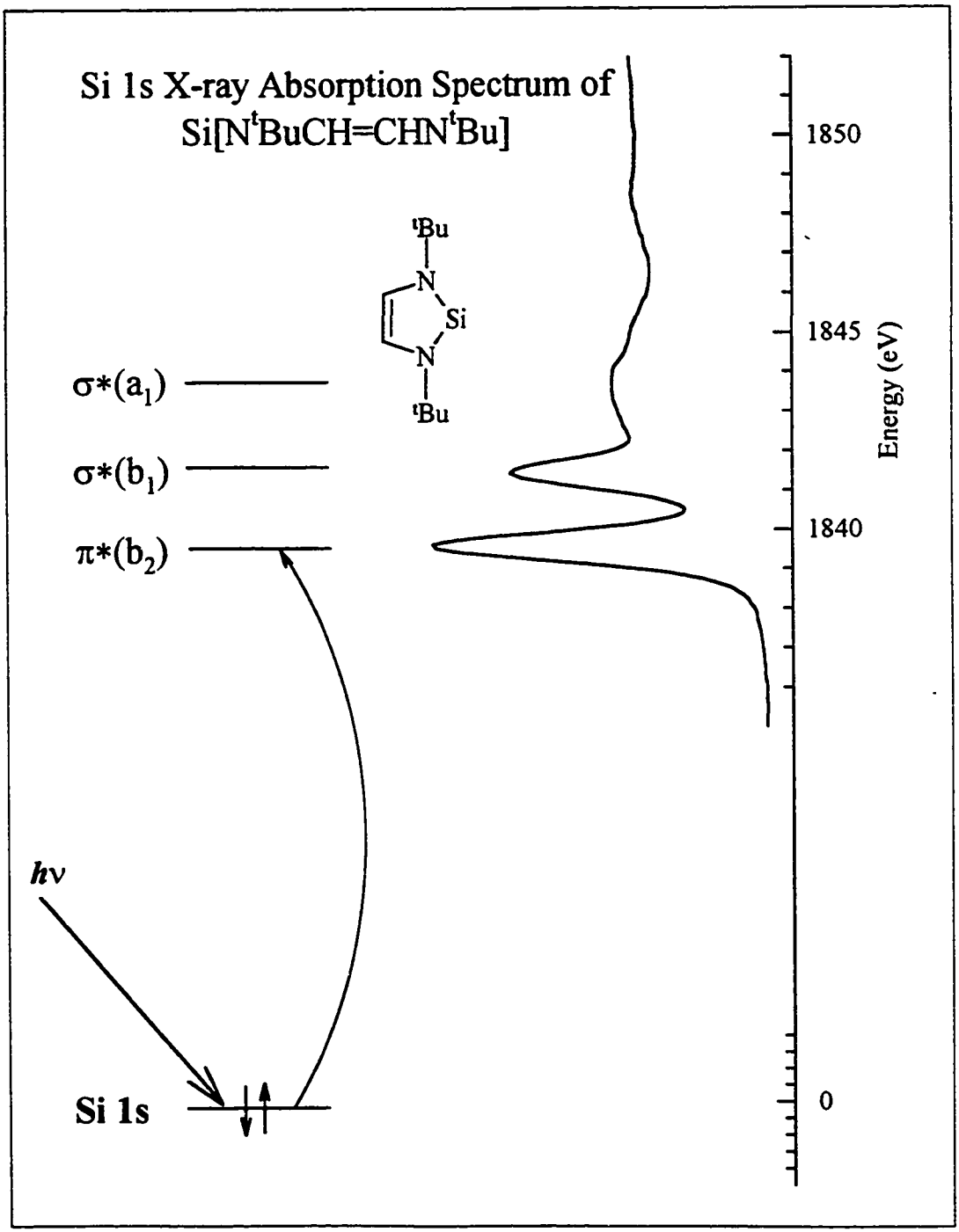

Figure 1.2.1 Core excitation by X-ray photoabsorption: Si 1s X-ray Absorption Spectrum of Si[N^{t}BuCH=CHN^{t}Bu] (§5B).

spherical grating x-ray monochromators has reduced this particular advantage. Nevertheless, ISEELS spectroscopy remains a relevant technique for several reasons. ISEELS spectroscopes can continuously scan a large energy range (i.e. 50 - 1000 eV using the McMaster ISEELS spectrometer), whereas x-ray monochromators require different gratings for different energy ranges. The energy resolution of the ISEELS spectrometer (with a constant band pass analyser; §2.2.2) is constant over this energy range, while the energy resolution of x-ray monochromators varies with the photon energy. The wide energy range of ISEELS is particularly useful as multiedge spectral investigations often give additional insight to spectral problems relative to investigations restricted to only one core edge. Gas phase ISEELS spectrometers have been configured for spectral studies of low volatility species that would otherwise be difficult using x-ray photoabsorption [W92]. These instruments have provided some of the best measurements of absolute photoabsorption cross sections [BH81]. Finally, the use of "lab based" electron impact experiments is often more convenient than synchrotron radiation based experiments.

In ISEELS spectroscopy, a high energy monochromatic electron beam is passed through the sample. The yield of inelastically-scattered electrons is measured with an electron spectrometer as a function of the energy loss at a small scattering angle θ. This process is presented in **Figure 1.3.1**. The energy distribution of the inelastically scattered electrons contains information on the probability of creation of core excited states by the scattered electron beam.

The process for inducing an inner shell transition using a high energy electron of

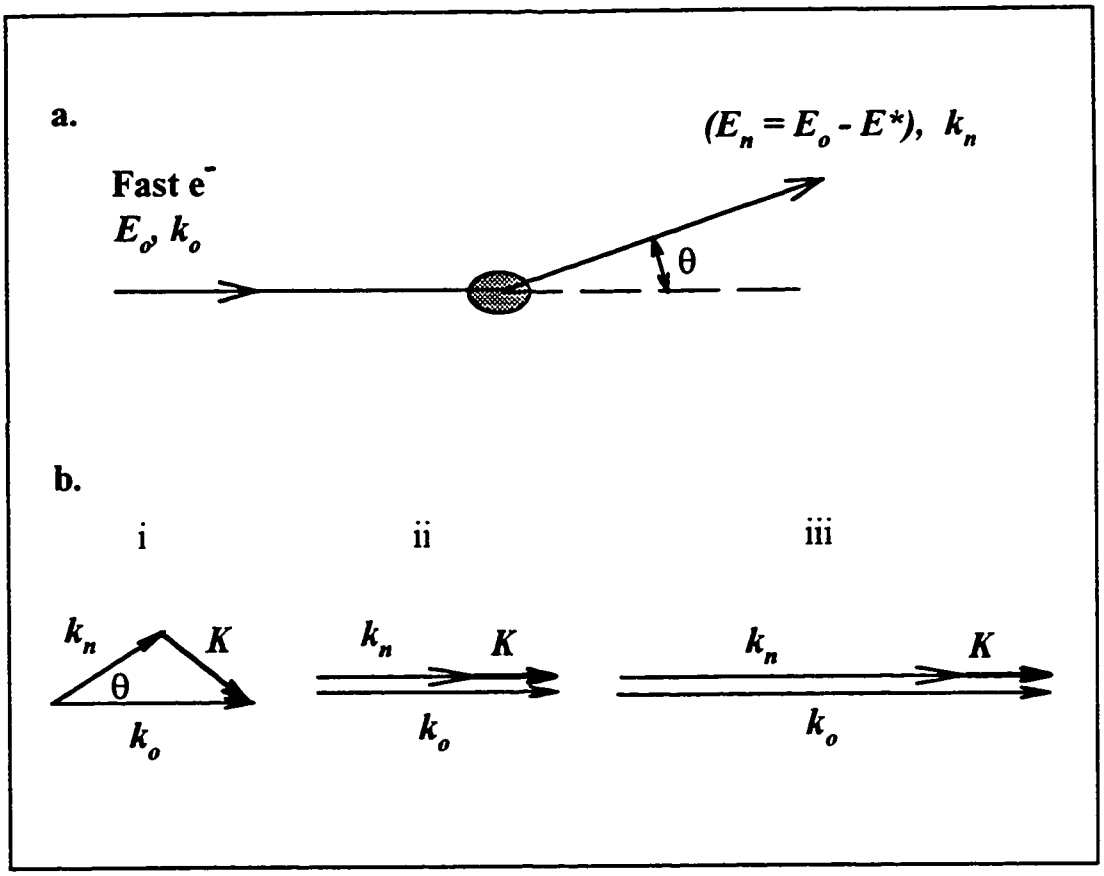

Figure 1.3.1 (a.) Illustration of the inelastic scattering of a fast electron by a molecular target: E_o, impact energy; E^*, energy loss; k_o and k_n, wavevectors of the fast incident electron before and after scattering; θ, scattering angle.
(b.) Transfered momentum, K, dependent on the scattering angle and/or the incident electron k_o. E^* has the same magnitude in each case. i.) small E_o, large θ; ii.) small E_o, small θ; iii.) large E_o, small θ.

impact energy E_o is:

$$\begin{array}{lccccccc} & M & + & e_{inc.} & \rightarrow & M^* & + & e_{scat.} \\ \text{Energy conservation} & & & E_0 & & E^* & & E_n \\ \text{Momentum conservation} & & & \boldsymbol{k_o} & & \boldsymbol{K} & & \boldsymbol{k_n} \end{array} \qquad (1.3.1)$$

where M refers to the free atom or molecule. The energy ($E^* = E_o - E_n$) lost by the inelastically-scattered electron in a single collision is equal to the excitation energy for the creation of the core excited state M^*.

It is important to note that ISEELS is a *non-resonant* technique. In electron-target collisions, energetic electrons can lose *any fraction* of their energy through electronic interactions with the target. This is in contrast to photoabsorption, in which photons are either absorbed or are transmitted unabsorbed. In ISEELS, the flux of inelastically scattered electrons with a certain energy is measured.

§1.3.1 Relationship Between Electron Scattering and X-ray Photoabsorption

In order to compare ISEELS spectra with NEXAFS spectra, the relationships between the techniques must be understood. In 1930, Bethe [B30] showed that there is a quantitative relationship between photoabsorption and inelastic scattering of fast electrons under conditions where the first Born approximation holds. Recent theoretical treatments of this relationship have been given by Inokuti [I71, IIT71] and Kim [K72], and have been reviewed by Brion and Hamnett [BH81].

The inelastic scattering of fast electrons by a molecule can be described by evaluating the probability for transitions from an initial state (wavefunction ψ_0) to a final state (wavefunction ψ_n). The number of electrons that have lost an energy E^* in a collision

with a molecule and are scattered in a direction characterized by the momentum $k_n = k_o - K$ (where K is the momentum transfer to the atom or molecule) is proportional to the double-differential cross section: [S92]

$$\frac{d^2\sigma_e}{dE^* dK} = f(K,E^*)\left|\left\langle \psi_n \left| \sum_{j=1}^{Z} e^{iK\bullet r_j} \right| \psi_o \right\rangle\right|^2 \qquad (1.3.2)$$

where $f(K, E^*)$ is a momentum and energy dependent function, and the summation is over all electrons. In the limit $K \cdot r_j \ll 1$ (where r_j is the radius of the initial core state), the exponential factor in equation 1.3.2 can be expanded as a power series:

$$e^{iK\bullet r_j} = 1 + iK\bullet r_j + \tfrac{1}{2}(iK\bullet r_j)^2 + \ldots. \qquad (1.3.3)$$

As the initial and final states (ψ_o and ψ_n) are orthogonal, the matrix element from the first term is equal to zero. The second term leads to the usual electric-dipole matrix element and the third term leads to a mixed quadrupole-octupole matrix element, and so on [I71]. When the momentum transfer K is small, the electric-dipole term dominates over the higher order terms.

By integrating over the finite angular acceptance of the spectrometer (up to θ_{max} from the incident beam direction) we obtain:

$$\frac{d\sigma_e}{dE^*} = f(E_o,E^*,\theta_{max})\left|\left\langle \psi_n \left| e_K\bullet r \right| \psi_o \right\rangle\right|^2 \qquad (1.3.4)$$

where E^* is the incident electron beam energy, $f(E_o, E^*, \theta_{max})$ is a kinematic function of

the energy loss, incident electron beam energy and the scattering angle, and e_k is a unit vector in the direction of momentum transfer $\boldsymbol{K}$. Compare equation 1.3.4 to the expression for x-ray absorption: [S92]

$$\sigma = f(h\nu,\boldsymbol{k})\left|\langle\psi_n|\boldsymbol{e}_E\bullet\boldsymbol{r}|\psi_o\rangle\right|^2 \qquad (1.3.5)$$

where $\boldsymbol{k}$ is the wave vector magnitude of the photoelectron and e_E is a unit vector in the direction of the electric field $\boldsymbol{E}$ of the x-ray photons. In the limit of small momentum transfer ($\boldsymbol{K} \to 0$), ISEELS spectra are dominated by electric-dipole transitions, where the vector $\boldsymbol{K}$ takes the role of the electric field vector $\boldsymbol{E}$ of x-rays. The full expression relating electron scattering with photoabsorption (including terms neglected in the simplified treatment above) is: [S92]

$$\frac{d\sigma_e}{dE^*} = 8mc^2\left(\frac{2\pi e^2}{hc}\right)E_o(E^*)^{-3}\sigma \qquad (1.3.6)$$

This equation provides a quantitative relationship between x-ray photoabsorption (σ) and electron scattering ($d\sigma/dE^*$) in small momentum transfer conditions.

The momentum transfer vector $\boldsymbol{K}$ depends on the scattering angle θ and the energy loss E^*. Its magnitude can be derived by applying the conservation of momentum to the electron-molecule collision: [BH81]

$$K^2 = |K|^2 = |k_o - k_n|^2 = k_o^2 + k_n^2 - 2k_ok_n\cos\theta \qquad (1.3.7)$$

A vector diagram illustrating this process is presented above in **Figure 1.3.1**. For small

angle scattering of the incident electron, the momentum transfer $\boldsymbol{K}$ is small according to Eq. 1.3.7. A larger relative electron impact energy (larger k_o) decreases the relative magnitude of the momentum transfer vector. In the "electric-dipole limit" - large impact energy, small scattering angle collisions and thus small momentum transfer - the scattered electron predominantly causes electric-dipole transitions. ISEELS spectra in this thesis were acquired near the electric-dipole limit in order to complement the electric-dipole NEXAFS spectra. Other researchers have used ISEELS spectroscopy in large angle scattering geometries to measure non-dipole electronic transitions [KT&77, SKR80, F95].

§1.4 Interpretation of Molecular Core Excitation Spectra

The features appearing in core excitation spectra arise from electronic transitions between the ground state and core excited states of a molecule. First, the terms used to describe core excited states will be reviewed. A *state* is described by a wavefunction, a mathematical construct that contains information about the location and motion of *all* electrons in the molecule. However, most core excitation features are described by a simpler one-electron picture, where an electron is excited from an initial (core) level to a final (unoccupied valence) level. Several complementary descriptions of the core excitation process are presented in **Figure 1.4.1**, for the intense N 1s → π^* feature observed in the N 1s core excitation spectrum of N_2. This transition is described in the one electron orbital picture as a transition from the N 1s level (1s σ_u and 1s σ_g) to the π_g^* level. The core excited state is also described in the one electron picture in terms of its electron configuration: (1s σ_u^{-1}, π_g) and (1s σ_g^{-1}, π_g). In the state picture, these core

excited states are described by the term symbols $^{1,3}\Pi_u$ and $^{1,3}\Pi_g$. The state term symbols describe all of the electrons in the molecule and thus can distinguish between the spin-allowed singlet core excited state $^1\Pi$ ($\Delta S = 0$) and the spin-forbidden triplet core excited state $^3\Pi$ ($\Delta S = 1$). At a fundamental level, any electronic transition is a process involving all electrons in a molecule, and the state picture is strictly correct. However, the one electron picture is a convenient description which is adequate for many core excitation transitions.

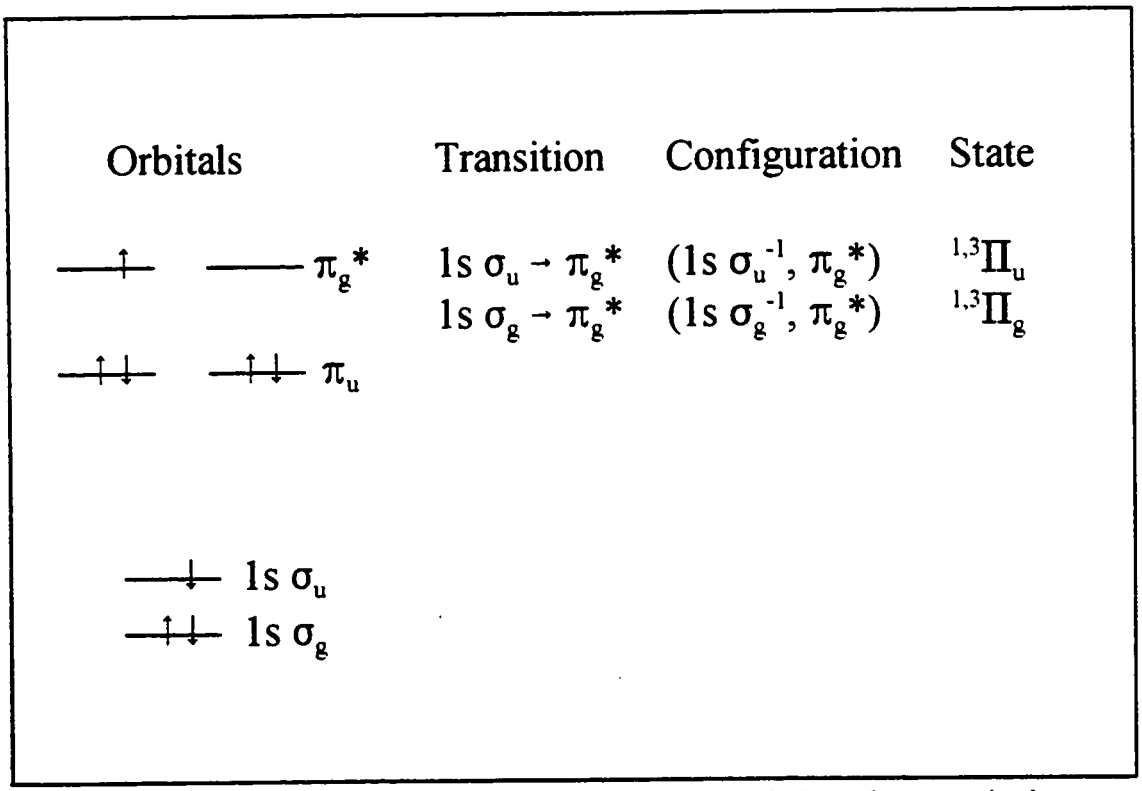

Figure 1.4.1 Orbital, transition, configuration and state description of core excitation, including non-dipole transitions.

In addition to transitions described as one electron transitions, two electron transitions are also observed in core excitation spectra. An example is the $(1s^{-1}, \pi, \pi^{*2})$ core excited transition that occurs at ~415 eV in the N 1s spectrum of N_2. Two electron

transitions are a relatively minor contribution to the spectra of complex molecules and polymers.

One electron transitions are classified in terms of the character of the final electronic level, which includes resonant "valence excitations" (i.e. core → π^* and core → σ^* transitions) and "Rydberg transitions" (core → Rydberg transitions). Rydberg features are weak in large molecules and are generally absent or attenuated in the spectra of solids. Extended X-ray Absorption Fine Structure (EXAFS) features are also present in core excitation spectra. EXAFS features are a weak fine structure extending hundreds of electron volts into the continuum. These features arise from the interference of the outgoing photoelectron wave with the component of the photoelectron wave backscattered by atoms surrounding the core excited atom [S88]. This signal can be Fourier processed to extract the radial distribution of the backscattering atoms. This technique is not used in this thesis and will not be discussed further.

The most dominant features observed in molecular core excitation spectra are attributed to resonant valence excitations, where a core electron is excited to an unoccupied valence level. In discussions of the core excitation spectra of organic and organometallic species, it is common to describe these transitions in terms of the molecular orbital (MO) character of the optical orbital. These transitions can also be described in terms of multiple scattering theory [S92]. While multiple scattering theory is complementary to the molecular orbital model, its language is quite different from that of molecular orbital theory. The MO description is familiar to chemists and will be the description used in this thesis.

Resonant core excitation transitions occur at energies relatively near the energy of the core electron ionization potential (IP). Features that occur below the IP are referred to as "bound" or "discrete" resonances, while resonant features that occur above the IP are referred to as "unbound" or "shape" resonances. Within the MO model, it is useful to distinguish the origin and nature of these resonances in terms of the nature of the optical orbital which has either π or σ character. The designation "π" or "σ" is not strictly correct for non-planar molecules and complex molecules and it is heavily oriented to the two-electron or valence-bond description of chemical bonding. While this description is relevant for some simple molecules, it is less relevant to organometallics, main group atoms, and electron deficient carborane molecules. A group theory identification of MOs is proper in all instances but not always informative. It can be useful to identify a "dominant" orbital character, such as the π or σ MO character at the core excited atom site. Final state MOs are typically antibonding and these levels are referred to as π* and σ* MOs (e.g. C 1s → π* transition). The specific nature of core → π*, core → σ* and core → Rydberg transitions will be discussed below, using the C 1s, N 1s and O 1s core excitation spectra of urea as an example.

§1.4.1 Core → π* Transitions

Core → π* transitions are observed in π bonded molecules whenever there is π* orbital density at the site of the core hole. The final levels in these transitions are usually the antibonding counterparts of the π-bonding MOs and the antibonding "π*" designation is generally applied. **Figure 1.4.2** presents the C 1s, N 1s and O 1s core excitation spectra

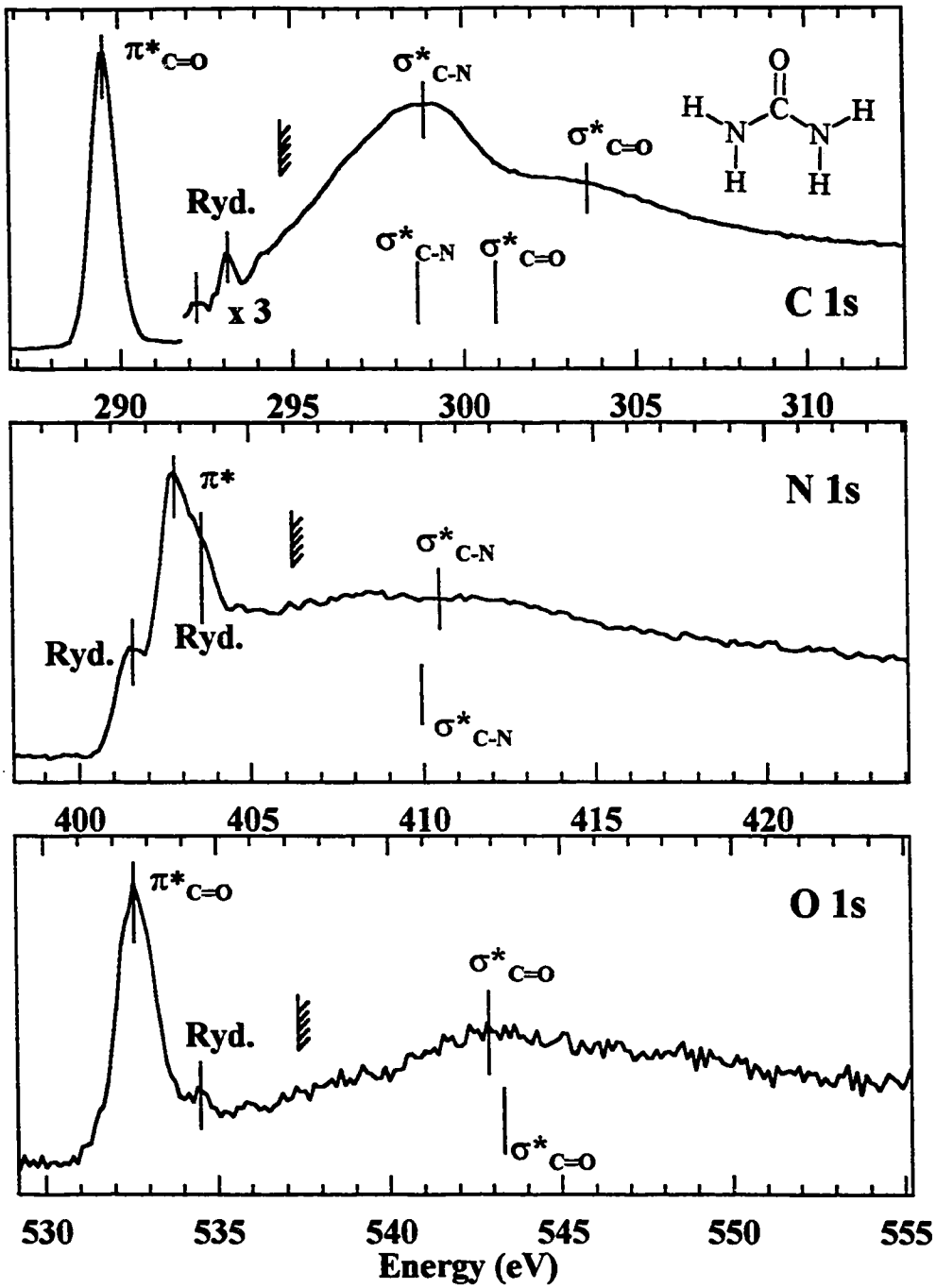

Figure 1.4.2 C 1s, N 1s and O 1s Inner Shell Electron Energy Loss Spectra (ISEELS) of urea. Ionization potentials (from Tables III-V, Chapter 4C) are indicated by hatched lines. Details of the acquisition, processing and analysis are discussed in Chapter 4C. Predictions based on the bond length correlation are indicated below the experimental trace (bond lengths from Chapter 4C, correlation from literature [SSH84]).

of urea (NH_2CONH_2), acquired by ISEELS spectroscopy (extracted from Chapter 4C). As urea has a carbonyl π-bond, the Highest Occupied Molecular Orbital (HOMO) is expected to be a $\pi_{C=O}$ MO and the Lowest Occupied Molecular Orbital (LUMO) is expected to be a $\pi^*_{C=O}$ MO. In the C 1s and O 1s spectra, the intense low energy feature is assigned as a transition from the core level (C 1s or O 1s) to the $\pi^*_{C=O}$ MO. This feature is intense because the $\pi^*_{C=O}$ MO has a high density on the carbon and oxygen atom sites in urea. In the N 1s spectrum of urea, a N 1s → π* transition is observed, but is heavily mixed with Rydberg transitions. This N 1s → π* transition originates from delocalization of the carbonyl $\pi^*_{C=O}$ density onto nitrogen. The special nature of Rydberg transitions and their mixing with resonant valence transitions will be discussed below (§1.4.3).

The energy and intensity of π* features can reflect the character of the π-bonds. The intensity of the π* transition increases with the π-bond order within a series of molecules containing the same atoms. For example, the intensity of the C 1s → π* transition in triply bonded CO is ~2.3 times larger than in doubly bonded H_2CO [MC&87, RI&88]. In this instance, there is a greater π*-density at the carbon atom site when the atom participates in two π-bonds instead of one.

In general, π* resonances are intense and narrow. The natural width of these resonances (in the absence of instrumental broadening) is determined by the lifetime of the core excited state and the vibrational motion of the molecule. A core excited state can be vibrationally split into bands, reflecting the excitation of vibrational modes in the molecule upon core excitation. The width of each vibrational state is determined by rate of core hole decay, which is manifest through the Heisenberg uncertainty principle in the width of the

spectral feature. The natural line width of the π^* resonance in CO, for example, is very narrow (65 ±10 meV) [TKR79], mainly reflecting the energy of the core level. Vibrational bands can be resolved in the high resolution spectra of molecules with narrow natural linewidths, as observed in the core excitation spectra of the several small molecules [TKR79, FKH94, CMS89].

§1.4.2 Core → σ^* Transitions

Core → σ^* transitions are observed in the spectra of all organic, organometallic and polymer species. These features are generally observed at higher energy than the π^* features in unsaturated molecules. Most core → σ^* transitions occur above the IP, although some core → σ^* states, specifically those associated with weak σ bonds can occur below the IP [IM&87].

Core → σ^* resonances that occur below and above the ionization potential are attributed to different physical mechanisms. Transitions to resonant states below the ionization potential can be described as transitions to unoccupied MOs. This description can be used for transitions to states above the ionization potential, where the transition is viewed as a two step process: excitation from a core orbital to an unoccupied MO, followed by rapid auto-ionization into the continuum [T83]. These features can also be described by multiple scattering theory [DDP85, DPS86], which is complementary [T83] to the MO description.

Core → σ^* transitions are very sensitive to the chemistry and bonding of a system. This is well illustrated by a "bond length correlation" model, which relates the term value (TV) of the σ^* feature with the σ-bond length.

The term value (TV) is given by:

$$\text{Term Value} = \text{Feature Energy} - \text{Ionization Potential.} \qquad (1.4.1)$$

This bond length correlation was established for σ bonds containing second row (B, C, N, O or F) atoms in diatomic and "psuedodiatomic" molecules such as acetylene [SG&89, SSH84, HBT89]. This correlation is presented in **Figure 1.4.3**, illustrating that shorter bonds have a higher relative σ* resonance energy. The bond correlations are grouped according to the sum of atomic numbers (Z) of the atoms forming the σ bond (for example N_2 with $\sum Z = 14$ is grouped with CO which also has $\sum Z = 14$). Parameters for a formula to predict σ* energies for a given bond length have been obtained from a least squares fit of data from many experimental spectra [SSH84].

The bond length correlation model was criticized by Piancestelli *et al.* [PL&87a,

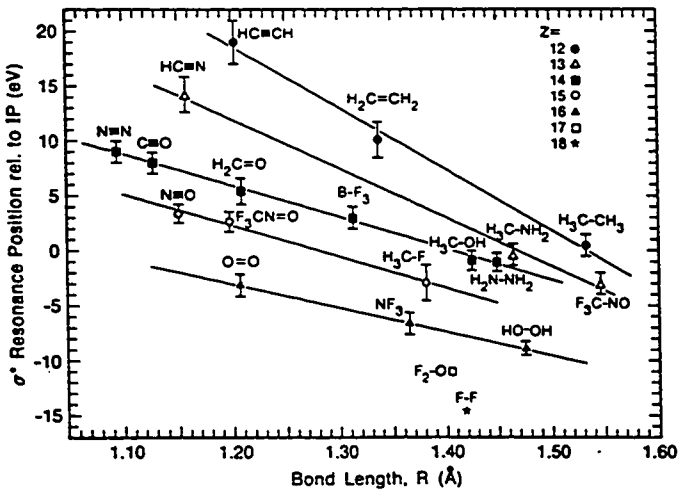

Figure 1.4.3 Empirical correlation between the σ* resonance position relative to the 1s ionization potential (IP) and the bond length R for simple non-conjugated molecules. All data are from K-shell spectra of free molecules. Each data point is labelled by the molecule it represents and the bond and bond type is explicitly indicated. The molecules are grouped according to the sum of atomic numbers of the bonded pair, Z [SSH84].

PL&87b], in part because of the failure of the model for conjugated molecules such as CO_2. Both Hitchcock and Stöhr [SSH84, HS87] and Piancastelli *et al.* [PL&87a, PL&87b] describe the σ*-behaviour in terms of a *multiple scattering* potential barrier model, rather than a model where σ* resonances are described in terms of MOs and covalent bonding [SG&89, LAL91]. The strength of a covalent bond is reflected by its length (shorter = stronger) and the concurrent stabilization of the σ energy and a destabilisation of the σ* energy. Thus, shorter bonds are expected to have a higher relative σ* energy. This is reflected in the "particle in a square well" argument presented by Sheehy *et al.* [SG&89]

The process of relating a specific σ* resonance with a specific covalent σ-bond is only strictly applicable in diatomic molecules. When the core excited atom is a participant in more than one σ-bond, the σ and σ* MOs are not necessarily bond specific but may be delocalized or "mixed" over several σ-bonds. In this case, the σ* resonances do not exclusively reflect the character of a specific bond. In "pseudodiatomic" molecules such as acetylene, the σ*(C-H) and σ*(C-C) resonances do not strongly mix and in this instance the bond length correlation is effective.

Both localized "bond specific" and delocalized or mixed core → σ* transitions are observed in the C 1s, N 1s and O 1s core excitation spectra of urea (Figure 1.4.2). In the O 1s spectrum of urea, the broad O 1s → $\sigma^*_{C=O}$ transition in the experimental spectrum is approximately at the same energy as that predicted by the bond length correlation.

In the C 1s spectrum of urea, σ*-delocalization has a much larger effect. The C1s spectrum of urea has two strong continuum resonances (298.8 eV and 303.5 eV). The lower resonance is at approximately at the same energy as the σ^*_{C-N} bond length

correlation prediction, while the higher resonance is ~2 eV higher energy than the $\sigma^*_{C=O}$ bond length correlation prediction. In MO calculations of urea (not shown), the σ* MOs are delocalized over both the C=O and C-N bonds. The "bond specific" σ^*_{C-N} and $\sigma^*_{C=O}$ labelling is maintained as the lower energy σ* transition has greater "C-N" character, and the higher energy σ* transition has greater "C=O" character (Chapter 4C).

Despite the limitations of the bond length correlation for complex molecules, the example of urea demonstrates that this model is still useful for forming a qualitative understanding of the spectra of molecules containing second row atoms. The extension of the bond length correlation to bonds containing third row atoms (P, S, Si, etc) has been attempted, but only a weak correlation was observed [HT88, HBT89].

The width of σ* features is determined by lifetime broadening and shape of the molecular potential. For σ* resonances, the lifetime of the $(core^{-1}; \sigma^*)$ core excited configuration is that of the quasibound excited state. Because of the high probability of decay of the quasibound states into continuum states, these higher energy σ* features are very broad. As well, σ* resonances have an asymmetric shape that originates from the increased ionization probability for higher energy photoelectrons and in some cases, vibrational broadening [S92].

§1.4.3 Rydberg and Mixed Valence-Rydberg Features

Rydberg orbitals are *atomic like* features observed in the core excitation spectra of atoms and molecules. In core – Rydberg transitions, the excited electron "sees" a hydrogenic core, where the core hole and nuclear charge is screened by the valence

electrons such that the nucleus and all non-excited electrons appears to the excited electron as a single entity with a +1 charge. Rydberg features are not as chemically sensitive as valence resonances, but their ubiquitous presence in the core excitation spectra of small molecules requires a consideration of their characteristics.

The energy of Rydberg states in a molecule should follow the Rydberg formula, where the term value of any member (n,ℓ) is given by: [R74]

$$TV = IP - E_n = R/(n - \delta_\ell)^2 \qquad (1.4.1)$$

where R is the Rydberg energy (13.6 eV) and δ_ℓ the quantum defect associated with the angular-momentum quantum number ℓ. The maximum electron density of a molecular Rydberg orbital exists outside the molecular core and its shape and number of nodal surfaces are similar to its atomic hydrogenic orbital counterpart.

Rydberg and valence core excited states can appear in the same energy region of a core excitation spectrum, especially in the core spectra of atoms with bonds to hydrogen. In these instances, extensive Rydberg-valence mixing can occur. This is observed in the C 1s spectrum of methane, where the Rydberg and σ^*(C-H) transitions are considered to overlap and mix strongly [S92].

The nature of Rydberg orbitals differs systematically between small and large molecules. When heavy atoms (non-hydrogen) are bonded to the core excited atom, the region of space which the Rydberg orbital occupies overlaps with that of the electron density of other atoms. This generally results in the attenuation of Rydberg features relative to their intensity in simpler molecules. In the core excitation spectra of condensed molecules and polymers, Rydberg transitions disappear or are attenuated [XJ&96], and

can be shifted to higher energy relative to in the gas phase [RH&93].

Some Rydberg transitions are observed in the C 1s, N 1s and O 1s core excitation of urea (Figure 1.4.2). The Rydberg transitions in the C 1s spectrum are particularly weak because carbon is coordinated by three heavy atoms. The Rydberg structure is also weak at the O 1s edge because the small O 1s orbital has a relatively small overlap with the spatially extended Rydberg orbitals. The N 1s spectrum of urea provides a vivid example of Rydberg/valence mixing, as the N 1s → Rydberg and N 1s → π^* occur in the same energy region. The identification and interpretation of these features is discussed in detail in Chapter 4C.

§1.4.4 Linear Dichroism of Resonant Features

The intensity of spectral features in the core excitation spectra of aligned molecules and polymers exhibits a linear dichroism. Specifically, the intensity of spectral features depends on the angle between the x-ray electric-field vector and the orientation of the electronic transition moment. The photon electric-field vector lies in the plane normal to the photon propagation direction. In common experimental conditions, the electric field vector $\boldsymbol{e}_E$ of synchrotron radiation is linearly polarized in the plane of the storage ring. Thus, angular dependance can occur in the spectra of aligned materials and is an important consideration in spectral interpretation.

The electric-dipole operator ($\boldsymbol{r}$) is a vector connecting the ground state with the final core excited state. In K shell core excitation, the initial electronic level (1s orbital) is spherical and does not contribute to the angular dependance. The intensity of the transition

is the largest when the electric field vector (e_E) of the radiation is aligned with electric-dipole vector ($e_E \cdot r = 1$). More generally, the transition intensity follows a $\cos^2\theta$ intensity behaviour, where θ is the angle between the electric-dipole vector and the electric-field vector.

$$I \propto |e_E \cdot r|^2 \propto \cos^2\theta \qquad (1.4.2)$$

This effect is best demonstrated by example: **Figure 1.4.4** presents the angle-dependent C 1s NEXAFS spectrum of poly(tetrafluoroethylene) (PTFE) thin films [ZS&94]. When the electric field vector e_E is directed perpendicular to the chain ($\alpha = 90°$), the intensity of transitions to $\sigma^*_{C\text{-}F}$ states (labelled "1" in Figure 1.4.4) are enhanced relative to $\sigma^*_{C\text{-}C}$ states (2). When the electric field vector e_E is directed along the chain ($\alpha = 0°$), the relative intensity of these transitions is reversed.

In gas phase measurements, the angular dependance is removed by rotational averaging of the molecules. The orientational dependance of NEXAFS has been used to determine the orientation of surface adsorbed molecules [S92] and the orientation of polymer chains [S92, ZS&94]. Angular dependance can also be present in electron energy loss spectroscopy of oriented materials. In this instance, the momentum transfer vector e_K plays the same role as the electric field vector in photoabsorption. EELS has also been used in this manner to determine the orientation of surface adsorbed molecules [HT95].

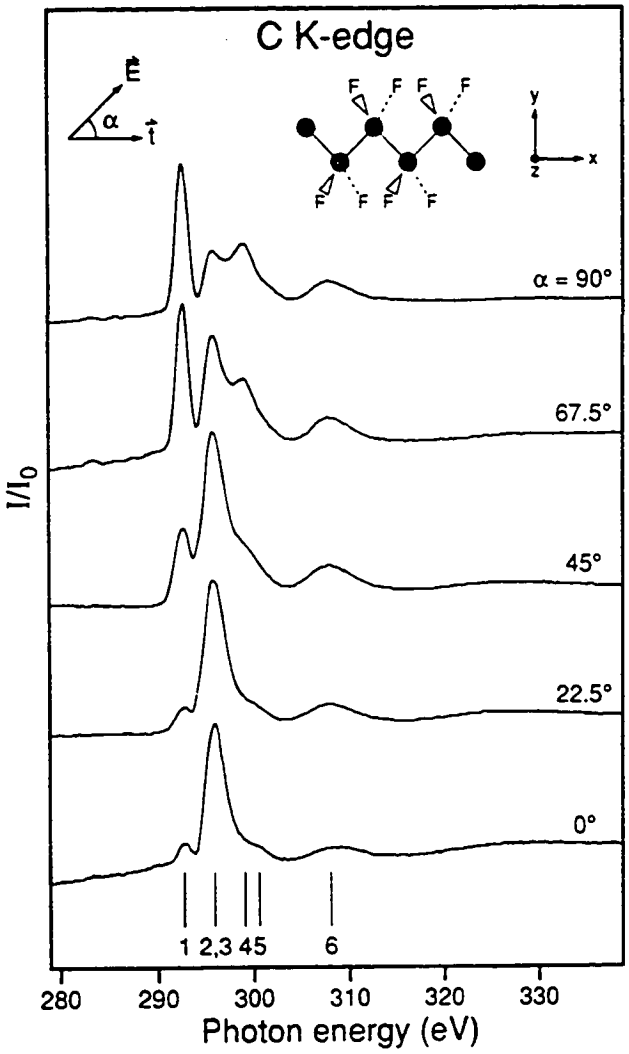

Figure 1.4.4 Polarization-dependant C 1s Near Edge X-ray Absorption Fine Structure Spectra (NEXAFS) of highly oriented poly(tetrafluoroethylene) at angles of $\alpha = 0°$, 22.5°, 45°, 67.5° and 90° between the *e* vector of the X-ray photons and the chain axis [ZS&94].

§1.5 Core Excitation Spectra of Polymers

The core excitation spectra of polymers are expected to manifest core → π^* and core → σ^* transitions like those observed in molecules. This follows from the fact that polymers are extended assemblies of the same building blocks that form organic molecules. Sometimes, the response of polymers to core excitation will differ from that of molecules because of the extended electronic structure of polymers and the effect that the solid phase has on the polymer spectra.

Core excitation spectroscopy is predominantly a *local* probe of electronic structure at the site of the core excited atom. A consequence of this "local probe" description is a "building block" approach to polymer spectra. Comparison to the spectra of structurally analogous molecules can be used to model and interpret polymer spectra [HUR92]. This approach assumes that electronic interactions between polymer repeat units is negligible. In polymers with long range electronic delocalization, a band structure approach is more applicable than this local building block description. Many polymers have a limited degree of electronic delocalization, within a repeat unit or over several repeat units. The identification of appropriate *intermediate* building blocks is an important aspect of this thesis.

§1.5.1 Building Block Models

The core excitation spectra of *saturated* molecules and polymers, such as polyethylene, are strongly determined by the *local* structural order at the core excited atom. In a simple view, we might envision the core excitation spectra of complex materials

as the superposition of "diatomic" (C-C, C-H) building blocks. Recall the description of core excitation features as $\pi^*_{C=O}$ or σ^*_{C-N} (§1.4), a description that is derived from a "valence bond" or "bond specific" view of core excitation spectroscopy.

A bond specific description of core excitation spectra is given by the pseudodiatomic building block model [S92]. An example of this building block model is presented in **Figure 1.5.1**, where the C 1s spectrum of the molecule acetonitrile (CH_3CN) is compared to the C 1s spectrum of ethane (CH_3CH_3) and hydrogen cyanide (HCN). Ethane and hydrogen cyanide contain the C-C and CN "diatomic" bonds present in acetonitrile, and the identification of the σ^*_{CN}, σ^*_{C-C} and π^*_{CN} "bond specific" features in acetonitrile is easy through a comparison with these "building block" molecules. This building block comparison is adequate for interpreting the spectrum of acetonitrile, but in more complex molecules, the π^* and σ^* MOs can be delocalized over part or all of the molecule. "Diatomic" building blocks can not account for more extensive π and σ delocalization, and a larger molecular fragment must be considered. This issue will be addressed in Chapter 4.

§1.5.2 Long Range Conjugation

In polymers with extensive, long range electronic delocalization, it is not useful to describe the unoccupied electronic structure in terms of "localized" π^* and σ^* features. A band structure approach has been used by some researchers. The core excitation spectrum of unsaturated polymers has been considered by Ågren [CA&95] within a band structure approach and vocabulary. In this approach, the nature of the interaction of the core hole

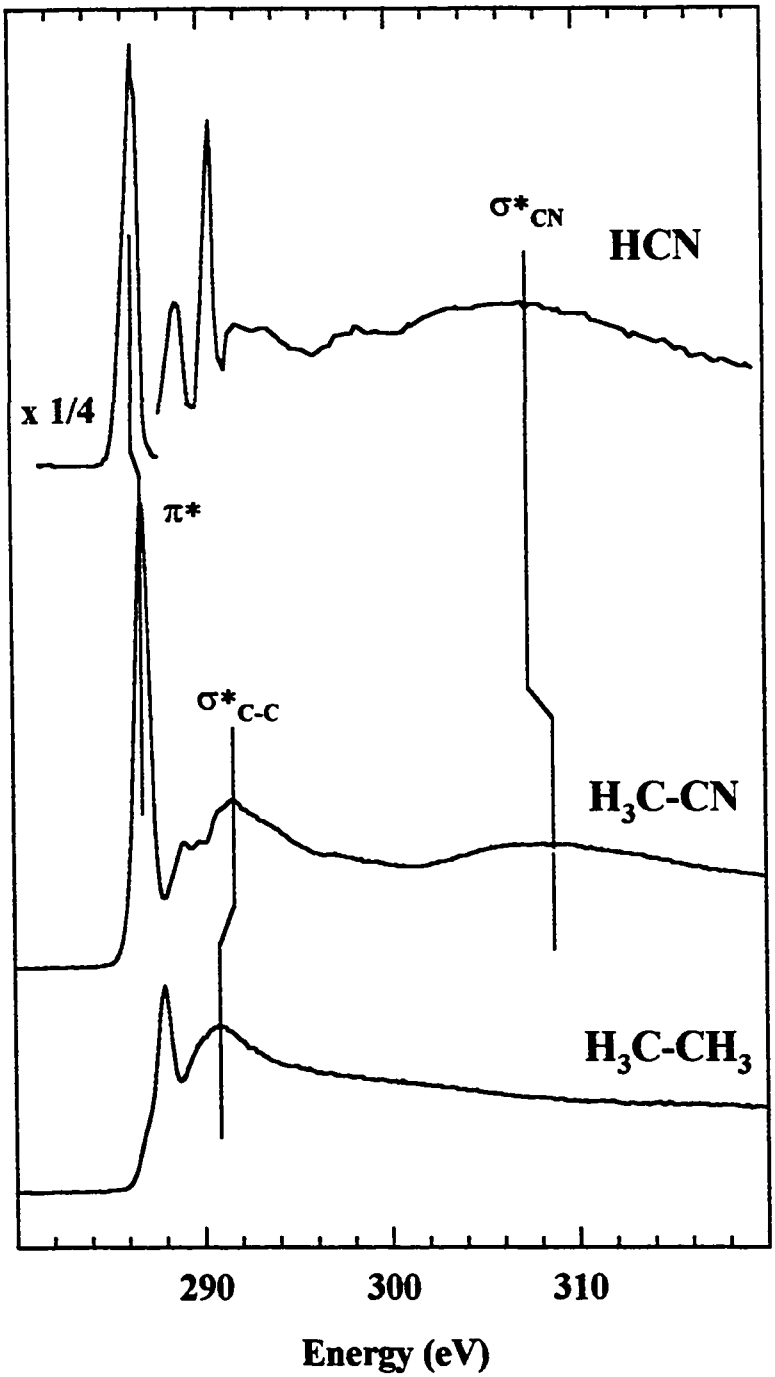

Figure 1.5.1 Demonstration of the building block model for C 1s core excitation spectra: Gas phase C 1s spectra of hydrogen cyanide (HCN), acetonitrile (H_3CCN) and ethane (H_3CCH_3) [S92].

with the excited electron is considered. If the core hole is "well screened" by the electrons in the polymer, then the excited electron is not bound to the core-excited atom site. If the core hole is poorly screened, the excited electron is bound to the core excited atom site, and the transition is called an "exciton". An exciton is defined as a "bound hydrogen like state" [V92], typically observed in the core spectra of semiconductors or insulators. When the bandwidth of the shallow core state ($core^{-1}$, π^*) is narrow, the effective mass of the core hole is large, and the photoelectron is "bound" to the site of the core hole. When the photoelectron is bound to the site of the core hole, the strong core hole-excited electron Coulombic interaction causes substantial relaxation of the optical orbital. This electronic relaxation is observed in molecules, which Ågren refers to as "trivially excitonic" [GA95].

In Ågren's calculations of the oligimer series $CH_3(CHCH)_nCH_3$ (n = 1, 2, 3, 5, 9), the excitonic character of the lowest C 1s → π^* transition was explored. In longer chains, the core hole is increasingly well screened by the delocalized π electrons, the photoelectron is less strongly bound to the core hole, and therefore the intensity of the C 1s → π^* transition decreases. As the chain length increases, there is a reduction in the π^* to σ^* intensity ratio [CA&95, GA95], indicating that the core → π^* transition shifts from an "excitonic" to a delocalized core excited states. In contrast, a similar study of polyacenes and graphite showed that an excitonic π^* transition persisted in the larger models and in graphite [AVC95].

The band structure description and the molecular orbital description are not necessarily mutually exclusive. For many systems, these models can describe the same phenomena using a different language. For the polymers analysed in this thesis, electronic

delocalization has a significant role in defining the core excitation spectra, but on a much shorter range. An *intermediate* building-block fragment approach will be presented and discussed in Chapter 4, where the critical range of electronic delocalization is considered.

§1.6 Spectromicroscopy of Polymers

Spectromicroscopy is an awkward word for a technique that combines *spectroscopy* with *microscopy*. This combination of techniques has two general forms: spectra can be acquired of small sample volumes, or microscopic images are acquired using electronic transitions to create the image contrast. In both methods, the imaging radiation (x-ray or electron) induces electronic transitions in the sample. In the context of this thesis and recent technical developments, core excitation spectroscopy is particularly relevant.

Two spectromicroscopy techniques are based on core excitation spectroscopy: Transmission Electron Microscopy - Electron Energy Loss Spectroscopy (TEM-EELS, §1.6.1) and Scanning Transmission X-ray Microscopy (STXM, §1.6.2). These techniques have recently been applied to the investigation of polymers.

1.6.1 Transition Electron Microscopy - Electron Energy Loss Spectroscopy

Transmission Electron Microscopy (TEM) is commonly used for materials analysis. A high energy, focussed electron beam is used to image thin samples at very high (reaching 2 Å) spatial resolution. The image contrast is formed by inelastic and elastic scattering of the electron beam by the sample. Inelastic scattering of the electron beam

induces vibrational and electronic excitations and structural deformation in the sample. Electronic excitation spectra can be obtained by measuring the energy distribution of inelastically scattered electrons by adding an energy dispersive detector (an Electron Energy Loss Spectrometer) to the TEM microscope. This spectroscopy is identical to gas phase ISEELS spectroscopy, except that it is performed on solids using the imaging electron beam of the microscope.

TEM-EELS spectromicroscopy is strongly advanced by the technological sophistication of commercial TEM microscopes. The high spatial imaging resolution permits spectroscopy of extremely small volumes. The electronic resolution of TEM-EELS depends on the resolution of the EELS analyser and the energy distribution of the imaging electron beam. With a field emission electron source, core excitation spectra with an electronic resolution of ~0.9 eV full width a half maximum (FWHM) are attainable with commercial EELS spectrometers [G97]. Higher electronic resolution (70 meV fwhm) has been demonstrated in custom built systems with electron beam monochromation [B92].

Plural scattering of the electron beam by the sample limits the thickness of samples that can be studied by TEM-EELS [E86], although moderate plural scattering effects can be removed by deconvolution [E86]. The limiting sample thickness depends on the composition of the material, but is generally less than 100 nm thick. The high vacuum requirements of TEM microscopes prevents the study of volatile and wet species. Radiation damage is also a concern in "soft" materials such as polymers. Parallel detection, sample cooling and special beam handling methods have been implemented to permit EELS studies of such materials. Beam damage and electronic resolution issues in

TEM-EELS have recently been evaluated by Rightor *et al.* [RH&97].

1.6.2 Scanning Transmission X-ray Microscopy

Scanning Transmission X-ray Microscopy (STXM) is a technique of burgeoning importance for the investigation of polymers. Its unique niche within the pantheon of microscopic techniques is that it is capable of detailed chemical speciation of "soft" materials (such as polymers) at a submicron spatial scale. This technique uses NEXAFS spectroscopy to provide a "chemical dimension" to microscopic images, either through NEXAFS spectra of small volumes or by NEXAFS-derived contrast in images. At present, there are two STXM instruments, at the National Synchrotron Light Source (NSLS, Brookhaven NY) and at the Advance Light Source (ALS, Berkeley CA), in addition to other types of x-ray microscopes [KJH95].

Figure 1.6.1 presents an illustration of an Scanning Transmission X-ray Microscope [AS&95]. The x-rays are diffractively focussed onto a sample by a Fresnel zone plate. The maximum spatial resolution is governed by the present limitations of nanofabrication technology in creating the zone plates. The typical focus resolution is ~ 55 nm, although smaller features can be discerned by image processing [JC91]. An order sorting aperture is used to only allow the first order diffracted x-rays to focus on the sample. An x-ray detector (Si photodiode or gas proportional counter) is used to measure the flux of x-rays transmitted through the sample. Images are formed by scanning the sample through the x-ray beam and measuring the x-ray flux at each sample position.

STXM microscopes can be operated in two modes: Images can be acquired at a

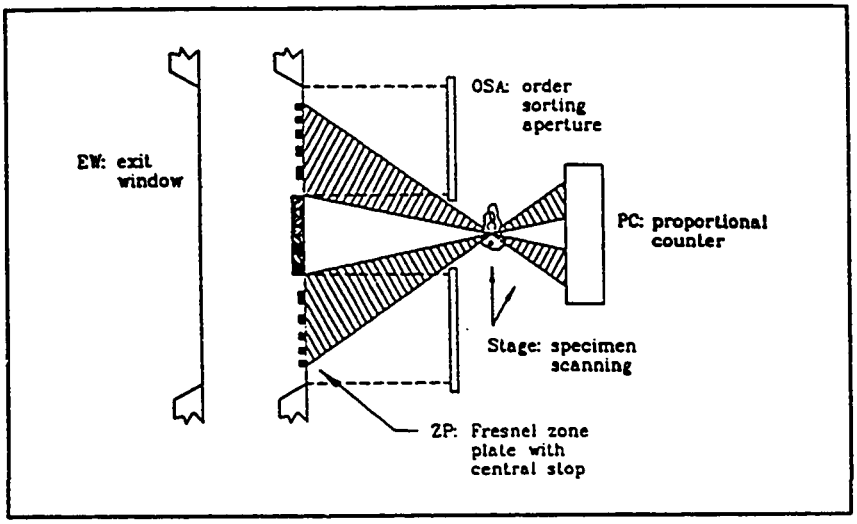

Figure 1.6.1 Schematic diagram of the major components of the Scanning Transmission X-ray Microscopy (STXM) [AS&95].

particular x-ray energy or NEXAFS spectra can be acquired of a microscopic region. **Figure 1.6.2** presents an example of each model. On the top panel of Fig 1.6.2 are two images of a polycarbonate (PC) - polyethylene terephthalate (PET) blend, one acquired at the energy of the maximum of the C 1s $\rightarrow \pi^*_{C=C}$ transition feature in PET (285.36 eV) and the other at the maximum of the C 1s $\rightarrow \pi^*_{C=C}$ transition feature in PC (285.69 eV). A contrast reversal, showing the distribution of PET and PC is observed in these images. The spectra of PET and PC acquired from a 0.1 μm^2 region are presented in the bottom panel of Figure 1.6.2. These micro-spectra are very sensitive to the chemical nature of the polymer.

STXM microscopy is of particular relevance for biological, environmental and polymeric samples. There is a "water window" between the C 1s (284 eV) and the O 1s (540 eV) core edges in which x-rays have a long transmission length (2 - 10 μm) in water [KJH95]. This allows the use of STXM for the investigation living cells and environmental

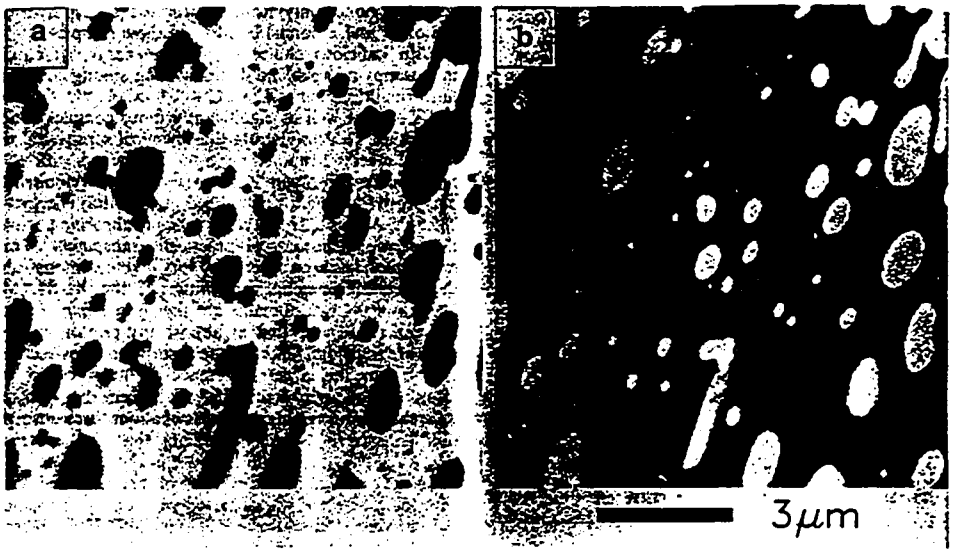

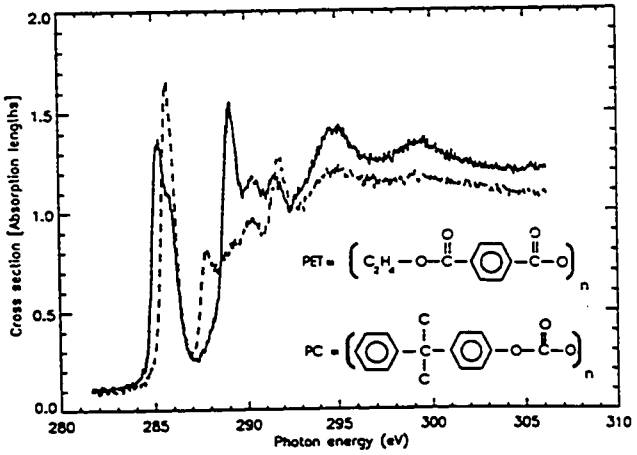

Figure 1.6.2 (top) X-ray micrographs of a polycarbonate (PC) poly(ethylene terephthalate) (PET) blend acquired at 285.36 eV (a) and 285.69 eV (b). (bottom) NEXAFS spectra acquired of a 0.1 μm^2 area in the PC/PET blend. PC: broken curve; PET: solid curve. [AS&95] (Linearity of the energy scale is incorrect above 290 eV).

samples in which the sample must be immersed in water. The application of STXM to polymers is driven by the lower x-ray beam damage than TEM-EELS, and the ability to perform detailed chemical speciation with the high electronic resolution available from modern x-ray monochromators [AS&95]. A careful comparison of TEM-EELS and STXM in terms of electronic resolution and beam damage has recently been presented by Rightor *et al.* [RH&97].

§1.7 Outline of Thesis Chapters

Chapter Two will outline the experimental techniques used for this thesis: Near Edge X-ray Absorption Fine Structure (NEXAFS) and Inner Shell Electron Energy Loss Spectroscopy (ISEELS). Chapter Three will present and discuss the calculational methods used in this thesis: Extended Hückel Molecular Orbital (EHMO) and *ab initio* calculations, and the approximations used to consider the effect of the core hole on the electronic structure. In Chapter Four, an analysis of spectroscopy of polyurethane and polyphthalate polymers will be discussed. In this analysis, the use of molecular building blocks, the effect of electronic delocalization and the application of calculational methods will be presented. In Chapter Five, the use of core excitation spectroscopy for the investigation of organosilane molecules is presented. Electronic delocalization is also important for understanding the spectroscopy these species, including aromaticity in silylenes, π-delocalization in phenyl silanes and the unique functional group fingerprint spectra of Si-Si bonds. General insights and conclusions developed from these investigations are presented in Chapter Six.

CHAPTER 2

EXPERIMENTAL

In this thesis, Near Edge X-ray Absorption Fine Structure (NEXAFS) and Inner Shell Electron Energy Loss Spectroscopy (ISEELS) have been used to examine the unoccupied electronic structure of molecules and polymers. The experimental apparatuses and details of the acquisition of core excitation spectra are presented in this chapter.

§2.1 NEXAFS Spectroscopy

Near Edge X-ray Absorption Fine Structure (NEXAFS) spectroscopy (also known as X-ray Absorption Spectroscopy (XAS) and X-ray Absorption Near Edge Structure (XANES)) can be performed on solid, liquid and gaseous samples over a wide energy range (<50 eV to >50 keV), accessing shallow and deep core atom levels in any material. The common source of x-rays used for NEXAFS experiments is synchrotron radiation, although less intense Bremsstrahlung sources can also be used [K88]. In NEXAFS spectroscopy, the attenuation of a photon beam by a sample is measured as a function of the photon energy. "Indirect" methods are often used for measuring NEXAFS spectra, because measuring the decay of core excited states is often easier than "direct" transmission detection methods

§2.1.1 Synchrotron Radiation

Synchrotron radiation provides an intense and continuous "white light" of x-ray photons. Conventional lab x-ray sources used for crystallography and medical x-ray imaging are much less intense and only produce x-rays at fixed wavelengths. Synchrotron radiation is emitted by the acceleration of relativistic charged particles (typically electrons) in a storage ring. Currently the main method for extracting synchrotron radiation is at the bending magnets of the storage ring. The synchrotron radiation is emitted tangentially to the electron path as it is radially accelerated by the bending magnet. Insertion devices (undulators and wigglers) consisting of alternating magnetic fields are used in straight sections of the storage ring to produce intense and partially coherent x-ray radiation. The energy distribution, intensity and angular divergence of the x-ray beam is dependent on several factors, including the electron beam current (~100's mA), electron energy (250 MeV - 5 GeV), the radius of curvature of the bending magnet (or the insertion device properties), and the spatial properties of the electron bunches in the storage ring. **Figure 2.1.1** presents the x-ray spectral brightness as function of photon energy for a variety of bending magnet and insertion device beamlines for the proposed Canadian Light Source [C96]. Here, "brightness" is defined as the flux of photons per second, per mm^2 sample area, per $mrad^2$ angular acceptance of the beam, per 0.1% bandwidth for a beam at an electron beam current of 100 mA. This diagram shows the wide energy range of synchrotron radiation, from <0.1 eV to 100 keV, and the choice and properties of bending magnets (dipoles) or insertion devices (wigglers and undulators) to obtain different beam energies and intensities. In comparison, rotating anode lab x-ray sources have a brightness

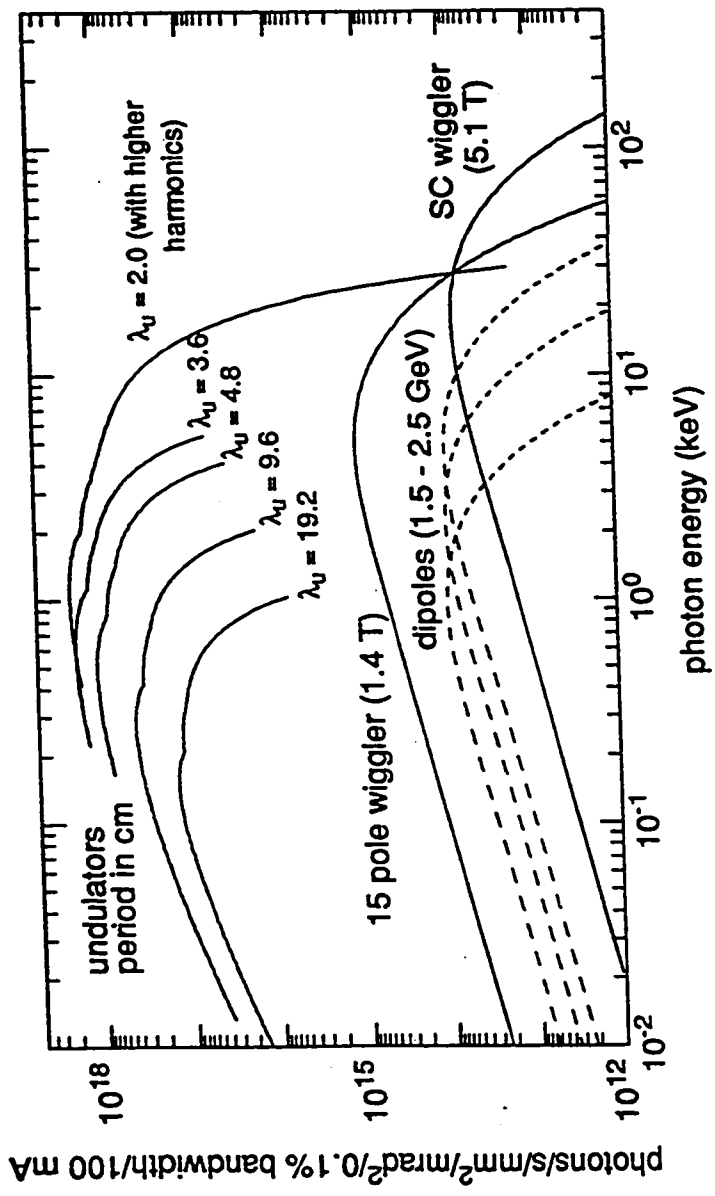

Figure 2.1.1 Brightness of bending magnet and undulator and wiggler insertion devices for the proposed 2.9 GeV Canadian Light Source (CLS) [C96]

of 10^7 (Al Kα) to 10^{10} (Cu Kα) photons /s/mm^2/mrad^2/0.1% bandwidth [K86].

For the NEXAFS spectra presented in this thesis, I have used the facilities of the Synchrotron Radiation Center (SRC, University of Wisconsin, Stoughton, WI). The experimental results collected by my collaborators were acquired using the facilities of the Advanced Light Source (ALS, Lawrence Berkeley National Lab), and the National Synchrotron Light Source (NSLS, Brookhaven National Lab).

2.1.2 Beamlines and Calibration

The "white light" of x-rays that is emitted from a synchrotron radiation source must be handled by a "x-ray beamline" for use in NEXAFS experiments. A beamline consists of a "front end", beamline optics and the experimental apparatus. The "front end" provides cooling from the high radiation heat load, fast closing valves for protecting the storage ring from accidental vacuum loss in the beamline and radiation protection hardware. Beamline optics are employed to direct, focus and select the energy of (monochromate) the x-ray photons for the experiment. The x-rays are energy selected by grating monochromators (grooved surfaces or crystals). The beamline consists of mirrors and entrance and exit slits for defining the beam size, position and the energy resolution.

The experimental apparatus or "end station" varies with the experiment. Some experiments are performed in ultra high vacuum and are directly connected to the synchrotron radiation source while others are performed in high vacuum and rely on differential pumping and/or windows to protect the beamline and storage ring vacuum.

The two beam lines used for this thesis are the Double Crystal Monochromator

(DCM) and the Grasshopper monochromator of the Canadian Synchrotron Radiation Facility (CSRF), located at the Synchrotron Radiation Center. The DCM monochromator has an effective energy range of 1700 - 4000 eV when using InSb(111) monochromator crystals [YM&92]. This monochromator has a resolution of 0.9 eV fwhm at the Si 1s edge (~1850 eV). This is twice the estimated Si 1s core hole broadening of ~0.4 eV [K79]. The Grasshopper monochromator has an effective energy range of 50 - 250 eV, depending on the gratings used. This monochromator has demonstrated a resolution of 0.06 eV at the Al $L_{2,3}$ core edge (73 eV) [TB&82].

Spectra recorded using the DCM monochromator were calibrated by setting the inflection point of the Si 1s spectrum of crystalline silicon to 1839.2 eV [HT&93]. While the DCM monochromator has a systematic error in the energy scale (~20 eV over an 1840 - 2800 eV range) [A96] this is not expected to significantly affect the short-range Si 1s NEXAFS spectra presented in this thesis.

Crystalline Si is also used as a calibrant species for spectra acquired using the Grasshopper monochromator, where the inflection point of the Si 2p spectrum of crystalline Si is set to 99.804 eV [BBT90].

§2.1.3 NEXAFS Detection techniques

The fundamental method of acquiring a photoabsorption spectrum is by a transmission measurement. In transmission detection, the attenuation of a photon beam by the sample is determined by measuring the flux before (I_o) and after (I) the sample. The transmission cross section is given by the Beer-Lambert law:

$$\ln\left(\frac{I(E)}{I_o(E)}\right) = -\sigma C x \qquad (2.1.1.)$$

where $I_o(E)$ and $I(E)$ is the photon flux before and after the sample, σ is the sample cross section, C is the concentration of molecules per unit volume, and x is the thickness of the sample (or the length of the cell for gases). The photon flux is typically measured using a gas ionization chamber filled with a gas that has a structureless absorption spectrum in the energy region of interest.

For several reasons, NEXAFS experiments are not typically performed in transmission mode. For solids, it is both difficult and inconvenient to make sufficiently thin samples. For gaseous atoms and molecules, transmission detection has a small dynamic range and it is thus difficult to record weak and strong features simultaneously.

Other detection methods are based on the detection of the decay of core excited states. There are two core hole decay mechanisms: Auger decay and fluorescent decay. In fluorescent decay, the core hole is refilled by a less tightly bound electron and the excess energy is carried away by x-ray emission. In Auger decay, the core hole is refilled by a less tightly bound electron and the excess energy is carried away by another electron. In both processes, the energy of the ejected photon or electron is specific to the element with the core hole. Auger and fluorescence are competing processes in the decay of core excited atoms. The Auger decay channel is dominant for low Z atoms and shallow core levels of high Z atoms (basically all core levels below 2 keV).

Since core excitation necessarily leads to core hole decay (within some short time,

$\tau < 10^{-14}$ s), these decay processes can be used to measure core excitation. Fluorescent yield (FY) detection is based on the detection of the fluorescent photons. The large relative escape depth of fluorescent photons makes FY sensitive to the "bulk" of the sample (as opposed to the surface). Total Ionization Yield (TIY) and Total Electron Yield (TEY) techniques are based on the ion and electron current created by core excitation and decay. These methods were used to acquire the gas and solid phase NEXAFS spectra presented in this thesis and are discussed further below.

Total Ionization Yield (TIY) Detection

Total Ionization Yield (TIY) detection is used to acquire gas phase NEXAFS spectra. This method measures the current of charged particles produced when x-rays ionize a gas. The ionization chamber used for Si 1s gas phase spectra on the DCM beamline is presented in **Figure 2.1.2**. This chamber is similar to that used for detection of the incident x-ray flux except that in this instance the chamber is filled with the sample of interest rather than a spectroscopically featureless gas. The sample gas chamber was separated from the beamline vacuum by a 25 μm thick Be window. Charged ions and electrons are produced by the x-ray ionization of the gas. The electrons produced by the core excitation and Auger decay further ionize molecules in the detector, resulting in a gas amplification of the ion yield signal. These particles are collected by applying a stable -45 V bias to the ion chamber electrodes and the ion current is measured with a Keithley picoampmeter. This ion current signal (I), and the output from the upstream (I_o) flux monitor are used to determine the core excitation spectrum (TIY $\propto (I/I_o)$) which is

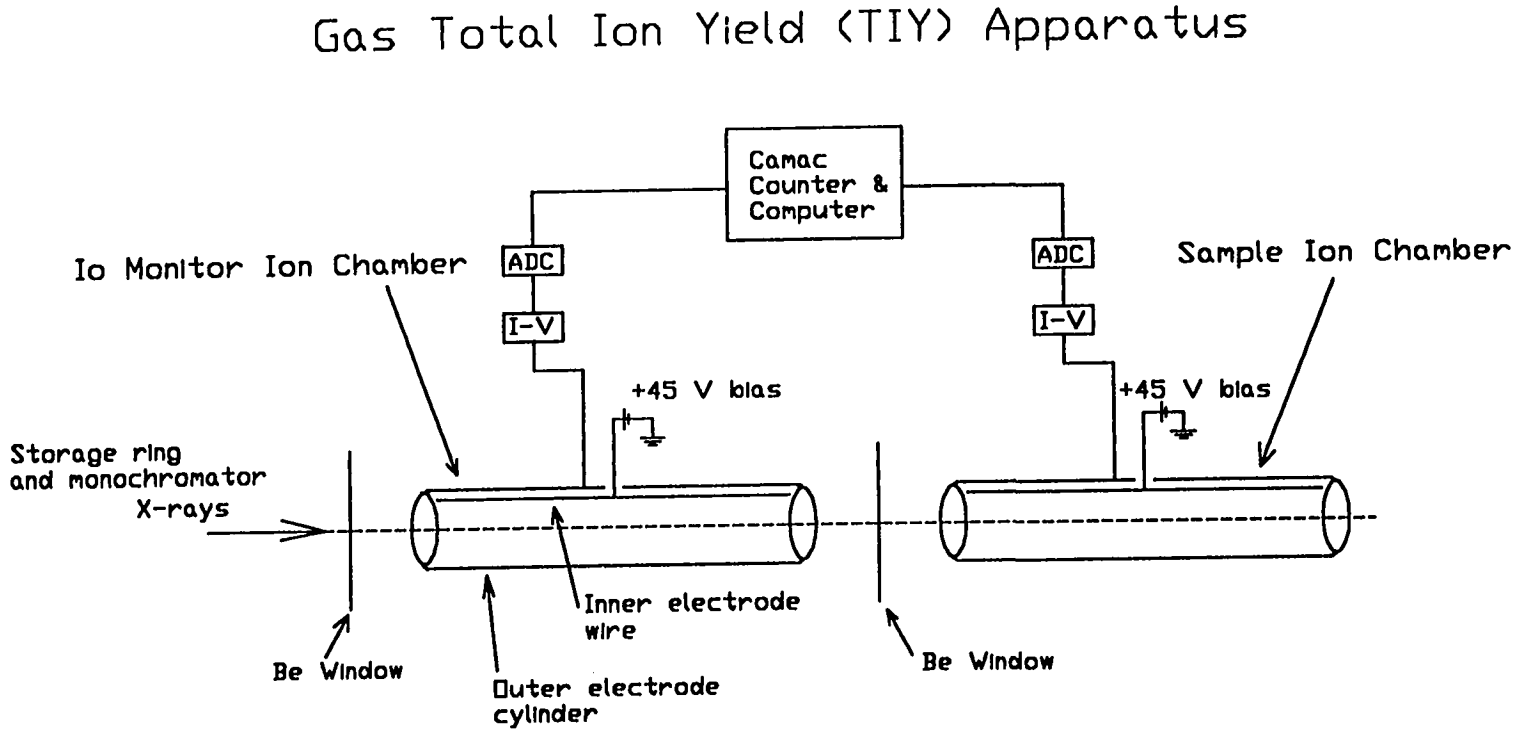

Figure 2.1.1 Gas Total Ion Yield Apparatus. Vacuum housing, support hardware and sample inlet lines excluded for clarity.

proportional to the absorption cross section.

In ion yield measurements, saturation effects can be present if the sample pressure is too high. Saturation can occur by self absorption, where absorption in the first part of the ionization cell is high enough to significantly reduce the flux to the further parts of the gas cell. Another possible distortion is ion saturation, where the high photon flux and high gas amplification makes the detection non linear. Saturation effects are illustrated in **Figure 2.1.3** for the Si 1s NEXAFS spectrum of trimethylmethoxysilane (Me_3SiOMe). For pressures below a certain level, the relative intensity of spectral features is invariant, but at higher pressures the relative area of the intense features are attenuated. The effect of saturation on the area of the S 1s → t_{1u} transition in SF_6 [HT88] is also illustrated in Figure 2.1.3. For the Si 1s NEXAFS spectra of organosilanes studied in this thesis, the threshold pressure was usually ~1 torr for molecules with one Si atom, ~0.5 torr for molecules with two Si atoms, and so on.

The ions detected by this method are created by photoionization and Auger decay of core excited atoms. It is important to consider how the Auger decay of core-*ionized* states behaves differently from the Auger decay of core-*excited* states. In core-ionized states, the core electron is removed from the molecule, and the subsequent Auger decay produces three or more charged particles (dissociative M^{+2} ions, a fast Auger electron and a slow photoelectron). Core-excited states are created below the ionization potential. The core electron is excited to some bound level (by a core → π^* transition, for example) and the Auger decay of this core excited molecule creates only two charged particles (M^+ and a fast electron). Thus one should expect a difference in the current of charged particles

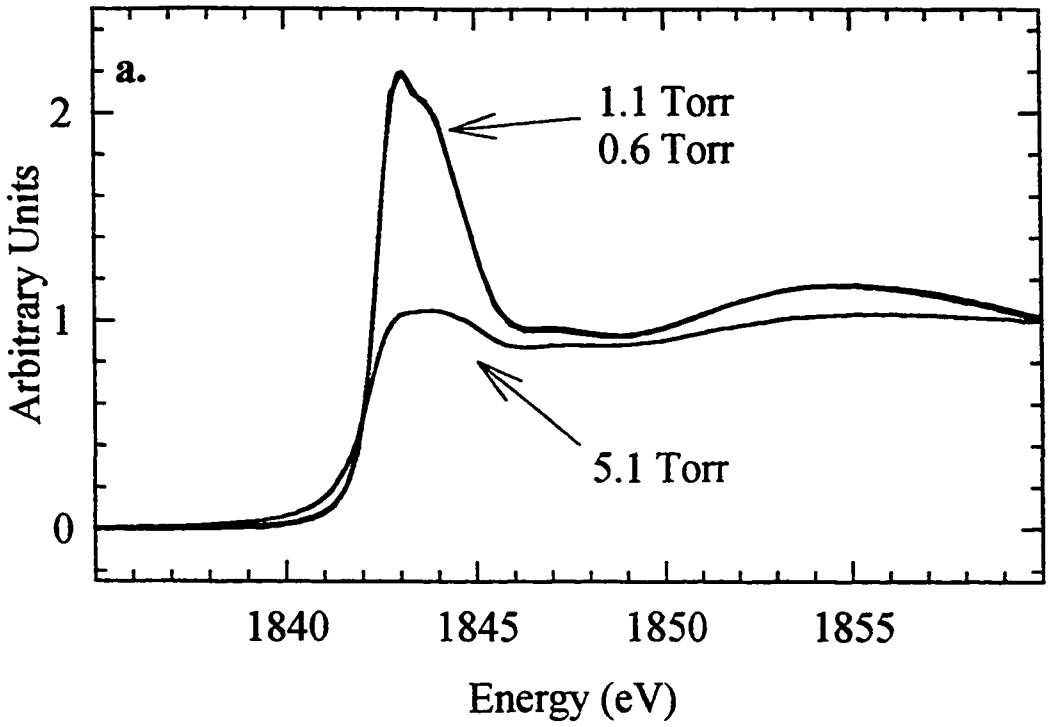

b.

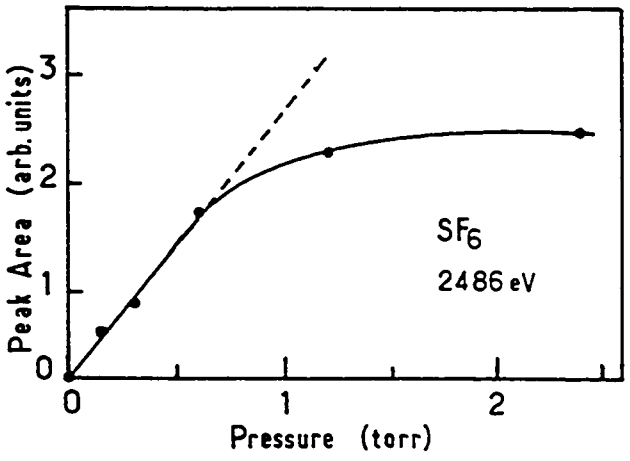

Figure 2.1.3 a.) Absorption saturation effect in the Si 1s spectrum of Me_3SiOMe b.) Variation with sample pressure of the area of the S 1s → t_{1u} peak (2486.0 eV) of SF_6 recorded with ion current detection [HT88].

produced above and below the ionization potential, per absorbed photon. This difference is less significant for high Z atoms since the gas amplification factor for the higher energy Auger electrons dominates the ion yield signal. For the S 1s edge, this difference was estimated to be < 5% [HT88]. Because the S 1s (~2740 eV) and Si 1s (~1840 eV) core edges are close in energy, it is reasonable to expect that these difference are also negligible in the Si 1s TIY NEXAFS spectra. However, in Si 2p NEXAFS spectra (~110 eV), the degree of gas amplification is less because the fast Auger electron is less energetic (Si LVV: ~100 eV). At ~20 eV per ion pair creation, the Si LVV Auger electron creates ~5 ion pairs, which corresponds to the creation of ~5 charged particles below the IP and ~6 above, a ~16 % difference.

Gas amplification also "tilts" the ion-yield core excitation spectrum. At higher energy, the photoelectron energy is greater and the gas amplification from these photoelectrons is increased. The spectra reported have been systematically corrected for this "bolometric" effect by scaling the spectral intensity by a factor 1/E.

Total Electron Yield (TEY) Detection

Total Electron Yield (TEY) detection is another indirect measure of the x-ray absorption cross section of solids and surfaces. The experimental set up used on the "EXAFS Chamber" on the DCM beamline is presented in **Figure 2.1.4.** The sample current associated with all electrons emitted by the sample after the absorption of an x-ray (elastically emitted Auger electrons, photoelectrons and inelastically scattered electrons) is measured with a bias applied to a ring above the sample. The current is measured with a

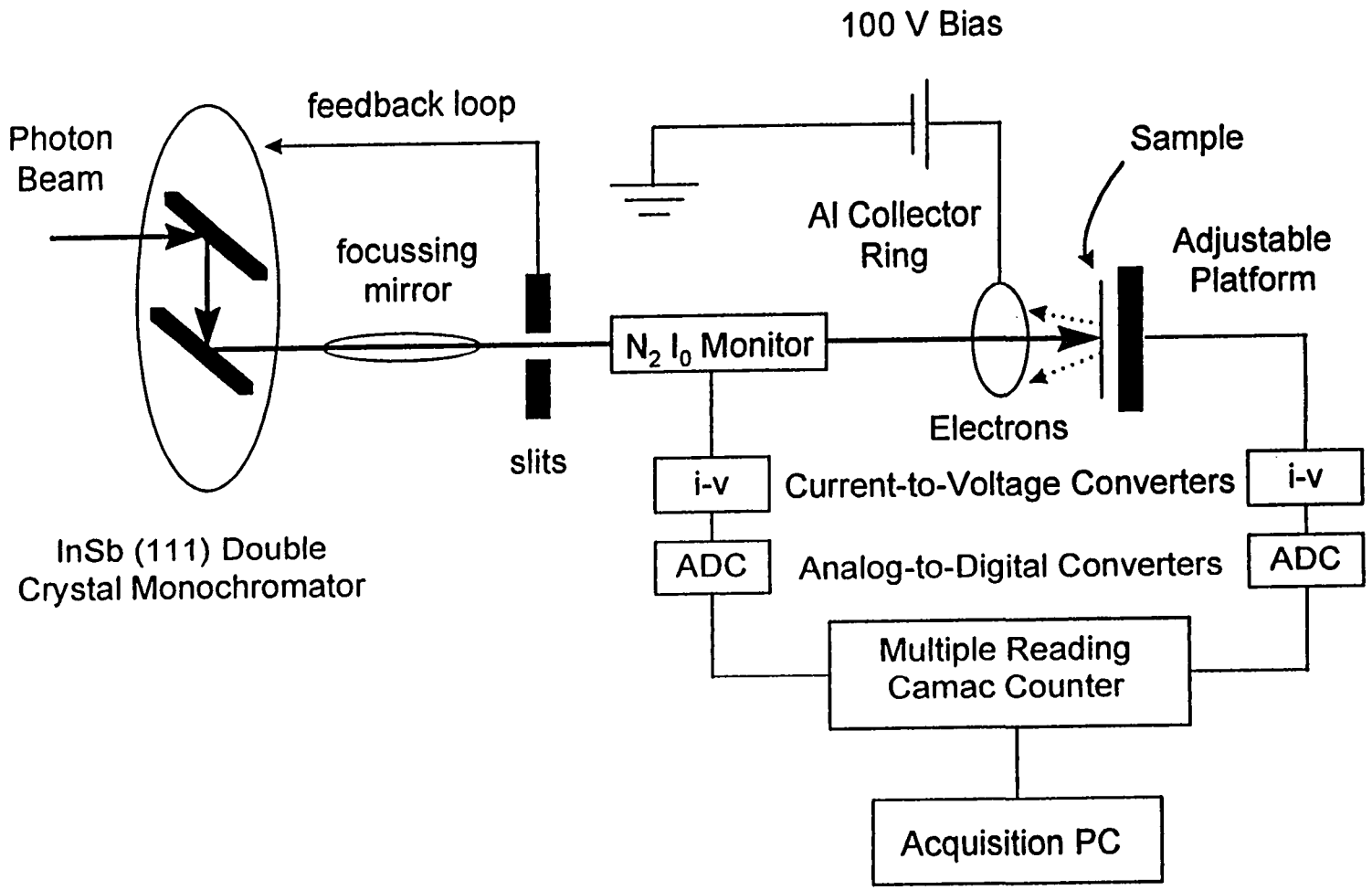

Figure 2.1.4 Schematic representation of the Double Crystal Monochromator (DCM) Beamline at the Synchrotron Radiation Center (SRC), University of Wisconsin, Stoughton, WI [A96].

Keithley picoammeter, and the ratio of the total electron signal (I), and the output from a flux monitor upstream (I_o) is the core excitation spectrum (TEY $\propto (I/I_o)$). This signal is approximately proportional to the "true" absorption spectrum. The escape depth of the photoelectrons limits the depth sensitivity of the technique to ~ 60 Å at the Si 1s edge.

§2.2 ISEELS Spectrometer

The Inner Shell Electron Energy Loss spectrometer used for all gas phase ISEELS measurements reported in this thesis was described previously [H90, W92]. The spectrometer was originally built by Steel [S82], modified by Newbury [N86] and Wen [W92] and was recently retrofitted by the author (§2.2.4). A schematic diagram of the spectrometer is presented in **Figure 2.2.1**. This spectrometer is operated under conditions of small momentum transfer to ensure that the electronic excitations measured are dominated by electric dipole allowed transitions. This entails a small scattering angle (~2°) and a high electron impact energy (2.5 keV + energy loss). The spectrometer resolution is dependant on the electron beam current and analyser pass energy, but is typically 0.75 eV full width at half maximum (fwhm) at a beam current of 20 μA and 0.5 eV fwhm for a beam current of ~1 μA.

The spectrometer consists of an electron source, deflectors for beam steering, a gas interaction cell, focussing lenses, an electrostatic analyser and a single electron counting channeltron. This is contained within a high vacuum chamber which is pumped by two diffusion pumps. Differential pumping of the gun chamber is used in order to protect the emitting surface the electron gun from attack by the sample gas. External

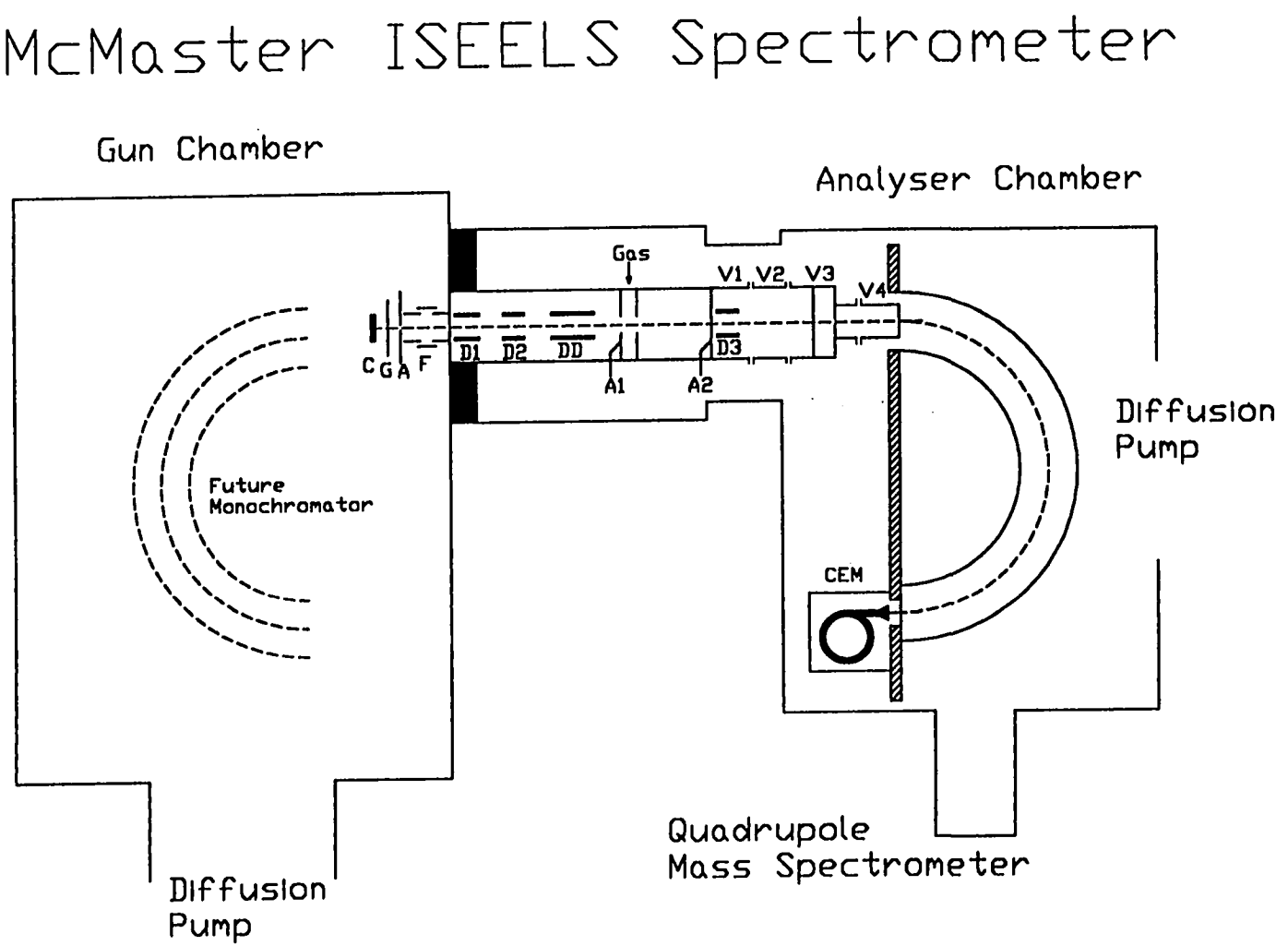

Figure 2.2.1 McMaster Inner Shell Electron Energy Loss Spectrometer.

Helmholtz coils are used to minimize the earth's magnetic field and optimize the electron trajectory in the spectrometer. A sample handling manifold, consisting of a rotary pump and leak valves, is used to control the pressure of sample and calibration gases in the spectrometer.

2.2.1 ISEELS Calibration and Spectral Processing

ISEELS spectra are calibrated by acquiring the spectra of a stable mixture of the analyte molecule and a reference compound. Reference compounds and the energy of distinct features in their spectra are presented in Table 2.2.1

Table 2.2.1 Reference Compounds used for ISEELS Spectroscopy [N86, SB84]

Reference Compound	Transition	Energy (eV)
CO_2	C 1s → π^* O 1s → π^*	290.74(4) [HI87] 535.4(2)
CO	C 1s → π^* O 1s → π^*	287.40(2) 534.21(9)
SF_6	S $2p_{1/2}$ → t_{2g} F 1s → a_{1g}	184.54(5) 688.27(15)
N_2	N 1s → π^*	401.10(2)
O_2	O 1s → π^*	530.8(2) [WB74]

A Fluke Model 45 five digit multimeter was used to establish the linearity of the energy scale on calibration scans.

The core excitation spectra associated with a particular core edge (acquired from both NEXAFS and ISEELS spectroscopy) are isolated from the underlying valence-shell and core ionization continua by subtracting a smooth curve determined from a curve fit of the function $a(E-b)^c$ to the pre-edge experimental signal. The background subtracted spectra are converted to absolute oscillator strength scales using previously described methods [HM94]. The form of spectral normalization used in this thesis is discussed specifically in each chapter.

§2.2.2 Electron Source, Steering and Analysis

The beam of electrons used in this spectrometer is produced by an oxide cathode electron gun. These electron guns are produced by Philips for commercial black and white televisions. Although these electron guns are designed to work at a high (25 kV) accelerating voltage, they are usually operated here at 2.5 kV and sometimes down to 500 V without great difficulty. The oxide cathode is susceptible to attack by some gases (i.e. strong oxidizers) and the work function of the emitting surface is modified by the presence of some species. Cathode degradation is reduced by differential pumping.

The electron beam is accelerated to its impact energy by a large positive voltage ($2.5\ keV + E_{loss} + E_{pass}$). The electron beam is directed toward the sample interaction region by a series of quadrupole deflectors **D1**, **D2** and **D3** (see Fig. 2.2.1). A double deflector (**DD**) system is used to prevent the main beam from entering the electrostatic analyser, where a large background would be created by electron scattering of the beam off the outer analyser sphere [WBW72]. Because of this electron background, zero-angle

scattering can not be measured. By virtue of the **DD** system, electrons scattered with an angle of 2° (±1°) pass through the angular selection aperture ($\mathbf{A_2}$). This scattered electron beam then passes through the decelerating lenses ($\mathbf{V_1}$ - $\mathbf{V_4}$), which slow down the scattered electrons to the pass energy of the analyser.

The analyser is an 180° hemispherical electrostatic analyser. This analyser is used in constant residual energy mode, where the pass energy (E_{pass}) of the analyser is kept constant and the impact energy (2.5 kV + E_{loss} + E_{pass}) of the electrons is varied. Electrons that enter the analyser with an energy eV_{pass} (≡ E_{pass}) will transverse the analyser with a circular path of radius R_{pass}. The pass energy is related to the analyser bowl voltages (V_{inner}, V_{outer}, $V = V_{inner} - V_{outer}$) by the formula:

$$V = V_{pass}\left(\frac{R_{outer}}{R_{inner}} - \frac{R_{inner}}{R_{outer}}\right) \qquad (2.2.1)$$

where R_{outer} and R_{inner} are the radii of the inner and outer bowls. In the ISEEL spectrometer, these dimensions are R_{inner} ~ 70 mm (2.745") and R_{outer} ~ 115 mm (4.535").

The energy resolution of the electrostatic analyser depends on the pass energy E_{pass} and the analyser properties:

$$\Delta E_{anal} = E_{pass}\left(\frac{r_a}{R_{pass}} + \alpha^2\right) \qquad (2.2.2)$$

where r_a is the radius of the entrance and exit apertures, R_{pass} is the radius of the electron trajectory, and α is the maximum acceptance half-angle. For this spectrometer, r_a = 1 mm

and R_{pass} ~ 92 mm (3.625"). A plot of the theoretical analyser energy resolution (ignoring α^2 terms) as a function of pass energy is presented in **Figure 2.2.2**. This spectrometer is typically operated with a pass energy of 40 - 50 V.

The spectrometer resolution is determined by the combination of the electron beam bandwidth (ΔE_{gun}) and the resolution of the electrostatic analyser (ΔE_{anal}) [W92] according to:

$$\Delta E \approx \sqrt{\Delta E_{gun}^2 + \Delta E_{anal}^2} \qquad (2.2.1)$$

The oxide cathode provides a reasonably monoenergetic beam ($\Delta E_{gun} \approx 0.4$ eV fwhm) and is presently used without additional monochromation. When the analyser is operated with a 50 V pass energy, the instrumental resolution is predicted to be ~0.68 eV.

The spectrometer's effective energy resolution is also strongly dependant on the electron beam current because space charge effects significantly degrade the resolution. The bottom part of Figure 2.2.2 presents the measured instrument resolution as a function of the beam current. This resolution is determined by measuring the full width at half maximum of the narrow C 1s → 3s Rydberg transition in CO_2.

§2.2.3 ISEELS Computer Control

The spectrometer data acquisition is controlled by a personal computer coupled to a scan-control crate and pulse counting crate. The scan voltage, which is applied to the cathode potential is generated by three power supplies in the scan-control crate. These separate power supplies are used to scan different energy ranges, each with 12 bit

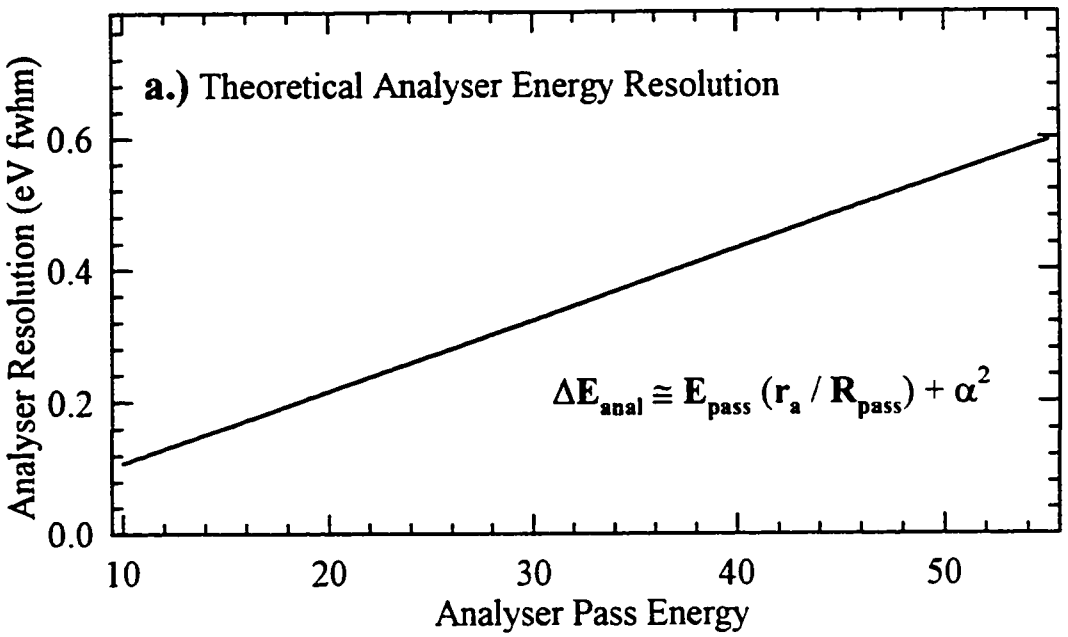

—— Calculated resolution of an electrostatic hemispherical analyser: pass radius R_a = 92.5 mm, entrance and exit aperature radius r_a = 1.0 mm. Angular acceptance term α neglected.

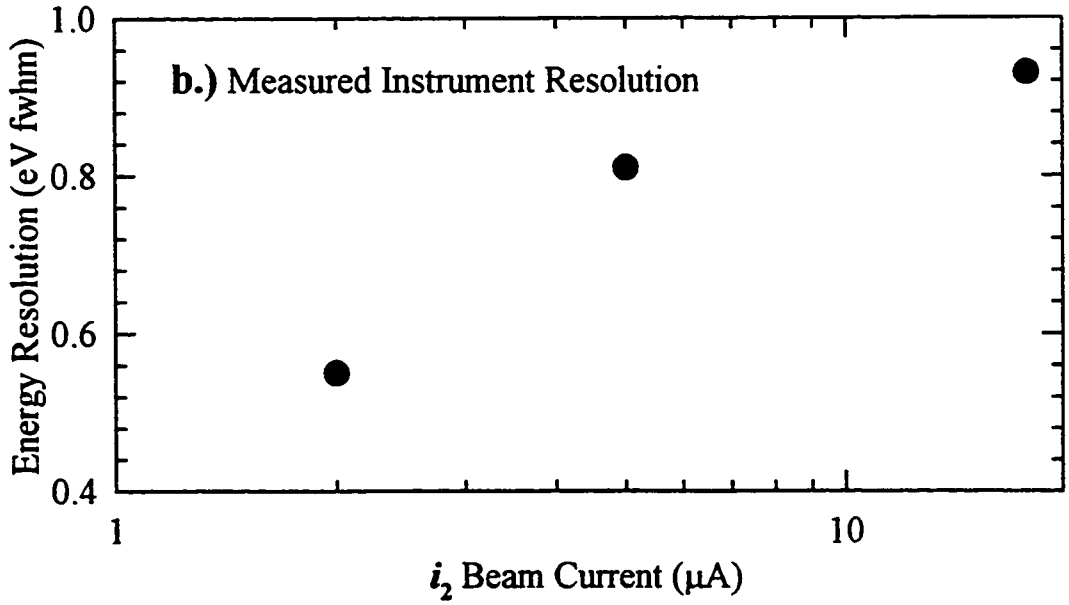

Figure 2.2.2 a.) Calculated energy resolution of the ISEELS hemispherical analyser; b.) Dependance of instrument resolution on beam energy (Vpass = 50 V; Feb. 1996).

resolution (High: 50 V range, ~12 mV resolution; Medium: 400 V range, ~100 mV resolution; Coarse: 1 kV range, ~0.25 V resolution) and digitally controlled by the computer. This electronics technology was developed by Tolmar Instruments for electron spectroscopy applications [TK94] and features low ripple voltages, can be floated to >2.5 kV, fast response time (ms) and an optically isolated digital to analog interface. The implementation of this system for a more complex, computer controlled spectrometer is discussed in the Ph.D. thesis of J. T. Francis [F95].

The I/O card that digitally controls the scan-crate also processes digital pulses from the channeltron/preamplifier circuit. The channeltron creates a charge pulse from electron impact. The charge pulses are amplified and a discriminator creates a digital (+5V) pulse when charge pulses are observed above a threshold. The pulse counting and scan voltage is controlled by the program MSPEC, written by Dr. T. Tyliszczak.

§2.2.4 ISEELS Upgrades

In the course of my graduate work, I performed several upgrades to the ISEEL spectrometer to improve the instrument's performance and reliability, and in preparation for the addition of an electron monochromator. This major retrofit was carried out in the summer of 1996, in addition to incremental improvements made throughout my graduate work.

The retrofit involved substantial changes to the physical structure of the ISEELS spectrometer. In order to accommodate a monochromator, I designed a larger vacuum chamber to replace the small gun vacuum chamber. This chamber is designed to encase a

moveable stage supporting an monochromator-electron gun assembly and a regular electron gun stage, allowing both monochromatized and unmonochromatized ("straight through") operation without breaking vacuum.

The new chamber is pumped by a higher speed vacuum pump and is connected by a wider tube. An Edwards Diffstak Series 100 diffusion pump (~10 cm diameter, 322 ℓ/s air pumping speed) replaced the Edwards Model E2 diffusion pump (~5 cm diameter, 150 ℓ/s air pumping speed). The old pump was connected to the gun chamber by a ~1 m long tube with a diameter of ~5 cm. The new pump is connected to the gun chamber by a 10 cm diameter tube of the same length. Even though the new gun chamber has a volume ~20 times greater than the old gun chamber, the base pressure of the new gun chamber is consistently better (before 3.4 $x10^{-6}$ torr ; after 1.3 $x10^{-7}$ torr).

The new gun chamber and gun pump could not be supported on the original spectrometer stand. I designed a new stand entirely of Aluminum to support the revised spectrometer structure and improve access to the components. It is interesting to note that the removal of the previous soft iron support table resulted in a slight decrease in the apparent spectrometer performance. In the new assembly, the instrument resolution decreased slightly and the count rate increased. In my "standard test conditions" (CO_2 pressure: 1 x 10^{-5} torr, beam current 10 μA, analyser $\Delta V = 50$ V), I typically attained a count rate of ~10,000 Hz on the intense CO_2 C 1s → π* transition at 290.74 eV (20:1 signal to background) and a resolution of ~0.7 eV fwhm on the narrow CO_2 C 1s → 3s Rydberg (292.7 eV) before the spectrometer refit. After the refit, the resolution decreased to ~0.95 eV fwhm and the count rate on the CO_2 C 1s → π* transition increased to 14,000

Hz (20:1 signal to background). This suggests that the magnetic components of the old spectrometer stand acted as a Wein filter, where the magnetic field enhanced the dispersion of electron energies in the analyser and lens stack. This increased the effective electronic resolution of the instrument on the older stand. The resolution "loss" was recovered by lowering the analyser pass energy, which returned the instrument closer to the previous operating conditions (Resolution: ~0.8 eV fwhm, count rate: 10,000 Hz, Analyser $\Delta V = 40$ V). When the current was dropped from 10 μA (my standard test conditions) to 1 μA, a resolution of 0.55 eV fwhm was observed.

With the assistance of Dr. Tyliszczak, I designed, built and installed an improved vacuum pump control electronics. This package includes relay control of all pumps, valves and critical voltages, with simple logic to put the spectrometer into a "safe" mode (diffusion pump isolation valves shut, high voltages off) after a power failure.

The sample gas manifold was redesigned and rebuilt during this upgrade. This gas manifold is often used for delivering "dirty" and "sticky" compounds into the gas cell and required frequent cleaning. This spectrometer is often used to record the N 1s ISEELS spectrum of nitrogen-containing molecules, so it is essential that the sample manifold be free of leaks. It was often difficult to attain a leak-free sample line after cleaning. The manifold was rebuilt to replace the swagelock fittings with VCR™ metal-seal fittings which are easier to rebuild and to maintain a seal.

Other improvements made on the spectrometer include the replacement of pressure gauges, improvement of the gun power supply and energy loss crate, and replacement of the preamplifier and discriminator circuit. A new Granville-Phillips Model 307 ionization

gauge controller was installed, with new ion and convectron gauges to replace the Pirani and convection gauges. The Pirani gauges contained a strong magnet and therefore could not be directly connected to the vacuum chamber. The new ion gauges are much more sensitive to the chamber pressure because they are now directly connected to the vacuum chambers. The older gun power supply components (focus, and grid and anode voltages) were replaced with Tolmar [TK94] components which are more stable and have less voltage ripple. The preamplifier and discriminator circuits were also replaced by a more sturdy Tolmar [TK94] circuit.

CHAPTER 3

MOLECULAR ORBITAL CALCULATIONS

Molecular orbital calculations are valuable for assisting the interpretation of the core excitation spectra of molecules and polymers. In applying theoretical methods to core excitation spectroscopy, the effect of the core hole on the electronic structure must be considered. Two methods for considering the core hole induced electronic relaxation, the Equivalent Ionic Core Virtual Orbital Model (EICVOM) and the Improved Virtual Orbital (IVO) method are presented. The application of these methods, in Extended Hückel Molecular Orbital (EHMO) and ab initio calculations are discussed.

§3.1 Introduction to Molecular Orbital Calculations

Molecular orbital calculations have been applied to the core excitation spectroscopy of many species, including organic molecules [AC&94, S92, HUR92], boranes and carboranes [HU&97, HW&93], organometallics [W92, RH89] and polymers [CA&95]. Multiple scattering [S92] and density functional calculations [EK&96] have also been used for calculating the core excitation and core level photoemission spectroscopy of molecules and polymers, but these methods will not be discussed here.

Molecular orbital calculations are considered within a "one electron picture" where the creation of a core excited state is described as a one electron transition from a core level to an unoccupied molecular orbital. Molecular orbital calculations are used to calculate the energies and orbital character of the optical orbital. In some programs, the

energy and character of the initial core level can also be calculated. Molecular orbital calculations can be performed at simple (semi-empirical) or higher (*ab initio*) levels of theory, with the obvious compromise between speed and quality. In this thesis, low-level Extended Hückel Molecular Orbital (EHMO) calculations and high-level *ab initio* calculations were used to interpret the core excitation spectra of organic and organometallic molecules. In general, EHMO calculations provide a useful but strictly qualitative consideration of core excitation spectra, and can be applied more easily to larger molecules than large basis set *ab initio* methods.

§3.2 Core Hole Relaxation

The creation of a core hole induces a significant perturbation of the molecular electronic structure. This perturbation must be considered when using MO calculations to interpret core excitation spectroscopy. While ground state MO calculations include solutions for the unoccupied MOs, these MOs are not an accurate description of the character and energy of the electronic levels probed by core excitation. A substantial relaxation of the occupied and unoccupied electronic levels is induced by the modification of the atomic core Coulomb potential (nucleus + core electrons). Two approximations are commonly used to consider core hole relaxation in MO calculations: the Equivalent Ionic Core Virtual Orbital Model (EICVOM) and the Improved Virtual Orbital (IVO) model. The basis of these approaches will be discussed below.

3.2.1 Equivalent Ionic Core Virtual Orbital Model

The simplest means to consider the effect of the core hole in MO calculations is the Equivalent Ionic Core Virtual Orbital Model (EICVOM) [S75], also known as the "Z+1" approximation. This model is based on the following observation: the charge of the atomic core (nucleus plus core electrons) of a core excited atom with atomic number Z is the same as the atomic core charge of the ground state "Z+1" atom. For example, the core charge of the core excited carbon atom (Z = 6; core charge = 5) is the same as the neutral nitrogen atom (Z =7, core charge = 5).

The application of the "Z+1" approximation in calculations requires two trivial changes to the calculation input file. An atom whose core excitation contribution is to be considered is replaced by its "Z+1" counterpart, and the charge of the molecule is set to +1 to preserve the correct valence electron count. No change in the molecular geometry is made.

The solution of calculations of the "Z+1" cation species provide the energies and wavefunctions of the unoccupied molecular orbitals in the presence of the approximated core hole. An example of the relaxation of the unoccupied molecular orbitals in the presence of the "Z+1" approximated core hole is presented in **Figure 3.2.1**. The energies (calculated by Extended Hückel Molecular Orbital calculations with the program CACAO [MP90]) and MO plots of the ground state unoccupied π^* MOs of dimethyl terephthalate are compared to those calculated with a "Z+1" approximated core hole at a C-H site in the phenyl ring (site indicated by an "*"). In general, the energies of the unoccupied MOs relax and the orbital character is reorganized in the presence of the "core hole". The

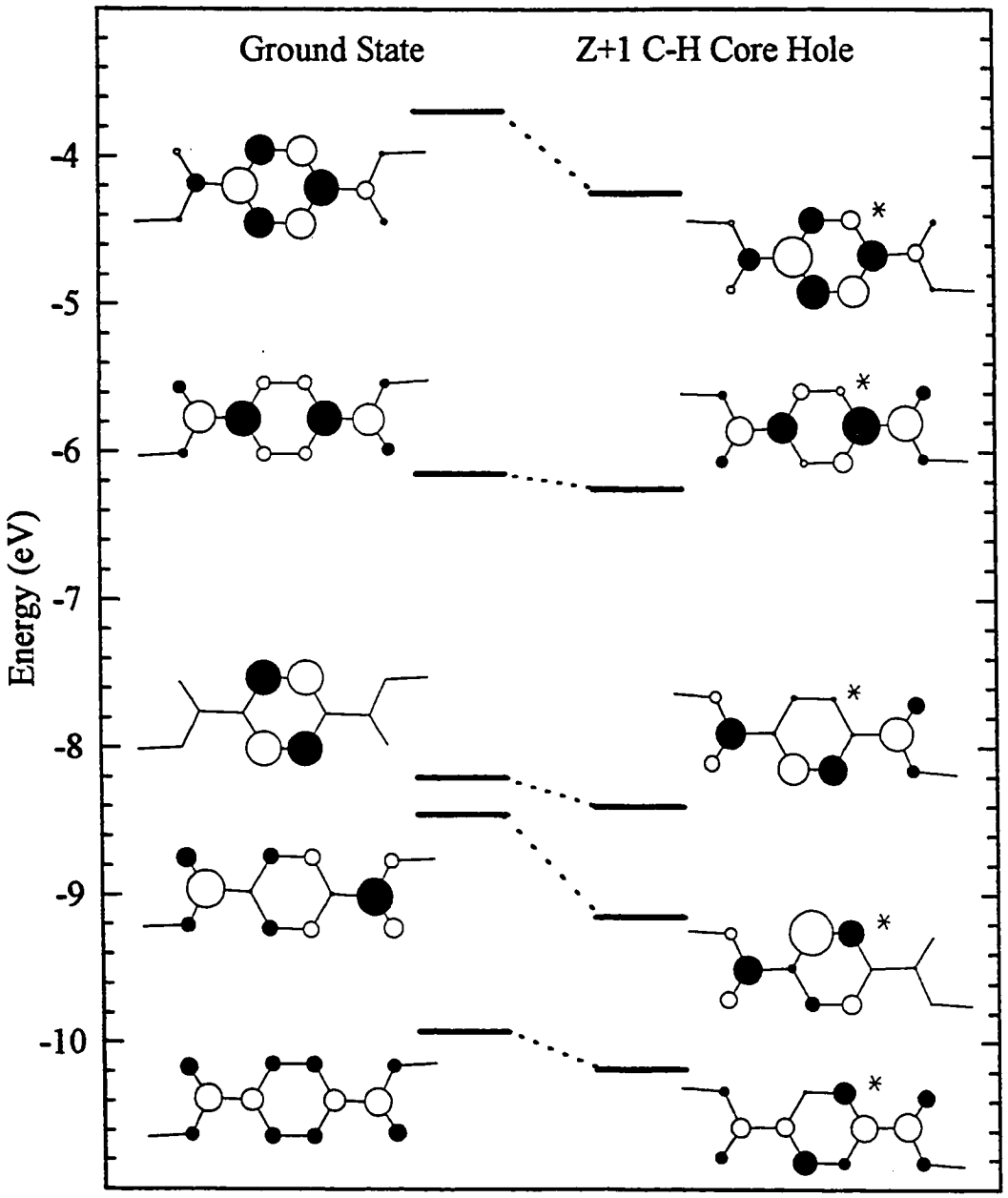

Figure 3.2.1 Energies and molecular orbital plots of the ground state and the C 1s(C-H) core excited state of dimethyl terephthalate, calculated using the "Z+1" approximation and Extended Huckel Molecular Orbital (EHMO) The site of the core hole is indicated by "*". The molecular geometry used is from §4D. The area of each circle is proportional to the C2p-π density.

implementation of the "Z+1" method with Extended Hückel Molecular Orbital (EHMO) calculations will be discussed below (§3.3).

3.2.2 Improved Virtual Orbitals

The final state of a core excitation transition can be described by the removal of a core electron from an inner orbital ϕ_i and an addition of this electron to an outer orbital ϕ_f. In the *Improved Virtual Orbital* (IVO) method [HG68], the core hole contribution to the molecular potential is explicitly considered, while the contribution of the excited outer shell electron is neglected. The molecular potential is that of the core ionized ion, an (N-1)-electron system with an electron missing in orbital ϕ_i. This approximation is enacted by replacing the usual Fock operator with a "static exchange" Fock operator that considers singlet ionization of electron ***i***: [HG68]

$$F_i^{EX} = F - J_i + 2K_i \qquad (3.2.1)$$

F is the usual Fock operator, and J_i and K_i are the Coulomb and exchange operators of the ionized electron. The static exchange Fock operator represents the removal of the ***ith*** electron from the usual Fock operator. The solutions of the Hamiltonian equations for the core ionized cation calculated with the static exchange Fock operator provides the energies and wavefunctions of the unoccupied molecular orbitals calculated in the presence of the core hole.

The core ionization potential can also be calculated using this method. The difference in total energy between a ground state calculation and a core ionized cation

calculation provides the energy required to ionize the core electron. This Δ-SCF method can provide excellent estimates for ionization potentials, as the relaxed potential can account for the effect of the large electronic relaxation that occurs upon core ionization [KSY92, AC&94]. This method is superior to Koopmans' method, in which the ionization potential is approximated by the negative of the calculated orbital energy ϵ of the AO or MO from which the electron is ionized. Koopmans' method is inaccurate because it neglects electronic relaxation and the change in correlation energy between the neutral molecule and the ion [L91].

§3.3 Extended Hückel Molecular Orbital Calculations

Extended Hückel Molecular Orbital (EHMO) calculations, employing the Z+1 approximation, have proven useful for interpreting the spectra of conjugated organic molecules [FH92, FH94, HUR92], organometallics [W92, RH87] and carboranes [HU&97, HW&93]. EHMO's utility is well expressed by the adage "quantitatively never right, qualitatively never wrong". Calculational accuracy is compromised for speed and simplicity. For large and complex molecules and polymers, EHMO can be a wise compromise to make.

Extended Hückel is a simple one electron "valence only" method, developed and applied by Hoffmann [H63]. In EHMO, the electronic Hamiltonian is taken as the sum of one-electron Hamiltonians: [L91]

$$H_{val} = \sum_i H_{eff}(i) \qquad (3.3.1)$$

and the MOs are considered as linear combinations of atomic orbitals (LCAO) of the

atoms:

$$\phi_i = \sum_r c_{ri} f_r \qquad (3.3.2)$$

where f_r is the atomic centred atomic orbitals (AOs) and c_{ri} are the coefficients weighing the AOs in the ϕ_i molecular orbital. In the EHMO Hamiltonian matrix, the value of the matrix elements:

$$H_{rs}^{eff} = \langle f_r | H^{eff} | f_s \rangle \qquad (3.3.3)$$

simply depends on the AOs f_r and f_s and some parameters. For r = s ($f_r = f_s$), the matrix element H_{rr}^{eff} is set equal to α, where α is the experimental orbital energy of AO f_r for atom r. For example, <H 1s|H^{eff}|H 1s> = -13.6 eV, the ionization energy of Hydrogen. For r≠s, the Hamiltonian matrix element H_{rs}^{eff} is given by the expression:

$$H_{rs}^{eff} = \tfrac{1}{2}K(H_{rr}^{eff} + H_{ss}^{eff})S_{rs} \qquad (3.3.4)$$

where S_{rs} is the overlap between f_r and f_s and K is a constant. In a very simple manner, EHMO calculations can reflect the effect of elemental identity and molecular geometry on the electronic structure of the molecule.

§3.3.1 Simulating Core Excitation Spectra from EHMO Calculations

It is useful to use "spectral simulations" to compare the results of core excitation calculations to experimental spectra. The process of creating a spectral simulation from an EHMO "Z+1" calculation has been described in detail before [FH92, HUR92] and a brief summary will be given here.

The energies of the unoccupied molecular orbitals (ϵ) from the EICVOM calculation are assumed to be related to the position of the core excitation spectral lines. In order to calculate the intensity of each transition to an unoccupied molecular orbital, the electric-dipole transition matrix element is considered. The electric-dipole matrix element can be expressed using the LCAO expansion of the initial and final states:

$$I \propto |\langle \Psi_{final} | \mu | \Psi_{initial} \rangle|^2 = |\langle \Sigma c_j \phi_j | \mu | \Sigma c_i \phi_i \rangle|^2 \qquad (3.3.5)$$

As EHMO is a "valence only" method that does not include solutions for core levels, we can not explicitly calculate the core - unoccupied MO electric-dipole integral. An approximate method, based on the "atomic propensity rule" is used instead.

In atomic electronic transitions, those with a change in orbital angular momentum of $\Delta\ell = \pm 1$ are formally allowed by electric-dipole selection rules (i.e. s ($\ell = 0$) - p ($\ell = 1$)). In a molecule, core excitation transitions are generally considered to follow an "atomic propensity rule" in which excitations are considered to obey atomic selection rules on the core excited atom (localized core hole picture). For example, K shell (1s) transitions occur predominantly to final levels with p orbital character. The "atomic propensity rule" can be applied to molecular core excitation because the initial core level remains essentially atomic-like in molecules. Because the electric-dipole allowed overlap spatially localizes the transition to the site of the core hole, the final level orbital density can be described as a sum of s, p, d, etc. atomic components centred on the core hole.

Based on the "atomic propensity rule", the electric-dipole matrix element for 1s core excitation is dominated by terms involving 1s AOs of the initial level and 2p AOs

localized at the site of the localized core excitation. Of the terms in Equation 3.3.5, the largest terms are those of the form $<c_{2p}\phi_{2p}|\mu|\phi_{1s}>$, where ϕ_{2p} and ϕ_{1s} are both centred on the core excited atom. This approach implicitly assumes that the core hole is localized to one atomic site and is not delocalized over the symmetry equivalent atomic sites in the molecule.

The sum of these dominant matrix elements of the form $<c_{2p}\phi_{2p}|\mu|\phi_{1s}>$ is proportional to the sum $\sum c^2(2p)$, where c(2p) is the coefficient of the 2p-AOs centred on the core excited atom. Therefore, in the atomic propensity approach, the intensity of a core → unoccupied MO transition is considered proportional to the sum of the squares (i.e. $\sum c^2(2p)$) of the coefficients of the AOs that are atomic-dipole coupled to the initial core orbital.

Figure 3.3.1 illustrates the process of generating a simulation spectrum from a "Z+1" calculation. An EHMO calculation was performed on dimethyl terephthalate using the program CACAO [MP90]. The "Z+1" approximation was enacted on a phenyl ring "C-H" carbon atom. (The molecular geometry used is documented in §4D). To simulate the transition to each unoccupied molecular orbital, a Gaussian function is generated with an area given by $\sum c^2(2p)$ and a position given by the calculated energy of the molecular orbital. In Figure 3.3.1, these Gaussian line shapes, each representing a core → unoccupied MO transitions are presented. The width of the Gaussian functions depends on the orbital energy in a manner that approximates the experimental trends of increasing line width for increasing core excited state energy. In this example, the linewidths used were 0.6 eV FWHM for orbitals with of $\epsilon < 0$ eV; 6.0 eV for $0 < \epsilon < 5$ eV; and 12.0 eV for $\epsilon > 5$ eV.

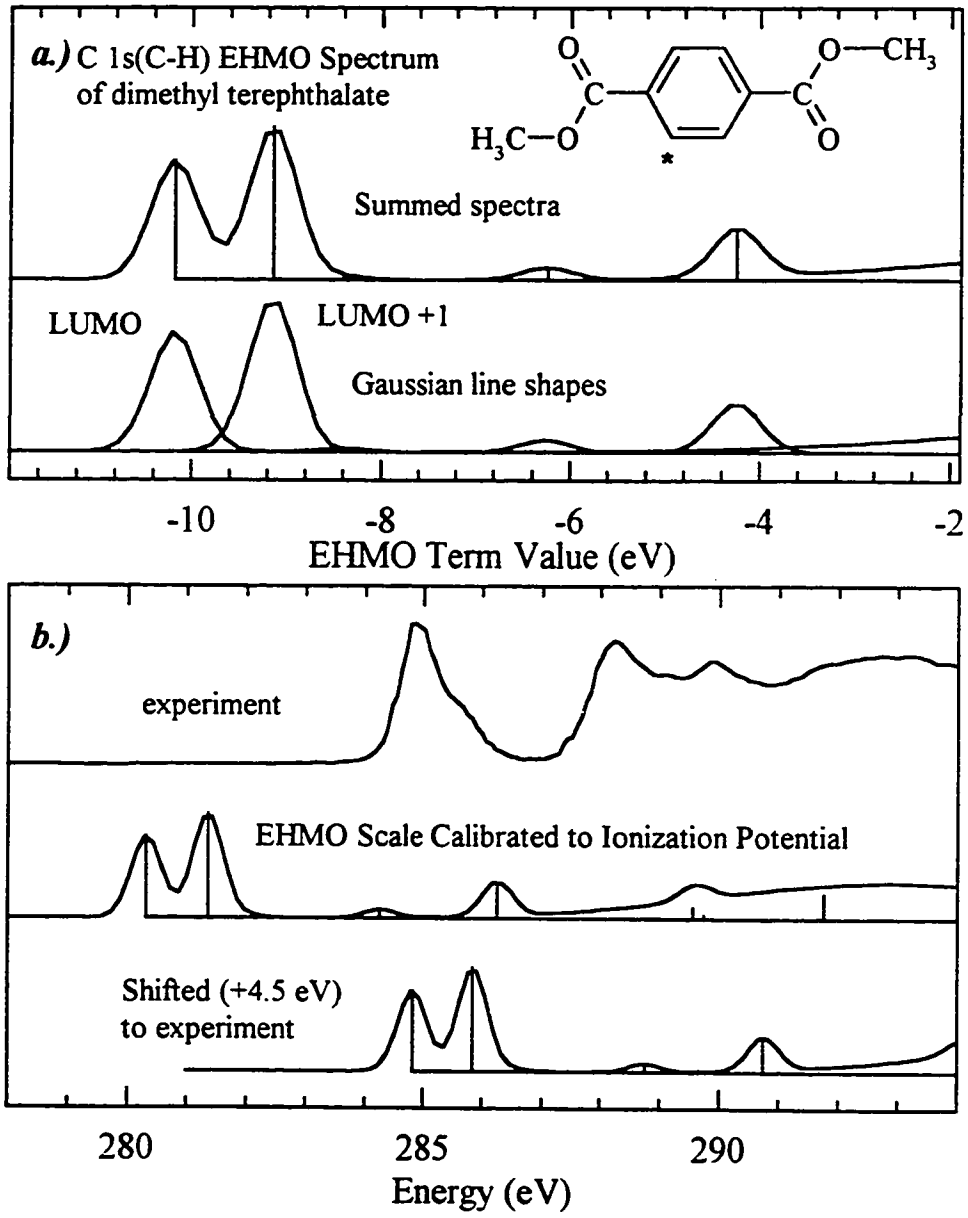

Figure 3.3.1 a.) EHMO Z+1 Simulation of the C 1s(C-H) spectrum dimethyl terephthalate. Gaussian line shapes representing transitions to each unoccupied molecular orbital (LUMO, LUMO+1, etc) are summed. The site of the core hole is indicated by "*".
b.) Alignment of the EHMO simulation spectrum with experiment. Zero of EHMO scale is set to the Ionization potential, then a "hard shift" of +4.5 eV is added to align the smulation with experiment.

The individual Gaussian lines are then summed to form the predicted spectrum. This spectrum simulation process is automated through the program SIMILE [H91]. SIMILE-spectra are generated for each symmetry inequivalent atom. After the application of appropriate chemical shifts for each atomic component, the spectra are summed to generate an overall EHMO-predicted spectrum for a molecule.

Since EHMO does not explicitly calculate core hole energies, it is not capable of providing absolute transition energies. Chemical shifts for each atomic simulation component are required in order to account for the difference in energy between the core levels in the molecule. There are two methods by which these chemical shifts are usually applied [HUR92]. In the first method, a specific, unambiguously interpretable feature, common to both the EHMO and experimental spectra, is used to calibrate the EHMO energy scale. In the EHMO simulation of the C 1s(C-H) component of dimethyl terephthalate C 1s spectrum (Figure 3.3.1), the first C 1s $\rightarrow \pi^*_{C=C}$ is unambiguous in both the EHMO and experimental spectrum. The first peak in the EHMO simulation can thus be calibrated to 284.86 eV [§4D].

In the second method, experimental or estimated ionization potentials are used to calibrate the spectral energy scale. For each symmetry inequivalent-EHMO spectrum, the zero of the EHMO energy scale is set to the ionization potential of the particular core excited atom. These spectra are then summed to form the EHMO spectrum for the entire molecule. Simulated spectra prepared by this method must be systematically shifted to align them with the experimental energy scale. In this example (Fig. 3.3.1), a "hard shift" of +4.5 eV is applied to align the spectrum with experiment. This particular method is

more appropriate for the core excitation of molecules with many different atomic components, as it is usually difficult to identify an unambiguous feature in the experimental spectrum for some atomic components.

Figure 3.3.2 presents the EHMO simulation of the full C 1s spectrum of dimethyl terephthalate, in comparison to experiment. The spectral components for each symmetry inequivalent position (C-H, C-R, C=O, and CH_3) were aligned, first by calibration to their IPs (Table 3, §4D), and then by a +4.5 eV hard shift. The components are summed, with a stoichometrically weighing appropriate for the component. The comparison of this particular EHMO simulation with experiment is discussed in §4D.

§3.4 *Ab Initio* Calculations

Ab initio calculations have been successfully applied to the core excitation spectra of organic [§4D], organometallic [§5B, 5D], electron deficient carboranes [HU&97], and polymers [AC&95]. *Ab initio* calculations can provide higher quality results than semiempirical methods, but they are calculationally much more intensive.

In this thesis, ab initio calculations have been performed using both the *Improved Virtual Orbital* (IVO) method and the "Z+1" method to account for core hole relaxation. In §5B, "Z+1" *ab initio* calculations were applied to the Si 1s, N 1s and C 1s core excitation spectra of the silylene Si[N^{t}BuCH=CHN^{t}Bu]. The implementation of the "Z+1" approximation in *ab initio* calculations is identical to that described for EHMO calculations in §3.3.1, so no further description will be given here.

IVO calculations were performed in this thesis for organic (§4D) and organosilane

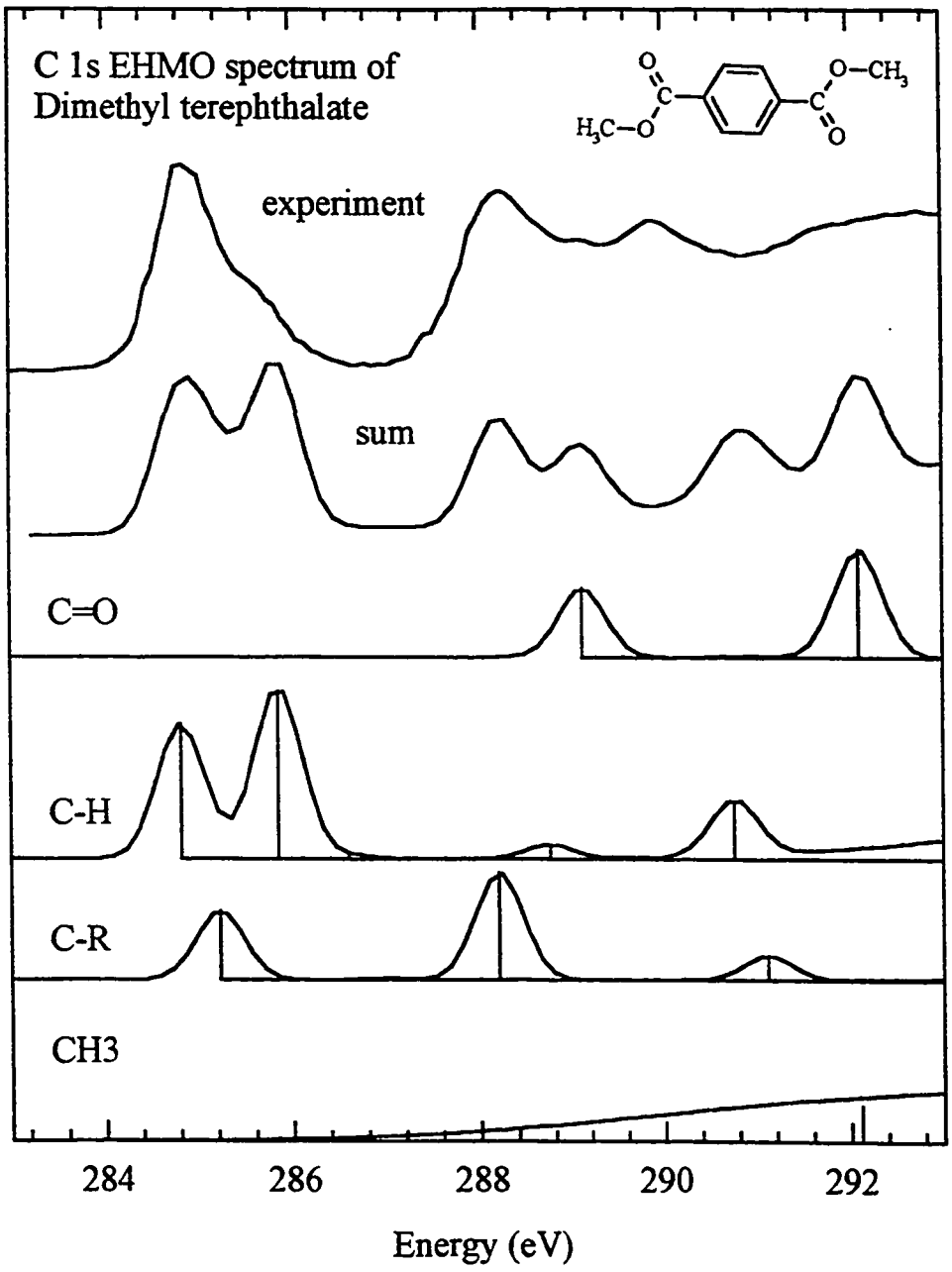

Figure 3.3.2 EHMO Simulation of the C 1s spectrum of dimethyl terephthalate, in comparison to experiment. Each component spectrum corresponds to a separate "Z+1" calculation. Details of the calculation presented in Figure 3.2.1, and details of the energy scale calibration are presented in Figure 3.3.1. The sum is weighted by the molecular stoichiometry.

(§5D) molecules. These calculations were carried out using the program GSCF3, written by Professor N. Kosugi [KK80]. The basis set used is that of Huzinaga et al. [HA&84]. For example, in the IVO calculation of dimethyl terephthalate (§4D) an extended basis set of (63/6) and (53/5) contracted Gaussian-type functions for C and O and (6) for H was used. The (63/6) basis set on carbon represents 6 s-type basis functions for the 1s electrons, 3 s-type basis functions for the 2s electrons, and 6 p-type functions for the 2p electrons. A double-zeta contraction scheme of (521/31) is applied for heavy atoms and (31) for H. The heavy atom onto which the core hole is to be placed has a very high quality basis set in order to obtain a localized core hole solution. For carbon, this contraction scheme is (311121/21111/1*), which includes a polarization function.

The calculation is performed in three steps. In the first step, the ground state MOs and the total ground state energy of the molecule is obtained. These results are used to determine which core MO will have the core hole. In the second step, the SCF solution is obtained for the doublet core ionized state of the molecule for a specified core hole [KK80]. The self consistent field of the core-ionized state defines the fully relaxed Hartree-Fock potential. The difference in total energy between the ground state calculation (first step) and the core-ionized state (second step) corresponds to the Δ-SCF ionization potential. In the final step, the core-excited state is obtained under the fully relaxed Hartree-Fock potential (the static exchange potential) determined in the second step. This calculation computes the "excited orbitals" by minimizing the excitation energy between the core levels ϕ_{I_s} and the excited orbitals ϕ_k, where ϕ_k is determined within the space spanned by the set of vacant orbitals determined for the core ionized molecule (step

2): [IKN78]

$$E(\phi_{1s} \rightarrow \phi_k) = -\epsilon_{1s} + \langle \phi_k | F - J_{1s} + 2K_{1s} | \phi_k \rangle \qquad (3.4.1)$$

This calculation provides term values and oscillator strengths for core excitation transitions. The electric-dipole transition matrix connecting the 1s $\rightarrow \phi_k$ transitions is explicitly evaluated.

The creation of simulation spectra from the IVO-*ab initio* results is similar to that used for the EHMO calculations (§3.3.1). Peaks are expressed as Gaussian functions, with a width following from experimental trends in the increasing line width with increasing core excited state energy. The calculated IPs are used to set the calculated term value scale to the experimental scale.

The construction of the IVO-*ab initio* simulation of the C 1s spectrum of dimethyl terephthalate is presented in §4D, Figure 4. The EHMO "Z+1" result and the IVO-*ab initio* result are compared to experiment in **Figure 3.4.1**. The feature of particular interest for this molecule is the splitting of the lowest energy feature. The EHMO-Z+1 calculation does not reproduce the relative intensity of the two components as well as the *ab initio*-IVO calculation.

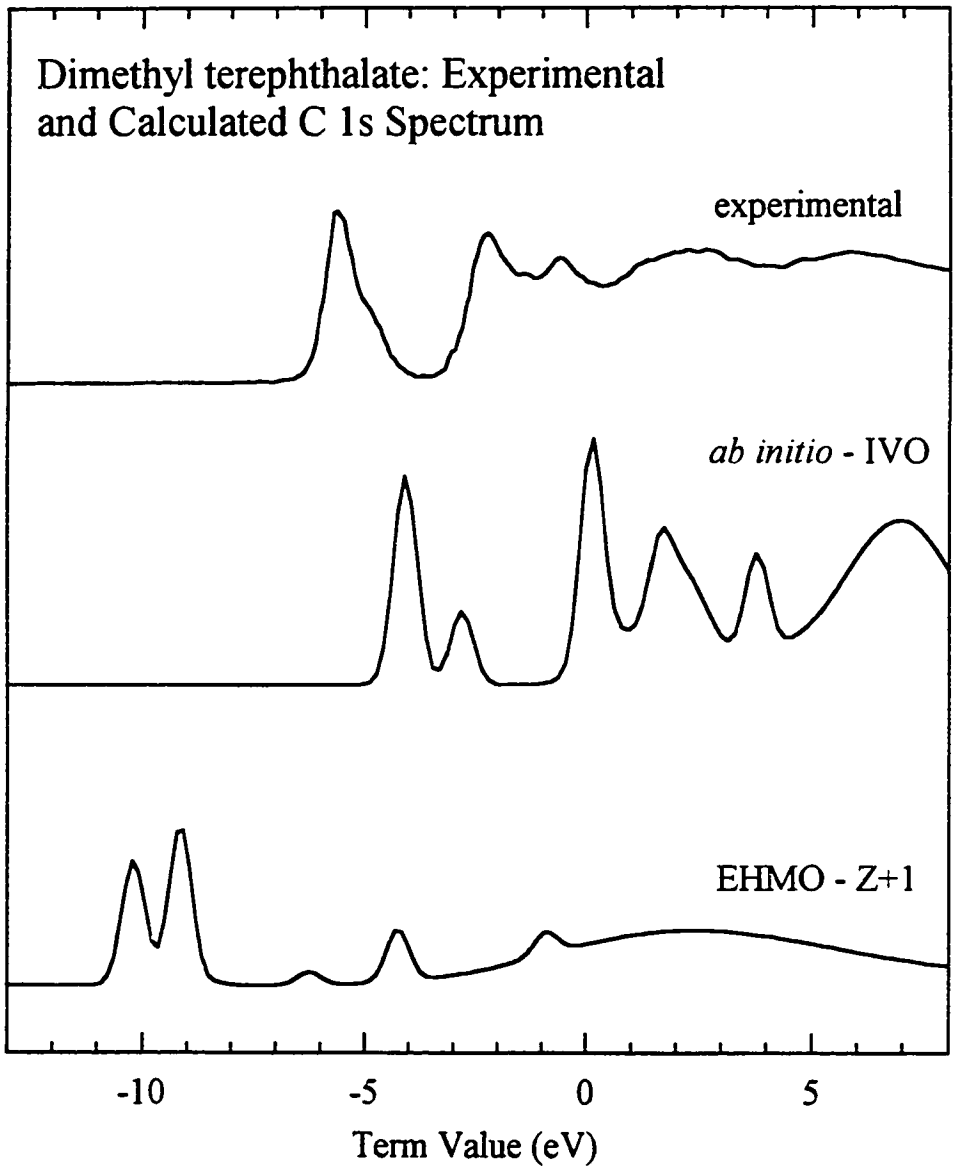

Figure 3.4.1 Comparison of the EHMO simulation spectrum generated by EHMO within the Z+1 method (Fig 3.3.2), *ab initio* calculations with the IVO method (§4D) and the experimental C 1s core excitation spectrum of dimethyl terephthalate.

CHAPTER 4A

MOLECULAR MODELS FOR POLYMER ANALYSIS

The application of core excitation spectroscopy to polymer speciation varies in complexity from simple fitting of spectral shapes ("fingerprinting") to detailed spectral interpretation, aided by quantum calculations. In this thesis, polyurethane and polyphthalate polymers are investigated. Molecular models are used to provide an empirical basis for distinguishing urea and carbamate linkages and hard and soft segments in polyurethane polymers. In polyphthalates, electronic delocalization in the π^*-manifold affects the core excitation spectra, giving rise to a remarkable sensitivity to polyphthalate isomerism. Molecular orbital calculations performed at simple (extended Hückel) and higher levels of theory (ab initio) are used to provide an understanding of molecular and polymer core excitation spectra. General guidelines for defining the critical size of the "molecular fragment" that defines the characteristic core excitation spectrum are discussed.

This chapter (4A) presents an overview of key results from my molecular model study of the core excitation spectroscopy of polyurethane and polyphthalate polymers. This material is presented in more detail in Chapters 4B, 4C and 4D as it was published in the scientific literature.

§4.1 Core Excitation Spectroscopy of Polyurethanes

Polyurethane polymers are produced for a wide range of applications, including

carpet backing, upholstery and car body panels. The physical form of these products ranges from rigid and flexible foams, elastomers, paints and coatings. The structure and morphology of polyurethane polymers on a sub-micron scale can be important to their physical and mechanical properties. Segregation of crystalline phases, side reactions and competing reaction products, unreacted monomer and additives are all possible sources of inhomogeneities on this spatial scale. The use of NEXAFS and STXM microscopy for the chemical speciation of microprecipitates in polyurethane polymers motivated this molecular model investigation.

In polyurethanes, there are three common linkages in the polymer backbone: urethane (also known as carbamate), urea and ether links. These linkages are formed by the polymerization of aromatic diisocyanates with diols or copolymerization with polyethers, as presented in **Figure 4.1.1.** Carbamate linkages are formed by the reaction of a diisocyanate monomer (OCN-Ar-NCO) with a diol (HO-R-OH). When water is added to the reaction mixture, two diisocyanates can react to form a urea linkage. The CO_2 gas produced in this reaction acts as an *in situ* blowing agent for foam formation. As well, polyether chains can be copolymerized into polyurethanes.

For this thesis, I have acquired gas phase ISEELS spectra of a range of urea, carbamate and ether molecules. These molecules were chosen to act as "building blocks" in polyurethane spectral analysis, to identify key features and to provide the basis for a detailed spectral interpretation. Details of the acquisition, processing and analysis of these spectra has been previously published and is presented in published form in §4B and §4C.

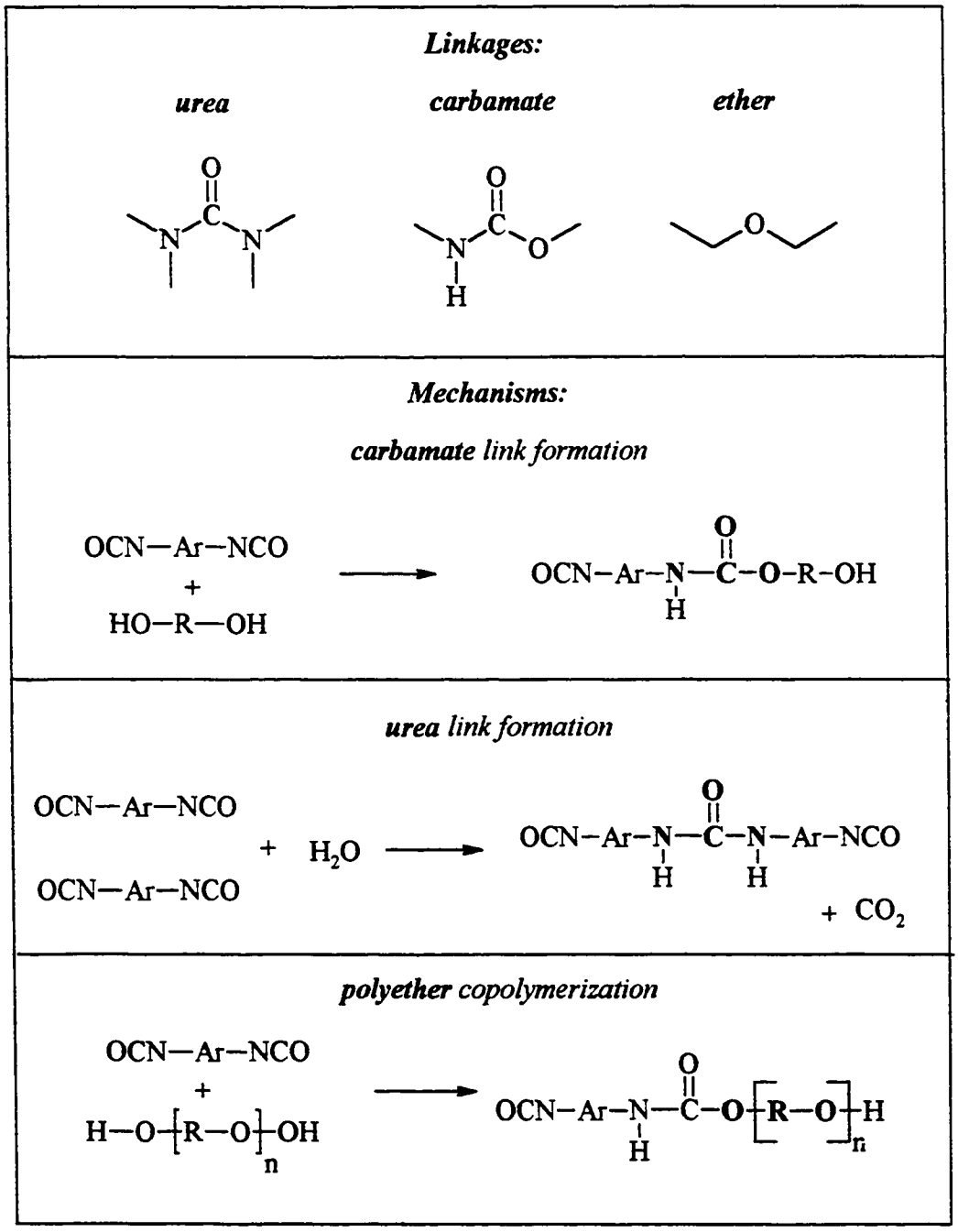

Figure 4.1.1 Functional groups in polyurethane polymers and their formation.

4.1.1 Distinguishing Urea and Carbamate Functional Groups in Polyurethanes

4.1.1.a Urea and Carbamate C 1s Spectra

Can core excitation spectroscopy distinguish between urea and carbamate functional groups? This question is central to the application of STXM microscopy to the character and origin of microprecipitates in polyurethane polymers, where both urea and carbamate linkages can be present. ISEEL spectra of three urea and four carbamate molecular models were investigated to answer this question. **Figure 4.1.2** presents the C 1s ISEEL spectra of phenyl urea and phenyl carbamate, which are models for urea and carbamate linkages in aromatic polyurethanes. The lowest energy feature in the C 1s spectra of molecules and polymers containing phenyl groups is the C 1s(C-H) → $\pi^*_{C=C}$

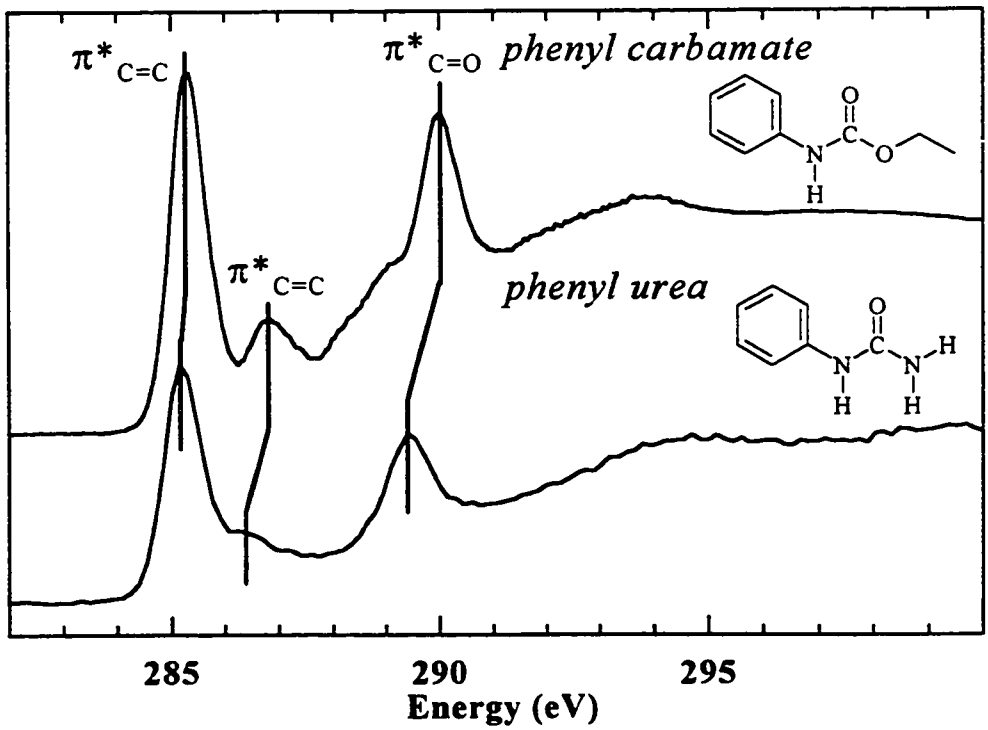

Figure 4.1.2 C 1s ISEEL Spectra of phenyl carbamate and phenyl urea.

transition at ~285 eV. The feature at ~286.5 eV is also a transition to the phenyl ring π^* level, except for this feature the initial C 1s core level is on the phenyl ring carbon atom to which the substituent is bonded. This feature occurs at higher energy because the C 1s binding energy of the substituted carbon is shifted by the inductive effect of the functional group. This feature is assigned as the C 1s(**C-R**) - $\pi^*_{C=C}$ transition. The shift between the C 1s(C-H) - $\pi^*_{C=C}$ and the C 1s(C-R) - $\pi^*_{C=C}$ transition depends on the identity of the "R" substituent.

The most critical feature observed in C 1s spectra for distinguishing urea and carbamate linkages is the C 1s(C=O) - $\pi^*_{C=O}$ transition that occurs at ~290 eV. The C 1s - $\pi^*_{C=O}$ transition in phenyl carbamate is ~0.6 eV higher than in phenyl urea. This shift is readily apparent in the spectra in Fig. 4.1.2.

Molecular orbital calculations were applied to understand the origin and character of this C 1s(C=O) - $\pi^*_{C=O}$ transition in phenyl urea and phenyl carbamate. **Figure 4.1.3** presents the results of an Extended Hückel Molecular Orbital (EHMO) calculation for the carbonyl (C=O) component of the C 1s spectra of phenyl urea and phenyl carbamate (extracted from Figures 4 and 9 in §4C). The left panel shows the "valence only" contribution to the spectra: The EHMO-calculated energy of the $\pi^*_{C=O}$ feature with respect to the ionization potential. The $\pi^*_{C=O}$ level in phenyl carbamate is 0.27 eV *lower* than in phenyl urea. When the carbonyl C 1s binding energy is accounted for (by setting the zero of the EHMO term value energy scale to the experimental ionization potential; middle panel) the C 1s(C=O) - $\pi^*_{C=O}$ transition energy is 0.49 eV *higher* in phenyl carbamate than in phenyl urea. This is close to the experimental difference of ~0.6 eV

(right panel). The binding energy shift arises from the difference in the atoms bonded to the carbonyl carbon atom between urea and carbamate. The valence $\pi^*_{C=O}$ shift reflects the differing nature of the delocalization of the carbonyl π^* density. Both of these effects contribute in an opposite sence, but the core binding energy shift dominates.

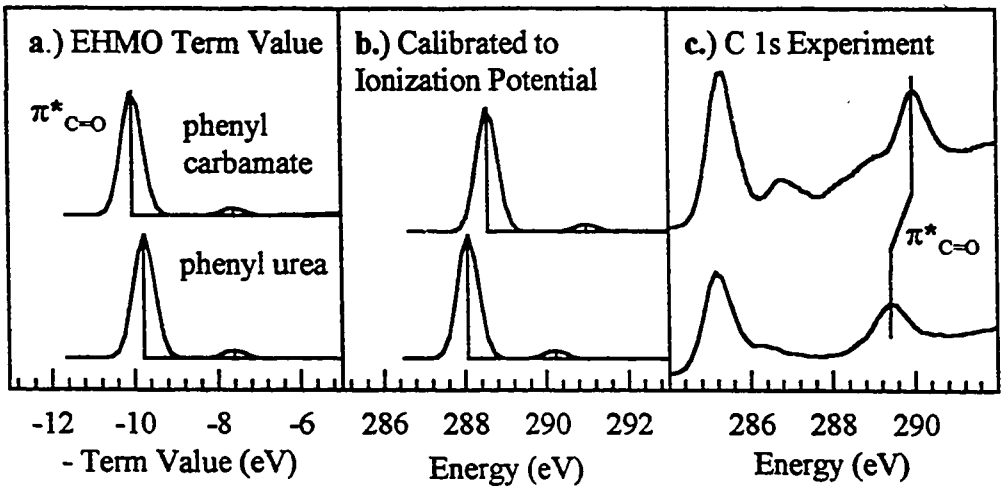

Figure 4.1.3 EHMO calculation of the C 1s(C=O) → π* component of the phenyl carbamate and phenyl urea spectrum. a.) Calculated results on a negative-term value scale (ϵ); b.) Calculated results with the zero of the EHMO term value scale set to experimental ionization potentials (urea: 288.84 eV, carbamate: 289.60 eV) [BB92]; c.) Experimental C 1s spectra of phenyl carbamate and phenyl urea.

The shift in the C 1s → $\pi^*_{C=O}$ transition energy of urea and carbamate linkages permits NEXAFS spectroscopy to distinguish these linkages. This effect has been useful in the C 1s NEXAFS and STXM microscopy of polyurethane polymers [WP&97]. **Figure 4.1.4** presents the C 1s NEXAFS spectra of two polyurethane polymers that contain only carbamate linkages, of a polyurethane-poly(propylene oxide) copolymer with a 50:50 ratio of urea and carbamate linkages [WP&97] and of a polyurea polymer (The MDI-TDI labels

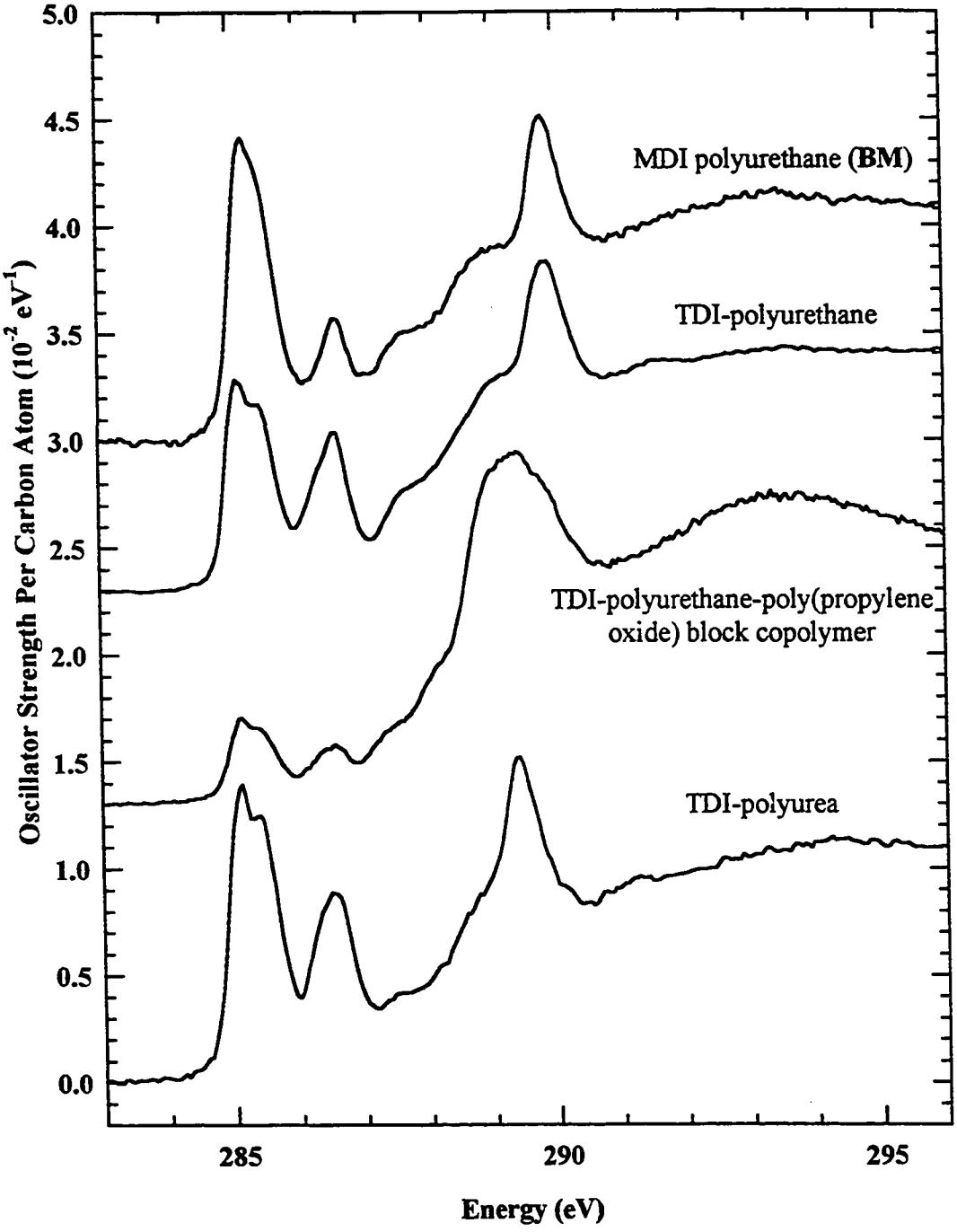

Figure 4.1.4 NEXAFS Spectra of polyurethane polymers: MDI-polyurethane (**BM**), TDI-polyurethane, TDI-polyurethane-poly(propylene oxide copolymer) (**#259**, mixed urea, urethane linkages) and TDI-polyurea [HRA96].

refer to the aromatic component and will be discussed below in §4.1.3). The C 1s(C=O) → $\pi^*_{C=O}$ feature is clearly observed at lower energy in the polyurea spectrum (bottom) than in the polyurethane spectrum (carbamate-linked, bottom two traces), demonstrating the ability of this transition to distinguish between carbamate and urea linkages. The polyurethane-poly(propylene oxide) copolymer contains a mixture of urea and carbamate linkages. The characteristic C 1s(C=O) → $\pi^*_{C=O}$ transitions of urea and carbamate are superimposed on the broad ether C 1s → σ^*_{C-O} transitions. A detailed analysis of the spectral line shape using appropriate polyurea and polyurethane models allows quantification of the urea/carbamate ratio with good precision [WP&97].

4.1.1.b Urea and Carbamate N 1s and O 1s Spectra

While the C 1s spectra of polyurethanes has been shown above to be capable of distinguishing urea and carbamate linkages, it is also useful to examine what might be learned from other core edges. From the chemical structure of the urea and carbamate linkages, it is reasonable to expect that the oxygen and nitrogen core edge spectra would be able to differentiate these linkages. In general, multi-edge studies are useful for providing additional information about materials than that obtained from only one core edge.

A detailed discussion of the acquisition and analysis of the N 1s and O 1s ISEEL spectra of urea, carbamate and ether molecular models is presented in §4C. Here, in **Figure 4.1.5**, the N 1s ISEELS spectra of phenyl urea and phenyl carbamate and the O 1s ISEELS spectra of phenyl urea, phenyl carbamate and diisopropyl ether are presented.

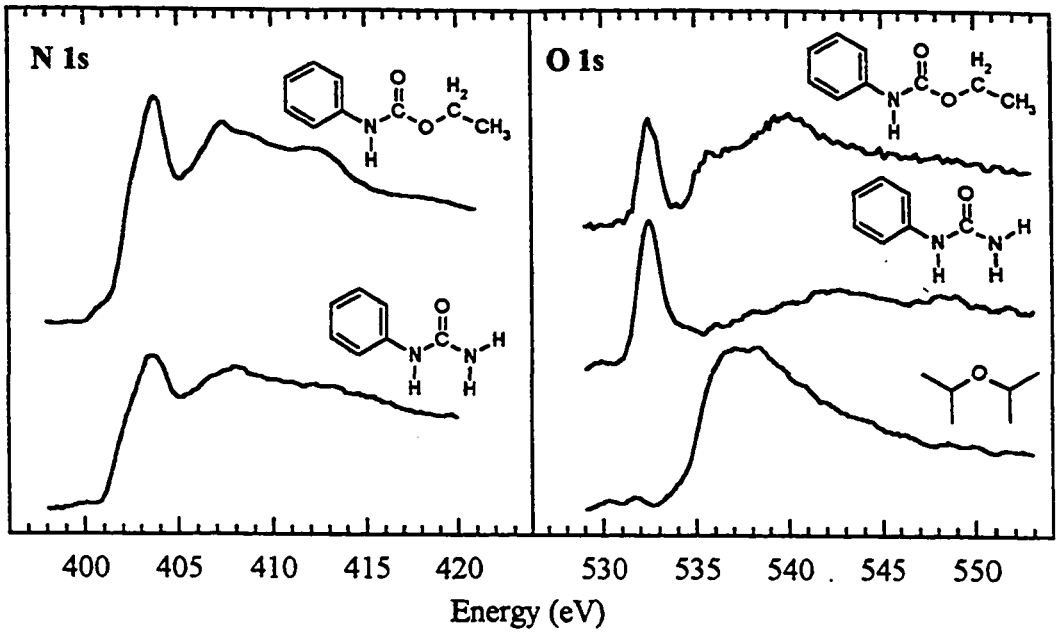

Figure 4.1.5 N 1s and O 1s Inner Shell Electron Energy Loss Spectra of phenyl carbamate, phenyl urea and diisopropyl ether.

Of particular interest in the N 1s spectra of the molecular models is the low energy N 1s → π* transition at ~403 eV. This feature is somewhat broader in the phenyl-substituted urea and carbamate molecules than in the unsubstituted molecules (See Figures 3 and 8 in §4C to compare). In the unsubstituted molecules, the $\pi^*_{C=O}$ feature originates from delocalization of the carbonyl π* density onto nitrogen, as illustrated by an MO diagram for urea (Figure 5, §4C). In the phenyl-substituted urea and carbamate molecules, π* density from *both* the carbonyl and phenyl groups is delocalized onto nitrogen and is probed by N 1s spectroscopy. Any possible pattern of π* mixing and splitting that might arise from this delocalization is not observed in these N 1s spectra, although the statistical quality of these spectra is relatively poor and the experimental resolution (~0.7 eV) may

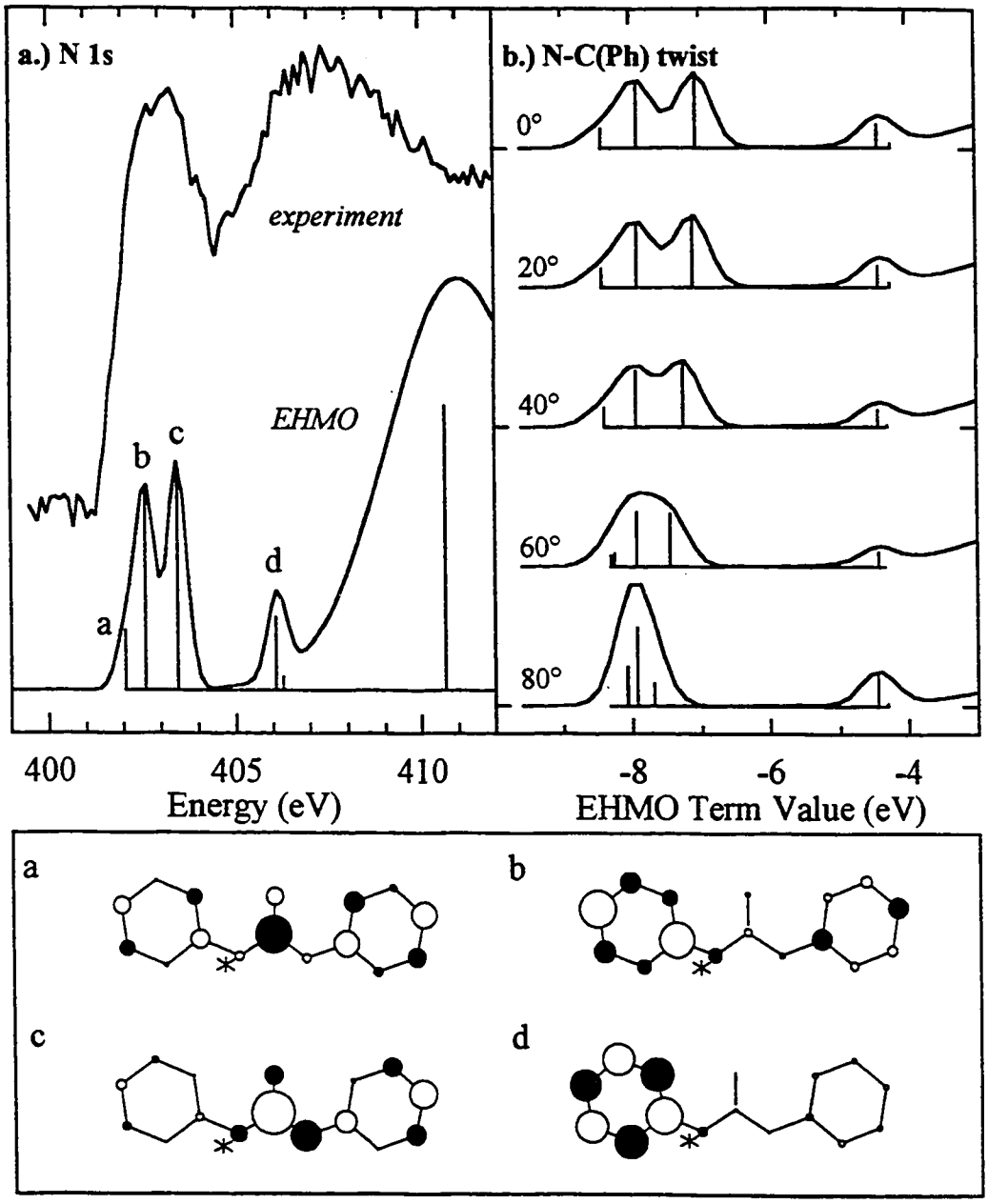

Figure 4.1.6 a.) Experimental N 1s spectrum of diphenyl urea, in comparison to the N 1s EHMO calculated spectrum of diphenyl urea. b.) N 1s EHMO spectra of diphenyl urea calculated for different values of the N-C(Ph) twist angle. Bottom: Plots of π^* MOs in panel 1.

not be adequate to resolve the complex character of this π^* band. Instead, MO calculations are used to show the potential complexity of the N 1s spectra.

In **Figure 4.1.6**, the experimental N 1s spectrum of diphenyl urea is compared to the EHMO-predicted N 1s spectrum of diphenyl urea, together with a calculational examination of the dependance of the N-C(ph) twist angle on the π^*-band (adapted from Figures 6-7 in §4C). The EHMO spectra predict that the N 1s → π^* band consists of several closely spaced N 1s → π^* transitions and that the splitting of these π^* features is dependant on the "twist" or conformation of the phenyl ring relative to the urea group. While skepticism regarding the capability of N 1s spectra to distinguish urea and carbamate linkages may be justified based on these experimental spectra, the EHMO calculations encourage further investigation at the N 1s core edge. At this point in time, the N 1s spectra of polyurethanes acquired by both TEM-EELS (§4B) and NEXAFS [HRA96] has not had adequate statistical precision to address this question.

Substantial differences are observed between the O 1s spectra of phenyl urea, phenyl carbamate and diisopropyl ether (Figure 4.1.5). The O 1s spectrum of diisopropyl ether is similar to that observed for oxygen coordinated by saturated alkyl groups, such as in diethyl ether (§4C), tetrahydrofuran and tetrahydropyran [NIH86]. Such spectra consist of weak Rydberg features and broad O 1s → σ^*_{C-O} resonances. The O 1s spectrum of phenyl urea originates from the single oxygen atom in the carbonyl group, while the phenyl carbamate O 1s spectrum originates from both carbonyl and -O-R oxygen atoms. Both spectra are dominated by the intense O 1s(C=O) → $\pi^*_{C=O}$ transition (at ~532.5 eV) and the higher energy O 1s(C=O) → $\sigma^*_{C=O}$ transition (at ~548 eV). In the O 1s spectrum of

phenyl carbamate, the O 1s(O-R) - $\pi^*_{C=O}$ transition (at ~536 eV) and the O 1s(O-R) - σ^*_{C-O} transition (at ~540 eV) are present as well. The presence of the -O-R transitions can be used to differentiate carbamate linkages from urea linkages at the O 1s core edge. O 1s TEM-EELS spectra of polymers containing varying amounts of poly(propylene oxide) and polyurethane are presented in Figure 5, §4B.

§4.1.2 Polyurethane Hard-Soft Model Studies

In order to calibrate the sensitivity of NEXAFS for polymer chemical speciation, it is useful to study the NEXAFS spectra of polymer models that have well determined structures. Three 4,4'-methylene diphenyldiisocyante (MDI) polyurethane-poly(propylene

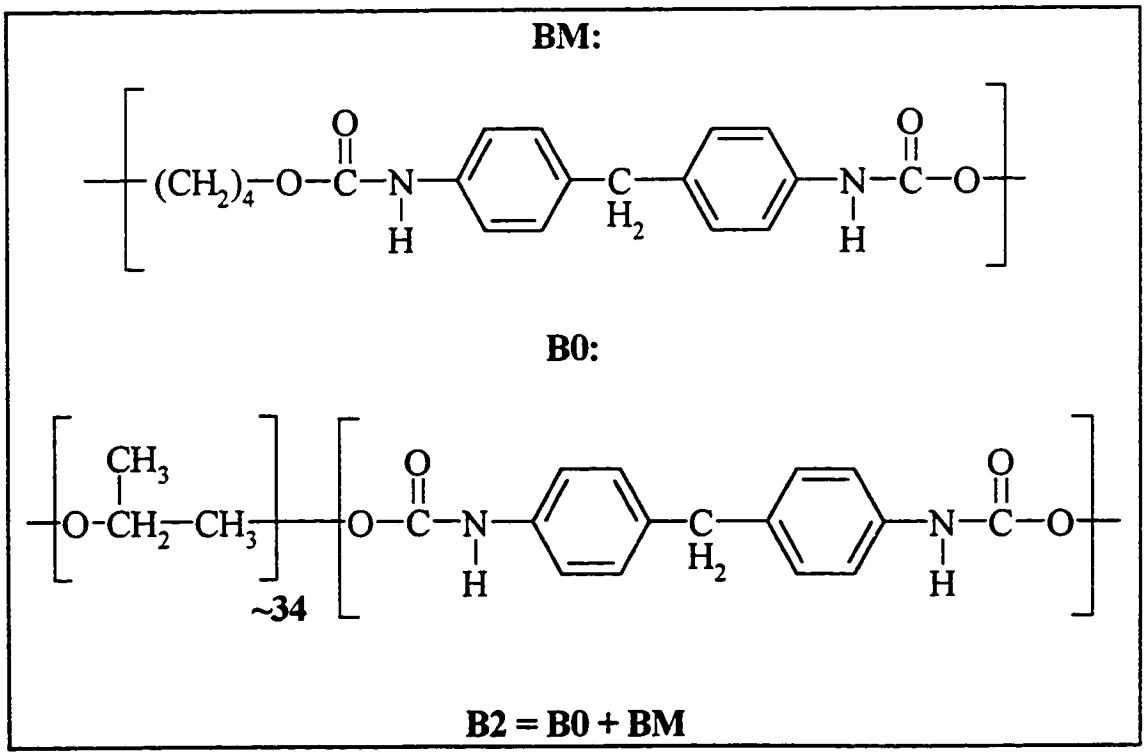

Figure 4.1.7 Structures of some 4,4'-methylene diphenyldiisocyanate (MDI)-poly(propylene oxide) copolymers.

oxide) (PPO) copolymers, formed with different polyurethane and poly(propylene oxide) concentrations [CH&86] are investigated. The structure of these polymer models (**B0**, **B2** and **BM**) is presented in **Figure 4.1.7**. The polymer **BM** is a "hard segment" polymer, formed by the polymerization of 4,4'-methylene diphenyldiisocyante (MDI) with butane diol (BDO). The polymer **B0** is a "soft segment" polymer, formed by the polymerization of MDI with PPO (with ~34 repeat units). The structure of polymer **B2** is intermediate - a sum of the structures of polymers **BM** and **B0**. The terms "soft segment" and "hard segment" arise from the physical character of these polymers. Polymers dominated by long saturated chains (such as poly(propylene oxide)) are relatively flexible (i.e. **B0** is a liquid), whereas the MDI polyurethane chains are relatively rigid because of electronic conjugation and hydrogen bonding.

Figure 4.1.8 presents a comparison of the C 1s EELS and NEXAFS spectra of the molecular models phenyl carbamate and diisopropyl ether, and the polymer models **B0**, **B2** and **BM** (adapted from Fig. 2. of §4B). The left panel presents the C 1s Electron Energy Loss spectra of polymers **B0**, **B2** and **BM**, recorded in a Transmission Electron Microscope with parallel EELS detection by R. Leapman (see §4B for details). The right panel presents the C 1s NEXAFS spectra of these polymers, recorded by Ade and Smith [AS96], using the Scanning Transmission X-ray Microscope (STXM) at the National Synchrotron Light Source (NSLS). This comparison between the polymer EELS and the molecular models is discussed below in §4B. The higher resolution NEXAFS spectra were acquired after publication of §4B so further discussion of this data is presented here. The comparison of the EELS and NEXAFS spectra demonstrates the advantages of higher

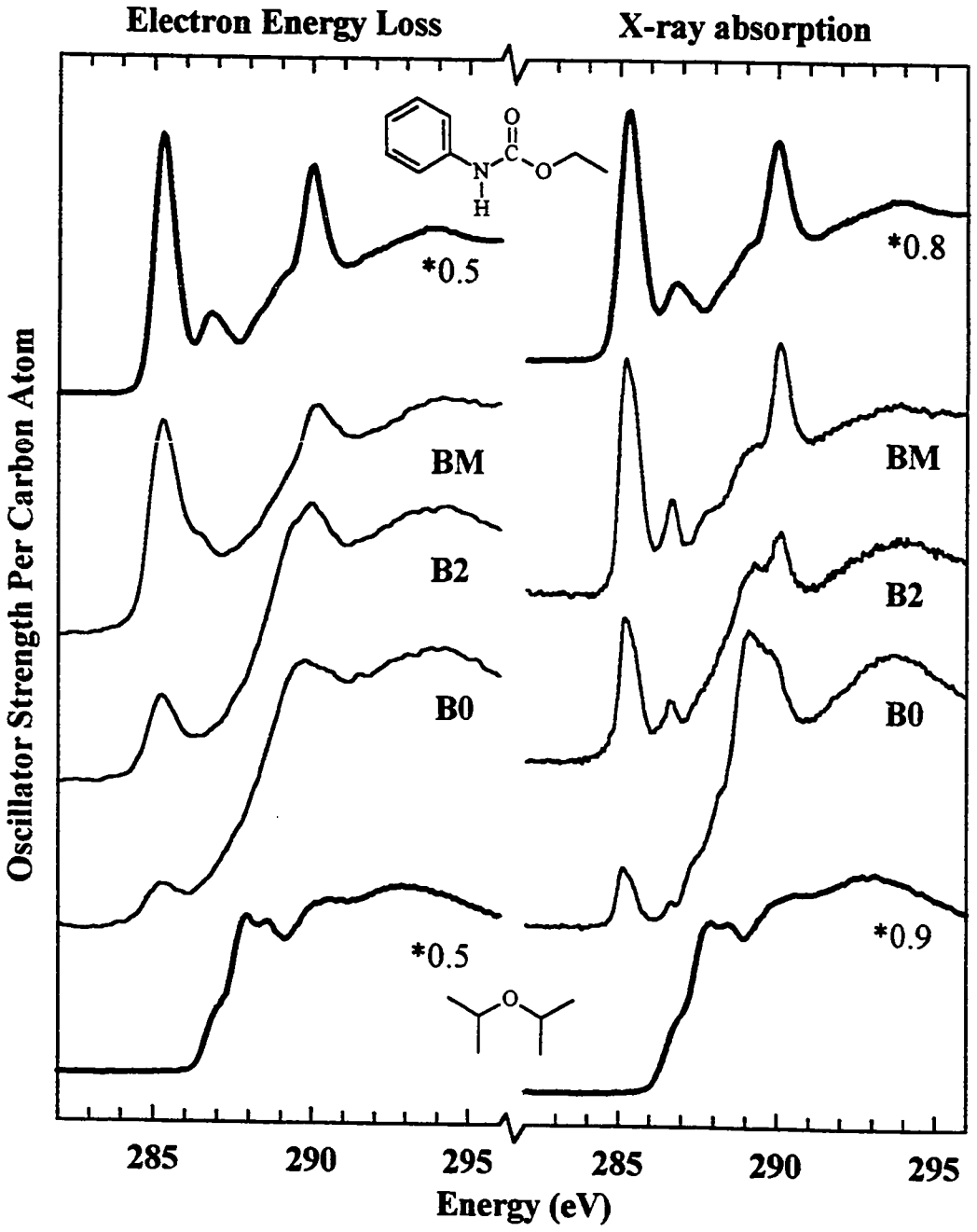

Figure 4.1.8 C 1s ISEELS Spectra of phenyl carbamate (top trace) and diisopropyl ether (bottom trace), compared to the C 1s EELS spectra (left panel) [UH&95a] and the C 1s NEXAFS spectra (right panel) [HRA96] of the **B0**, **B2** and **BM** MDI polymer models.

electronic resolution and the use of x-ray absorption spectroscopy, both of which make STXM a powerful tool for polymer analysis.

The dominant features © 1s(C-H) → $\pi^*_{C=C}$: ~285 eV and C 1s(C=O) → $\pi^*_{C=O}$: ~290 eV) in the polyurethane spectra are resolved by the EELS and NEXAFS techniques. The intensity of these C 1s → π* features is proportional to the relative concentration of these components in each polymer. The C 1s(C-R) → $\pi^*_{C=C}$ transition in the MDI-dilute polymers **B0** and **B2** can be resolved in the NEXAFS spectra but is not resolved in the EELS spectra. The strong correspondence between the spectrum of phenyl carbamate and the **BM** NEXAFS spectrum demonstrates the effectiveness of this molecular model. In the structure of **BM** (see Fig 4.1.7) there are two identifiable "phenyl carbamate" substructures per repeat unit. While there are small differences between the polymer and molecular model (such as the absence of the methylene unit), these differences are not expected to be significant. Saturated units can be thought of as "brick walls" with respect to electronic delocalization. By dividing the polymer into "molecular units" at these saturated units, spectra based on these molecular units should be good models for the polymer spectra. This is demonstrated by the similarity of the core spectra of phenyl carbamate to those of the polymer **BM**.

The correspondence between the soft segment dominated polymers (**B0**, **B2**) with the soft segment molecular model (diisopropyl ether) is much poorer. In the low energy region (286-289 eV) of the diisopropyl ether C 1s spectrum, there is a complicated pattern of Rydberg transitions. In the C 1s spectrum of **B0** (which is dominated by poly(propylene oxide)) there are weak shoulders at these energies but the spectrum is dominated by σ*

features at higher energy (288 - 290 eV). The weak shoulders may correspond to the Rydberg features observed in the gas phase spectrum of diisopropyl ether, as Rydberg features are typically attenuated or shifted to higher energy in solid phase spectra. However, the most significant difference between the molecular model and the polymer

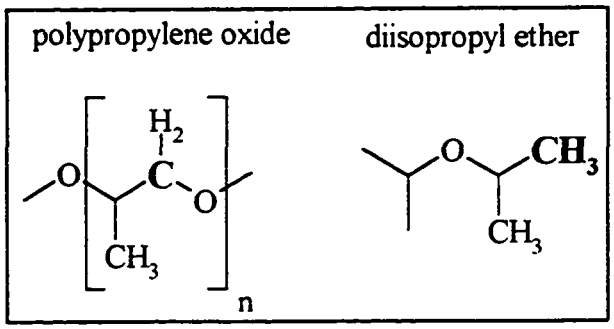

Figure 4.1.9 Structures of polypropylene oxide and diisopropyl ether.

spectra is a consequence of structural differences. The structure of PPO and diisopropyl ether is presented in **Figure 4.1.9**. The carbon atom site that differs between the molecule and polymer is highlighted in bold type. The C 1s → $\sigma^*_{C\text{-}O}$ feature (at ~290 eV) is larger in the polymer spectrum because there is one more C-O bond (at the CH_2 site) in the polymer repeat unit than in the molecular model. In this case, the chain -CH_2- unit is poorly modeled by the CH_3 group in diisopropyl ether.

While the use of diisopropyl ether as a model for the spectrum of the PPO component in **B0** and **B2** is limited, this comparison does demonstrate how core excitation spectra of saturated polymers such as PPO are dominated by the nearest atom environment.

4.1.3 Distinguishing MDI and TDI Polyurethanes

Two types of diisocyanate monomers are largely used for commercial polyurethane production: toluene diisocyanate (TDI) and 4,4'-methylene diphenyldiisoctanate (MDI). TDI monomers are produced as a mixture of 2,6- and 2,4- isomers (20:80). The structure of these monomers are presented in **Figure 4.1.10**. Polymers formed from these monomers are referred to as "TDI" or "MDI" polyurethanes.

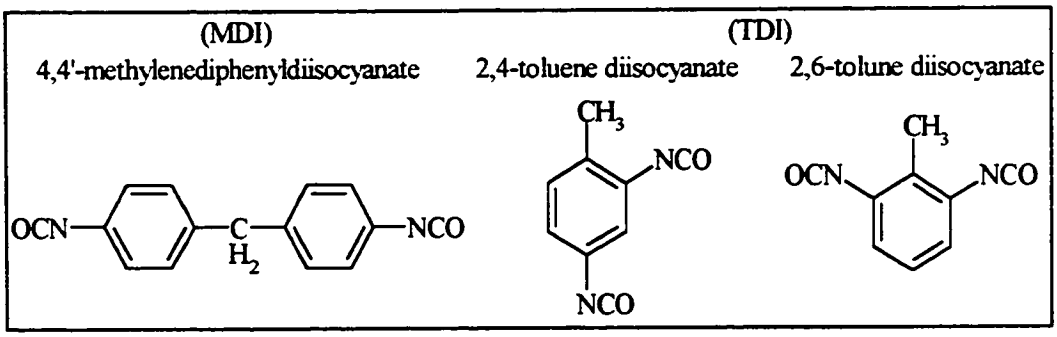

Figure 4.1.10 Structures of MDI and TDI polyurethane diisocyanate monomers.

Because features originating from the phenyl ring are strikingly dominant in C 1s core excitation spectra, MDI and TDI polymers and their monomers can be readily differentiated by core excitation spectroscopy. The spectra of molecular models demonstrating this is presented in **Figure 4.1.11**. The C 1s spectra of phenyl carbamate and MDI *bis* ethyl carbamate are very similar, which is not surprising because there are two "phenyl carbamate" substructures in the MDI *bis* ethyl carbamate molecule. In the region of the C 1s - $\pi^*_{C=C}$ transitions (285 - 287 eV), the TDI *bis* methyl carbamate C 1s spectrum is very different from that of MDI *bis* ethyl carbamate. A simple rationale can be applied to understand this difference. In TDI molecules and polymers, there are two C-N bonds and one C-C bond per phenyl ring, while in MDI molecules and polymers, there is

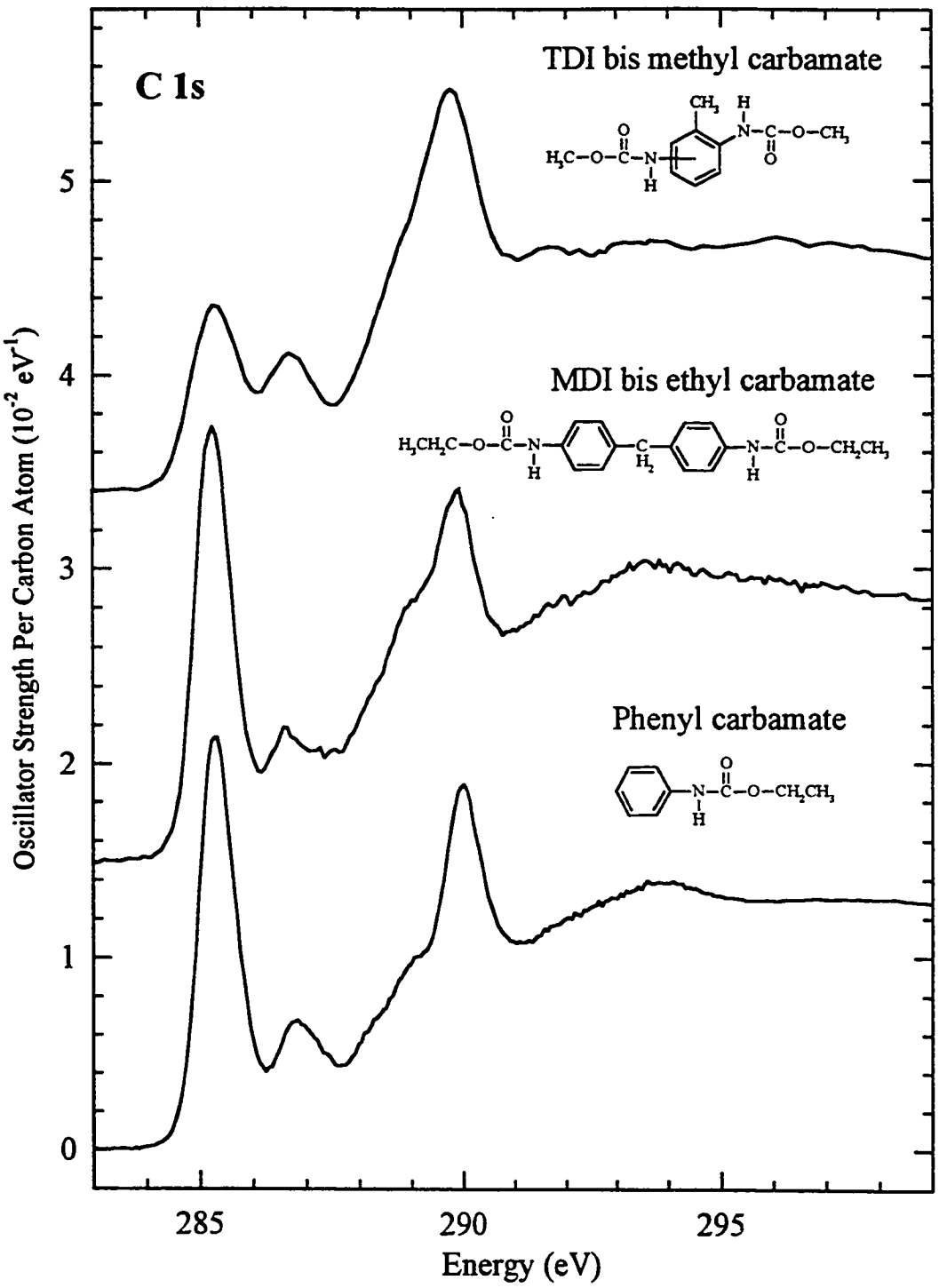

Figure 4.1.11 C 1s ISEELS spectra of TDI *bis* methyl carbamate, MDI *bis* ethyl carbamate and phenyl carbamate [U94]. Offsets of 3.4 and 1.5 (10^{-2} eV^{-1}) have been used for clarity in the spectra of TDI bis methyl carbamate and MDI bis methyl carbamate.

one C-N bond and one C-C bond per phenyl ring. This difference results in an decrease of the C 1s(C-H) → $\pi^*_{C=C}$ transition intensity and an increase in the C 1s(C-R) → $\pi^*_{C=C}$ transition intensity in TDI systems relative to MDI systems. This simple difference has been quite useful in the STXM analysis of polyurethanes. The reader is challenged to identify which monomer (TDI or MDI) was used in the manufacture of the polyurethanes whose spectra are presented in Figures 4.1.8 and 4.1.4. (Hint: compare to the molecular model spectra in Figure 4.1.11).

§4.2 Core Excitation Spectroscopy of Polyphthalate Polymers

Polyphthalates are a class of aryl polyesters, including poly(ethylene terephthalate) (PET) which is commonly used in soft drink packaging. This thesis presents a molecular model study of the core excitation spectra of PET and the related polymers poly(diallyl isophthalate) and poly(diallyl phthalate) which are substitutional isomers of PET in the phthalate segment (-CO_2-Ph-CO_2-) of the polymer chain. The structures of these polymers are presented in **Figure 4.2.1**. The core excitation spectra of polyphthalates can be quite complex and can be a significant challenge for spectral analysis.

§4.2.1 What makes an Appropriate Molecular Model?

In the study of MDI polyurethane polymers (§4.1), a molecular model that represented *part* of the polymer repeat unit (phenyl carbamate) was an adequate model for the polymer. In polyphthalates, the form of an appropriate molecular model must be evaluated. **Figure 4.2.2** presents the C 1s NEXAFS spectra of poly(ethylene

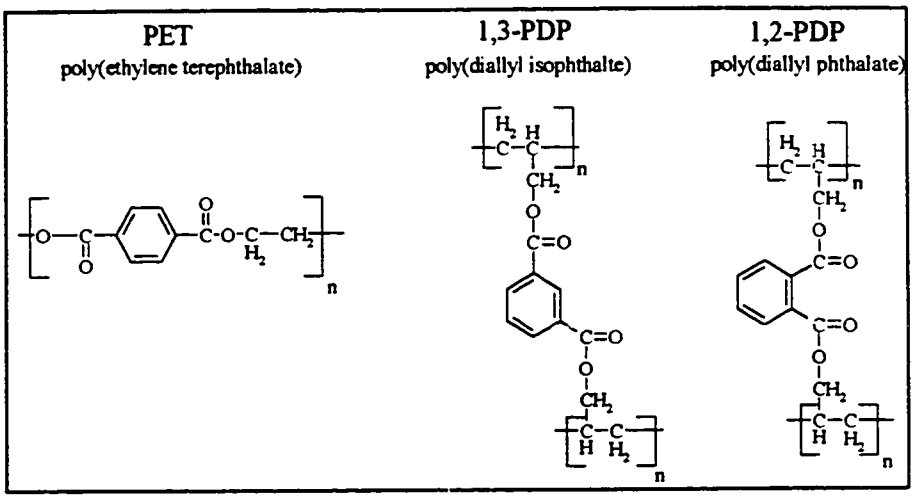

Figure 4.2.1 Chemical Structures for the polymers poly(ethylene terephthalate) (**PET**), poly(diallyl isophthalate) (**1,3-PDP**) and poly(diallyl phthalate) (**1,2-PDP**).

terephthalate), in comparison to the C 1s ISEELS spectrum of dimethyl terephthalate [§4D], ethyl benzoate [HUR92], and a simulation formed by the sum of benzene [HB77] and formic acid [IH87]. If the spectrum of such a material is viewed as a sum of functional-group building blocks, then the spectrum of PET could be simulated by combining the spectrum of a phenyl ring model (benzene) with a carboxylate model (formic acid). The simulation reflects the general form of the polymer spectra, specifically the presence of C 1s(C-H) → $\pi^*_{C=C}$ and C 1s(C=O) → $\pi^*_{C=O}$ transitions. Ethyl benzoate represents of a subfragment of the PET repeat unit. π-delocalization between the phenyl ring and the methyl carboxylate group is considered in the ethyl benzoate model, but not with the same "para" pattern as in PET. The best molecular model for PET is dimethyl terephthalate (1,4-DMP), which represents the polymer repeat unit divided at the ethyl linkage. The unique splitting of the C 1s(C-H) → $\pi^*_{C=C}$ feature observed in PET is also observed in the C 1s spectrum of 1,4-DMP but is *not* observed in the spectrum of ethyl benzoate or the benzene + formic acid simulation. We might assume that this splitting

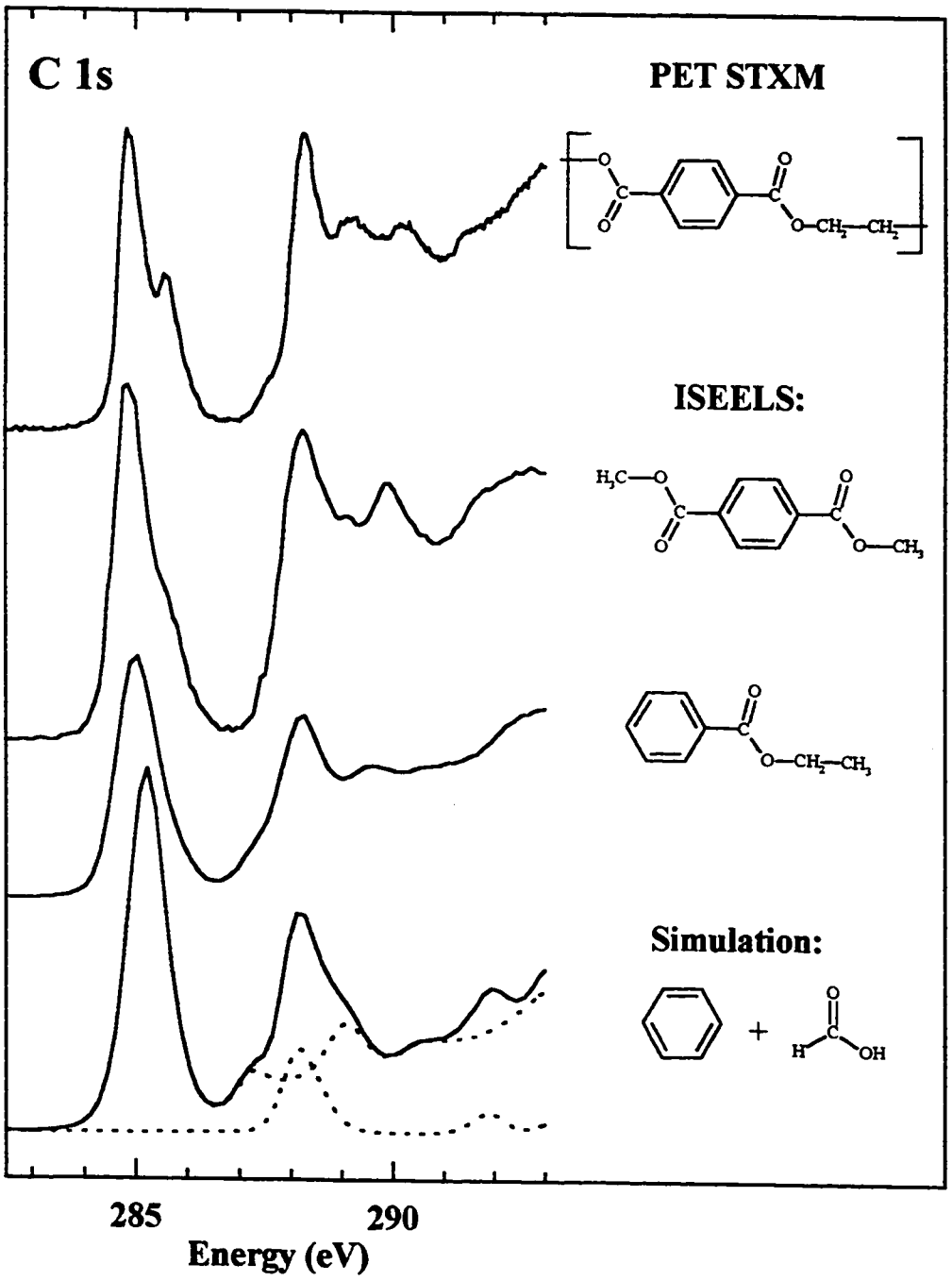

Figure 4.2.2 C 1s NEXAFS spectrum of poly(ethylene terephthalate) (**PET**), compared to the C 1s ISEELS spectra of dimethly terephthalate (**1,4-DMP**), ethyl benzoate and a simulation formed from the sum of benzene and formic acid.

arises from a "C-R" core level shift of the phenyl ring carbon bonded to the methyl carboxylate group, but this conclusion is inconsistent with the spectra of poly(diallyl isophthalate), poly(diallyl phthalate), 1,3-dimethyl isophthalate and 1,2-dimethyl phthalate which are presented below.

Differences in the 288-293 eV energy region also bear on the choice of molecular model. This region is best reproduced by 1,4-DMP, suggesting that the phenyl and methyl carboxylate groups interact in a way that significantly affects the C 1s → π* spectroscopy. While it would be trivial to note that 1,4-DMP is the most similar to the polymer, this by itself is not the critical origin of the spectral similarity. The spectral details can only be properly considered when the molecular model include the same linkages of *unsaturated* components as the polymer. Through π-delocalization, unsaturated components introduce a non-local structure sensitivity to core excitation spectroscopy. The spectroscopic probe is still "local", but the local electronic structure is perturbed by delocalization.

§4.2.2 Poly(phthalate) NEXAFS Spectroscopy

In addition to the core excitation spectra of poly(ethylene terephthalate) (PET), the core excitation spectra of poly(diallyl phthalate) (1,3-PDP) and poly(diallyl isophthalate) (1,2-PDP) have also been studied (See Figure 4.2.1 for structures). The phthalate segments ($-CO_2-Ph-CO_2-$) of these polymers are isomers, where the substitution pattern of the ester groups on the phenyl ring differs (para: PET; meta: poly(diallyl isophthalate); ortho: poly(diallyl phthalate)). The polymers themselves are not isomers, as the alkyl link between the phthalate units in 1,3-PDP and 1,2-PDP is different from that in PET.

Details of the acquisition of the C 1s and O 1s ISEELS spectra of the molecular models 1,4-dimethyl terephthalate (1,4-DMP), 1,3-dimethyl isophthalate (1,3-DMP) and 1,2-dimethyl phthalate (1,2-DMP) are discussed below in §4D. The low energy range of the C 1s (283 - 292 eV) and O 1s spectra (529 - 538 eV) of these molecules is reproduced in **Figure 4.2.3.** The energy of the main C 1s(C-H) → $\pi^*_{C=C}$ transition shifts upward by 0.26 eV between 1,4-DMP and 1,2-DMP, and the shape of this π^*-band changes substantially between 1,4-DMP and the other molecules. The main C 1s(C=O) → $\pi^*_{C=O}$ transition shifts upwards by 0.3 eV, and the O 1s → $\pi^*_{C=O}$(+) transition shifts upwards by 0.47 eV. These shifts are *real*, as the calibration precision of the energy loss scale is better than 0.05 eV (with an accuracy of better than 0.1 eV). These changes result from differences in the π-delocalization between the phenyl ring and the methyl carboxylate

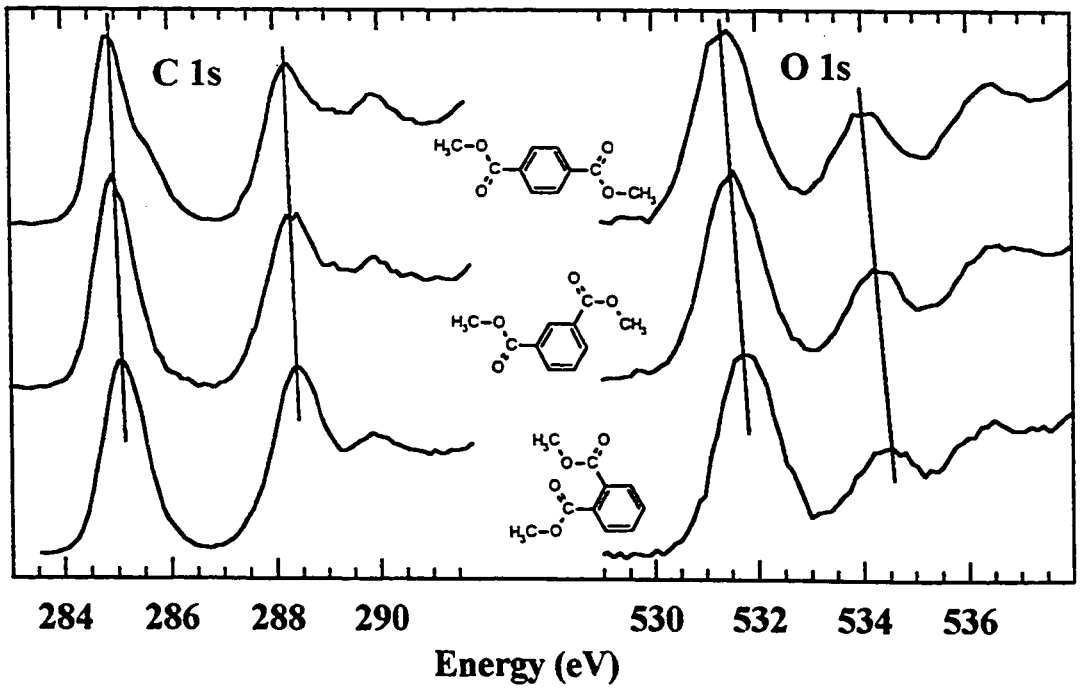

Figure 4.2.3 C 1s and O 1s Inner Shell Electron Energy Loss Spectra (ISEELS) of dimethyl terephthalate (1,4-DMP, top); dimethyl isophthalate (1,3-DMP, middle) and dimethyl phthalate (1,2-DMP; bottom).

groups as a function of ring substitution. To understand the nature of this delocalization, MO calculations are employed (§4.2.3).

A comparison of the C 1s spectra of the polyphthalates and these molecular models is presented and discussed below in §4D. The similarity between the polymer and molecular model spectra is quite good, except for differences that arise from the differing instrumental resolution. These molecular models differ from the polymer structures in their representation of the alkyl component. Because the saturated alkyl linkages act as a "brick wall" with respect to electronic delocalization, adjacent phthalate units in the polymer chain are not expected to interact. The molecules 1,4-DMP, 1,3-DMP and 1,2-DMP are excellent models for the polyphthalate polymers because they account for the relevant extent of delocalization and because they are structurally differentiated from the polymer at the saturated linkage.

§4.2.3 Spectral Interpretation and MO Calculations

A detailed understanding of the spectral features in polyphthalate NEXAFS spectra is important for the effective application of NEXAFS for polymer speciation. Initially, EHMO calculations were used to examine the spectra of PET [UH&96]. The results of EHMO calculations for the C 1s spectrum of 1,4-DMP were presented above in Figure 3.3.2. This EHMO calculation predicted that the splitting of the first C 1s $\rightarrow \pi^*$ band arises from a splitting of the C 1s(C-H) $\rightarrow \pi^*_{C=C}$ transition into two features. This contradicted what had been first assumed - that the higher energy shoulders in the 1,4-DMP $\pi^*_{C=C}$ band originated from a substituent shift (a "C-R" shift). The relative intensity of the two $\pi^*_{C=C}$

components in the EHMO calculation does not match experiment. This difference between the EHMO calculation and experiment is a source of concern since EHMO calculations have a good history of reproducing the character of π^* features in the spectra of unsaturated organic molecules [FH92, FH94, HUR92]. Because of this suspicion, high level *ab initio* improved virtual orbital (IVO) calculations were undertaken for 1,4-DMP, 1,3-DMP and 1,2-DMP. These results are presented in Figure 4 in §4D. The *ab initio*-IVO results reproduce the relative intensities of the π^* band in 1,4-DMP and PET and the energy shifts of the $\pi^*_{C=O}$ features referred to above.

The splitting of the C 1s(C-H) → $\pi^*_{C=C}$ transition in 1,4-DMP and PET is in itself unusual and is deserving of special attention. It is useful to examine the MO character of the optical orbitals for these transitions to better understand the core spectrum. An orbital energy correlation diagram for the LUMO and LUMO+1 of ground state benzene, 1,3-DMP and 1,4-DMP, and the C 1s(C-H) core excited states of 1,3-DMP and 1,4-DMP is presented below (Figure 6, §4D). In benzene, the LUMO level is a degenerate e_{2u} π^* MO. When a core hole is created on a benzene carbon, the degeneracy of the e_{2u} levels is lost. The lower energy e_{2u} orbital has substantial orbital density at the site of the core hole, resulting in a very strong C 1s → π^* feature. The second lowest e_{2u} level of benzene has no orbital density at the site of the core excited atom. When the core hole in the calculation is moved to a different atom position in the benzene ring, the spatial distribution of this e_{2u} orbital changes so that there is no $2p\pi^*$ density at the site of the core hole (i.e. this MO "avoids" the core hole). In 1,4-DMP, the para substitution of the two methyl carboxylate group appears to "pin" the electron distribution of the (LUMO+1) level, such that a

portion of the e_{2u}-derived orbital density remains at the site of the C 1s(C-H) core excited atom. By examining the (LUMO+1) MO of 1,3-DMP, we observe that the corresponding pinning does not occur. This "pinning" is strongly related to the nature of π-delocalization between the phenyl ring and *para* methyl carboxylate substituents. This effect is also observed in the C 1s ISEELS spectrum of para-quinone [FH92]. This is an example of where relatively "long range" effects can modify the otherwise local probe of core excitation spectroscopy.

§4.3 Electronic Delocalization and Spatial Extent of Structural Sensitivity

In the molecular models and polymers examined above, I have examined the core excitation spectra of several previously unstudied functional groups (in particular, urea and carbamate), and the spectra of these functional groups in environments with extensive π-delocalization. π-delocalization adds complexity to the normally "locally" driven interpretation of the core excitation spectroscopy of organic molecules and polymers. I wish to briefly review the aspect of the "size sensitivity" of core excitation and its relation to π-delocalization, from the behaviors of saturated systems, "localized" π-systems, and delocalized π-systems.

The core excitation spectra of saturated molecules and polymers can often be understood from the identity of the atoms in the first coordination shell of the core excited atom. The C 1s → σ* features in the spectrum of the model diisopropyl ether differed from that in the C 1s spectrum of poly(propylene oxide) because the molecular model did not entirely reproduce the next-neighbour environment of the polymer. In saturated polymers,

a "fragment" approach, where the fragment contains the same first coordination shell, is appropriate.

In some instances, π^* features are also relatively localized. The important C 1s(C=O) → $\pi^*_{C=O}$ feature in urea and carbamate differed in energy primarily because of the difference in the carbonyl C 1s binding energy. The carbonyl C 1s → $\pi^*_{C=O}$ energy shift was also observed in the same manner between the simpler molecules urea and urethane (§4C), so this $\pi^*_{C=O}$ is most strongly affected by the local structure and less so by electronic delocalization. In polyphthalates, a model that includes the full extent of the π-delocalization was required, but specifically a model that reproduces the same *pattern* of delocalization. For example, ethyl benzoate was not an adequate model for PET, while 1,4-DMP was adequate.

CHAPTER 4B

Analysis of Polyurethanes Using Core Excitation Spectroscopy. Part I: Model Polyurethane Foam Polymers

The following work documents the C 1s, N 1s and O 1s core excitation spectra of model methylenediphenyldiisocyanate (MDI) polyurethanes and compares these spectra to the core excitation spectra of small molecule analogue species. This work has been published in the Journal of Polymer Science (*J. Polym. Sci: Part B: Polym. Phys.* **33**, 1593, 1995) and is presented here in published form. The right to reprint this article was retained by the author and authorization has been obtained from the coauthors.

The author of this thesis acquired all the gas phase spectra of the small molecule analogues presented in this paper, was a major contributor in developing the analysis of the spectra and helped write the paper in collaboration with Prof. A. P. Hitchcock and Dr. E. G. Rightor. The polymer core excitation spectra were acquired by Dr. E. G. Rightor and Dr. R. D. Leapman.

Analysis of Polyurethanes Using Core Excitation Spectroscopy. Part I: Model Polyurethane Foam Polymers

S. G. URQUHART, A. P. HITCHCOCK,*[1] R. D. LEAPMAN,[2] R. D. PRIESTER,[3] and E. G. RIGHTOR[3]

[1]Institute for Materials Research, McMaster University, Hamilton, Ont., Canada, L8S 4M1; [2]Biomedical Engineering and Instrumentation Program NCRR, National Institutes of Health, Bethesda, Maryland 20892; [3]Dow Chemical USA, Bldg. B-1225, Freeport, Texas 77541

SYNOPSIS

The C 1s, N 1s, and O 1s excitation spectra of model methylenediphenyldiisocyanate (MDI) polyurethanes with well known structures have been recorded using electron energy loss spectroscopy (EELS) in an electron microscope. These spectra are compared to the core excitation spectra of selected small molecule analogue species (recorded by gas phase EELS) in order to identify transitions characteristic of various structural components found in polyurethanes. A more detailed report on the small molecule analogue spectra is presented in the following article. Spectral features characteristic of the different structural components in polyurethanes are identified in the spectra of the model polymers. These can be used as the basis for chemical studies of micron or submicron sized segregated phases in flexible polyurethane polymers. © 1995 John Wiley & Sons, Inc.

Keywords: polyurethanes • phase segregation • analysis by core excitation spectroscopy

INTRODUCTION

Polyurethanes are generally composed of alternating hard- and soft-segment units. The hard segments are composed of isocyanate and/or a chain extender, while the soft segments are composed of long chain polyethers or polyesters. Segregation of the hard segments is believed to provide a high level of cross-linking and to be responsible for the morphology and excellent performance properties of polyurethanes. Many researchers have been involved in characterizing the hard segments in order to provide a better understanding of the relationship between the reaction mixture, the composition of the resultant polymer, and its physical properties. In order to provide a context for the application of new methods for spatially resolved analysis of segregated phases in polyurethanes, it is appropriate to briefly review selected studies on the nature of this segregation.

The chemistry and morphology of polyurethanes can be complex and the use of models has been crucial in previous work. Brunette and co-workers[1] characterized a set of model methylenediphenyldiisocyanate (MDI)/butane diol (BDO)/poly(propylene oxide) (PPO) polymers using dynamic mechanical spectroscopy (DMS), Fourier transform infrared (FTIR), and differential scanning calorimetry (DSC). Their results strongly suggested that the length of the hard segment was important in the phase segregation process. Christenson, Armisted and co-workers[2] used independent model compound studies to support these arguments and highlight the importance of hydrogen bonding. The Miller and Harrell groups have also been actively involved in the correlation of hard segment length and distribution with ultimate polymer performance.[3] More recently Kintaner and co-workers[4] and Okamoto et al.[5] have used deuterium nuclear magnetic resonance (NMR) to study MDI/BDO hard segments. Using deuterium-labeled BDO they were able to observe multiple species of varying crystalline/amorphous nature which provided line shapes and relaxation times characteristic of the hard and soft segments. Blackwell et al.[6] have used single crystal x-ray methods to study a variety of model MDI/diol hard segments. These studies provided average bond lengths, bond angles, and bond torsion angles which

* To whom correspondence should be addressed.

Journal of Polymer Science: Part B: Polymer Physics, Vol. 33, 1583–1602 (1995)
 CCC 0887-6266/95/111583-10

Hard Segment MDI Urethane Polymer (BM)

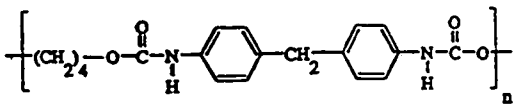

Soft Segment MDI Urethane Polymer (B0)

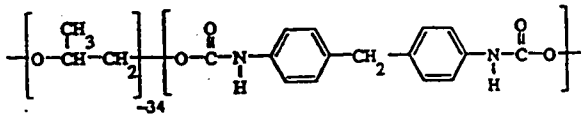

Model MDI-Based Urethane Polymer (B2)

OCN-X-NCO Soft:

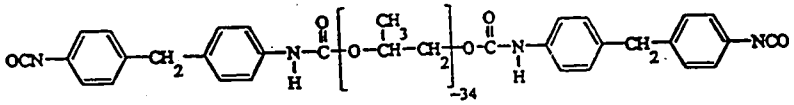

HO-Y-OH Hard:

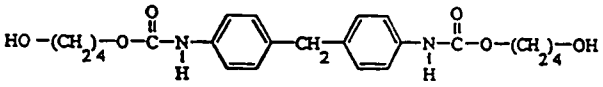

B2

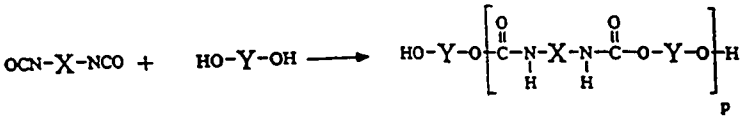

Scheme 1

were generally consistent with the fiber repeat units observed previously. Lastly, Camargo and coworkers[7] have investigated the effect of mixing and catalysis on the phase separation and morphology of MDI/BDO hard segments. Their results were interpreted using simplified phase diagrams which provided an improved understanding of domain evolution. These efforts, in conjunction with many others, have provided a basic level of understanding of phase segregation in polyurethanes. However, a new generation of analytical techniques and investigational approaches are needed to provide additional detail about the composition, purity, and morphology of these hard segment-containing materials. Speciation, as well as compositional information, is required on a spatial scale of 0.1 μm or smaller to fully elucidate the structure–performance relationship.

Spectroscopies involving the excitation and ionization of inner shell (core) electrons are sensitive

to the local environment of the core excited atom[8] and thus have excellent ability to provide speciation information. For this reason, core excitation spectroscopies, such as electron energy loss spectroscopy (EELS)[9-11] or x-ray absorption (NEXAFS) techniques[12-15] have experienced increased usage in the analysis of polymers. When coupled with appropriate instrumentation (electron or soft x-ray microscopes) both EELS and NEXAFS can provide effective analysis at high spatial resolution, as outlined in a recent comparison of EELS and NEXAFS of poly(ethyleneterephthlate) (PET).[16] State-of-the-art spatial resolution of electron microscopes is several orders of magnitude better than that currently available with soft x-ray microscopes and thus it is particularly of interest to investigate the polymer analysis capability of EELS in microscopes. However there are greater radiation damage problems with electron impact than with soft x-ray absorption so it is desirable to investigate both techniques.

The interpretation of core excitation spectra of polymers is a significant challenge. A reasonable understanding of the near edge spectral features is required in order to deduce the local polymer composition from spatially resolved core excitation spectra. Core excitation spectra of gas phase molecules that are analogues to polymer structures (i.e., share common substructures) can be used to provide the appropriate interpretational framework. This approach has been used recently[16,17] to help interpret the C 1s and O 1s spectra of PET recorded using EELS with parallel detection in a transmission electron microscope.

The application of core spectroscopy to the microanalysis of polyurethane foams in particular motivates the selection of samples studied in this work. Polyurethanes based on MDI are commonly found both as elastomers, generally consisting of MDI and BDO, and flexible foams, generally consisting of MDI and polyureas. We now focus on the spectral transitions expected for MDI-based foams which contain variable mixtures of hard and soft segments. The hard segments are composed of MDI-based repeat units such as those in the model polymer BM (scheme A). These segments are relatively rigid because of electron conjugation and hydrogen bonding, which helps drive the organization of the soft and hard segments into a complicated morphology. Soft segment regions are dominated by long chain saturated hydrocarbons or ethers, such as in the model polymer B0. These segments are relatively flexible because of the presence of many different conformations associated with rotation about C—C and C—O single bonds. In MDI polyurethanes, for which B2 is an appropriate model, the soft segments consist of a long chain of isopropyl ether linked to the hard segments by a urethane linkage.

Recently Briggs and Beamson have reported an extensive study of the x-ray photoelectron (ESCA) spectra of polyureas.[18] The present work builds on that study, in particular by investigating the characterization of model polymers related to substructures of water-blown polyurethane. As in earlier studies,[17] comparisons of the core excitation spectra of model polymer and small molecule analogue compounds are required to develop an understanding of how EELS can be used to identify individual components and thus determine how their interactions produce a given morphology. The B0, BM, and B2 polyurethane model compounds (scheme A) were investigated previously by Christenson et al.[2] The present study of the C 1s, N 1s, and O 1s spectra of the B0, BM, and B2 polymer model compounds aids spectral structure correlations and provides a bridge between the small molecule analogues studied by gas phase spectroscopy[19] and studies of phase-segregated polyurethane foams using electron microscope-based EELS or NEXAFS microscopy.[20,21] The focus of this work was to characterize the fine structure in the core edge spectra of polyurethane structures which could be used to identify features in foams. Our experimental setup was optimized for data collection at the C 1s edge, with care taken to minimize radiation damage. The sample thicknesses were not optimal for the weaker N 1s and O 1s edges, and thus the data quality is somewhat lower for these edges. Given this, the comparison to gas phase spectra was helpful for identifying transitions of analytical interest.

The core excitation spectra of model compounds are useful for simulating the spectra of complex molecules and polymers only when the near edge features depend primarily on the local electronic environment of the core excited atom. In a "building block" approach,[12,13] spectra of appropriate small molecule analogues can be added to simulate a complex spectrum. However, in systems with extensive electronic delocalization, the building block model has only limited applicability. Comparisons of the spectra of substituted and unsubstituted molecules along with extended Hückel molecular orbital (EHMO) calculations have been used to characterize the effect of electronic delocalization on the spectra of the small molecule analogues, as described in the following article.[19] The results of the small molecule analogue studies are briefly summarized to form a basis for the inter-

pretation of the spectra of the polyurethane model polymers.

EXPERIMENTAL

Materials

Full details of the preparation and characterization of the model polymer samples have been presented previously.[2] The B2 and BM polymers are solid while the B0 species is a viscous liquid. All three species were dissolved in dimethylformamide and cast on liquid water. A thin film of the polymer was picked up on a holey carbon film. Unsupported polymer areas were used for the parallel-EELS measurements.

Polymer Parallel EELS

Initially EELS spectra were recorded using a JEOL 2000FX transmission electron microscope with a LaB_6 filament and a Gatan 666 parallel-EELS system (as in ref. 17). Under the operating conditions employed, the resolution was 1.2 eV as measured from the full width at half maximum (FWHM) of the elastic peak, which was inadequate to resolve important near edge features expected from the gas phase studies. The present studies were carried out with a scanning transmission electron microscope (STEM) (VG Microscopes model HB501) equipped with a field emission filament and a parallel EELS spectrometer (Gatan Model 666).[22-24] The narrow energy width of the field-emission distribution enabled acquisition of higher quality spectra (0.5 eV FWHM resolution). A vacuum of below 5×10^{-9} mbar was maintained in the specimen chamber. The sample was cooled to 100 K in order to minimize radiation damage during analysis. The spectrometer collection semiangle (β) was 20 mrad and the probe convergence semiangle (α) was 3 mrad.

Suitable areas were selected at low electron dose (< 10 e^-/nm^2) from the annular dark-field STEM image. Spectra were acquired from 5 to 10 μm diameter regions by scanning the specimen at low magnification. In order to achieve optimal energy resolution it was necessary to descan movement of the spectrum over the detector by applying a synchronized voltage to the spectrometer drift tube.[25] In order to minimize radiation damage the probe beam was defocussed to a diameter of about 100 nm during the spectrum acquisition and the beam was rastered over the region of interest so as to achieve a uniform electron dose distribution. The electron dose was approximately 100 e^-/nm^2 for the carbon K-edge and 400 e^-/nm^2 for the oxygen K-edge spectra.

The point spread function of the Gatan parallel detector was deconvoluted from the raw data. This significantly reduced broad tails which were present in the as-recorded data. The deconvoluted spectra were then background subtracted to isolate the signal for a single atomic edge. Plural scattering introduces additional structure in the ionization continuum about 20–25 eV above the onset of the core excitation. This complicates use of atomic cross sections for oscillator strength normalization. In order to allow quantitative comparison of the small molecule and polymer spectra the background subtracted polymer spectra have been normalized at 310 eV in the C 1s, 415 eV in the N 1s, and 550 eV in the O 1s spectra, in the region above the core → valence transitions but before the onset of plural scattering.

Gas Phase EELS

Details of the procedures used to acquire the spectra of the gas phase model compounds are presented in the following article.[19]

RESULTS AND DISCUSSION

Gas Phase Spectra of Small Molecule Analogues

Small model compounds were chosen that reflect the structural and chemical components of MDI polyurethane foams. A comprehensive description of the spectroscopy of these molecules is presented in the following article.[19] The spectra of several compounds that are particularly suitable models for the B0, B2, and BM polymers are presented and discussed briefly. Figure 1 compares the core excitation spectra of gas phase diisopropyl ether, *N*-phenyl urea, and ethyl *N*-phenyl carbamate. Diisopropyl ether is a model for the isopropyl ether chain of the soft segment polyurethane polymer. Ethyl *N*-phenyl carbamate is a model for the phenyl urethane component of the hard segment of the polyurethane polymer. *N*-phenyl urea is also shown to illustrate how EELS can distinguish urethane (carbamate) and urea polymer linkages.

The dominant feature of the C 1s spectra of both phenyl-substituted species is the C 1s(Ph, C—H) → $1\pi^*_{C=C}$ transition at ~ 285 eV which is an unambiguous identifier of the phenyl functional group. The C 1s(C—R) → $1\pi^*_{C=C}$ transition ap-

pears as a small peak at 286.8 eV in the C 1s spectrum of ethyl *N*-phenyl carbamate and as a shoulder at 286.4 eV in the spectrum of *N*-phenyl urea. This feature, which is characteristic of phenyl rings with electronegative substituents, is displaced from the main C 1s(Ph, C—H) → $\pi^*_{C=C}$ transition chiefly by the shift in the ionization potential (IP) at the substitution site. The peak at ~ 290 eV which appears in both urea and carbamate species is primarily the C 1s(C=O) → $\pi^*_{C=O}$, with a minor contribution at lower energy from the C 1s(Ph, C=H) → $2\pi^*_{C=C}$ transition. In the case of ethyl *N*-phenyl carbamate, this feature is at slightly higher energy and it exhibits distinct low energy shoulders, which are attributed to the C 1s(C—R) → $2\pi^*_{C=C}$ and the C 1s(CH_2) → $2\pi^*_{C=O}$ transitions. At higher energies (293–310 eV) there are several broad C 1s → $\sigma^*_{C=C}$ resonances which have the "double-humped" shape characteristic of phenyl groups.

The C 1s spectrum of diisopropyl ether is considerably different from the urea and carbamate spectra. Because of the saturated character of ethers there are no sharp low-lying spectral features. The main spectral intensity (290–294) is associated with broad C 1s → σ^*_{N-C-O} and C 1s → σ^*_{C-C} resonances which are characteristic of saturated species. The shoulders and weak, relatively narrow peaks at ca. 287–290 eV are identified as C 1s → Rydberg transitions.[19] Since Rydberg orbitals overlap and become diffuse in the condensed state, core → Rydberg transitions are not expected to be observable in solid-state spectra of polyethers. Based on these models, it is clear that C 1s spectroscopy can readily distinguish the soft segment polyether structure from the hard segment, carbamate-like structure. With adequate spectral energy resolution it should be possible to use the differences between 286–292 eV to distinguish urea and carbamate based structures.

The N 1s spectra of *N*-phenyl urea and ethyl *N*-phenyl carbamate (Fig. 1) are quite similar to each other. The main intensity (406–415 eV) is associated with N 1s → $\sigma^*_{N-C=O}$ and → σ^*_{N-Ph} resonances. The relatively sharp lines at ca. 404 eV are a combination of several closely spaced N 1s → π^* and weak N 1s → Rydberg transitions. While the latter should not contribute to solid-state spectra, the N 1s → π^*

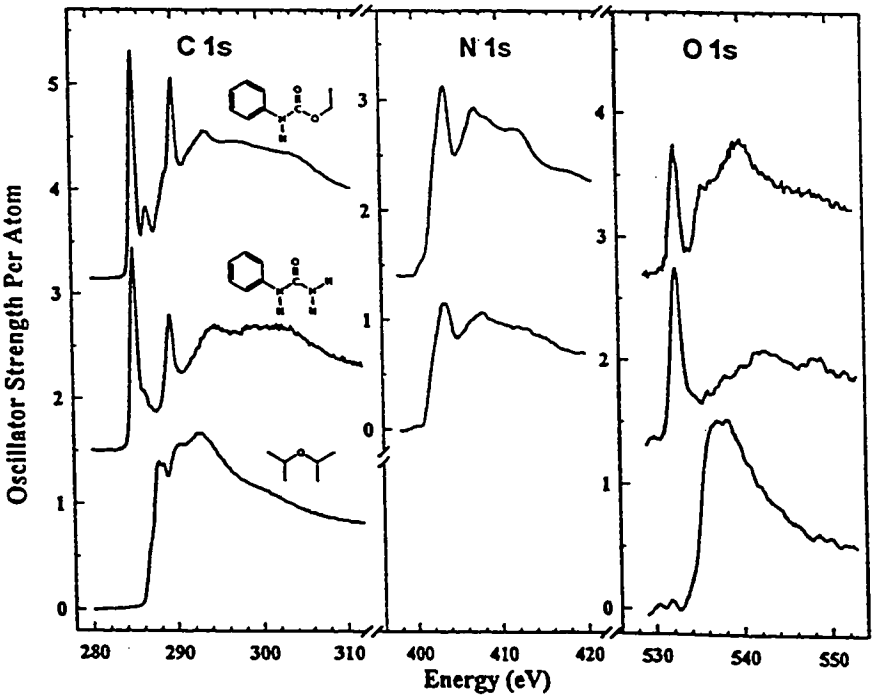

Figure 1. C 1s, N 1s, and O 1s oscillator strength spectra of diisopropyl ether, *N*-phenyl urea, and ethyl *N*-phenyl carbamate, derived from inner shell electron energy loss spectra recorded using 2.5 keV final electron energy, 2° scattering angle, and 0.7 eV FWHM resolution.

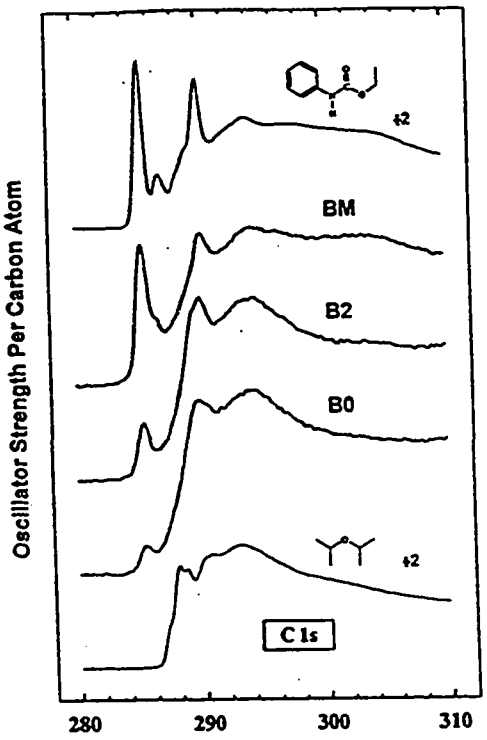

Figure 2. C 1s spectra of the BM, B2, and B0 polymer models for MDI polyurethanes compared to the C 1s spectra of gas phase ethyl *N*-phenyl carbamate and diisopropyl ether. The polymer spectra, which were recorded using parallel EELS, have been background subtracted and normalized to an atomic oscillator strength per carbon atom of 0.0081 eV^{-1} at 310 eV.

features should be detected. In principle the π^* features are of considerable interest since, according to the model compound studies,[19] the spectral detail in this region is sensitive to the extent of delocalization of the phenyl π density onto the N atoms which in turn is controlled by the phenyl twist angle. There are small but identifiable differences between the N 1s spectra of *N*-phenyl urea and ethyl *N*-phenyl carbamate. However, very high quality N 1s spectra of polymers would be required to use these differences to distinguish urea and carbamate components. This will be difficult because of the very low N atom density and the multiplicity of possible environments associated with varying degrees of hydrogen bonding in real polyurethane polymers.

The O 1s spectra of diisopropyl ether, *N*-phenyl urea, and ethyl *N*-phenyl carbamate presented in Figure 1 illustrate that O 1s spectroscopy provide perhaps the easiest means to distinguish various polyurethane structures. As at the C 1s edge, hard and soft segments are easily distinguished by the presence or absence of the intense, sharp $\pi^*_{C=O}$ resonance at 533 eV. In addition, the O 1s spectra of the carbamate differs considerably from that of the urea since the carbamate contains O 1s(C—O) → $\pi^*_{C=O}$ transitions at 536 eV and a broad C1s(C—O) → σ^*_{C-O} resonance at 540 eV whereas the main feature in the same region of the O 1s spectrum of *N*-phenyl urea is the O 1s(C=O) → $\sigma^*_{C=O}$ resonance at 542 eV. The *N*-phenyl urea O 1s spectrum is much simpler than that of ethyl *N*-phenyl carbamate because there is only one oxygen environment. As at the C 1s edge, the O 1s spectrum of diisopropyl ether does not contain any strong features below the IP but rather it is dominated by the broad σ^*_{C-O} resonance.

Core Excitation Spectra of Model Polymers

C 1s Spectra of BM, B2 and B0

The C 1s spectra of the BM, B2, and B0 model polymers recorded by parallel-EELS are presented in Figure 2. The C 1s spectra of diisopropyl ether and ethyl *N*-phenyl carbamate are also plotted as models

Table I. Energies and Proposed Assignments for the C 1s Spectral Features of BM, B2, and B0 Model Polyurethane Polymers

Energy (eV)			Assignment			
BM	B2	B0	Ph(C—H)	Ph(C—N)	C=O	C—O
285.3	285.4	285.3	$1\pi^*_{C=C}$*			
286.4 (sh)				$1\pi^*_{C=C}$		
290.0	290.0	290	$2\pi^*_{C=C}$*		$\pi^*_{C=O}$	$\pi^*_{C=O}$
294	294	294	σ^*_{C-C},$\sigma^*_{C=C}$(1)	σ^*_{C-C},$\sigma^*_{C=C}$(1)		σ^*_{C-O}
394	304		$\sigma^*_{C=C}$(2)	$\sigma^*_{C=C}$(2)	$\sigma^*_{C=O}$	

* $1\pi^*_{C=C}$ corresponds to the e_{1u} π^* orbital, while $2\pi^*_{C=C}$ corresponds to the b_{2g} π^* orbital in benzene.

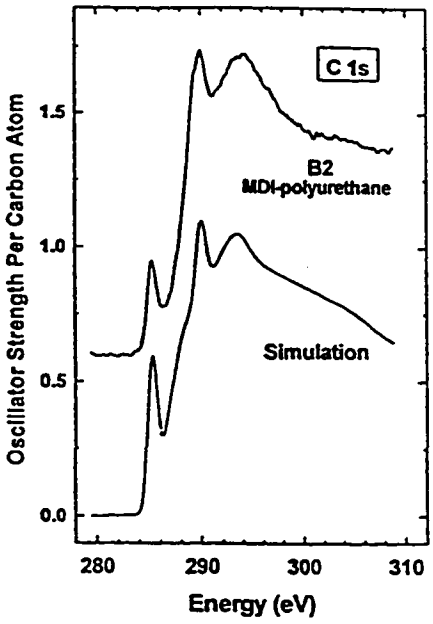

Figure 3. C 1s spectrum of B2 compared to a simulation constructed from the sum of 17 times the spectrum of diisopropyl ether and 12 times that of ethyl *N*-phenyl carbamate (with correct per-molecule rather than per-atom intensity normalization). After constructing the simulation, the result was smoothed until the width of the $\pi^*_{C=C}$ peak matched that of B2.

for the ether component of the soft segment and the MDI bis(ethylurethane) unit which dominates the hard segment. Energies and tentative assignments of the spectral features are presented in Table I. There are clearly systematic changes in the C 1s spectra of these model polymers. The first peak (ca. 285 eV) increases in intensity from B0 through B2 to BM. In addition, there are changes in the region between 288 and 300 eV. The evolution of these features and the correlation with changes in the polymer structure can be understood through comparison to the small molecule spectra.

In each unit of BM, there are 12 phenyl carbons, 5 saturated carbons, and 2 carbonyl carbons (see scheme A). The C 1s spectrum of BM reflects this mixture as deduced by comparison to the C 1s spectrum of ethyl *N*-phenyl carbamate, the closest small molecule analogue among the species we have studied. The spectra of B2 and B0 are modified from that of BM by the addition of features characteristic of the polyether soft segment. The sharp feature observed at about 285 eV in the C 1s spectra of all three model polymers is clearly the C 1s(Ph, C—H) → $\pi^*_{C=C}$ transition at the phenyl rings, which occurs at the same energy as the corresponding transition in ethyl *N*-phenyl carbamate. The shoulder at 286.5 eV in BM is attributed to the C 1s(C—R) → $1\pi^*_{C=C}$ excitation. The corresponding feature in B2 and B0 is masked by the additional ether spectral components. The sharp structure and accompanying low energy shoulder which is observed prominently at around 290 eV in BM, more weakly in B2, and with little contrast in B0, is attributed to a mixture of transitions of which the C 1s(C=O) → $\pi^*_{C=O}$ transition is the origin of the sharpest component. The broad features at 294 and 304 eV are σ^* resonances in the characteristic benzenoid "double-humped" pattern.

B0, the soft segment model polymer, consists mostly of isopropyl ether groups terminated by MDI. Its C 1s spectrum is much closer to that of diisopropyl ether than that of ethyl *N*-phenyl carbamate, although the 285 eV feature associated with the MDI aromatic rings remains visible. The continuum is dominated by the σ^*_{C-C} resonance at 293 eV. The $\pi^*_{C=O}$ and higher energy σ^* contributions are very weak. Note that while ethyl *N*-phenyl carbamate and diisopropyl ether were selected as the small molecule analogues for the hard and soft segments, respectively, the study of a range of molecules in each of the ether, urea and carbamate classes[19] has greatly contributed to the confidence of both our comparison and spectral interpretation.

B2 has structural components of both BM and B0. Thus its spectrum is expected to have aspects similar to the spectra of both BM and B0 as well as the small molecule analogues. Figure 3 compares the C 1s spectrum of the B2 model polyurethane to a simulation constructed from a sum of the C 1s EELS spectra of diisopropyl ether and ethyl *N*-phenyl carbamate with proportions chosen according to the stoichiometry of B2. There is a strong correspondence between the simulation and the experimental spectrum. Relative to the experimental spectrum,

Table II. Intensities of the C 1s → $\pi^*_{C=C}$ Transition on BM, B2, and B0

Species	I(π^*)[a]	Relative C1s(Ph)[b]	Ratio[c]
BM	1.16(4)	0.63	1.8(1)
B2	0.39(3)	0.33	1.2(1)
B0	0.21(3)	0.12	1.7(2)

[a] Intensity based on normalization at 310 eV to 0.0081 eV^{-1} (atomic value).
[b] Number of phenyl carbon atoms divided by total number of carbon atoms in the repeat unit.
[c] Ratio of column 2/column 3.

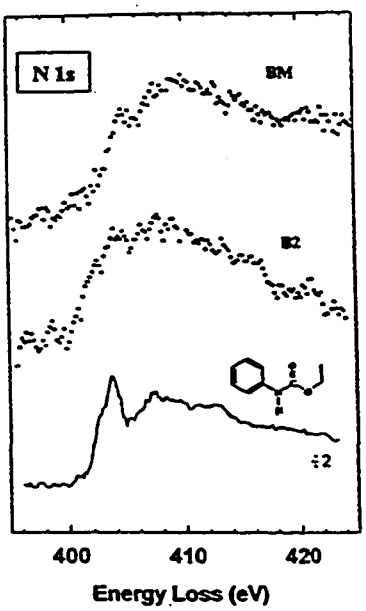

Figure 4. N 1s spectra of BM and B0 recorded by parallel-EELS, compared to the N 1s spectrum of ethyl *N*-phenyl carbamate. The polymer spectra have been background subtracted and normalized to an atomic oscillator strength per nitrogen atom of 0.0058 eV^{-1} at 415 eV.

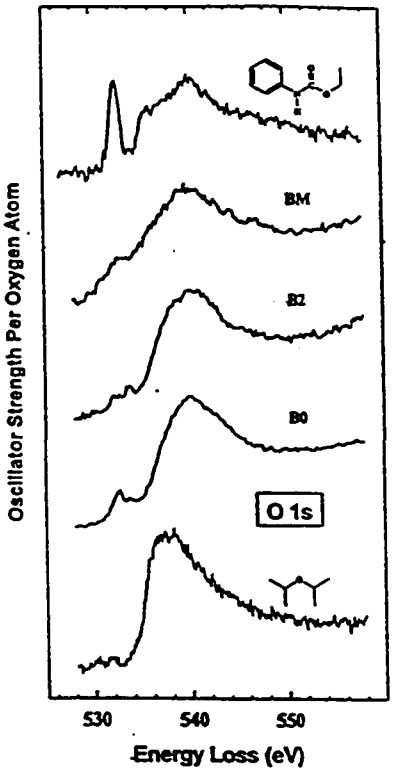

Figure 5. O 1s spectra of BM, B2, and B0 recorded by parallel-EELS, compared to the O 1s spectra of gas phase ethyl *N*-phenyl carbamate and diisopropyl ether. The polymer spectra have been background subtracted and normalized to an atomic oscillator strength per oxygen atom of 0.0048 eV^{-1} at 550 eV.

the simulation exhibits excess signal between ~ 287 and ~ 289 eV which arises from the C 1s → Rydberg transitions in the C 1s spectrum of gas phase diisopropyl ether. As expected, Rydberg transitions are not seen in the condensed state. The first feature of the B2 spectrum is clearly the C 1s(Ph, C—H) → $1\pi^*_{C=C}$ transition. The C 1s(C—R) → $1\pi^*_{C-C}$ contribution which is expected at 287.4 eV,[19] is not resolved, probably because it is obscured by the onset of the strong σ^*_{C-C} and σ^*_{C-O} features at higher energy. The broad peak at ~ 294 eV in B2 arises from the C 1s(CH_x) → $\sigma^*_{C-C}/\sigma^*_{C-O}$ transitions. Its position is slightly lower than that of the maximum in the simulation, perhaps reflecting changes in the chemical environment of the ether carbons due to the extended chain structure of the polymer.

The intensities of corresponding C 1s spectral features in BM, B0, and B2 can be used to estimate the relative functional group composition. Accurate spectral normalization is essential for a valid quantification. As summarized in Table II, the decrease in the intensity of the C 1s(Ph, C—H) → $1\pi^*_{C=C}$ transition in the sequence BM, B2, B0 approximately tracks the changing stoichiometric ratio of phenyl to nonphenyl carbons.

Table III. Energies and Proposed Assignments for the N 1s Spectral Features of BM and B2 Model Polyurethane Polymers

Energy (eV)		
BM	B2	Assignment
403.5	403.8	π^*
408(2)	408(2)	σ^*_{C-N}

N 1s Spectra of BM and B2

The N 1s spectra of the BM (hard segment model) and B2 (model MDI-polyurethane polymer) are compared with the N 1s spectrum of ethyl *N*-phenyl carbamate in Figure 4. The energies and tentative assignments of the spectral features of the two polymer species are presented in Table III. The present

Table IV. Energies and Proposed Assignments for the O 1s Spectral Features of BM, B2, and B0 Model Polyurethane Polymers

Energy (eV)			Assignment	
BM	B2	B0	O 1s(C=O)	O 1s(C—O)
	532.1	532.6	$\pi^*_{C=O}$	
534.0(4)	533.7	533.8		$\pi^*_{C=O}$
	538 (sh)	537 (sh)		σ^*_{C-O}(ether)
541.5	540	540		σ^*_{C-O}(carbamate)
548(2)			$\sigma^*_{C=O}$	

experimental conditions limit the statistical precision that can be achieved in these spectra because it is necessary to keep the total dose below ~ 400 e^-/nm^2 to avoid radiation damage. This dose limitation is not such a problem for the C 1s spectra because of the much larger atomic fraction and the higher ionization cross section for carbon relative to nitrogen. In fact, for B0 with a nitrogen atomic fraction of < 0.02, it was not possible to discern the N 1s fine structure, although a weak nitrogen core edge was observed. For BM and B2 it is possible to distinguish the π^* resonance with reasonable confidence. However, the π^* resonance is less well resolved in the polymer spectra than in the N 1s spectrum of ethyl *N*-phenyl carbamate. In part this can be attributed to broadening by the detector point-spread function.[26] No attempt was made to correct for this by deconvolution because of the high noise level.

In the future, schemes may be available for improving the counting statistics by averaging noisy spectra recorded over extended regions of the specimen.[25] The use of cooled charge couple device (CCD) arrays with higher detective quantum efficiency is expected to provide a further improvement in spectral quality. This is important because considerable detailed information is potentially available from the N 1s spectra. For example, the width of the N 1s → π^* transition may reflect variation in hydrogen bonding. Hydrogen bonding can force a nonplanar geometry, thereby reducing conjugation with the phenyl ring and resulting in a weaker and higher energy shifted N 1s → π^* structure. The sensitivity of N 1s → π^* transitions to the twist angle about the N atom is explored using extended Hückel calculations in the following article.[19]

O 1s Spectra of BM, B2, and B0

Useful information about the ratio of ether and carbamate components is available from oxygen 1s spectra. The O 1s spectra of BM, B2, and B0 are presented in Figure 5 in comparison with the O 1s spectra of ethyl *N*-phenyl carbamate and diisopropyl ether. Energies and tentative assignments of the spectral features are presented in Table IV. The polymer spectra are all dominated by the σ^* resonance at 540–541 eV associated with the polyether components. In addition, the spectra of all three polymers exhibit weak π^*_{C-O} structures between 532 and 534 eV. The π^*_{C-O} is more intense in the spectrum from BM than in B2 or B0, consistent with the greater amount of carbonyl oxygen in the former compound. However, the amplitude of the π^*_{C-O} peak is much smaller than in ethyl *N*-phenyl carbamate, even in the case of BM which should have approximately the same carbonyl content. This result may be due to preferential radiation damage of the carbonyl groups even at the low electron dose of 400 e^-/nm^2 that was used to record the present data. It is known that oxygen is particularly sensitive to radiation damage by fast electrons.[27] Again, improved detectors and acquisition techniques should eventually allow more reliable O 1s spectra to be collected.

SUMMARY

The core excitation spectra of three polymers which are models for phase-segregated MDI polyurethane foams have been reported and analyzed by comparison to the spectra of gas phase model compounds. This evaluation of the polymer spectra has provided insights into spectral-structure relationships for polyurethane systems. Core excitation spectroscopy carried out in electron, or x-ray microscopes,[21] can obtain chemical information from submicron segregated phases in polyurethanes which provides a useful new tool for studying these materials. Core excitation spectromicroscopy, along with results

from several complementary methods, are being combined with the wealth of previously obtained information in order to improve the understanding of the mechanism of phase segregation and its influence on physical properties in these complicated systems.

This research has been supported by Dow Chemical U.S.A. and the Natural Science and Engineering Research Council of Canada. S.G.U. thanks Dr. Ed Rightor for helpful guidance and Dow Chemical for its financial support. Additionally, the authors thank Bob Turner, Gene Young, John McClusky, Chester Norman, and Chris Christenson for helpful discussions, sample preparation, and support. We also thank Stanley Sun (NIH) for assistance with the EELS experiments.

REFERENCES AND NOTES

1. C. M. Brunette, S. L. Hsu, and W. J. MacKnight, *Macromolecules*, **15**, 71 (1982).
2a. C. P. Christenson, M. A. Harthcock, M. D. Meadows, H. L. Spell, W. L. Howard, M. W. Creswick, R. E. Guerra, and R. B. Turner, *J. Polym. Sci. B: Polym. Phys.*, **24**, 1401 (1986).
2b. J. Armisted, G. Wilkes, and R. Turner, *J. Appl. Polym. Sci.*, **35**, 601 (1988).
3a. J. A. Miller, S. B. Lin, K. K. S. Hwang, K. S. Wu, P. E. Gibson, and S. L. Cooper, *Macromolecules*, **18**, 32 (1985).
3b. L. L. Harrell, *Macromolecules*, **2**, 607 (1969).
4. A. Kintanar, L. W. Jelinski, I. Gancarz, and J. T. Koberstein, *Macromolecules*, **19**, 1876 (1986).
5. D. T. Okamoto, E. M. O'Connell, S. L. Cooper, and T. W. Root, *J. Polym. Sci. B: Polym. Phys.*, **31**, 1163 (1993).
6. J. Blackwell, J. R. Quay, and M. R. Nagarajan, *J. Polym. Sci. B: Polym. Phys.*, **22**, 1247 (1984).
7. R. E. Camargo, C. W. Macosko, M. V. Tirrell, and S. T. Wellinghoff, *Polym. Eng. Sci.*, **22**, 719 (1982).
8. A. P. Hitchcock, *Physica Scripta*, **T31**, 159 (1990).
9. J. Fink, *Z. Phys. B*, **61**, 463 (1985); J. Fink, B. Scheerer, W. Wernet, M. Monkenbusch, G. Wegner, H.-J. Freund, and H. Gonska, *Phys. Rev. B*, **34**, 1101 (1986); F. Hofer, W. F. Geymeye, and E. Ingolic, *Proc. XI Int. Cong. Electron Microscopy* Kyoto, 1986, p. 323.
10. J. J. Ritsko, L. J. Brillson, R. W. Bigelow, and T. J. Fabish, *J. Chem. Phys.*, **69**, 3931 (1978); J. J. Ritsko and R. W. Bigelow, *J. Chem. Phys.*, **69**, 4162 (1978).
11. G. Crecelius, J. Fink, J. J. Ritsko, M. Stamm, H. J. Freund, and H. Gonska, *Phys. Rev. B*, **28**, 1802 (1983).
12. D. C. Koningsberger and R. Prins, Eds., *X-Ray Absorption Spectroscopy*, Wiley, New York, 1988; J. Stöhr, *NEXAFS Spectroscopy*, Springer Ser. Surf. Sci., Springer-Verlag, Heidelberg, 1992.
13. D. A. Outka and J. Stöhr, in *Chemistry and Physics of Solid Surfaces*, Springer Ser. Surf. Sci. 10, R. Vanselow and R. Howe, Eds., Springer, Berlin, 1988, p. 201.
14. J. L. Jordan-Sweet, C. A. Kovac, M. J. Goldberg, and J. F. Morar, *J. Chem. Phys.*, **89**, 2482 (1988); T. Ohta, K. Seki, T. Yokoyama, I. Morisada, and K. Edamatsu, *Phys. Scripta*, **41**, 150 (1990); E. Umbach, *Prog. Surf. Sci.*, **35**, 113 (1990).
15. H. Ade, X. Zhang, S. Cameron, C. Costello, J. Kirz, and S. Williams, *Science*, **258**, 972 (1992).
16. E. G. Rightor, G. Mitchell, D. Fischer, A. P. Hitchcock, S. G. Urquhart, and R. D. Leapman, to be submitted.
17. A. P. Hitchcock, S. G. Urquhart, and E. G. Rightor, *J. Phys. Chem.*, **96**, 8736 (1992); E. G. Rightor, G. P. Young, S. G. Urquhart, and A. P. Hitchcock, *Microscopy: The Key Research Tool*, **22**, 67 (1992).
18. D. Briggs and G. Beamson, *Anal. Chem.*, **65**, 1517 (1993).
19. S. G. Urquhart, A. P. Hitchcock, E. G. Rightor, and R. D. Priester, *J. Polym. Sci. B: Polym. Phys.*, **33**, 1994.
20. H. Ade, K. Zhang, S. Cameron, G. Costello, J. Kirz, and S. Williams, *Science*, **258**, 972 (1992); H. Ade and B. Hsiao, *Science*, **262**, 1429 (1993).
21. H. Ade, A. P. Smith, S. Cameron, R. Cieslinski, B. Hsiao, G. Mitchell, E. Rightor, *Polymer* (submitted).
22. O. L. Krivanek, C. C. Ahn, and R. B. Keeney, *Ultramicroscopy*, **22**, 103 (1987).
23. O. L. Krivanek, J. H. Paterson, and H. R. Poppa, in *Proc. 47th Annual Meeting Elect. Micros. Soc. Am.*, G. W. Bailey, Ed., San Francisco Press, San Francisco, 1989, p. 410.
24. R. D. Leapman and S. B. Andrews, *J. Microsc.*, **161**, 3 (1991).
25. J. A. Hunt, R. D. Leapman, and D. B. Williams, *Microbeam Anal.*, **2**, 272 (1993).
26. R. F. Egerton, Y.-Y. Yang, and S. C. Cheng, *Ultramicroscopy*, **48**, 239 (1993).
27. B. J. Ciliax, K. L. Kirk, and R. D. Leapman, *Ultramicroscopy*, **48**, 13 (1993).

Received August 4, 1994
Revised December 2, 1994
Accepted January 25, 1995

CHAPTER 4C

Analysis of Polyurethanes Using Core Excitation Spectroscopy. Part II: Inner-Shell Spectra of Ether, Urea and Carbamate Model Compounds

The following work documents the C 1s, N 1s and O 1s core excitation spectra of a series of ether, urea and carbamate molecules, and the use of Extended Hückel Molecular Orbital (EHMO) calculations for interpreting these spectra. This work has been published in the Journal of Polymer Science (*J. Polym. Sci: Part B: Polym. Phys.* **33**, 1603, 1995.) and is presented here in published form. The right to reprint this article was retained by the author and authorization has been obtained from the coauthors.

The author of this thesis performed the experimental work and calculations presented in this paper, was a major contributor in developing the spectral analysis, and wrote the bulk of the paper in collaboration with Prof. A. P. Hitchcock and Dr. E. G. Rightor.

Analysis of Polyurethanes Using Core Excitation Spectroscopy. Part II: Inner Shell Spectra of Ether, Urea and Carbamate Model Compounds

S. G. URQUHART,[1] A. P. HITCHCOCK,*[1] R. D. PRIESTER,[2] and E. G. RIGHTOR[2]

[1]Institute for Materials Research, McMaster University, Hamilton, Ont., Canada, L8S 4M1; [2]Dow Chemical U.S.A., Bldg. B-1225, Freeport, Texas 77541

SYNOPSIS

Core excitation spectra of selected small molecule analogue species have been acquired to assist interpretation of the core excitation spectra of model methylenediphenyldiisocyanate (MDI) polyurethane polymers. Oscillator strength spectra for C 1s and O 1s core excitation of diethyl ether and diisopropyl ether; C 1s, N 1s, and O 1s core excitation of urea, *N*-phenyl urea, *N,N'*-diphenyl urea, ethyl carbamate, *N*-phenyl carbamate, *N*-phenyl *N*-methyl carbamate, and benzyl carbamate have been derived from gas phase electron energy loss spectra (EELS). Extended Hückel Molecular Orbital (EHMO) calculations are used to assist assignment and to interpret the effect of π-electron delocalization on the gas phase spectra. Functional group identification by core excitation is explored for the purpose of using core excitation spectra for microanalysis of polyurethane polymers. © 1995 John Wiley & Sons, Inc.

Keywords: polyurethanes • core excitation spectroscopy • NEXAFS • EELS • EHMO • molecular models of polymer subunits

INTRODUCTION

Part I of this series of articles[1] explored the use of core excitation spectroscopy for compositional analysis of polyurethane polymers. In particular, transitions characteristic of various functional groups were identified in order to gain insight into how spatially resolved core excitation spectroscopy could be used to identify segregated species in polyurethane foams. Compositional information is required to provide an improved understanding of phase separation processes in polyurethanes and to assist in the correlation of phase separation effects with ultimate polymer performance. Core excitation spectroscopy[2] is well suited to this sort of problem since the spectral features are very sensitive to local chemical structure and since very high spatial resolution can be obtained in electron or soft x-ray microscopes.

The use of core excitation spectroscopy to study polymers of an unknown composition is greatly facilitated by complementary studies of related gas phase molecular compounds. First, such studies help to identify potential problems of radiation damage. Second, EELS spectra of gas phase molecules that are analogues to polymer structures can assist in the development of correct interpretations of polymer spectra. This approach has been used recently[3] in studying the C 1s and O 1s spectra of poly(ethylene terephthalate) (PET) recorded using EELS with parallel detection in a transmission electron microscope.[4] The selection of molecules studied here is motivated by their application as models for microanalysis of polyurethane foam polymers, in particular, those based on 4,4'-methylenediphenyldiisocyanate (MDI). The chosen model compounds reflect the carbamate, urea, and ether chain elements of these polymers.[5] Figure 1, which includes some of the data presented in part I, illustrates the rele-

* To whom correspondence should be addressed.

Journal of Polymer Science: Part B: Polymer Physics, Vol. 33, 1603-1620 (1995)
 CCC 0887-6266/95/111603-18

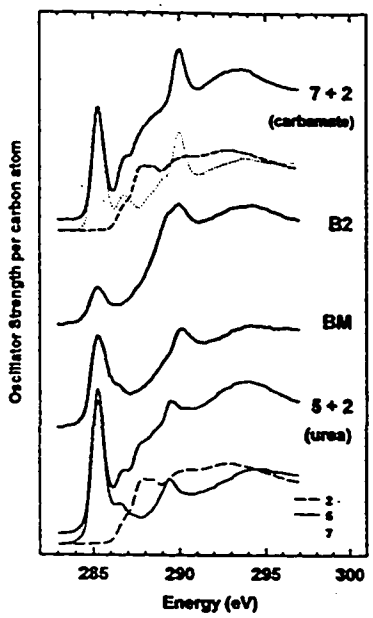

Figure 1. Comparison of the C 1s spectra of MDI-polyurethane polymer models (B2—mixed hard, soft segment species; BM—carbamate hard segment) with simulations of a mixed hard-soft segment based on sums of the spectra of di-isopropyl ether (2), phenyl carbamate (7) (upper curve), and diphenylurea (5) (lower curve). The dashed lines indicate the di-isopropyl ether, phenylcarbamate, and diphenylurea spectra used in the simulation. A 1 : 1 composition was assumed for the simulation.

vance of these model compound studies to polymer microanalysis. One concern in polyurethane analysis is the ability to distinguish urea and carbamate components, even when they are present as only a fraction of a given micro-region of a polymer sample. As Figure 1 illustrates, comparisons of polymer spectra with simulations generated from the spectra of model compounds can be very useful in evaluating the capability of core excitation to make this distinction. The composition of the B2 and BM model polymer materials is given in part I.[1] There is a better match of the polymer $\pi^*_{C=O}$ resonance at 290 eV to that in the carbamate-based simulation than to that in the urea-based simulation. While the composition of the B2 and BM polymer models was known before this investigation, Figure 1 demonstrates that C 1s spectra can differentiate urea and carbamate functionalities which may be present in poorly characterized complex polymers.

It is useful to measure and analyze the spectra of a variety of urea and carbamate compounds in order to develop a valid understanding of the relationship between a given molecular structure and the appearance of its associated core excitation spectrum. An important aspect of the differences in urea and carbamate spectra is the nature of the electronic delocalization between the phenyl ring and the urea or carbamate group. Both chemical series and semi-empirical calculations have been used to investigate this. From a wider range of small molecule models that were studied, this article reports the C 1s and O 1s spectra of diethyl ether (1) and diisopropyl ether (2); and the C 1s, N 1s, and O 1s spectra of urea (3); *N*-phenyl urea (4); *N,N'*-diphenyl urea (5); ethyl carbamate (6); ethyl *N*-phenyl carbamate (7); ethyl *N*-methyl *N*-phenyl carbamate (8); and benzyl carbamate (9) (code numbers refer to scheme A). The numerical codes are used as labels for the molecules throughout the text.

When the core excitation spectrum depends primarily on the immediate environment of the core excited atom, the spectra of model compounds can be used to provide useful simulations of the spectra of complex molecules and polymers. In this so-called "building block" approach[6,7] spectra of appropriate small molecule analogues can be summed to simulate the spectrum of a more complex material such as a multicomponent polymer. In molecules with extensive electronic delocalization, the building block model may have limited applicability. Quantum chemical calculations such as the extended Hückel molecular orbital (EHMO) scheme, are particularly important for spectral interpretation in such cases. The EHMO results help to interpret the core spectra of the phenyl-substituted small molecule analogues and provide additional insight into the relationship between core excitation spectral features and molecular structure.

EXPERIMENTAL

Materials

The small molecule model samples were all obtained commercially from Aldrich, except for ethyl *N*-phenyl carbamate (7) (Accurate Chemical). All samples were 99% stated purity, except for *N*-methyl *N*-phenyl carbamate (8) (96%), *N,N'*-diphenyl urea (5) (98%), and *N*-phenyl urea (4) (97%). *N*-methyl *N*-phenol carbamate (9) was vacuum distilled before use. All other samples were used without further purification.

Ethers

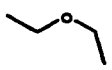

(1) Diethyl ether

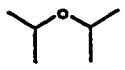

(2) Diisopropyl ether

Ureas

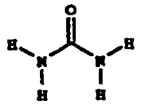

(3) Urea

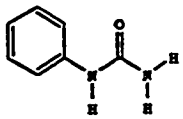

(4) N-phenyl urea

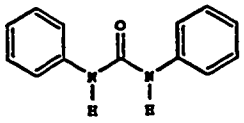

(5) N,N'-diphenyl urea (carbanilide)

Carbamates

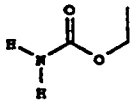

(6) Ethyl Carbamate (urethane)

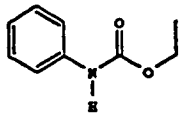

(7) Ethyl N-phenyl Carbamate (phenyl urethane)

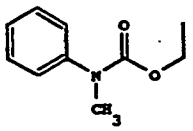

(8) Ethyl N-methyl, N-phenyl carbamate

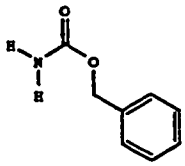

(9) Benzyl Carbamate

Scheme A

Gas Phase EELS

The inner shell electron energy loss spectra (IS-EELS) were recorded using the McMaster gas phase spectrometer,[8] operated under inelastic scattering conditions under which electric dipole transitions dominate. The final electron energy was 2.5 keV, the scattering angle was 2°, and the resolution was 0.7 eV full width half maximum (FWHM).

In order to obtain an adequate vapor pressure of low volatility compounds the spectrometer uses an internally mounted quartz-halogen bulb to heat the gas cell. Water-cooled plates at either end of the gas cell reduced sample migration and deposition beyond the gas cell region. Even with these condensation plates there was a gradual buildup of insulating deposits on the electron optics which eventually degraded the spectrometer performance. Small amounts (ca. 50 mg) of these compounds were placed in an aluminum tube attached directly to the gas cell. Compounds (3–7, 9) were run in this manner. The more volatile samples, (2, 3, and 8) were introduced into the gas cell through a leak valve.

Multiple spectra were obtained to confirm reproducibility and to check for impurity contributions or the onset of decomposition at higher heating temperatures. Absolute energy scales were established by recording the spectrum with a stable mixture of the analyte and a standard calibrant species (CO_2, CO, O_2, or N_2,[9] as documented in the tables of spectral data assignments). The as-recorded spectra were converted to absolute oscillator

Table I. Molecular Geometries used for EHMO Calculations

Parameter	3[a]	4[b]	5[b]	6[c]	7[c]
$R_{C=O}$(Å)	1.21	1.208	1.208	1.223	1.223
R_{C-N}(Å)	1.37	1.358	1.358	1.344	1.344
R_{N-H}(Å)	0.99	0.96	0.96	0.99	0.99
R_{N-Ph}(Å)	—	1.374	1.374	—	1.374
$R_{C=C}$(Å)	—	1.39	1.39	—	1.39
R_{C-H}(Å)	—	0.95	0.95	1.08	1.08
$R_{(CO)-O}$(Å)	—	—	—	1.348	1.348
R_{C-C}(Å)	—	—	—	1.514	1.514
R_{O-CH_2}(Å)	—	—	—	1.454	1.454
∠(OC—N)	123°	124.2°	124.2°	125°	125°
∠(CN—H)	112°	115.4°	115.4°	120°	120°
∠(CN—Ph)	—	128.2°	128.2°	—	128.2°
∠(HN—H)	131°	—	—	131°	—
∠(C—C—C)	—	120°	120°	—	120°

[a] Estimated from crystalographic[37] and calculated geometries.[38] A planar structure was assumed.
[b] Estimated from solid-state crystalographic data[38] and molecular mechanic (MM2) calculations.[38] The amide and phenyl rings are assumed to lie in the same plane. The crystalographic study[38] has shown that the phenyl and amide moieties are planar individually in the solid state, but that the phenyl rings are twisted 36–43° about the N—Ph bond. The molecular mechanic study[38] predicted a twist of 2° in the gas phase.
[c] Derived from an ab initio structure optimization using a 6-31G* basis set.[39]

strengths using procedures discussed and tested previously.[10] This involved subtraction of a background generated by extrapolation of a fit of the pre-edge experimental data to the function $a(E-b)^c$ (a, b, c are fitted parameters) in order to isolate the signal associated with a particular core edge. The background subtracted spectra were corrected for the kinematic factor connecting energy loss and photoabsorption intensities[11] and then normalized to an absolute oscillator strength scale by calibrating the intensity of the nonresonant ionization continuum of the analyte spectrum to that of tabulated atomic continuum oscillator strengths.[12]

EHMO Calculations

Spectral assignments have been assisted by comparisons to semiempirical extended Hückel molecular orbital (EHMO) calculations of urea (3), *N*-phenyl urea (4), *N,N'*-diphenyl urea (5), ethyl carbamate (6), ethyl *N*-phenyl carbamate (7), and formamide. The default parameters of the EHMO program[13] were used. The molecular geometries are outlined in Table I. The procedures we use to apply EHMO to core excitation spectroscopy have been documented in earlier studies of organometallic,[14-16] conjugated organic,[17] and polymer analogue molecules.[2]

Predictions of core excitation spectra were generated from the EHMO output using the equivalent ionic core virtual orbital model (EICVOM) procedures described previously.[2,15-17] Briefly, a calculation is performed on a singly charged molecule in which the core excited atom is replaced with the Z + 1 atom—for example the C 1s spectrum of the ring-substitutional site in *N*-phenyl urea (C 1s(C-R)) is derived from the EHMO calculation for singly charged *N*-phenyl urea modified by replacing the substituted ring carbon with an N atom. The energies of virtual molecular orbitals (VMO) of this EICVOM species are assumed to be related to the position of the core excitation spectral lines. For each VMO a spectral peak is generated with an area given by $\Sigma c^2(2p)$, where $c(2p)$ is the LCAO coefficient of the $2p$ atomic orbital density on the core excited atom in that VMO. The peak is given a Gaussian line shape with a width which depends on the orbital energy in a manner which approximates experimental trends in increasing linewidth with increasing core excited state energy. The linewidths were 0.6 eV FWHM for orbitals of $\epsilon < -2$ eV; 4.0 eV for $-2 < \epsilon < 2$ eV; 6.0 eV for $2 < \epsilon < 5$ eV; and 12 eV for $\epsilon > 5.0$ eV. The individual gaussian lines are summed to form the predicted spectrum for core excitation at a single site. The predicted spectra over all sites

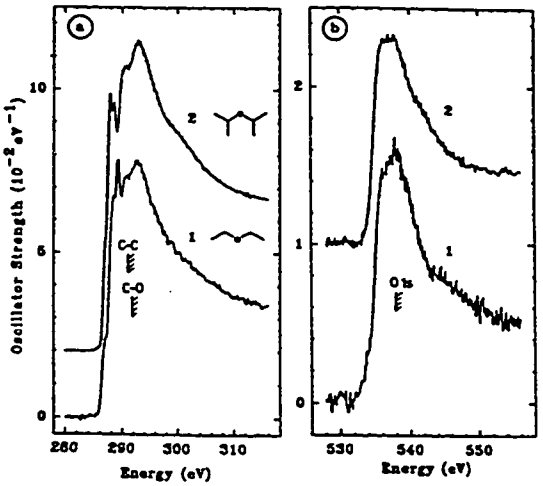

Figure 2. (a) C 1s and (b) O 1s oscillator strength spectra of diethyl ether (1) and diisopropyl ether (2), derived from inner-shell electron energy loss spectra recorded using 2.5 keV final electron energy, 2° scattering angle and 0.7 eV full width half maximum (FWHM) resolution. Signal from O_2 was subtracted from both O 1s spectra. The hatched lines indicate the IPs as measured by XPS,[34] or estimated from IPs of related species.

are then summed to generate an overall EHMO-predicted spectrum.

EHMO does not explicitly calculate core hole energies and thus it is not capable of providing absolute transition energies. A specific, unambiguously interpretable feature, common to both the EHMO and the experimental spectra, is used to calibrate the EHMO energy scale. The individual EHMO spectra from symmetry inequivalent sites are first calibrated individually by setting the zero of the EHMO orbital energy scale to the measured or estimated ionization potential (IP) of the particular core excited atom. These spectra are then summed to form the EHMO spectrum for the entire molecule. The EHMO spectrum prepared by this IP-alignment procedure is then shifted to align it with experiment at an unambiguously assignable feature (typically the lowest energy 1s → π^* transition).

Plots of individual molecular orbitals are generated from the EHMO results using the CACAO program.[18] These plots are very helpful in relating spectral features to structural aspects of the molecules and in visualizing the effect of core hole relaxation on particular orbitals by comparison of the same orbital in the ground state and the EICVOM approximation to the core excited state.[2]

RESULTS AND DISCUSSION

We note that in order to give a good overview of the spectral comparisons it has been necessary to present the data in a relatively compact form. For those interested, the spectral data can be obtained from a database according to instructions given in.[2]

Ethers

The two *ether* compounds are analogues to the ether linkages present in polyurethane polymers either as bridges between carbamate groups (created by the reaction of a diol with the diisocyanate in the formation of the polyurethane chain) or as the extended polyether soft segment chains.[5,19]

The C 1s and O 1s spectra of diethyl ether (1) and diisopropyl ether (2) are presented in Figure 2. Energies, term values, and proposed assignments of the features of these spectra are presented in Table II. The C 1s spectra of the two ether molecules are quite similar, differing mainly in relative intensities of the features below the ionization threshold. Based on the C 1s spectra of other saturated species,[20,21] the low energy region of the C 1s spectrum (286-292 eV) is expected to be dominated by states of mainly Rydberg[22] character, with perhaps some σ^*_{C-H} valence character.[23] In these ether species, the interpretation is complicated by the presence of two closely spaced C 1s ionization limits and the broadness of the features. The intensity of the first two shoulders on the leading edge of the C 1s spectra are proportional to the number of CH_x groups in each species. These features are assigned to C 1s(CH_x) → 3*s* and 3*p* Rydberg transitions. The most intense feature in each spectrum is the broad C 1s → σ^* resonance at ~293 eV, with weaker, broader σ^* resonances at higher energy. Based on the EHMO results these resonances have both σ^*_{C-O} and σ^*_{C-C} character.

The O 1s spectra of the ether compounds are more similar than their C 1s spectra, as is expected from the similarity of the immediate chemical environment of the oxygen atoms in the two compounds. The O 1s spectra of the ethers are composed of weak 1s → Rydberg transitions appearing as poorly defined shoulders below the IP and an intense, broad O 1s → σ^*_{C-O} transition at 538 eV. The Rydberg structure is much weaker at the O 1s than at the C 1s edge, as expected from the much smaller size of the O 1s core orbital and thus smaller overlap with the spatially extended Rydberg orbitals.

Table II Energies, Term Values and Proposed Assignments for the C 1s and O 1s Spectral Features of Diethyl Ether (1) and Diisopropyl Ether (2)

A. C 1s

	1			2			Assignment	
#	E (eV)	T (CH_3)	T (CH_2)	E (eV)	T (CH_3)	T (CH)	CH_3	CH_2O
1 sh	287.1	4.0		286.9	4.2		3s	
2				287.9[a]		4.1		$3s/\sigma^*_{C-H}$
3	288.6	2.5		288.5	2.6		3p	
4	289.26[a]		2.7	289.4		2.6		3p
5	290.7		1.3	290.5		1.5		σ^*_{C-O}
IP	291.1[b]			291.1[b]			IP	
IP	292.0[b]			292.0[b]				IP
6	292.7	−1.6	−0.7	292.8	−1.7	−0.8	σ^*_{C-C}	σ^*_{C-O}
7				301(1)	−10	−9	$\sigma^*_{C-C}/\sigma^*_{C-H}$	

B. O 1s

	1		2		
#	E (eV)[c]	T	E (eV)[c]	T	Assignment
1 sh	534.0	4.1	534.2	3.9	3s
2 sh	536.1(3)	2.0	535.8(3)	2.3	3p
IP	538.1[d]		538.1[d]		IP
3	538	0	538	0	$\sigma^*_{C-O}(-)$[e]
4 br	546	−8	544	−6	$\sigma^*_{C-C}/\sigma^*_{C-O}(+)$[e]

[a] Calibration: (1): −1.47(4) eV relative to 1s → π^* in CO_2 (290.74 eV)[8]; (2): −2.8(1) eV relative to CO_2.
[b] IPs estimated from other species: CH_3 from ethanol (291.1 eV); CH_2 from ethanol (292.5 eV).[24]
[c] Calibration: Energy scales set by 1s → π^* of impurity O_2 (530.8 eV).[8] An O_2 signal amounting to 10–20% of the ether signal was subtracted to obtain each of the spectra plotted in Fig. 2.
[d] IP from XPS.[24] The IPs of 2 are assumed to be the same as those of 1.
[e] $\sigma^*_{C-O}(+)$ and $\sigma^*_{C-O}(-)$ refer to the relative phases of left and right σ^*_{C-O} components of this molecular orbital.

Ureas

Amide structures occur in polyurethanes when water is added to the polymerization reaction mixture.[5] The formation of urea linkages competes with the formation of carbamate linkages. Thus the proportion and distribution of urea links in the polymer cannot be predicted from the reagent stoichiometry. If spectral features specific to the urea functional group can be identified, this could provide a means for measuring the urea content in various segregated phases. Urea (3) is the simplest model of the amide linkage while *N*-phenyl urea (4) and *N,N'*-diphenyl urea (5) are closer models to the chemical environment in polymers containing phenyl urea units.

The C 1s, N 1s, and O 1s spectra of urea, *N*-phenyl urea and *N,N'*-diphenyl urea are presented in Figure 3. Energies, term values, and tentative assignments of the features of these spectra are presented in Tables III, IV, and V. The C 1s spectrum of 3 is dominated by an intense C 1s → $\pi^*_{C=O}$ transition at 289.53 eV, characteristic of the carbonyl functional group. Weak Rydberg features, similar to those seen in CO,[24] are observed between 292 and 294 eV. The strong broad features at 299 and 304 eV are assigned to 1s → σ^*_{C-N} and 1s → $\sigma^*_{C=O}$ transitions, similar to those seen in the C 1s spectra of CH_3NH_2[25] and CO,[24] respectively.

The C 1s spectra of the phenyl-substituted ureas, 4 and 5 (Fig. 3), are significantly different from that of 3 because of the contribution of C 1s excitation at the phenyl groups. The strong feature at 285.2 eV in 4 and 5 is characteristic of C 1s spectra of benzenoid species. It is attributed to the C 1s(C—H) → $1\sigma^*_{C=C}$ transitions in the benzene ring carbons.[2] The C 1s(C=O) → $\pi^*_{C=O}$ transition is still clearly ob-

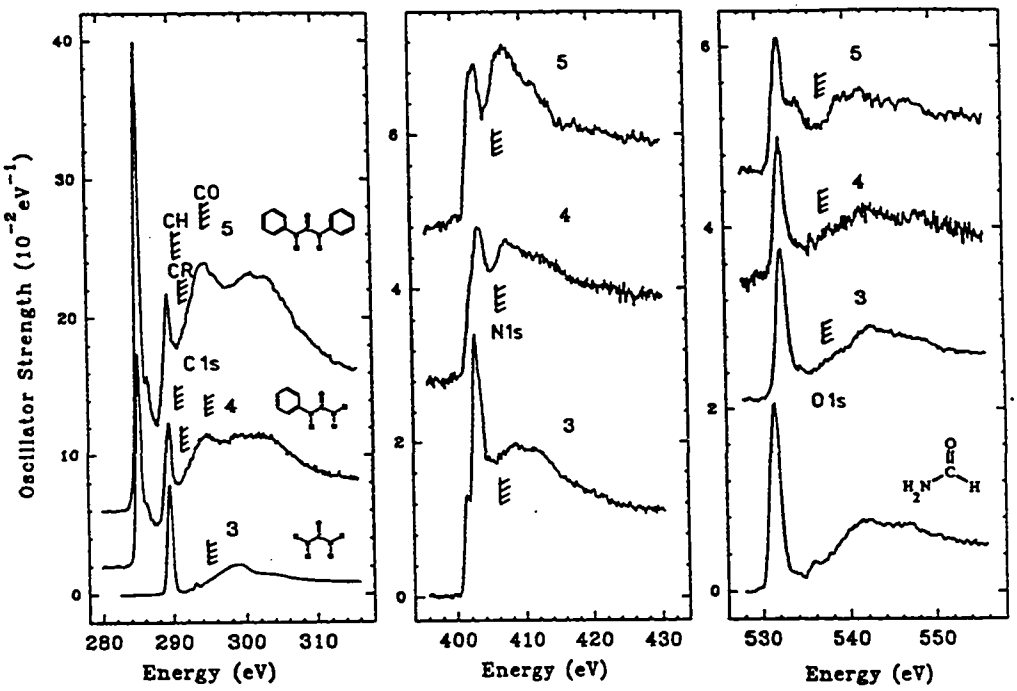

Figure 3. C 1s, N 1s and O 1s oscillator strength spectra of urea (3), *N*-phenyl urea (4), and *N,N'*-diphenyl urea (5). Signal from N_2 was subtracted from the N 1s spectra of 3 and 5, and signal from O_2 was subtracted from the O 1s spectrum of 3. The O 1s spectrum of formaldehyde[33] is included for comparison. See the caption to Fig. 2 for experimental details.

served at ca. 289.5 eV in the C 1s spectra of both phenyl ureas. The amplitude of the weak feature at ~ 286.5 eV between the C 1s (Ph,C—H) → $1\pi^*_{C=C}$ and C 1s(C=O) → $\pi^*_{C=O}$ transitions increases in proportion to the number of phenyl groups (i.e., it is twice as intense in 5 as in 4). This feature is attributed to the C 1s(C—R) → $1\pi^*_{C=C}$ transition (i.e., the transition at the functionalized carbon of the phenyl ring). In aniline, the C 1s IP of the phenyl carbon bonded to the nitrogen atom is 1.3 eV higher than the C 1s IP of the five other carbon atoms of the phenyl ring.[26] This chemical shift is also seen in the core excitation spectra of substituted benzenes such as the monohalobenzenes[27] and aniline.[28,29] The shift between the C 1s(C—H) → $1\pi^*_{C=C}$ and C 1s(C—R) → $1\pi^*_{C=C}$ transitions in aniline is 1.46(2) eV[29] which is similar to the 1.3 eV shift between the corresponding peaks in 4 and 5. The C 1s(C—H) → $2\pi^*_{C=C}$ transition (the $2\pi^*_{C=C}$ orbital corresponds to the b_{2g} π^* orbital in benzene) is expected to occur around 289 eV, in the region of the C 1s(C=O) → $\pi^*_{C=O}$ transition.[30] This is likely the origin of the shoulder at ca. 288.5 eV which has a larger intensity in 5 than in 4. The shape and energy of the σ^* resonances at and above the ionization potential are characteristic of benzenoid systems,[2,30] with additional contributions from σ^*_{C-N} and $\sigma^*_{C=O}$ resonances at 299 and 304 eV.

Figure 4 compares the C 1s spectrum of *N*-phenyl urea with that predicted by EHMO. Molecular orbital plots are presented for selected lines. Overall there is reasonable agreement between calculation and experiment. The details of the component spectra are consistent with the spectral interpretation outlined above. Since the σ^* orbitals are delocalized in the ground state of conjugated species such as 5, one might expect a large number of intense 1s → π^* transitions spread over a 4–6 eV spectral range. However, as found in previous studies,[2,16,17] core hole relaxation perturbs the MOs so that the lowest energy 1s → π^* transition dominates each component spectrum. Even so, there are additional, weaker 1s → π^* transitions at higher energy. These reflect the π-delocalization and thus are more sensitive to the full molecular structure. Delocalization of the $\pi^*_{C=O}$ orbital onto the phenyl ring results in the higher energy π^* peak (e) in the C 1s(C=O) component. Similarly the bands labelled b and c in the

Table III. Energies(eV), Term Values (eV), and Proposed Assignments for the Features in the C 1s Spectra of Urea (3), *N*-phenyl Urea (4), and *N,N'*-diphenyl Urea (5)

A. C 1s of Urea (3)

#	Energy	T	Assignment
1	289.53[a]	5.3	$\pi^*_{C=O}$
2	292.2	2.6	3s
3	293.1	1.7	3p
4	294.1	0.7	4p
IP	294.8[b]		IP
5	298.8(4)	−4.0	σ^*_{C-N}
6	303.5(6)	−8.7	$\sigma^*_{C=O}$

B. C 1s of *N*-phenyl Urea (4) and *N,N'*-diphenyl urea (5)

	4				5				Assignment		
#	E(eV)	T(C—H)	T(C—R)	T(C=O)	E(eV)	T(C—H)	T(C—R)	T(C=O)	C—H	C—R	C=O
1	285.17[c]	5.2			285.22[c]	5.2			$1\pi^*_{C=C}$		
2 sh	286.4		4.6		286.5		4.7			$1\pi^*_{C=C}$	
3 sh	287.1	3.3			287.2	3.2			3s		
4 sh	288.5	1.9			288.3	2.1			$2\pi^*_{C=C}$		
5	289.4			5.1	289.4			5.0			$\pi^*_{C=O}$
IP	290.4[d]				290.4[d]				IP		
IP	291.0[d]				291.2[d]					IP	
IP	294.5[d]				294.5[d]						IP
6	294.6	−4.2	−3.6		294.5	−4.1	−3.3		$\sigma^*_{C=C}(1)$	$\sigma^*_{C=C}(1)$	
7	299.1(4)			−4.6	300.6(5)			−5.5			σ^*_{C-N}
8 br	302	−12	−11	−8	303	−13	−12	−8	$\sigma^*_{C=C}(2)$	$\sigma^*_{C=C}(2)$	$\sigma^*_{C=O}$

[a] Calibration: (3) + 2.13(3) eV relative to CO.
[b] IP from XPS.[34]
[c] Calibration: (4): −5.57(3) relative to CO_2; (5): −5.52(5) eV relative to CO_2.
[d] IP's estimated from other species: C—H from C_6H_6 (290.4 eV); C—N from $C_6H_5NH_2$ (291.2 eV); C=O from $(CH_3)_2NCOH$ (293.45 eV).[34] The solid-state IPs of (4) are known[40] and the chemical shifts are consistent with these estimates.

C 1s(C—H) component are a reflection of delocalization.

The C 1s spectra of these model ureas indicate that urea linkages present in MDI polyurethane foams may be identified through C 1s spectroscopy by observation of the combination of the C 1s → $\pi^*_{C=O}$ transition at ~ 289.5 eV and the C 1s(C—H) → $1\pi^*_{C=C}$ transition at 285.2 eV in the appropriate relative intensity. In the real polymers however these transitions may be broadened which would complicate the analysis.

In contrast to the C 1s spectra, the N 1s spectra of 3, 4, and 5 (Fig. 3) are quite similar to each other. The low energy range of the N 1s spectra is expected to be complex, as both N 1s → Rydberg and N 1s → π^* transitions are expected to overlap in this region. Although bonding at the nitrogen atom is formally saturated there is considerable delocalization of the $\pi^*_{C=O}$ orbital onto the neighboring amide N atom. This can be represented by zwitterionic and hydroxyimine tautomeric representations of the structure.[35] The intensity of the N 1s → π^* transition is a measure of the extent of delocalization of the $\pi^*_{C=O}$ orbital onto the amide nitrogen. It is important to differentiate between core → Rydberg and core → valence transitions, as valence transitions are expected to dominate the spectra of polymers. The experimental spectrum of 3 shows a well-resolved peak at 401.5 eV, an intense peak at 402.7 eV and a higher energy shoulder at 403.7 eV. It is difficult to judge, a priori, which feature is a N 1s → π^* and which is a N 1s → Rydberg transition. Comparison of the N 1s spectra of 3 with those of ammonia,[31] methyl amine,[32] and formamide[33] is helpful in this regard. The broad band around 411 eV in the N 1s spectrum of 3 is attributed to N 1s → σ^* transitions for which the σ^* orbitals have mixed σ^*_{N-H} and σ^*_{C-N} character according to the EHMO calculations.

Table IV. Energies, Term Values and Proposed Assignments for the N 1s Spectral Features of Urea (3), *N*-phenyl Urea (4) and *N, N'*-diphenyl Urea (5)

	3		4		5[a]		
#	E(eV)	T	E(eV)	T	E(eV)	T	Assignment
1	401.5	4.6	401.6	4.1	401.7	4.0	3s
2					402.5	3.2	π^{*c}
3	402.7[b]	3.4	403.6[b]	2.4	403.2	2.5	π^{*}
4 sh	403.7	2.4			404.1	1.6	3p
5					404.8	0.9	π^{*c}
6	404.7	1.4					4p
IP	406.1[d]		405.7[e]		405.7[e]		IP
7	408	−2	408	−2	407.4(8)	−2	σ^{2}_{C-N}
8	411	−5	414	−8	412	−6	σ^{2}_{C-N}

[a] Calibration: (5): Energy scale set by 1s → π^* of impurity N_2. An N_2 signal amounting to 40–50% of the signal was subtracted to obtain the spectra plotted in Fig. 3.

[b] Calibration: (3): +1.5 eV relative to the 1s → π^* in N_2 (401.1 eV)[5]; (4): +2.5(2) eV relative to N_2.

[c] Assignment of these extra features as additional π^*-related structure is supported by the EHMO calculations and Gaussian curve fit (see Fig. 6).

[d] IP from XPS.[34]

[e] IPs estimated from related species: $(NH_2)_2CO$ (406.1 eV) and $C_6H_5NH_2$ (405.3 eV).[34]

Figure 5 compares the N 1s spectrum of 3 with that of formamide, and with EHMO-predicted spectra for both species. The experimental spectra are presented on a term value scale, established from the experimental IPs.[34] Both EHMO spectra have been shifted *equally* so as to align the first feature in the EHMO prediction with that in the experimental N 1s spectrum of formamide. The first feature in the N 1s spectrum of formamide has been assigned as a mixture of N 1s → π^* and N 1s → 3s Rydberg transitions.[33] EHMO cannot reproduce Rydberg transitions since these are constructed from higher-*n* atomic orbitals which are not used in EHMO. Thus comparison of the EHMO and experimental spectra provides a means of identifying π^* and Rydberg transitions. The EHMO calculations predict that both species have a relatively intense N 1s → π^* transition with that in 3 at higher energy than that in formamide. The predicted energy of the π^* transition in 3 aligns well with the second feature in the experimental spectrum of 3. This is the basis for our assignment of the second peak (at 402.7 eV) as the main π^* resonance in 3. The good alignment of the first peak in the experimental

Table V. Energies, Term Values and Proposed Assignments for the O 1s Spectral Features of Urea (3), *N*-phenyl Urea (4) and *N,N'*-diphenyl Urea (5)

	3		4		5		
#	E(eV)	T	E(eV)	T	E(eV)	T	Assignment
1	532.5[a]	4.7	532.5[a]	4.7	532.5[a]	4.7	$\pi^{2}_{C=O}$
2					534.4	2.8	π^{2}_{C-N}
3	534.4	2.8	534.6	2.6			3s
IP	537.2[b]		537.2[b]		537.2[b]		IP
4	538	−1			539	−2	double excitation
5	543	−5	543	−6	540	−3	σ^{2}_{C-N}
6	549	−12	548	−11	548	−11	$\sigma^{2}_{C=O}$

[a] Calibration: (3): −2.9(1) eV relative to O 1s → π^* in CO_2. (535.4 eV)[35]; (4): −2.9(1) eV relative to CO_2; (5): −2.9(1) eV relative to CO_2.

[b] IP of 3 from XPS.[34] The O 1s IP of 4 and 5 are estimated to be the same as 3.

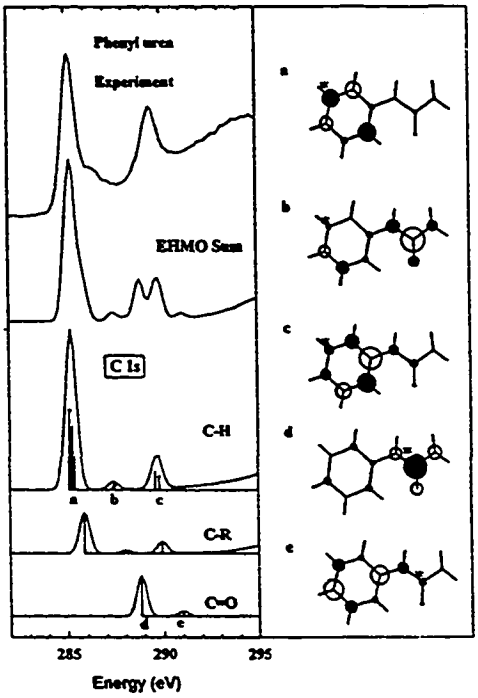

Figure 4. (left) Comparison of the experimental C 1s spectrum of *N*-phenyl urea (4) to that predicted by EHMO calculations within the EICVOM model. The calculated spectrum is the sum of components for each of the symmetry inequivalent carbons, which are indicated as the lower three curves. See text for further details of the calculation and spectral generation. (right) Plots of π^* MOs (z-projection of $2p\pi$ density predicted by EHMO) corresponding to selected spectral lines (a–e). The core-excited atom is starred. The meta C—H components of the C 1s(C—H) spectrum are indicated in the left hand figure. The geometry used for the calculation of 4 is presented in Table I.

spectrum of 3 (that at 401.5 eV) with the first peak in formamide suggests that both have Rydberg components. Based on this alignment and the term value, we attribute the first feature in the N 1s spectrum of 3 to the N 1s → 3s Rydberg transition. The N 1s → 3p transition is then assigned to be overlapped with the π^* feature at 402.7 eV.

The N 1s spectra of the phenyl-substituted ureas (4, 5) (Fig. 3) are quite similar to that of 3 although the discrete structure is weaker relative to the continuum. The low energy region is expected to contain both N 1s → Rydberg and N 1s → π^* transitions. The two small shoulders on the low energy edge of the first intense transition in 4 are approximately half as intense as the Rydberg transitions in 3. They are assigned to the N 1s(NH_2) → 3s and 3p transitions, respectively. These shoulders are entirely absent in the spectrum of 5. The decrease in the intensity of the Rydberg-assigned features in the sequence 3, 4, 5 is consistent with the decreasing fraction of $-NH_2$ groups in each molecule and increasing size. The systematic reduction in the intensity of the N 1s → π^* feature around 403 eV through 3, 4, and 5 can be explained by sterically enforced nonplanarity at the N atom with phenyl substitution which will reduce the ring-nitrogen $2p\pi$ overlap and thus the intensity of the N 1s → π^* transition.

N 1s → π^* transitions in the phenyl-substituted ureas might be expected to be more complex than in urea since there may be delocalization of $\pi^*_{C=C}$

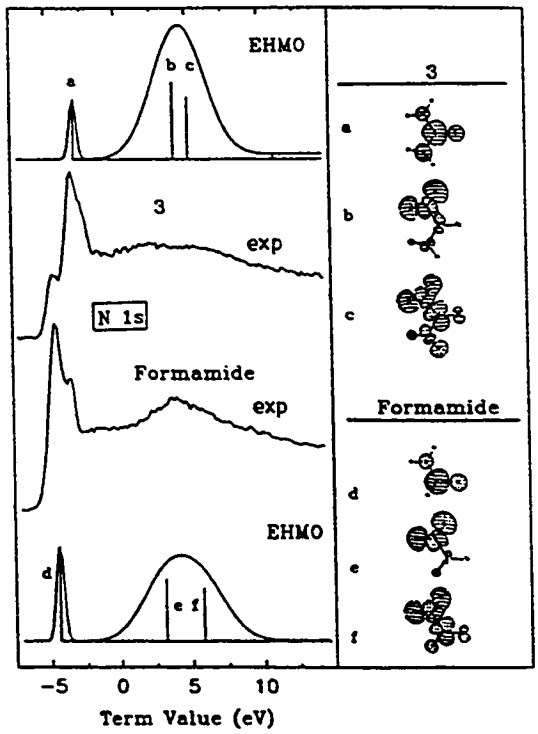

Figure 5. (left) The N 1s spectra of urea (3) and formamide[23] plotted on a term value scale (T=IP −E), compared with the calculated EHMO spectra of 3 and formamide. Both EHMO spectra were shifted equally by +4.5 eV so as to align the EHMO and experimental N 1s → π^* transition in formamide. (right) Plots of the orbitals from the EHMO-EICVOM calculations. See the caption to Fig. 4 for further details on the generation of the EHMO spectra. An experimental geometry was used for formamide;[41] the geometry used for the calculation of 3 is presented in Table I.

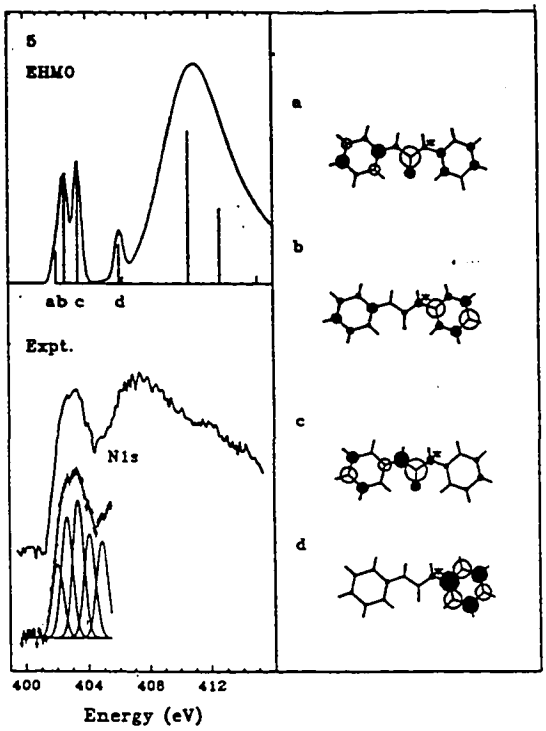

Figure 6. (left) Comparison of the experimental N 1s spectrum of planar *N,N'*-diphenyl urea (5) to that predicted by EHMO calculations. The result of a Gaussian curve fit of the discrete N 1s → π* structure is also shown. See the caption to Fig. 4 for further details; the geometry used for the EHMO calculation of the planar conformer of 5 is presented in Table I. (right) Molecular orbital plots (z-projection of 2pπ density predicted by EHMO) for selected orbitals.

density from the phenyl rings onto the N atom. This is an instance where EHMO calculations are useful since they allow one to evaluate the effect on the N 1s spectrum of delocalization of the phenyl π-electron density onto the N atoms. Figure 6 presents the EHMO N 1s spectrum of 5 in comparison to its experimental spectrum. Figure 6 also includes the result of a Gaussian curve fit of the broad, structured N 1s → π* region. While this curve fit is not a unique result it does provide an indication of the number, relative intensity, and position of the components. There is reasonably good agreement between the relative energies and intensities of the EHMO and experimental spectrum in the π* region. EHMO predicts that the first feature is composed of three N 1s → π* transitions where the three π* orbitals (a, b, c) consist of different mixtures of N $2p_z$, $\pi^*_{C=O}$ and delocalized π* orbital density of the phenyl rings. EHMO also predicts there will be a higher energy N 1s → π* transition (d) which should appear experimentally around 406 eV based on alignment of the EHMO spectrum at the first band. This high energy π* orbital is mainly located on the phenyl rings. This feature likely corresponds to the band at 405 eV identified by the curve fit. EHMO also predicts two strong near continuum resonances of $\sigma^*_{N-C=O/N-Ph}$ character which may correspond to the two broad features in the experimental spectrum at ~ 408 and ~ 412 eV.

The EHMO calculation for the N 1s spectrum of 5 described above was carried out using a planar molecular geometry. In the solid state the phenyl rings of 5 are twisted 20–40° out of the plane of the urea group.[38] It is possible the gas phase structures of 4 and 5 will differ from those of the solid state since hydrogen bonding plays an important role in dictating the solid-state conformation. Ab initio calculations of the geometry of isolated urea and phenyl-substituted ureas indicate that a nonplanar amine group is energetically more favorable[36] but

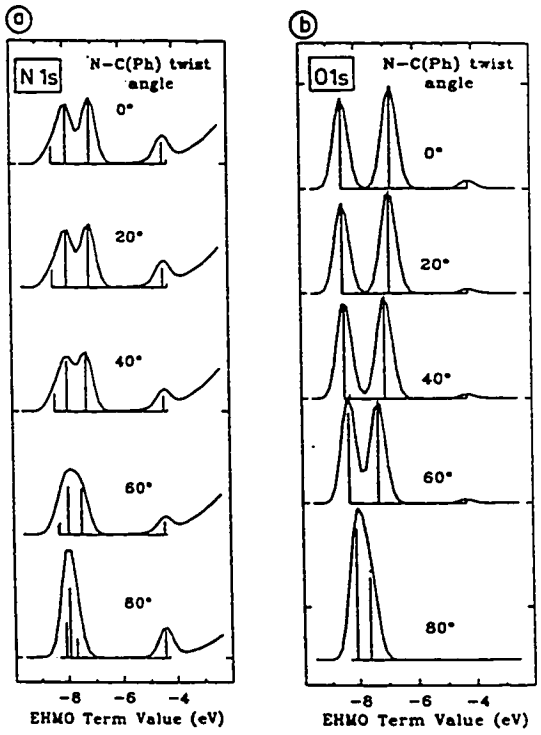

Figure 7. N 1s and O 1s EHMO spectra of *N,N'*-diphenyl urea (5) calculated for different values of the N—C(Ph) bond angle. The nonphenyl twist angle aspects of the geometry of 5 are presented in Table I.

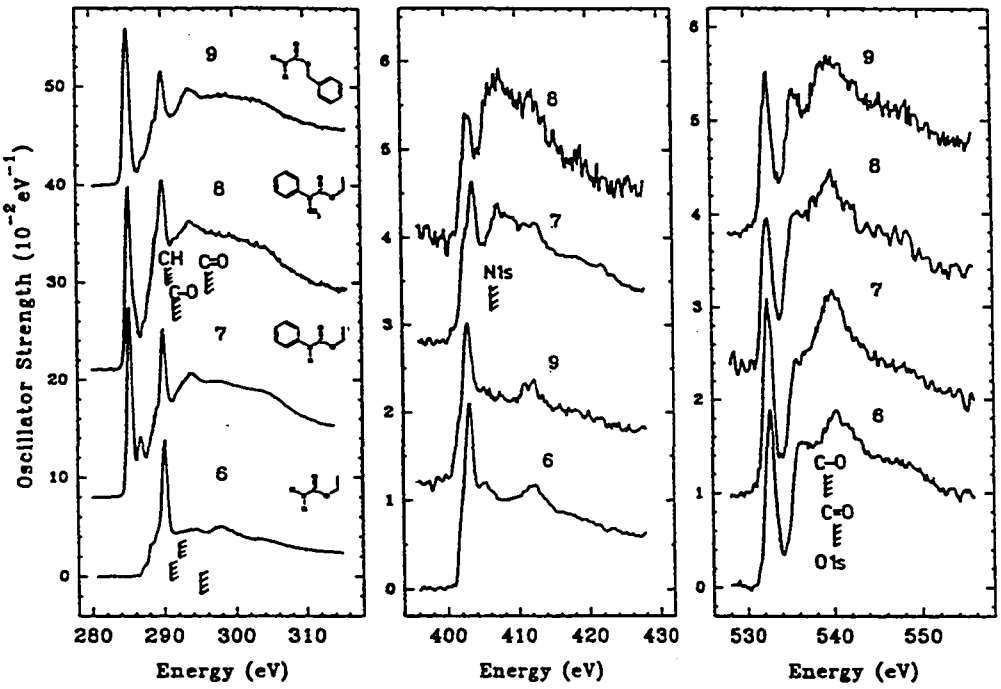

Figure 8. C 1s, N 1s, and O 1s oscillator strength spectra of ethyl carbamate (6), ethyl *N*-phenyl carbamate (7), ethyl *N*-methyl, *N*-phenyl carbamate (8), and benzyl carbamate (9). The order of plotting of the N 1s spectra differs from that used for the C 1s and O 1s spectra in order to emphasize the relationship between the intensity of the 403 eV peak to the number of N—H hydrogen atoms. See caption to Fig. 2 for experimental details.

they suggest that the twist angle should be smaller in the gas phase than in the solid state. An EHMO investigation of the dependence of the core spectra of 5 on the phenyl twist angle has been carried out in order to gain insight into how core excitation spectroscopy might be sensitive to ring-carbonyl nonplanarity associated with hydrogen bonding or steric hindrance effects. The latter is important in isocyanate molecules since the methyl groups attached at the amide nitrogen atom force nonplanarity of the phenyl rings and the carbonyl group.

Figure 7 presents the EHMO N 1s spectra of 5 calculated for a series of different N—C(Ph) dihedral angles. It is evident from the EHMO spectrum calculated for the planar geometry that delocalization of π^* density from the phenyl rings significantly perturbs the N 1s spectrum of 5 from that of 3 (urea). From geometric overlap considerations one expects that this delocalization would decrease if the phenyl rings twist out of the plane of the carbonyl group. While one expects decoupling of $\pi^*_{C=O}$ and π^*_{ring} density as the N—C(Ph) bond twist angle increases, the core excited nitrogen can be viewed as being both in the plane of the phenyl ring and in the plane of the carbonyl moiety, as the twist is about the N—C(Ph) bond. Thus extensive delocalization may occur up to quite large twist angles. EHMO calculations on nonplanar urea (not shown) demonstrate that the planarity at the N atom affects both the orbital energy and the orbital character. A nonplanar environment is expected in cases of strong hydrogen bonding. This is likely more important than N—C(C=O) bond rotation (i.e., amide twist) in determining the shape of the core edge. Changes are observed in the EHMO N 1s spectrum of diphenyl urea (5) as a function of phenyl twist angle (Fig. 7a), but these are relatively minor between 0° and 40°. At very large twist angles (80°) the split in the π^* structure collapses and EHMO predicts that only a single π^* peak should be observed. This indicates that the splitting associated with delocalization is almost completely eliminated when the phenyl group

twist approaches 90°. Corresponding effects of the twist angle on the O 1s → $\pi^*_{C=O}$ transition in 5 (Fig. 7b) are discussed below.

If one assumes diphenyl urea adopts a near planar geometry as the lowest energy conformation, as we have assumed for the calculation shown in Figure 6, the predicted splitting of the N 1s → π^* transitions associated with delocalization should be large enough to be detected with our experimental resolution. In fact, a splitting is not observed although the width of the N 1s → π^* resonance is significantly larger in 5 than in 3. This may be evidence for the existence of a number of different gas phase conformations each with significant but slightly different π^* splitting resulting in a broad band (see Fig. 6). This EHMO study strongly suggests that there is a distribution of nonplanar conformations of 5 (and presumably also 4) in the gas phase. Comparison of experiment and calculation could be used to estimate the average twist angle, although more precise N 1s spectra are required.

Based on the O 1s spectra of other carbonyl compounds,[33] the O 1s spectra of 3, 4, and 5 are expected to be rather similar, in each case dominated by O 1s → $\pi^*_{C=O}$ and O 1s → $\sigma^*_{C=O}$ transitions. The O 1s spectra of 3, 4 and 5 are presented in Figure 3, in comparison to that of formamide.[33] As in other carbonyl compounds, the $\pi^*_{C=O}$ feature occurs at essentially the same energy in all three species. Its energy is about 0.5 eV higher than the O 1s → π^* transition in formamide. This shift is similar to that found for the N 1s → π^* transitions (see Fig. 5). The other dominant O 1s spectral feature is the broad $\sigma^*_{C=O}$ resonance at 542 eV. EHMO calculations for 3 (not shown) support our spectral assignments.

Figure 7b presents the EHMO O 1s spectra of 5 for different N—C(Ph) bond angles. The spectrum calculated for the planar geometry and modest twist angles predicts two π^* features which should be readily resolved in our experiment. According to EHMO, it is only at extreme phenyl twist that the π^* splitting should become undetectable. A distribution of phenyl ring orientations is likely the origin of the larger width of the O 1s → $\pi^*_{C=O}$ transition in 5 than in 4 or 3.

Carbamates

Carbamate structures are characteristic of hard segment linkages in polyurethane polymers. Ethyl carbamate (6) and the *N*-phenyl substituted carbamates (7, 8) are models for this aspect of polyurethane polymers. Benzyl carbamate (9) was studied to investigate the sensitivity of core spectroscopy to distinguishing *N*-versus ethyl-bonding of the phenyl group. The C 1s, N 1s, and O 1s spectra of these species are presented in Figure 8. Energies, term values, and tentative assignments of the spectral features are presented in Tables VI, VII, and VIII. The C 1s spectrum of 6 is the superposition of the contributions of the carbonyl and the two saturated, ether-like carbons. It can be interpreted by comparison to the C 1s spectra of urea (Fig. 3) and diethyl ether (Fig. 2). The shoulders on the low energy side of the C 1s → $\pi^*_{C=O}$ transition of 6 arise from C 1s(CH_x) → Rydberg transitions at the ethyl carbons. The C 1s(C=O) → $\sigma^*_{C=O}$ resonance in 6 occurs at 304 eV, similar to that in 3. The other σ^* features are different because of the differences between 3 and 6 in bonding at the carbonyl carbon centre.

The interpretation of the C 1s spectrum of 6 can be extended to the phenyl-substituted ethyl carbamates by using the building block model. The additional contribution of C 1s excitations at the phenyl substituent can be described using the C 1s spectrum of benzene[30] as long as one takes into account the C 1s(C—R) energy shift, where C—R is the ring carbon to which the ethyl carbamate group is attached. Ethyl *N*-methyl *N*-phenyl carbamate (8) has a C 1s spectrum rather similar to that of 7. The C 1s transitions characteristic of the phenyl ring dominate the C 1s spectra of all three phenyl-substituted species.

Delocalization in the phenyl carbamates can be examined by EHMO calculations. Figure 9 compares the C 1s spectrum of 7 to the EHMO prediction. The EHMO spectra for the C 1s(Ph,C—H), C 1s(C—R), and C 1s(C=O) components are remarkably similar to the corresponding components in the EHMO calculation of 4 (see Fig. 4). EHMO accurately predicts the shift of the C 1s(C—R) → $1\pi^*_{C=C}$ relative to the C 1s(C=O) → $\pi^*_{C=O}$ transition. It also shows a small transition to a delocalized π^* orbital at the phenyl carbons, which may correspond to the experimental feature at ca. 287 eV. Relative to the prediction of the building block model this feature is unexpected. The C 1s(C=O) → $\pi^*_{C=O}$ and the C 1s(Ph,C—H) → $2\pi^*_{C=C}$ transitions overlap, with the carbonyl peak at lower energy as in *N*-phenyl urea. Comparison of the EHMO predictions for the $-CH_2-$ and $-CH_3$ components demonstrates there is delocalization of the carbonyl π electron density onto the methylene carbon but not on the methyl carbon of the ethyl group.

Table VI. Energies, Term Values, and Proposed Assignments for the C 1s Spectral Features of Ethyl Carbamate (6), Ethyl *N*-phenyl Carbamate (7), Ethyl *N*-phenyl *N*-methyl Carbamate (8), and Benzyl Carbamate (9)

A. C 1s of ethyl carbamate (6)

					Assignments		
#	E(eV)	T(CH_3)	T(CH_2)	T(C=O)	CH_3	CH_2	C=O
1 sh	287.3	3.7			3s		
2 sh	288.3	2.7	3.7		3p	3s	
3 sh	288.9		3.1			3p	
4	290.05[a]			4.95			$\pi^*_{C=O}$
IP	291[b]				IP		
IP	292[b]					IP	
5	294.0	−3.0	−2.0		$\sigma^*_{C-C/C-H}$	$\sigma^*_{C-O/C-C}$	
IP	295[b]						IP
6	298.0(2)		−6.0	−3.0		σ^*_{C-O}	σ^*_{C-O}
7 br	304			−9			$\sigma^*_{C=O}$

B. C 1s of ethyl *N* phenyl carbamate (7)

		Term values					Assignments				
	E(eV)	Ph(CH)	CH_x	C—R	CH_2O	C=O	Ph(C—H)	CH_x	C—R	CH_2O	C=O
1	285.26[c]	5.0					$1\pi^*_{C=C}$				
2	286.8			4.7					$1\pi^*_{C=C}$		
3	287.4	2.9	4.1				$2\pi^*_{C=C}$		3s		
4 sh	288.3		2.2					3p			
5 sh	289.0	1.2		2.6	2.6		4p		$2\pi^*$	$1\pi^*_{C=C}$	
6	290.0					6.0					$\pi^*_{C=O}$
IP	290.3[d]						IP				
IP	290.5[d]							IP			
IP	291.6[d]								IP	IP	
7	293.8	−3.8		−2			$\sigma^*_{C=C}(1)$		$\sigma^*_{C=C}(1)$		
IP	296[d]										IP
8	298				−6	−2				σ^*_{C-O}	σ^*_{C-O}
9	304(2)	−14		−12		−8	$\sigma^*_{C=C}(2)$		$\sigma^*_{C=C}(2)$		$\sigma^*_{C=O}$

C. C 1s of ethyl *N*-methyl *N*-phenyl carbamate (8)

		T (eV)					Assignments				
#	E(eV)	Ph(C—H)	CH_3	C—R	N—CH_3 CH_2O	C=O	Ph(C—H)	CH_3	C—R	NCH_3 CH_2O	C=O
1	285.26[e]	5.0					$1\pi^*_{C=C}$				
2 sh	286.3	(4.0)					$(1\pi^*_{C=C})^f$				
3	287.4			4.2					$1\pi^*_{C=C}$		
4 sh	288.2	2.1	2.3				$2\pi^*_{C=C}$	3s			
5 sh	289.2		1.3					3p			
6	290.0					5.9					$\pi^*_{C=O}$
IP	290.3[g]						IP				
IP	290.5[g]							IP			
IP	291.6[g]								IP		
IP	292.0[g]									IP	
7	294	−4		−3	−2		$\sigma^*_{C=C}(1)$	$\sigma^*_{C=C}(1)$		$\sigma^*_{C-O}, \sigma^*_{C-N}$	
IP	296[g]										IP
8	303	−13		−12		−7	$\sigma^*_{C=C}(2)$	$\sigma^*_{C=C}(2)$			σ^*_{C-O}

Table VI. Continued

D. C 1s of benzyl carbamate (9)

		T (eV)			Assignments			
#	E(eV)	Ph(C—H)	C—R	C=O	Ph(C—H)	C—R	CH_2	C=O
1	285.23[b]	5.2			$1\pi^*_{C=C}$			
2	287.3		4.3			$1\pi^*_{C=C}$		
3	289.0		2.6			$2\pi^*_{C=C}$		
4	290.0			6.0				$\pi^*_{C=O}$
IP	290.4[i]				IP			
IP	291.6[i]					IP		
IP	292.0[i]						IP	
5	294	−4	−3		$\sigma^*_{C=C}(1)$	$\sigma^*_{C=C}(1)$		
IP	296[i]							IP
6	299	−9	−8		$\sigma^*_{C=C}(2)$	$\sigma^*_{C=C}(2)$		
7	304			−8				$\sigma^*_{C=O}$

[a] Calibration: (6): −2.65(4) eV relative to CO (287.40 eV).[9]
[b] IPs of 6 estimated from other species: CH_3 from ethanol (291.1 eV); CH_2 from ethanol (292.5 eV); CO from $(CH_3CO)_2O$ (294.4 eV); CO from $(NH_2)_2CO$ (294.84 eV).[34]
[c] Calibration: −2.14(4) eV relative to CO.
[d] IPs of 7 estimated from: CH_3 from $(CH_3)_2NCHO$ (292.03 eV); CO from $(CH_3)_2NCHO$ (293.45 eV); CH from benzene (290.3 eV); C—NH_2 from $C_6H_5NH_2$ (291.38 eV); CO from $(CH_3CO)_2O$ (295.4 eV).[34]
[e] Calibration: −5.48(3) eV relative to CO_2.
[f] This shoulder is tentatively attributed to excitations from the ortho ring carbons to the $1\pi^*$ orbital. A chemical shift as large as 0.8 eV is plausible.
[g] IPs of 8 estimated from: CH_3 from $(CH_3)_2NCHO$ (292.03 eV); CO from $(CH_3)_2NCHO$ (293.45 eV); CH from benzene (290.3 eV); C—NH_2 from $C_6H_5NH_2$ (291.38 eV); CO from $(CH_3CO)_2O$ (295.4 eV).[34]
[h] Calibration: −2.17(4) eV relative to CO.
[i] IP's of 9 estimated from: C_6H_6 (290.4 eV); C_6H_5O (C—OH) (292.0 eV); $(CH_3CO)_2O$ (C=O) (295.4 eV).[34]

The N 1s spectra of the carbamates (Fig. 8) are expected to be similar to the N 1s spectra of similarly substituted ureas. For example, the first neighbor environment of the nitrogen atom in benzyl carbamate (9) and ethyl carbamate (6) are identical to that in urea (3). The similarity of local structure is reflected in the similarity of their N 1s spectra. The addition of a phenyl group in 7 and 8 modifies the N 1s spectrum in ways similar to the change between the spectra of 3 and 4, 5. The N 1s spectra of the carbamates each exhibit a low energy N 1s → π^* transition. There is a shoulder on the low energy

Table VII. Energies, Term Values, and Proposed Assignments for the N 1s Spectral Features of Ethyl Carbamate (6), Ethyl *N*-phenyl Carbamate (7), *N*-methyl *N*-phenyl Carbamate (8) and Benzyl Carbamate (9)

	6		7[a]		8[a]		9		
	E(eV)	T	E(eV)	T	E(eV)	T	E(eV)	T	Assignment
1 sh	402.0	3.5	402.5	3.5			401.6	4.7	3s, σ^*_{N-H}
2	403.05[b]	2.9	403.7(3)	2.3	403.2(3)	2.8	402.94[b]	3.4	3p, $\pi^*_{C=O}$
4	405.1	1.6	405.2	0.8	404.4	1.2	405.2	1.1	4p
IP	406.3[c]		406[c]		406[c]		406.3[c]		IP
4			407	−1	407	−1	407	−1	σ^*_{N-C}
5	412	−6	412	−6	412	−6	412	−6	σ^*_{N-C}

[a] The N 1s spectra of 7 and 8 were calibrated on the 1s → π^* feature of impurity N_2. This signal was subtracted for the plot presented in Fig. 8.
[b] Calibration: (6) 1.95(3) eV relative to N_2; (9) 1.85(3) relative to N_2.
[c] IPs estimated from other species: N from NH_2CHO (406.4 eV); N from CH_3NHCOH (405.8 eV); N from $C_6H_5NH_2$ (405.3 eV).[34]

Table VIII. Energies, Term Values and Proposed Assignments for the O 1s Spectral Features of Ethyl Carbamate (6), Ethyl *N*-phenyl Carbamate (7), *N*-methyl *N*-phenyl Carbamate (8) and Benzyl Carbamate (9)

	6			7			8			9			Assignment	
	E(eV)	T(C=O)	T(C—O)	E(eV)	T(C=O)	T(C—O)	E(eV)	T(C=O)	T(C—O)	E(eV)	T(C=O)	T(C—O)	C=O	C—O
1	532.8[a]	7.2		532.5[a]	7.3		532.6[a]	7.3		532.62[a]	7.2		$\pi^*_{C=O}$	
2	536.6		2.5	535.7		3.1	535.8		3.0	535.9		3.0		$\pi^*_{C=O}$
IP	539[b]			538.8[b]			538.8[b]			538.9[c]				IP
IP	540[b]			539.8[b]			539.8[b]			539.8[c]			IP	
3	540		-1	540		-1	540		-1	540		-1		σ^*_{C-O}
4 br	548	-8		548	-8		548	-8		549	-9		$\sigma^*_{C=O}$	

[a] Calibration: (6) 1.96(6) eV; (7) 1.76(11) eV; (8) 1.7(1) eV; (9) 1.7(1) eV relative to 1s → π^* in O_2 (530.8 eV).[3]
[b] IPs estimated from other species: CO from $(CH_3CO)_2O$ (539.66 eV); C—O—C from $(CH_3CO)_2O$ (538.56 eV).[34]
[c] IPs estimated from other species: CO from C_4H_8O (538.9 eV); C=O from $(CH_3CO)_2O$ (539.66 eV).[34]

side of this transition in 6 and 9. This is expected to be a N 1s(NH_2) → 3s Rydberg transition, similar to that seen in 3 and 4. The continuum maximum at 411 eV is attributed to N 1s → σ^*_{C-N} transitions. It is similar in position, but it has a different shape than the structure attributed to σ^*_{C-N} in urea 3 and the phenyl ureas.

The N 1s spectra of 7 and 8 have a broad peak at about 408 eV. This is attributed to N 1s → σ^*_{C-N} transitions consistent with the phenyl and methyl substitution at the nitrogen site in these carbamate species and similar to that seen in the N 1s spectra of the similarly substituted ureas. The N 1s spectra of ureas and carbamates with similar amine substitution exhibit only minor differences, so the N 1s spectra of polymers may be of limited use for providing a unique identification of carbamate relative to urea functionality. In addition there is much

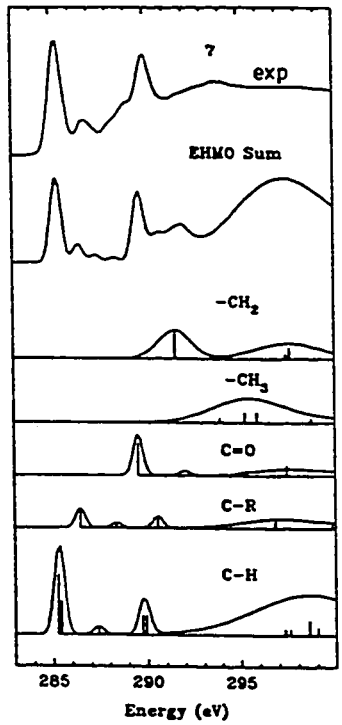

Figure 9. Comparison of the experimental C 1s spectrum of ethyl *N*-phenyl carbamate (7) to that predicted by EHMO calculations. See the caption to Fig. 4 for further details. A Gaussian linewidth of 4.0 eV was used for the C 1s(C=O) peak at 297 eV (ϵ = −2.17 eV) and the C 1s(CH_3) peak at 294 eV (ϵ = −2.06 eV); a width of 2.0 eV was used for the C 1s(CH_2) peak at 292 eV (ϵ = −5.07 eV). The geometry used for 7 is presented in Table I.

less nitrogen than carbon or oxygen in the polyurethane polymers and thus it will be particularly difficult to acquire high quality N 1s spectra on account of the necessarily low signal to background ratio.

The carbonyl and ether oxygen atoms in ethyl carbamate and the substituted carbamates each have a common local environment which leads to very similar O 1s spectra in all four carbamate species (Fig. 8). The O 1s spectrum of ethyl carbamate (6) can be interpreted by comparison to the O 1s spectra of diethyl ether (Fig. 2) and urea (Fig. 3). The feature at 533 eV in the ethyl carbamate spectrum is clearly the O 1s(C═O) → $\pi^*_{C=O}$ transition. The feature at 536 eV is attributed to O 1s(C—O) → $\pi^*_{C=O}$ transitions which have a non-zero intensity on account of delocalization of the $\pi^*_{C=O}$ orbital. A similar pattern is seen in all four carbamates and in the O 1s spectra of other esters, such as methyl formate.[20] The broad resonance at 540 eV is attributed to O 1s → σ^*_{C-O} transitions at the ether oxygen. The O 1s(C═O) → $\sigma^*_{C=O}$ resonance occurs at 548 eV. The similarities among the carbamate O 1s spectra and their contrast to those of the ethers and ureas (Figs. 2 and 3) mean that the O 1s edge should be particularly useful for identifying carbamate structures in polymer blends.

SUMMARY

The inner shell excitation spectra of 9 molecules (25 spectra in total), whose structures are related to elements of the structure of MDI polyurethane foams, have been recorded and analyzed with the aid of spectral trends and comparison to EHMO calculations. As found in other systems, the local sensitivity of core excitation spectroscopy provides a useful tool for microanalysis of polyurethanes. The gas phase spectra demonstrate that, if the spectra from all atomic edges are considered, inner shell spectroscopy offers the capability of distinguishing the various functional groups present in MDI polyurethanes. The characteristic C 1s, N 1s, and O 1s signals associated with ether, phenyl, and carbonyl groups provides a means of distinguishing ether-dominated soft segment from the urea and carbamate dominated hard segment functionalities. The O 1s and C 1s spectra are better suited than the N 1s spectrum to differentiating urea and carbamate linkages. The core excitation spectra are also sensitive to details of electronic delocalization. Appropriate analysis may provide useful insight into polymer conformational phenomena. In order to fully exploit the chemical sensitivity of core excitation spectroscopy for polymer analysis it is important to record spectra with adequate spectral resolution (ideally 0.5 eV or less) and with good signal to noise ratio (> 50). These requirements present a challenge to the analysis of polyurethane foams using electron microscope based EELS at high spatial resolution since spectra with sufficient spectral resolution and statistical precision must be obtained before significant radiation damage has occurred. Techniques such as positional averaging,[42] and monochromation of the probe beam,[43] have good potential for improving EELS for polymer analysis.

This research has been supported by Dow Chemical U.S.A. and the Natural Science and Engineering Research Council of Canada. The authors would like to thank Carlo Meali for generously supplying the CACAO molecular orbital plotting program. S.G.U. would like to thank Dr. Ed Rightor for helpful guidance and Dow Chemical for its financial support.

REFERENCES AND NOTES

1. S. G. Urquhart, A. P. Hitchcock, R. D. Leapman, E. G. Rightor, and R. D. Priester, *J. Polym. Sci. Polym. Phys.*, Part I, (1994).
2. A. P. Hitchcock and D. C. Mancini, *J. Electron Spectrosc.*, **67**, 1 (1994).
3. A. P. Hitchcock, S. G. Urquhart, and E. G. Rightor, *J. Phys. Chem.*, **96**, 8736 (1992).
4. E. G. Rightor, G. P. Young, S. G. Urquhart, and A. P. Hitchcock, *Microscopy: The Key Research Tool*, **22**, 67 (1992); E. G. Rightor, G. Mitchell, D. Fischer, A. P. Hitchcock, S. G. Urquhart, R. D. Leapman, A. Yeh, and J. L. Gland, *J. Phys. Chem.*, (1995).
5. (a) M. P. Stevens, *Polymer Chemistry: An Introduction*, Oxford University Press, New York, 1990, p. 440; (b) J. L. Kroschwitz, ed., *Concise Encyclopedia of Polymer Science and Engineering*, Wiley, New York, 1990, p. 890.
6. D. C. Koningsberger and R. Prins, eds., *X-ray Absorption Spectroscopy*, Wiley New York, 1988; J. Stöhr, *NEXAFS Spectroscopy*, Springer Ser. Surf. Sci., Springer-Verlag, Heidelberg, 1992.
7. D. A. Outka and J. Stöhr, in *Chemistry and Physics of Solid Surfaces*, Springer Ser. Surf. Sci., R. Vanselow and R. Howe, eds., Springer, Berlin, 1988, p. 201.
8. A. P. Hitchcock, *Physica Scripta*, **T31**, 159 (1990).
9. R. N. S. Sodhi and C. E. Brion, *J. Electron Spectrosc.*, **34**, 363 (1984).
10. R. A. McLaren, S. A. C. Clark, I. Ishii, and A. P. Hitchcock, *Phys. Rev. A*, **36**, 1683 (1987); A. P. Hitchcock and D. C. Mancini, *J. Electron Spectrosc.*, **67**, 1 (1994).

11. M. Inokuti, *Rev. Mod. Phys.*, **43**, 297 (1971).
12. B. L. Henke, P. Lee, T. J. Tanaka, R. L. Shimabukuro, and B. K. Fujikawa, *At. Data Nucl. Data Tables*, **27**, 1 (1982).
13. J. Howell, A. Rossi, D. Wallace, K. Haraki, and R. Hoffmann, FORTICON8 Program QCMP011 from Quantum Chemical Program Exchange, Creative Arts Bldg, Indiana University, Bloomington, IN, 47405.
14. E. Rühl and A. P. Hitchcock, *J. Am. Chem. Soc.*, **111**, 5069 (1989).
15. E. Rühl, A. T. Wen, and A. P. Hitchcock, *J. Electron Spectrosc.*, **57**, 137 (1991).
16. A. T. Wen, E. Rühl, and A. P. Hitchcock, *Organometallics*, **11**, 2559 (1992).
17. J. T. Francis and A. P. Hitchcock, *J. Phys. Chem.*, **96**, 6598 (1992).
18. C. Mealli, and D. M. Proserpio, *J. Chem. Ed.*, **67**, 339 (1990).
19. (a) C. P. Christenson, M. A. Harthcock, M. D. Meadows, W. L. Spell, M. W. Creswick, R. E. Guerra, and R. B. Turner, *J. Polym. Sci. Polym. Phys.*, **24**, 1401 (1986); (b) J. Armisted, G. Wilkes, and R. Turner, *J. Appl. Polym. Sci.*, **35**, 601, (1988).
20. I. Ishii, and A. P. Hitchcock, *J. Electron Spectrosc.*, **42**, 11 (1987).
21. I. Ishii, and A. P. Hitchcock, *J. Electron Spectrosc.*, **46**, 55 (1988).
22. M. B. Robin, *Higher Excited States of Polyatomic Molecules*, Academic Press, New York, Vol. 1, 2, 1975; vol. 3, 1985.
23. J. Stöhr, D. A. Outka, K. Baberschke, D. Arvanitis, and J. A. Horsley, *Phys. Rev. B.*, **36**, 2976 (1991).
24. G. R. Wight, C. E. Brion, and M. J. Van der Wiel, *J. Electron Spectrosc.*, **1**, 457 (1972/3).
25. R. N. S. Sodhi and C. E. Brion, *J. Electron Spectrosc. and Rel. Phen.*, **36**, 187 (1985).
26. T. Ohta, T. Fujikawa, and J. Kuroda, *J. Bull Chem. Soc. Jpn.*, **48**, 2017 (1975).
27. A. P. Hitchcock, M. Pocock, C. E. Brion, M. S. Banna, D. C. Frost, C. A. McDowell, and B. Wallbank, *J. Electron Spectrosc.*, **13**, 345 (1978).
28. J. L. Solomon, R. J. Madix, and J. Stöhr, *Surf. Sci.*, **255**, 12 (1991).
29. C. Turci, S. G. Urquhart, and A. P. Hitchcock (unpublished).
30. J. A. Horsley, J. Stöhr, A. P. Hitchcock, D. C. Newbury, A. L. Johnson, and F. Sette, *J. Chem. Phys.*, **83**, 6099 (1985).
31. G. R. Wight and C. E. Brion, *J. Electron Spectrosc.*, **4**, 24 (1974).
32. R. N. S. Sodhi and C. E. Brion, *J. Electron Spectrosc.*, **37**, 125 (1985).
33. I. Ishii and A. P. Hitchcock, *J. Chem. Phys.*, **87**, 830 (1987).
34. W. L. Jolly, K. D. Bomben, and C. J. Eyermann, *At. Data Nucl. Data Tables.*, **31**, 109 (1984).
35. K. Oichi, E. Ito, K. Seki, T. Araki, S. Narioka, H. Ishii, T. Okajima, T. Yokoyama, and T. Ohta, *Photon Factory Report*, 282 (1992).
36. (a) R. J. Meier and B. Coussens, *J. Mol. Struct.*, **253**, 25 (1992); (b) M. Kontoyyianni and J. P. Bowen, *J. Comp. Chem.*, **13**, 657 (1992).
37. A. Caron, and J. Donohue, *Acta. Cryst.*, **B25**, 404 (1969).
38. W. Dannecker, J. Kopf, and H. Rust, *Cryst. Struct. Comm.*, **8**, 429 (1979).
39. M. Remko and S. Scheiner, *J. Mol. Struct. (Theochem)*, **180**, 175 (1988).
40. G. Beamson and D. Briggs, *High Resolution XPS of Organic Polymers: The Scienta ESCA300 Database*, John Wiley and Sons, New York, 1993.
41. Landolt-Bornstein, ed., *Structure Data of Free Polyatomic Molecules*, New Series II, **7** (1987).
42. J. A. Hunt, R. D. Leapman, and D. B. Williams, *Microbeam Analysis*, **2**, 272 (1993).
43. P. E. Batson, N. D. Browning, and D. A. Muller, *MSA Bull.*, **24**, 371 (1994).

Received August 4, 1994
Revised December 2, 1994
Accepted January 25, 1995

CHAPTER 4D

Inner-shell Excitation of Polymer and Monomer Isomers of Dimethyl Phthalate

The following work documents the C 1s X-ray absorption spectra of poly(diallyl phthalate), poly(diallyl isophthalate) and poly(ethylene terephthalate), the C 1s and O 1s electron energy loss spectra of dimethyl phthalate, dimethyl isophthalate and dimethyl terephthalate, and *ab initio* calculations of the C 1s and O 1s core excitation spectra of dimethyl phthalate, dimethyl isophthalate and dimethyl terephthalate. This work has been published in the Journal of Physical Chemistry B. (*J. Phys. Chem. B.* 101, 2267, 1997) and is presented here in published form. The right to reprint this article was retained by the author and authorization has been obtained from the coauthors.

The author of this thesis acquired the electron energy loss spectra and performed the *ab initio* calculations, developed most of the spectral analysis, and wrote this paper in collaboration with Prof. A. P. Hitchcock, Prof. H. Ade, A. P. Smith and Dr. E. G. Rightor. The X-ray absorption spectra were acquired by A. P. Smith.

Inner-Shell Excitation Spectroscopy of Polymer and Monomer Isomers of Dimethyl Phthalate

S. G. Urquhart,† A. P. Hitchcock,*,† A. P. Smith,‡ H. Ade,‡ and E. G. Rightor§

Department of Chemistry, McMaster University, Hamilton, Ontario, Canada L8S 4M1, Department of Physics, North Carolina State University, Raleigh, North Carolina 27695, and Analytical Sciences, B-1470, Dow Chemical, Freeport, Texas 77541

Received: October 31, 1996; In Final Form: January 10, 1997®

The C 1s X-ray absorption spectra (XAS) of poly(diallyl phthalate), poly(diallyl isophthalate), and poly(ethylene terephthalate) (PET) have been recorded using transmission detection. The phthalate segments of these polymers are isomers with different patterns of substitution (ortho, meta, para) of the methyl carboxylate groups on the phenyl ring. The C 1s and O 1s electron energy loss spectra (EELS) of the corresponding isomeric monomers, dimethyl phthalate, dimethyl isophthalate, and dimethyl terephthalate, have also been recorded in the gas phase using inelastic electron scattering under conditions dominated by electric dipole transitions. Good agreement is found in overall shape and in the energies of the spectral features of the same isomer in monomeric (EELS) versus polymeric (XAS) form. *Ab initio* calculations are used to provide a detailed interpretation of the spectra, in particular the origin of the isomeric variations. The analytical potential for using inner shell excitation spectroscopy to identify isomeric character and to map spatial distributions of polymer isomeric substitution is assessed.

1. Introduction

This work extends earlier studies[1–3] of the core excitation spectroscopy of poly(ethylene terephthalate) (PET), a ubiquitous polymer often found in packaging applications, and its small molecule analogue, 1,4-dimethyl terephthalate (1,4-DMP), which is the repeat unit of PET. Core excitation, using either synchrotron-based X-ray absorption (XAS) in a scanning transmission X-ray microscope (STXM) or electron energy loss spectroscopy (EELS) in a transmission electron microscope (TEM), is finding increasing applications in chemical speciation at a microscopic scale.[4] We are interested in determining if isomeric polyphthalates can be analytically differentiated by changes in their C 1s and/or O 1s near edge spectra. Such a capability could be of use in tracking isomeric selectivity in phase segregation phenomena in polymers of mixed polyphthalates. To investigate the sensitivity of inner-shell excitation spectroscopy to the ring substitution pattern in phthalate-based polymers, we have studied both monomer standards and isomeric phthalate polymers.

Investigation of the degree of correspondence of the core spectra of monomers and polymers is a further motivation for this study. The validity of the use of small molecule (in this case monomer) species as standards for polymer spectra has been discussed and demonstrated previously.[5–8] The combination of several experimental techniques, along with semiempirical extended Hückel (EHMO) calculations of 1,4-DMP, has helped elucidate assignments of the spectral features of both polymer and monomer.[3] Other monomer–polymer comparisons include comparisons of phenylurethane to polyurethane,[2] and phenylurea to polyurea.[9] In many cases there is a close correspondence between the core spectra of monomer and polymer. This is true especially when there is no difference in degree of saturation between the monomer and the polymer and when there is minimal interaction among adjacent monomer units of a single polymer chain or among adjacent chains.

In this paper, we report the C 1s X-ray absorption spectra of poly(diallyl phthalate) (1,2–PDP), poly(diallyl isophthalate) (1,3-PDP), and poly(ethylene terephthalate) (1,4-PET or PET) and the C 1s and O 1s inner-shell electron energy loss (ISEELS) of the three isomeric monomers: dimethyl phthalate (1,2-DMP), dimethyl isophthalate (1,3-DMP), and dimethyl terephthalate (1,4–DMP) (see Chart 1). ISEELS is particularly suited for gas phase studies, while XAS in the STXM is exactly the technique for which this work is helping to develop quantification capabilities. Strictly speaking only two of the three polymers are isomers because of the different alkyl linkage. However, because the saturated fragment in which the polymers differ has no effect on π^* conjugation, the π^* aspect of the polymer spectra can be compared as if the polymers were isomers.

Semiempirical EHMO methods have proven useful for assignment of spectral features, even though EHMO does not give accurate absolute core excitation energies. Typically orbital eigenvalues (ϵ) in a "Z+1" calculation are interpreted as relative term values ($-\epsilon \approx \mathrm{TV} = \mathrm{IP} - E_{ex}$) which are placed on an absolute scale using experimental core level ionization potentials (IPs). In the case of 1,4-DMP, the quality of the agreement between the experimental and the EHMO calculated spectrum is poor[7] when compared to that found in other applications of EHMO to core excitation. EHMO was never able to reproduce important aspects of the experimental C 1s spectrum of 1,4-DMP, particularly the splitting of the lowest energy $\pi^*_{C=C}$ band, even when a range of plausible geometries were explored. For this reason we have used *ab initio* calculations based on Kosugi's "GSCF3" methodology[10] to provide improved theoretical results upon which to base our spectral interpretations. We report the results of GSCF3 calculations of the C 1s and O 1s absorption spectra of 1,4-DMP, 1,3-DMP, and 1,2-DMP.

2. Experimental Section

X-ray absorption measurements were made using the scanning transmission X-ray microscope (STXM) at the X-1A beamline

† McMaster University.
‡ North Carolina State University.
§ Dow Chemical.
® Abstract published in *Advance ACS Abstracts*, March 1, 1997.

CHART 1

1,4-DMP
dimethyl terephthalate

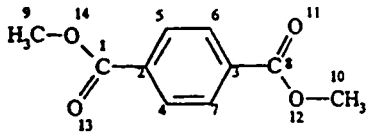

1,3-DMP
dimethyl isophthalate

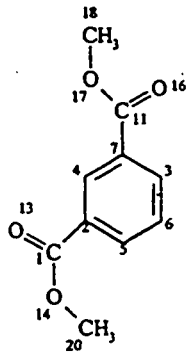

1,2-DMP
dimethyl phthalate

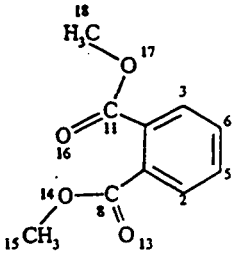

1,4-PET
poly(ethylene terephthalate)

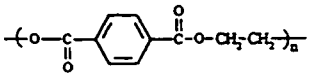

1,3-PDP
poly(diallyl isophthalte)

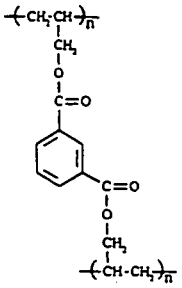

1,2-PDP
poly(diallyl phthalate)

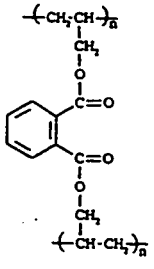

at the National Synchrotron Light Source (NSLS). Details of the apparatus and operating procedures have been provided elsewhere.[3,12,13] The polymer samples were obtained from Scientific Polymer Products (PET density 1.385; 1,3-PDP density 1.256, degree of polymerization 20; 1,2-PDP density 1.267, degree of polymerization 10). The PET sample was microtomed at room temperature to prepare ~0.1 μm thick sections for the C 1s spectrum. The 1,3-PDP and 1,2-PDP polymer samples were prepared by evaporating a 0.1 wt % solution of the polymer in acetone to form thin polymer films on carbon-coated TEM grids.

Spectra were acquired with an atmosphere of He gas in the microscope enclosure.[11] The energy resolution was about 0.3 eV. Spectral acquisition time was less than 1 min per energy scan, which represents approximately 5% of the critical dose in the case of PET. We assume that the critical dose of 1,2-PDP and 1,3-PDP is similar to that measured for PET.[3] In addition, the spectra for 1,2-PDP and 1,3-PDP were acquired under defocused beam conditions.

The energy scales of the C 1s spectra were determined by simultaneously measuring the C 1s spectrum of the polymer and CO_2 gas mixed with He gas in the microscope enclosure. The C 1s $\rightarrow$ 3s Rydberg peak at 292.80 eV[14] is used for calibration. The derived position of the main $\pi^*_{C=C}$ peak of PET is 284.8(1) eV. The estimated 0.1 eV uncertainty is largely associated with the uncertainties in a small correction for nonlinearity of the energy scale, which was variable in time but which amounted to as much as 0.2 eV in the 8 eV difference between the energies of the π^* peaks in PET and CO_2. The π^* energy for PET is in agreement with that of the main peak in the ISEELS of 1,4-DMP (284.86(6) eV).

The gas phase energy loss spectrometer has been described previously.[15] Spectra were recorded using a final electron energy of 2.5 keV, a scattering angle of 2°, and a resolution of 0.6 eV fwhm. Under these conditions electric dipole transitions dominate. Small angle rather than zero-degree scattering is used in order to prevent the main electron beam from entering the analyzer and creating a large background. The solid 1,4-DMP and 1,3-DMP samples and the liquid 1,2-DMP sample were introduced directly in a small metal cell directly attached to the collision cell. This normally provided adequate intensity, although gentle heating of the collision cell and sample to ~40

TABLE 1: Calculated Geometries of 1,4-DMP, 1,3-DMP, and 1,2-DMP[a]

	1,4-DMP	1,3-DMP	1,2-DMP	crystal[29]	PET[30]
Bond Lengths (Å)					
C−C(ring) average	1.383	1.383	1.384	1.385	1.35
C−H (ring)	1.069	1.070	1.069	1.070	1.07
C−(CO_2Me)	1.480	1.475	1.487	1.486	1.49
C=O	1.207	1.207	1.205	1.23	1.27
(CO)−O	1.346	1.347	1.342	1.331	1.34
O−Me	1.454	1.453	1.453	1.450	1.44
C−H(Me)	1.078	1.078	1.078	0.93	
Bond Angles (deg)					
C(Ph)−C(O)−OMe	112.6	112.5	113.0		
C(Ph)−C=O	124.9	125.0	126.4		
(OC)−O-Me	118.2	118.2	118.4		
Ph−CO_2Me	planar	planar	nonplanar		
1,2-DMP Dihedral Angles (See Chart 1 for Atom Labeling) (deg)					
2-1-7-8			−19.5		
3-2-11-12			−41.5		

[a] The molecular structures were obtained from an *ab initio* self-consistent-field (SCF) geometry optimization (3-21G* basis set). Harmonic frequency calculations were performed to verify that these structures represent the minima on the potential energy surface. Conformations are presented in Chart 1. The total energies for the minimum energy conformations are −680.185, −680.187, and −680.167 au for 1,4-DMP, 1,3-DMP and 1,2-DMP, respectively. In a fully planar geometry the total energy for 1,2-DMP is −680.156 au.

°C was used in some cases to obtain higher vapor pressure. All three DMP isomers were obtained from Aldrich (stated purity >99%). Absolute energy scales were determined by recording spectra of a mixture of the molecule and CO_2.

The spectra of the gas phase monomer and solid polymer were converted to an absolute oscillator strength scale using standard methods[16] that are based on background subtraction and normalization of the far continuum to atomic oscillator strengths.[17]

3. Calculations

The ground state structures of 1,4-DMP, 1,3-DMP, and 1,2-DMP were provided from an *ab initio* geometry optimization performed with a 3-21G* basis set using the program SPARTAN.[18] The effect of the methyl carboxylate conformation on the total energy was explored. For example, the C_{2h} configuration of 1,4-DMP has a lower energy than the C_{2v} configuration. Similar determinations were made for the 1,2-DMP and 1,3-DMP structures. Harmonic vibrational frequencies were calculated (3-21G* basis) to verify that the lowest energy optimized structures indeed represent minima in the potential energy surface. The lowest energy conformation is planar for 1,4-DMP and 1,3-DMP, but in 1,2-DMP the methyl carboxylate groups are forced out of plane by steric effects. These geometries are listed in Table 1. Chart 1 presents the atom numbering used to identify atomic-specific contributions to the calculated core excitation spectra.

The core-ionized and core excited states of 1,4-DMP, 1,3-DMP, and 1,2-DMP were obtained by *ab initio* self-consistent-field (SCF) calculations with explicit consideration of the core hole[19] and with the localized core hole picture. These calculations were performed using the *ab initio* program "GSCF3".[10] The basis set used is the extended basis set taken from (63/6) and (53/5) contracted Gaussian-type functions for C and O and (6) for H of Huzinaga et al.,[20] where the contraction scheme was (311121/21111/1*) for atoms with a core hole, (521/31) for heavy atoms with no core hole, and (31) for H. The core excited states were obtained with the improved virtual orbital (IVO) method.[21] The relaxed Hartree−Fock (HF) potential is essential in accurately considering large electronic reorganization upon inner-shell hole creation; therefore, the IVO method based on the relaxed HF potential is superior to the method using the ground state orbitals. This method has been shown to be quite accurate in predicting term values and intensities of core — Rydberg excitations,[22,23] and provides a good first-order approximation to the energies and intensities of core — valence excitations.[24] Gaussian line widths used in generating the simulated spectra from the *ab initio* results were 0.6 eV fwhm for orbitals of eigenvalue (ϵ) $-15 < \epsilon < 0$, 1.2 eV for $0 < \epsilon < 4$ in the C 1s simulation; and 0.8 eV fwhm for orbitals of eigenvalue (ϵ) $-15 < \epsilon < 0$, 1.2 eV for $0 < \epsilon < 4$ in the O 1s simulation. These widths were chosen to be similar to the experimentally observed line widths.

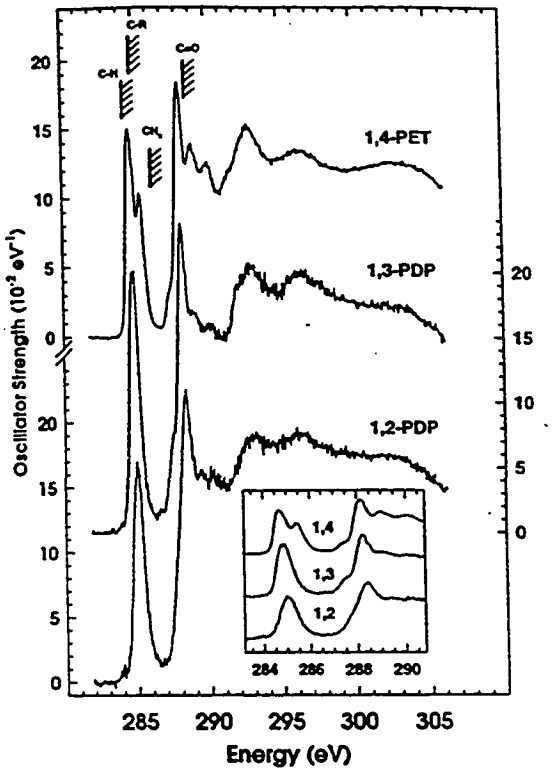

Figure 1. Comparison of C 1s oscillator strengths derived from x-ray absorption spectra of 1,2-PDP, 1,3-PDP, and 1,4-PET polymers, recorded by transmission through a solid thin film in a scanning transmission X-ray microscope (STXM) at X-1A of NSLS. The solid state IPs[31] are indicated by hatched lines. The inset shows an expansion of the π^* region.

Molecular orbital diagrams of the LUMO and (LUMO+1) π^* states of the C 1s(C−H) core excited states of 1,4-DMP, 1,3-DMP, and the ground state of benzene and 1,3-DMP have also been prepared. The orbital energies and wave functions for 1,3-DMP and 1,4-DMP were taken from the above calculations. The ground state of benzene was calculated using an identical basis set and the experimental geometry.[25]

4. Results and Discussion

4.1. C 1s Spectra. Figure 1 compares the C 1s X-ray absorption spectra of the 1,2-PDP, 1,3-PDP and 1,4-PET polymers. Figure 2 presents the corresponding C 1s spectra of the gas phase monomers 1,2-DMP, 1,3-DMP, and 1,4-DMP,

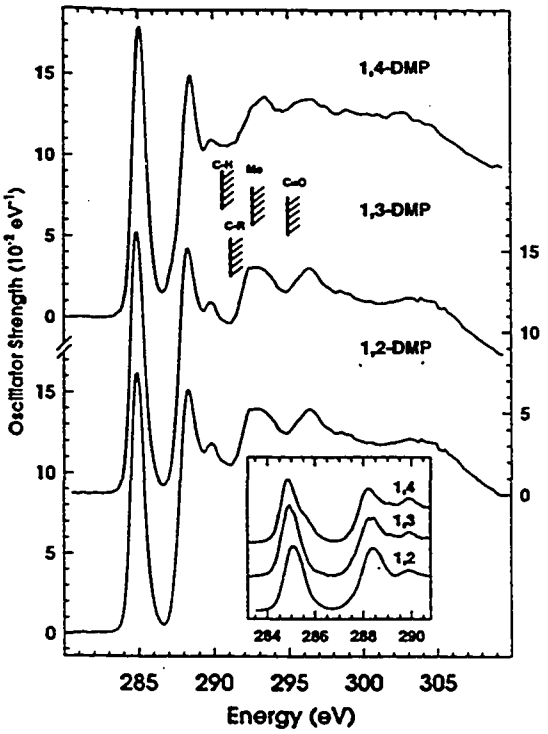

Figure 2. Comparison of the C 1s oscillator strength spectra of monomeric 1,2-, 1,3-, and 1,4-DMP, derived from gas phase, inner-shell electron energy loss measurements carried out in the electric dipole scattering regime (2° scattering angle, 2.5 keV final electron energy, 0.6 eV fwhm resolution). The inset shows an expansion of the π^* region. The hatched lines indicate estimated gas phase C 1s IPs.

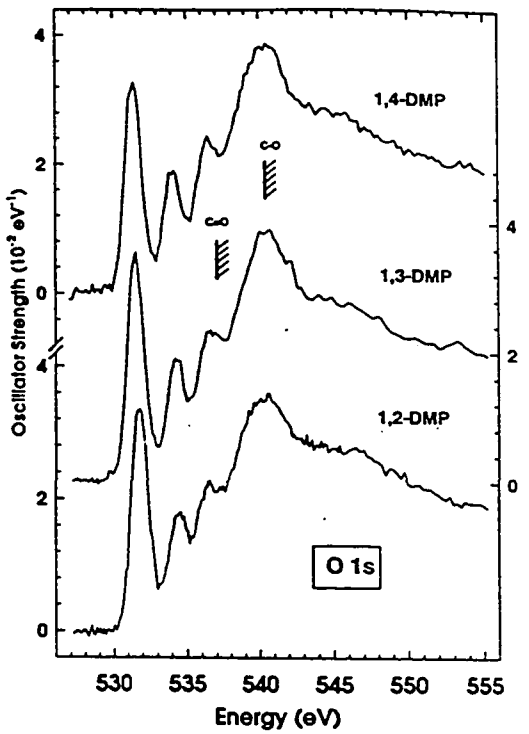

Figure 3. Comparison of the O 1s oscillator strength spectra of monomeric 1,2-, 1,3-, and 1,4-DMP, derived from gas phase EELS (see caption to Figure 2 for experimental details). The hatched lines indicate estimated gas phase O 1s IPs.

all recorded by energy loss spectroscopy. Figure 3 presents the O 1s spectra of the monomers. In all cases the spectra are converted to absolute oscillator strength scales, after subtraction of underlying valence and lower energy core excitation signal. Note the oscillator strength scale refers to that of the repeat unit or full molecule as opposed to a per-atom basis, which has been used in some earlier work. The repeat units of 1,2-PDP, 1,3-PDP, and 1,4-PET have 14, 14, and 10 carbon atoms, respectively, whereas all of the DMP monomers have only 10 carbon atoms. This is why the continuum intensity in the 1,2-PDP and 1,3-PDP C 1s spectra is larger than that in all of the other species.

Tables 2, 3, and 4 summarize the energies, estimated term values (TV = ionization potential (IP) − transition energy (E)), and proposed assignments for the C 1s and O 1s spectra of the three isomeric monomers and polymers. The C 1s spectra predicted from the GSCF3 *ab initio* calculations of 1,4-DMP, 1,3-DMP, and 1,2-DMP are presented in Figure 4, in comparison to the experimental spectra of the related polymers. Since the monomer and polymer spectra are generally similar, the calculations are compared to the polymer XAS spectra instead of the more appropriate monomer spectra because of the added information provided by the higher resolution. The relative positions of the calculated component spectra are set using the calculated C 1s ionization energies. The full spectrum was generated by summing the components in stoichiometric proportion. The calculated energies are higher than the absolute experimental energies, with the energy difference between calculated and experimental features increasing for transitions that occur at higher energy, such as the C 1s(C=O) → $\pi^*_{C=O}$ transition. For the lowest energy 1s → π^* transition, the energy difference is ~2 eV for the C 1s spectra and ~1 eV for the O 1s spectra. The calculated energies, term values, oscillator strengths, and ionization potentials for the C 1s and O 1s spectra are presented in Tables 5 and 6, respectively.

In general the assignments follow those proposed for PET in our earlier studies.[1-3] Here we focus the discussion on some of the differences among these three species, in particular the change in shape of the lowest energy π^* band in the C 1s spectrum and the energy shifts that are found in both the C 1s and O 1s spectra. On the basis of the effect of substitutional pattern on relative stability and chemical reactivity, one might expect that the electronic structure of the 1,2 and 1,4 isomers should be similar, while that of the 1,3 isomer might differ. However, because steric interactions cause the geometry of 1,2-DMP to be nonplanar, its orbital interactions are expected to be quite different and thus the expected correspondence with the para isomer should be reduced. Overall the spectra of the three isomers are quite similar, although there are some notable differences. The energy of the main C 1s → $\pi^*_{C=C}$ shifts upward by 0.26 eV, while the main O 1s → $\pi^*_{C=O}$ peak shifts upward in energy by 0.47 eV between 1,4-, and 1,2-DMP. These isomeric shifts of the energy of the main π^* transitions are reproduced by the *ab initio* calculations. In addition, the lowest energy C 1s → π^* band in 1,4-DMP has a different shape than that for the 1,3- and 1,2-DMP isomers (see inset of Figures 1 and 2). Finally, the energy of the weak band at 290 eV in the higher energy end of the $\pi^*_{C=O}$ region is dependent on the isomer. All of the energy shifts are real since the calibration precision of the energy loss scale is better than 0.05 eV (with an accuracy of better than 0.1 eV). It is likely that the isomeric shifts in the $\pi^*_{C=C}$ and $\pi^*_{C=O}$ peak positions arise mainly from

TABLE 2: Experimental Energies (*E*, eV) and Assignments for Features in the C 1s Spectra of Polymers: Poly(ethylene terephthalate) (1,4-PET), Poly(diallyl isophthalate) (1,3-PDP), and Poly(diallyl phthalate) (1,2-PDP)

				assignment			
	1,4-PET	1,3-PDP	1,2-PDP	C−H	C−R	CH_x	C=O
IP[b]	284.7	284.6	284.6	IP			
1	284.8[a]	284.87[a]	285.05[a]	π^*_{C-C}	π^*_{C-C}		
IP[b]	285.2	285.1	285.1		IP		
2	285.43			π^*_{C-C}			π^*_{C-C}
IP[b]	286.2	286.2	286.2			IP	
3 (sh)	287.4	287.5	287.6			σ^*_{C-H}	
4	288.27	288.21	288.38				$\pi^*_{C-O}(+)$
IP[b]	288.7	288.7	288.7				IP
5	289.0	289.2	289.4	$\pi^*_{C-C/C-O}$			
6	290.1	290.3	290.3				$\pi^*_{C-O}(-)$
7 (sh)	291.6	291.6					
8 (sh)	292.8	293.0	293.1	σ^*_1(Bz)			$\sigma^*_{C-O}/\pi^*_{C-O}$(mix)
9	296.4	296.3	296.2	σ^*_2(Bz)			
10	303.3	303.2	302.8				σ^*_{C-O}

[a] Calibration: Energy scales were determined by simultaneously measuring the C 1s spectrum of the polymer and CO_2 (admixed with He in the microscope enclosure). The C 1s → 3s Rydberg peak at 292.80 eV[14] is used for calibration. [b] From XPS.[31]

TABLE 3: Experimental Energies (*E*, eV), Term Values, and Assignments for Features in the C 1s Spectra of Dimethyl Terephthalate (1,4-DMP), Dimethyl Isophthalate (1,3-DMP), and Dimethyl Phthalate (1,2-DMP)

	dimethyl terephthalate (1,4-DMP)					dimethyl isophthalate (1,3-DMP)					dimethyl phthalate (1,2-DMP)					assignment			
	energy	term value				energy	term value				energy	term value							
	(eV)	T_{C-H}	T_{C-R}	T_{Me}	$T_{C=O}$	(eV)	T_{C-H}	T_{C-R}	T_{Me}	$T_{C=O}$	(eV)	T_{C-H}	T_{C-R}	T_{Me}	$T_{C=O}$	C−H	C−R	Me	C=O
1	284.86[a]	5.6	6.1			284.95[b]	5.6	6.1			285.12[c]	5.4	5.9			π^*_{C-C} (a)	π^*_{C-C}		
2	285.7	4.8														π^*_{C-C} (b)			
3	287.4			5.2							287.2			5.2				σ^*_{C-H}	
4	288.2		2.8		6.7	288.4		2.6		6.5	288.5		2.5		6.4		$\pi^*_{C-C/C-O}$		$\pi^*_{C-O}(+)$
5	289.1	2.4														$\pi^*_{C-C/C-O}$			
6	289.9				5.0	289.9				5.0	289.9				5.0				$\pi^*_{C-O}(-)$
IP[d]	290.5					290.5					290.5					IP			
IP[d]	291.0					291.0					291.0						IP		
IP[d]	292.6					292.6					292.6							IP	
IP[d]	294.9					294.9					294.9								IP
7	292.8	−2.3	−1.8		2.1	293.0	−2.5	−2.0		1.9	293.3	−2.8	−2.3		1.6	σ^*_1(Bz)	σ^*_{C-O}		π^*_{C-O}(mix)
8	296.3	−5.8				296.4	−5.9				296.3	−5.8				σ^*_2(Bz)			
9	304				−9	304				−9	304				−9				σ^*_{C-O}

[a] Calibration: −5.88(6) eV relative to π^* of CO_2 (290.74 eV). [b] Calibration: −5.79(3) eV relative to π^* of CO_2. [c] Calibration: −5.62(3) eV relative to π^* of CO_2. [d] The IPs were estimated from those of related species.[32] Note that the underscore in the following indicates the site of core ionization. C_6H_6, 290.3 eV; $\underline{C}H_3CO_2CH_3$, 291.3; $CH_3CO_2\underline{C}H_3$, 292.6; $CH_3\underline{C}O_2CH_3$, 294.9 eV.

TABLE 4: Experimental Energies (*E*, eV), Term Values, and Assignments for Features in the O 1s Spectra of Dimethyl Terephthalate (1,4-DMP), Dimethyl Isophthalate (1,3-DMP), and Dimethyl Phthalate (1,2-DMP)

	1,4-DMP			1,3-DMP			1,2-DMP				
		TV			TV			TV		assignment	
	energy (eV)	$T_{C=O}$	T_{C-O}	energy (eV)	$T_{C=O}$	T_{C-O}	energy (eV)	$T_{C=O}$	T_{C-O}	C=O	C−O
1	531.5[a]	5.5		531.53[b]		5.5	531.77[c]		5.2	$\pi^*_{C-O}(+)$	
2	534.0	3.0		534.3	2.7		534.5	2.5		$\pi^*_{C-O}(-)$	$\pi^*_{C-O}(+)$
3	536.4		4.1	536.8		3.7	536.5		4.0	$\pi^*_{C-O,C=C}$	$\pi^*_{C-O}(-)$
IP[d]	537.0			537.0			537.0			IP	
IP[d]	540.5			540.5			540.5				IP
4	540.3		0.2	540.5		0	540.4		0.1		σ^*_{C-O}
5	546	9		546	9		546	9		σ^*_{C-O}	

[a] Calibration: −3.9(1) eV relative to π^* of CO_2 (535.4 eV). [b] Calibration: −3.87(2) eV relative to π^* of CO_2. [c] Calibration: −2.34(4) eV relative to π^* of CO (534.11(8) eV). [d] Estimated from the XPS IPs of related species:[32] $CH_3\underline{C}O-OCH_3$, 537.0; $CH_3O-\underline{O}CH_3$, 540.5 eV.

the changing nature of π^*_{C-C} and π^*_{C-O} mixing. Similar changes were observed recently in the 1s spectra of nitroanilines.[26]

The *ab initio* calculations (Figures 4 and 5) mirror the isomer-related changes in the core excitation spectra. The energy and width of the first C 1s → π^*_{C-C} transition changes between 1,4-DMP and 1,2-DMP, as found experimentally. The width of this transition in the 1,3 and 1,2 species is a consequence of the overlap of multiple phenyl ring (C−H) contributions. The energy shift occurs because some of the C 1s(C−H) → π^*_{C-C} and C 1s(C−R) → π^*_{C-C} components in 1,3-DMP and in 1,2-DMP are shifted to higher energy and overlap (note that C−R refers to the ring carbon to which the methyl carboxylate is attached). The isomeric changes observed in the C 1s(C=O) → π^*_{C-O} transition are also reproduced, although there is a clear "stretching" of the calculated energy scale relative to the experimental one. The *ab initio* results show that the increase in the energy of the main π^*_{C-O} transition between 1,4-DMP and 1,2-DMP arises from a competition between a small decrease in the C 1s binding energy and a larger increase in the

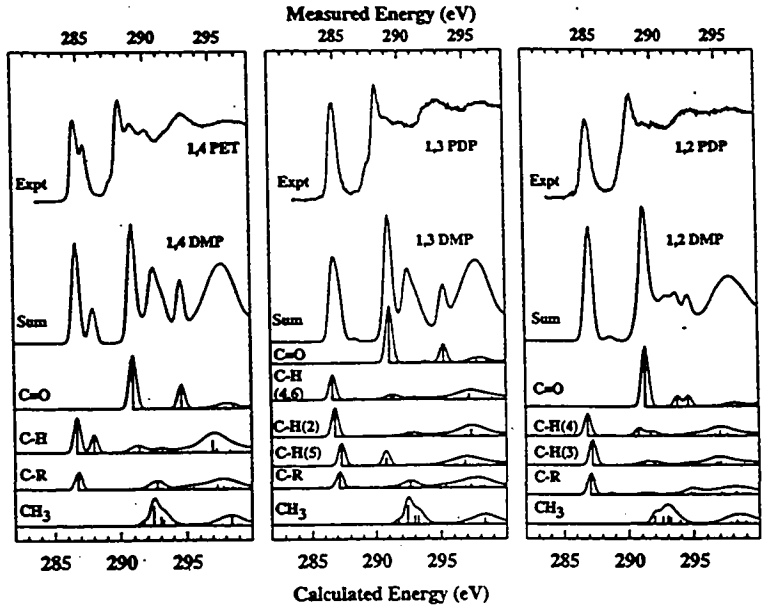

Figure 4. *Ab initio* calculations for the C 1s spectra of 1,4-DMP, 1,3-DMP, and 1,2-DMP, in comparison to the experimental C 1s X-ray absorption spectra of 1,4-PET, 1,3-PDP, and 1,2-PDP. Each component spectrum corresponds to an IVO calculation at a specific site (see Chart 1 for atom numbering). The excitation energy is the sum of the calculated term values for individual transitions and the calculated absolute IPs. *Note there is a 2.0 eV difference in the energy scales used to plot the experimental and calculated results.* The peak areas are the calculated absolute oscillator strengths. The sum is weighted by stoichiometry.

TABLE 5: Calculated Energies, Term Values, and Oscillator Strengths for C 1s → π^* Transitions of 1,4-DMP, 1,3-DMP, and 1,2-DMP

1,4-DMP

	C 1s C−H(2,3,5,6)			C 1s C−R(1,4)			C 1s C=O(7,11)			C 1s CH_3(10,14)[a]		
	E (eV)	TV (eV)	OS	*E* (eV)	TV (eV)	OS	*E* (eV)	TV (eV)	OS	*E* (eV)	TV (eV)	OS
IP	290.842			291.212			295.711			292.990		
1	286.73	4.12	0.0619	286.82	4.39	0.0304	290.97	4.75	0.0933	290.67	2.32	0.0000
2	288.02	2.82	0.0317	289.16	2.06	0.0000	294.63	1.08	0.0420	291.72	1.27	0.0083
3	290.96	−0.11	0.0058	291.12	0.10	0.0011	294.81	0.90	0.0000	292.45	0.54	0.0343

1,3-DMP

	C 1s C−H(4,6)			C 1s C−H(2)			C 1s CH(5)			C 1s C−R(1,3)			C 1s C=O(7,11)			C 1s CH_3(10,14)[a]		
feature[a]	E (eV)	TV (eV)	OS	E (eV)	TV (eV)	OS	E (eV)	TV (eV)	OS	E (eV)	TV (eV)	OS	E (eV)	TV (eV)	OS	E (eV)	TV (eV)	OS
IP	291.091			290.986			290.826			291.112			295.659			292.968		
1	286.74	4.35	0.0436	286.84	4.15	0.0252	287.33	3.50	0.0196	287.17	3.94	0.0283	291.09	4.57	0.1002	291.00	1.97	0.0001
2	288.46	2.63	0.0015	287.86	3.13	0.0000	287.58	3.25	0.0000	288.38	2.73	0.0011	293.90	1.76	0.0027	291.71	1.26	0.0083
3	291.26	−0.17	0.0074	291.46	−0.48	0.0000	290.81	0.01	0.0069	291.29	−0.18	0.0044	295.26	0.40	0.0333	292.28	0.69	0.0003

1,2-DMP

	C 1s C−H(3,6)			C 1s C−H(4,5)			C 1s C−R(1,2)			C 1s C=O(7,11)			C 1s CH_3(10,14)[b]		
	E (eV)	TV (eV)	OS	E (eV)	TV (eV)	OS	E (eV)	TV (eV)	OS	E (eV)	TV (eV)	OS	E (eV)	TV (eV)	OS
IP	290.898			290.95			291.240			295.551			292.533		
1	287.26	3.64	0.0448	286.89	4.06	0.0387	287.12	4.12	0.0373	291.28	4.27	0.1053	290.58	1.95	0.0024
2	287.78	3.12	0.0073	288.47	2.48	0.0014	288.77	2.47	0.0033	293.79	1.77	0.0187	291.69	0.84	0.0018
3	291.62	−0.72	0.0099	291.63	−0.67	0.0153	291.35	−0.11	0.0073	294.62	0.92	0.0189	291.94	0.60	0.0133

[a] For C 1s(C−H) and C 1s (C−R) excitation; feature 1 is mainly $\pi^*_{C=C}$ (lower energy component from the $1\pi^*(e_{1u})$ orbital of benzene); 2 is the higher energy component of the $1\pi^*$ (e_{1u}); and 3 is the main $\pi^*_{C-O}(+)$ orbital. For excitation at the other carbon sites, these are the 3 lowest energy virtual orbitals. [b] Tabulated C 1s(CH_3) → final state transitions for methyl carbons include π^* and σ^* final states.

$\pi^*_{C=O}$ term value. The dominant term value change indicates the important role of π^* mixing in these molecules, especially the mixing of the two carbonyl π^* orbitals.

In 1,4-DMP, there is a second, relatively intense transition at 285.7 eV that is absent in the spectra of both 1,3-DMP and 1,2-DMP. The *ab initio* calculations clearly show that the 285.7 eV peak is associated with C 1s(C−H) excitation to the second component of the $1\pi^*$ orbital, i.e. the higher energy of the two orbitals that correlate with the e_{1u} orbital of benzene (see Figure 6). Extended Hückel molecular orbital (EHMO) calculations previously performed for 1,4-DMP also predicted that the second transition originated from the C−H carbons.[7] However, the

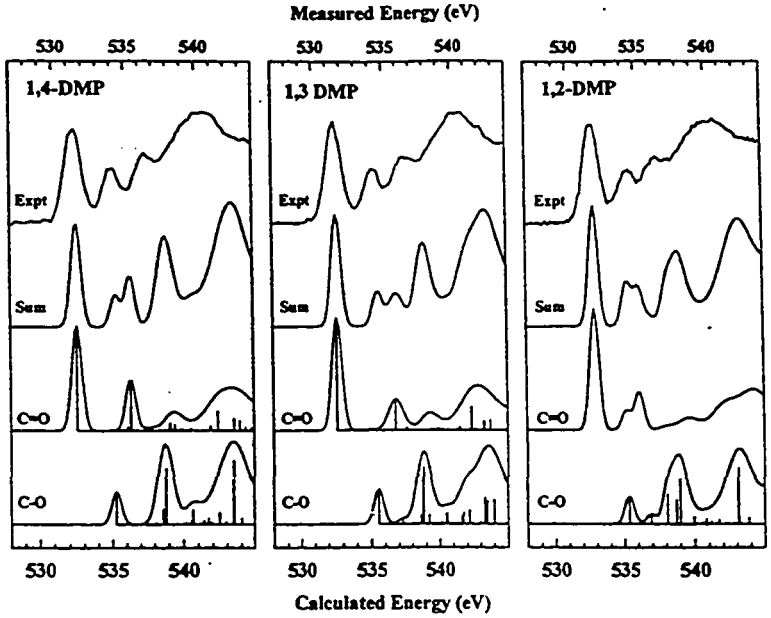

Figure 5. *Ab initio* calculations for the O 1s spectra of 1,4-DMP, 1,3-DMP and 1,2-DMP. Each component spectrum corresponds to an IVO calculation of core excitation at a specific site (see Chart 1 for atom numbering). The excitation energies are the sum of the term values for individual transitions and the calculated absolute IPs. *Note there is a ~1 eV difference in the presentation of the energy scales for the experimental and calculated energy scales.* The peak areas are the calculated absolute oscillator strengths.

TABLE 6: Calculated Energies, Term Values, and Oscillator Strengths for O 1s → π* Transitions of 1,4-DMP, 1,3-DMP, and 1,2-DMP

	O 1s(C=O) (8,12)			O 1s(C−O) (9,13)		
feature[a]	*E* (eV)	TV (eV)	OS	*E* (eV)	TV (eV)	OS
			1,4-DMP			
IP	536.854			538.583		
1	532.44	4.30	0.0155	535.28	3.30	0.0047
2	536.10	0.76	0.0005	538.13	0.45	0.0002
3	536.33	0.53	0.0072	538.65	−0.07	0.0033
			1,3-DMP			
IP	536.708			538.547		
1	532.65	4.06	0.0166	535.54	3.06	0.0051
2	535.11	1.60	0.0001	537.27	1.28	0.0007
3	536.79	-0.08	0.0066	538.83	−0.28	0.0123
			1,2-DMP			
IP	536.662			538.137		
1	532.89	3.77	0.0179	535.36	2.77	0.0040
2	535.18	1.49	0.0028	536.94	1.20	0.0014
3	536.14	0.53	0.0057	538.09	0.04	0.0043

[a] Feature 1 is $\pi^*_{C-O}(+)$, feature 2 is $\pi^*_{C-O}(-)$, and feature 3 is π^*_{C-O} in character.

EHMO calculation did not reproduce correctly the relative intensity of the first and second transition. In particular, the second transition was predicted to be significantly larger than the first.[7] The *ab initio* result confirms the EHMO attribution of the origin of the second transition and, in addition, reasonably reproduces the relative intensity of the first two transitions.

As EHMO calculations have had a good track record at reproducing the C 1s → π* transitions,[1,2] we have made further comparisons with the *ab initio* results in order to determine if the error in the relative intensities of the first two transitions in 1,4-DMP is related to assumptions made in our implementation of EHMO to core excitation or whether it is simply a reflection of the limitations of EHMO wave functions. Two assumptions that might be questioned are the use of the Z+1 approximation to correct for core hole relaxation and the use of N 2p coefficients to estimate spectral intensities. In the improved virtual orbital method of the GSCF3 *ab initio* package the core hole is included explicitly and the transition matrix element integrals are evaluated in full. However, it is possible to use GSCF3 in modes similar to the way we use EHMO, i.e. using orbital coefficients from Z+1 ground state calculations to approximate transition intensities. The EHMO Z+1 (EICVOM) result for 1,4-DMP has been compared to the result from the *ab initio* Z+1 calculation, as well as to an IVO−*ab initio* calculation in which the orbital coefficient is used to approximate intensities. All of the *ab initio* calculations used the same basis set, with the same level of expansion. The three ways of carrying out the GSCF3 calculation are compared to the EHMO result for 1,4-PET in Figure 7. Only the first two transitions are presented. While the term value differs with the calculation technique, all of the *ab initio* results qualitatively reproduce the relative intensity of the first and second transition, while the EHMO−EICVOM result does not. From Figure 7, we conclude that the shortcomings of EHMO are not simply a matter of limitations of the EICVOM model or the approximation in which $\sum c^2(2p)$ is used as the relative intensity, but rather they are associated with inadequacies of the EHMO wave functions themselves.

The prominent second peak in 1,4-DMP and its absence in the 1,2- and 1,3-DMP isomers suggest that a unique pattern of orbital mixing occurs in 1,4-DMP that does not exist in 1,3-DMP or 1,2-DMP. The nature of this mixing can be determined by examining the molecular orbitals corresponding to these final states. Figure 6 presents an orbital correlation diagram illustrating the relationships of the LUMO and (LUMO+1) π* MOs of the ground state and the C 1s(C−H) core excited state of 1,4-DMP and 1,3-DMP and the ground state of benzene. The first π* transition is to a final state similar to one of the π* e_{2u} MOs of benzene, mixed with a positive combination (same phase on each methyl carboxylate group) of π^*_{C-O} orbital

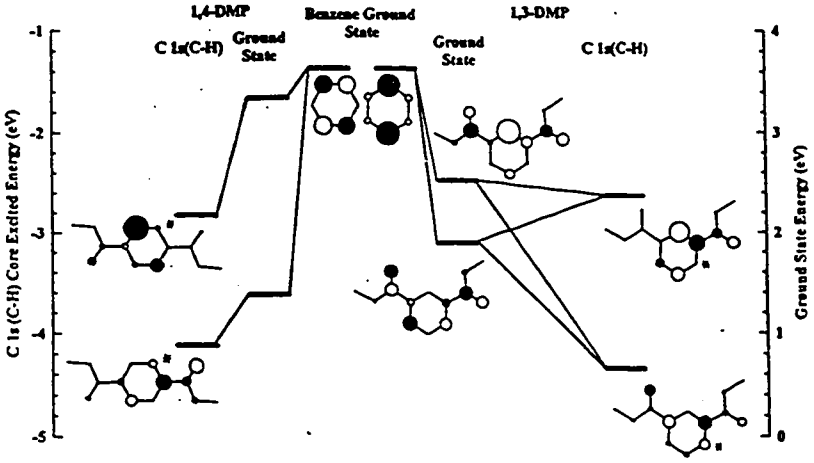

Figure 6. Orbital correlation diagram of the LUMO and (LUMO+1) π^* orbitals of the ground state and the C 1s(C−H) core excited states of 1,4-DMP and 1,3-DMP and of the ground state of benzene. The diameter of the circles is proportional to the $2p\pi$ orbital density on each atom in the molecular orbital. For visibility, the diameters of the circles on the methyl carboxylate group have been increased by a factor of 5. The "*" designates the site of the core hole.

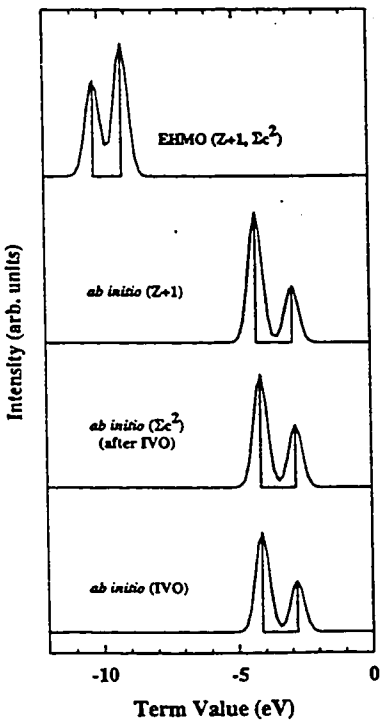

Figure 7. Comparison of the C 1s(C−H) spectrum of 1,4-DMP evaluated by extended Hückel molecular orbital calculations using the equivalent ionic core virtual orbital model (EICVOM, Z+1); *ab initio* EICVOM (Z+1) calculation; the IVO−*ab initio* (GSCF3) calculation with intensities approximated by 2p coefficients; and the IVO calculation using the full transition matrix element.

density. The second peak is evolved as well from the benzene π^* e_{2u} MO mixed with $\pi^*_{C=O}$ orbital density of the methyl carboxylate group on the opposite side of the molecule from the core excited center. Typically, the second lowest e_{2u}-derived level (LUMO+1) in a substituted benzene ring has no orbital density on the core excited carbon (see Figure 6 for MOs of C 1s excited and ground state 1,3-DMP). As the core hole is moved to different sites on the phenyl ring, the spatial distribution of this orbital changes so that there is no $2p\pi^*$ density at the site of the core hole. This trend has been observed in several other recent EHMO studies of substituted aromatic systems.[1,2] However, in 1,4-DMP, the para substitution of the two methyl carboxylate group appears to "pin" the electron distribution in the (LUMO+1) level, such that a portion of the e_{2u}-derived orbital density remains at the site of the C 1s(C−H) core excited atom. Examining the (LUMO+1) MO of 1,3-DMP, we observe that the corresponding pinning does not occur, so that there is no $2p\pi^*$ density at the C 1s(C−H) core excited atom in the higher energy of the two e_{2u}-derived MOs. In the (LUMO+1) of 1,3-DMP, the methyl carboxylate group has the same phase relationship to the ring as it has in 1,4-DMP, but the core excited carbon site now has no $2p\pi^*$ orbital density. This picture of a systematic influence of para substitution on the spatial distribution of the higher of the two e_{2u}-derived MOs is a recurring theme in core excitation in disubstituted phenyl groups.[1,2] In the absence of other perturbations, such as a ligand−ring delocalization which is dependent on the pattern of isomeric substitution, one may expect to see a second C 1s $\rightarrow 1\pi^*_{C=C}$ signal in para species, but not in the meta or ortho species. A distinct ~0.5 eV splitting of the main $\pi^*_{C=C}$ feature in *p*-xylene has been observed in recent studies of the C 1s spectra of the isomeric xylenes, supporting this outlook.[27]

The features in the region above the C 1s(C−H) $\rightarrow 1\pi^*_{C=C}$ transitions are less well resolved because this region has contributions from all of the carbon atoms in the polymer or monomer. In the spectra of the polymers and monomers there is a shoulder at ~287.5 eV. This shoulder is approximately of equal height in the monomer spectra, but is more than twice as large in the spectra of 1,3-PDP and 1,2-PDP than in the spectrum of 1,4-PET. This intensity difference provides a basis for assigning this feature to C 1s(CH_x) $\rightarrow \sigma^*_{C-H}$ transitions, since the intensity trends correlate well with the different alkyl bridge structure of the polymers. The *ab initio* calculations (Figure 4) predict that the C 1s(CH_3) $\rightarrow \sigma^*_{C-H}$ transitions occur at somewhat higher energy. This is an example of an energy scale "stretching" that occurs in the GSCF3 calculations at the level of basis set we are using. The effect is particularly clear for the C 1s(C=O) $\rightarrow \pi^*_{C=O}$ transitions. For transitions at higher

energy, more caution is required for interpretation, and the use of empirical observations is especially helpful.

The 288−292 eV region is dominated by a mixture of C 1s(C=O) → π^*_{C-O} and C 1s(C−H) → $2\pi^*_{C-C}$ transitions (the $2\pi^*_{C-C}$ orbital is derived from the π^* b_{2g} orbital of benzene). In general these features involve excitation to delocalized upper levels of mixed $\pi^*_{C-C/C=O}$ character (see Figure 5 of ref 3). The intense feature at ~288.3 eV in the spectra of the monomers and polymers is assigned to the C 1s(C=O) → $\pi^*_{C-O}(+)$ transition, where "+" refers to the in-phase relationship of the two contributing π^*_{C-O} portions. The transition at ~289 eV is assigned as a C 1s(C−H) → $\pi^*_{C-C/C=O}$ transition, and the transition at ~290 eV is assigned as the C 1s(C=O) → $\pi^*_{C-O}(-)$ transition. All of these transitions are superimposed on a broad background from C 1s(CH_x) → σ^*_{C-C} transitions.

With the exception of the effect of resolution and a few key differences outlined below, the polymer C 1s spectra are very similar to the monomer spectra. In 1,4-PET orientational effects are possible because 1,4-PET has a propensity to be crystalline. However polarization dependent XAS of our 1,4-PET sample showed less than 5% variation between grazing and normal incidence. A small difference is expected between 1,4-PET and 1,4-DMP because the monomer model represents the ethyl bridge as two terminal methyl groups. In principle the spectra of methyl and ethyl groups differ,[28] but since the features from saturated sites are broad and masked by the sharper spectral features of the saturated carbon sites, this difference is not observed in these systems. The 1,3-PDP and 1,2-PDP polymers have a substantially different alkyl bridge structure, with more carbons per repeat unit than 1,4-PET. The associated spectral changes are small, although the longer alkyl group does increase the spectral cross section in 1,2- and 1,3-PDP. Another possible source of differences between polymer and monomer spectra is electronic interactions between neighboring repeat units in the polymer. However, in these phthalate polymers the alkyl bridge acts as a barrier to π^* delocalization between polymer repeat units. Thus the π^* electronic environment of the polymers is expected to be very similar to that of the corresponding monomer. The considerable degree of similarity of the C 1s spectra of monomer and polymer (compare Figures 1 and 2) supports this interpretation. A significant difference between the polymer and monomer spectra exists in the relative intensities of the π^*_{C-O} region (288−290 eV), with that for the polymer being larger than that for the monomer. This can be seen by comparing the total oscillator strength of the π^*_{C-O} region in the polymers (Figure 1) with that of the monomers (Figure 2). A large part of this difference is likely the larger contribution of the saturated alkyl linkages in the polymer than in the monomer. Finally there is a clear difference in the intensity of the 289 eV feature between polymer and monomer, with the polymer signal being in all cases more intense than that of the corresponding monomer. This difference may be a signature of an unexpected degree of delocalization between adjacent repeat units of the polymer. It is interesting that this feature is most intense in 1,4-PET, the species in which interunit interactions might be expected to be strongest.

4.2. O 1s Spectra. In the experimental (Figure 3) and calculated (Figure 5) O 1s spectra of the isomeric phthalate molecules the π^* energies evolve as a function of isomerism in a manner similar to that observed in the C 1s spectra. The energy of the first O 1s → π^* peak increases between 1,4-DMP and 1,2-DMP. The *ab initio* calculations predict that the first peak is a O 1s → $\pi^*_{C-O}(+)$ transition in each phthalate. The increase in the energy of this transition from 1,4- to 1,2-DMP is the result of a larger decrease in term value (~virtual level binding energy) than a simultaneous increase in O 1s(C=O) binding energy, as the two methoxy carboxyl groups are brought closer to each other. This balancing effect (i.e. the opposite isomeric influence on the 1s binding energy and the π^* term value) is very similar to that observed in the calculated C 1s excitation spectrum. The second O 1s spectral feature is assigned as a combination of O 1s(C=O) → $\pi^*_{C-O}(-)$ and O 1s(C−O) → $\pi^*_{C-O}(+)$ transitions, although the *ab initio* calculation predicts that these two transitions should be resolved. The third feature is assigned as the O 1s(C−O) → $\pi^*_{C-O}(-)$ transition, on the basis of the calculations. The main continuum signal at 540 eV is attributed to O 1s(C−O) → σ^*_{C-O} transitions, while the shoulder at 545 eV is attributed to O 1s(C=O) → σ^*_{C-O} transitions. The shift in the position of the main π^*_{C-O} peak is clearly the feature with the most analytical potential for monitoring isomeric character at the O 1s edge.

5. Summary

We have shown that 1,2-, 1,3-, and 1,4-substitution of two ester functionalities on a single benzene ring results in characteristic differences in both C 1s and O 1s spectra that are detectable in the X-ray absorption spectra of polymers and the inner-shell electron energy loss spectra of monomers. Differences arise from the nature of π^* delocalization between the π^*_{C-O} orbitals of the methyl carboxylate groups and the π^*_{C-C} orbitals of the phenyl ring. In 1,4-DMP, an unusual pinning of the normally silent (LUMO+1) level produces an added feature in the C 1s spectra. This suggests that symmetry and orbital mixing considerations can play an otherwise unexpected role in determining the C 1s spectra of phenyl systems. The major features of the C 1s and O 1s spectra of 1,4-DMP, 1,3-DMP, and 1,2-DMP have been reproduced through *ab initio* GSCF3 calculations.

This study has shown that small but measurable differences in energy and shape exist in the core excitation spectra of the phthalate isomers. These characteristics could provide the basis for mapping phase segregation in phthalate-based polymers prepared from mixed 1,2- and-1,4-substituted precursors. For example, imaging at 285.4 eV could be used to map the spatial distribution of 1,4-PET in a mixed 1,2/1,4 system. Accurate energy scales and good energy resolution will be required.

Acknowledgment. This work was supported financially by NSERC (Canada) and Dow Chemical. We thank N. Kosugi for providing access to the GSCF3 code and helpful assistance with its use. We thank J. Kirz and C. Jacobsen and their groups for the development and maintenance of the X1-STXM at NSLS. The zone plates were provided through an IBM−LBNL collaboration between E. Anderson, D. Attwood, and D. Kern. Parts of this work were performed at the NSLS, which is supported by the Department of Energy, Office of Basic Energy Sciences. H.A. gratefully acknowledges an NSF Young Investigator Award (DMR-9458060) and support from Dow Chemical.

References and Notes

(1) Rightor, E. G.; Young, G. P.; Urquhart, S. G.; Hitchcock, A. P. *Microsc.: Key Res. Tool* 1992, *22*, 67. Hitchcock, A. P.; Urquhart, S. G.; Rightor, E. G. *J. Phys. Chem.* 1992, *96*, 8736.

(2) Urquhart, S. G.; Hitchcock, A. P.; Rightor, E. G.; Priester, R. D.; Leapman, R. D. *J. Polym. Sci. Part B: Polym. Phys.* 1995, *33*, 1593, 1603.

(3) Rightor, E. G.; Hitchcock, A. P.; Ade, H.; Leapman, R. D.; Urquhart, S. G.; Smith, A. P.; Mitchell, G. E.; Fischer, D.; Shin, H. J., Warwick, T. *J. Phys. Chem B* 1997, *101*, 1950.

(4) Ade, H.; Zhang, X.; Cameron, S.; Costello, C.; Williams, S. *Science* 1992, *258*, 972. Ade, H.; Smith, A.; Cameron, S.; Cielinski, R.; Mitchell,

G. E.; Hsiao, B.; Rightor, E. G. *Polymer* **1995**, *36*, 1843. Leapman, R. D. In *Transmission Electron Energy Loss Spectroscopy in Materials Science*; Disko, M. M., Ahn, C. C., Fultz, B., Eds.; Materials Research Society: Pittsburgh, PA, 1992; p 47.

(5) Outka, D. A.; Stohr, J. *Springer Ser. Surf. Sci.* **1989**, *109*, 201.

(6) Jordan-Sweet, J. L.; Kovac, C. A.; Goldberg, M. J.; Morar, J. F. *J. Chem. Phys.* **1989**, *89*, 2482.

(7) Urquhart, S. G.; Hitchcock, A. P.; Rightor, E. G.; Smith, P. A.; Ade, H. *Proc. Mat. Res. Soc.* (Spring meeting, 1996), in press.

(8) Urquhart, S. G.; Hitchcock, A. P.; Rightor, E. G.; Priester, R. D. *J. Polym. Sci. Part B: Polym. Phys.* **1995**, *33*, 1603.

(9) Ade, H.; Smith, A. P.; Rightor, E. G.; Hitchcock, A. P.; Urquhart, S. G. *J. Microsc. Soc. Am.*, in preparation.

(10) Kosugi, N. *Theor. Chim. Acta* **1987**, *72*, 149.

(11) Smith, A. P.; Coffey, T.; Ade, H. In *X-ray Microscopy and Spectromicroscopy*; Thieme, J., Schmahl, G., Umbach, E., Rudolph, D., Eds.; Springer-Verlag: Heidelberg, 1997.

(12) Jacobsen, C.; Williams, S.; Anderson, E.; Brown, M. T.; Buckley, C. J.; Kern, D.; Kirz, J.; Rivers, M.; Zhang, X. *Opt. Commun.* **1991**, *86*, 351. Zhang, X.; Jacobsen, C.; Williams, S. In *Soft X-ray Microscopy*; Jacobsen, C., Trebes, J., Eds.; *Proc. SPIE* **1992**, *1741*, 251.

(13) Kirz, J.; Ade, H.; Howells, M.; Jacobsen, C.; Ko, C.-H.; Lindaas, S.; McNulty, I.; Sayre, D.; Williams, S.; Zhang, X. *Rev. Sci. Instrum.* **1992**, *63*, 557.

(14) Ma, Y.; Chen. C. T.; Meigs, G.; Randall, K.; Sette, F. *Phys. Rev. A* **1991**, *44*, 1848.

(15) Hitchcock, A. P. *Phys. Scr.* **1990**, *T31* 159.

(16) Hitchcock, A. P.; Mancini, D. C. *J. Electron Spectrosc.* **1994**, *33*, 1.

(17) Henke, B. L.; Lee, P.; Tanaka, T. J.; Shimabukuro, R. L.; Fujikawa, B. K. *At. Data Nucl. Data Tables* **1982**, *27*, 1.

(18) *Spartan* version 4.0; Wavefunction Inc.: 18401 Von Karman Ave., #370, Irvine, CA 92715.

(19) Kosugi, N.; Kuroda, H. *Chem. Phys. Lett.* **1980**, *74*, 490.

(20) Huzinaga, S.; Andzelm, J.; Klobukowski, M.; Radzio-Andzelm, E.; Sasaki,Y.; Tatewaki, H. *Gaussian Basis Sets for Molecular Calculations*; Elsevier: Amsterdam, 1984.

(21) Hunt, W. J.; Goddard, W. A., III *Chem. Phys. Lett.* **1969**, *3*, 414.

(22) Kosugi, N.; Shigemasa, E.; Yagishita, A. *Chem. Phys. Lett.* **1992**, *190*, 481.

(23) Kosugi, N.; Adachi, J.; Shigemasa, E.; Yagishita, A. *J. Chem. Phys.* **1992**, *97*, 8842.

(24) Iwata, S.; Kosugi, N.; Nomura, O. *Jpn. J. App. Phys.* **1978**, *17-S2*, 109.

(25) Kuchitsu, K, Ed. *Structure Data of Free Polyatomic Molecules*, Vol. 7 Landolt-Bornstein, New Series II; Springer: Berlin, 1976.

(26) Turci, C. C.; Urquhart, S. G.; Hitchcock, A. P. *Can. J. Chem.* **1996**, *74*, 851.

(27) Huo, B.; Urquhart, S. G.; Eustatiu, U. G.; Hitchcock, A. P. In preparation.

(28) Hitchcock, A. P.; Ishii. I. *J. Electron Spectrosc.* **1987**, *42*, 11.

(29) Brisse, P. F.; Pérez, S. *Acta Crystallogr. B* **1976**, *32*, 2110.

(30) Daubeny, R. D.; Bunn, C. W.; Brown, C. J. *Proc. R. Soc. London A* **1954**, *226*, 531. Arnott, S.; Wonacott, A. J. *Polymer* **1966**, *7*, 157.

(31) Beamson, G.; Briggs, D. *High Resolution XPS of Organic Polymers: The Scienta ESCA300 Database*; Wiley: New York, 1992. The narrowest line in their XPS spectrum of PET is 0.85 eV fwhm (C 1s(C=O)), whereas the C 1s(ring) peak is 1.0 eV wide. Two Gaussian peaks in a 2:1 intensity ratio, each with 0.85 eV width, that are separated by 0.5 eV give a near symmetric peak 1.0 eV in width. From this we conclude that the C 1s(C−R) IP is ~0.5 eV above the C 1s(C−H) IP. The present calculated IPs, which predict a C 1s(C−H)/C 1s(C−R) shift of 0.37 eV in 1,4-PET, are in agreement with this observation. A lower resolution XPS spectrum of PET, along with a discussion of the dependence of the XPS on conformation, is given in the following: Boulanger, P.; Pireaux, J. J.; Berbist, J. J.; Delhalle, J. *J. Electron Spectrosc.* **1993**, *63*, 53.

(32) Jolly, W. L.; Bomben, K. D.; Eyermann, C. J. *At. Data Nucl. Data Tables* **1984**, *31*, 109.

CHAPTER 5A

ORGANOSILANE CORE EXCITATION SPECTROSCOPY

The structural-spectral relationships in the core excitation spectroscopy of organosilane molecules are investigated in this thesis. This chapter reviews the major themes of this research, presented in detail in Chapters 5B-5D. The core excitation spectroscopy of silylenes, of molecules containing Si-O and Si-Si bonds and of phenyl-Si π-delocalization are reviewed. The concept of functional group "fingerprinting" and the role of π-delocalization are extended to organosilane molecules.

§5.1 Si-O Bonding

The Si-O bond is an unusual, strong and flexible chemical bond. The core excitation spectroscopy of molecules containing Si-O bonds was investigated for several reasons. It was hypothesized that the presence of "hyperconjugation" or "(d-p)-π" backbonding in organosilanes could be investigated by core excitation spectroscopy, and that changes in the Si-O bond strength could be reflected in the core spectra. This study is presented in Chapter 5D in published form and is briefly reviewed here.

In the series of molecules Me_3SiO-X (X = H, CH_3, $SiMe_3$), the Si-O bond strength was experimentally measured to differ by 10% (D(Si-OH) = 536 kJ/mole; D(Si-OMe) = 477 kJ/mole; D(Si-OSi) = 549 kJ/mole) [W89]. If this bond strength difference is driven by a hyperconjugation mechanism (in which the oxygen lone electron pairs are delocalized into antibonding Si-C σ* MOs) or by a (d-p)-π backbonding mechanism (in which the

oxygen lone pairs are delocalized into unoccupied Si 3d AOs), it might be possible to observe differences in the Si edge core excitation spectra. However, the Si 1s spectra of the molecules Me_3SiOH, Me_3SiOMe and $Me_3SiOSiMe_3$ are very similar (Figure 1, Chapter 5D), as are the Si 2p spectra of Me_3SiOMe and $Me_3SiOSiMe_3$ (Figure 3, Chapter 5D, the Si 2p spectrum of Me_3SiOH was not recorded). The similarity of the spectra indicates that core excitation spectroscopy is not very sensitive to the Si-O bond strength differences.

Both the hyperconjugation model and the (d-p)π backbonding model are based in the covalent bonding model, where in-phase overlap of orbital density creates bonding MOs. A stronger covalent bond is reflected in stabilized bonding MOs and destabilized antibonding MOs. The observation of core → σ^*_{Si-O} features in the Me_3SiOX species indicates that there is *some* covalent character to these Si-O bonds. The lack of substantial differences between the core → σ^*_{Si-O} features between the spectra of these molecules suggests that differences in covalent bonding character are not responsible for the Si-O bond strength differences. Recent studies have argued that the Si-O bond has a predominantly ionic character [GJ96]. If the change in Si-O bond strength in the Me_3SiO-X molecules arises from a difference in the *ionic bonding strength*, than this bond strength difference should not be observed in covalently derived spectral features. The results presented in this thesis are consistent with this interpretation.

§5.2 Core Excitation Spectroscopy of Silylenes

In this thesis, the core excitation spectroscopy of a series of silylene molecules was studied at all possible core edges (Si 1s, Si 2s, Si 2p, C 1s and N 1s). *Silylenes* are a class

of molecules in which the silicon atom is dicoordinate and divalent. These particular silylene molecules, discovered by M. Denk [DRH94, DL&94] are the first thermodynamically stable silylenes synthesized. Their chemical stability is hypothesized to arise from cyclic π-delocalization in the silylene-containing heterocycle [DG&94]. By examining the core excitation spectroscopy of silylenes at different core edges, the unoccupied electronic structure can be examined site-by-site in the silylene heterocycle.

Figure 5.2.1 presents the structures of the two silylene molecules examined in this thesis. The ring carbon atoms in the molecule on the left (termed here as *silylene*, or **1**) are unsaturated, while the ring carbon atoms of the molecule on the right (termed here as *saturated silylene*, or **2**) are saturated. In addition, two similar organosilane molecules in which the Si atom is dihydrogenated were also studied. Full details of this study are presented in Chapter 5B.

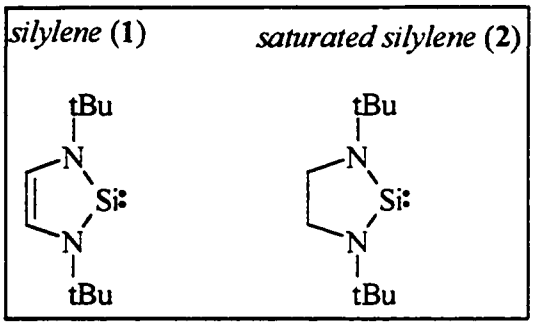

Figure 5.2.1 Structures of silylene (**1**) and saturated silylene (**2**).

Figure 5.2.2 presents the Si 1s NEXAFS spectrum and the Si 2p, C 1s and N 1s ISEELS spectrum of silylene. In each core edge spectrum, the lowest energy core → $\pi^*(b_2)$ transition is identified. Since core excitation is a *locally sensitive probe* of the unoccupied electronic density, only the π^* density *at the core hole site* (e.g. Si, N, C) is probed in the core edge spectra (i.e. Si 1s, N 1s, C 1s). This result (in conjunction with the MO calculations presented in Chapter 5B) illustrates that the *same* π^* LUMO level is delocalized onto each atomic site in the silylene heterocycle. In contrast, the C 1s

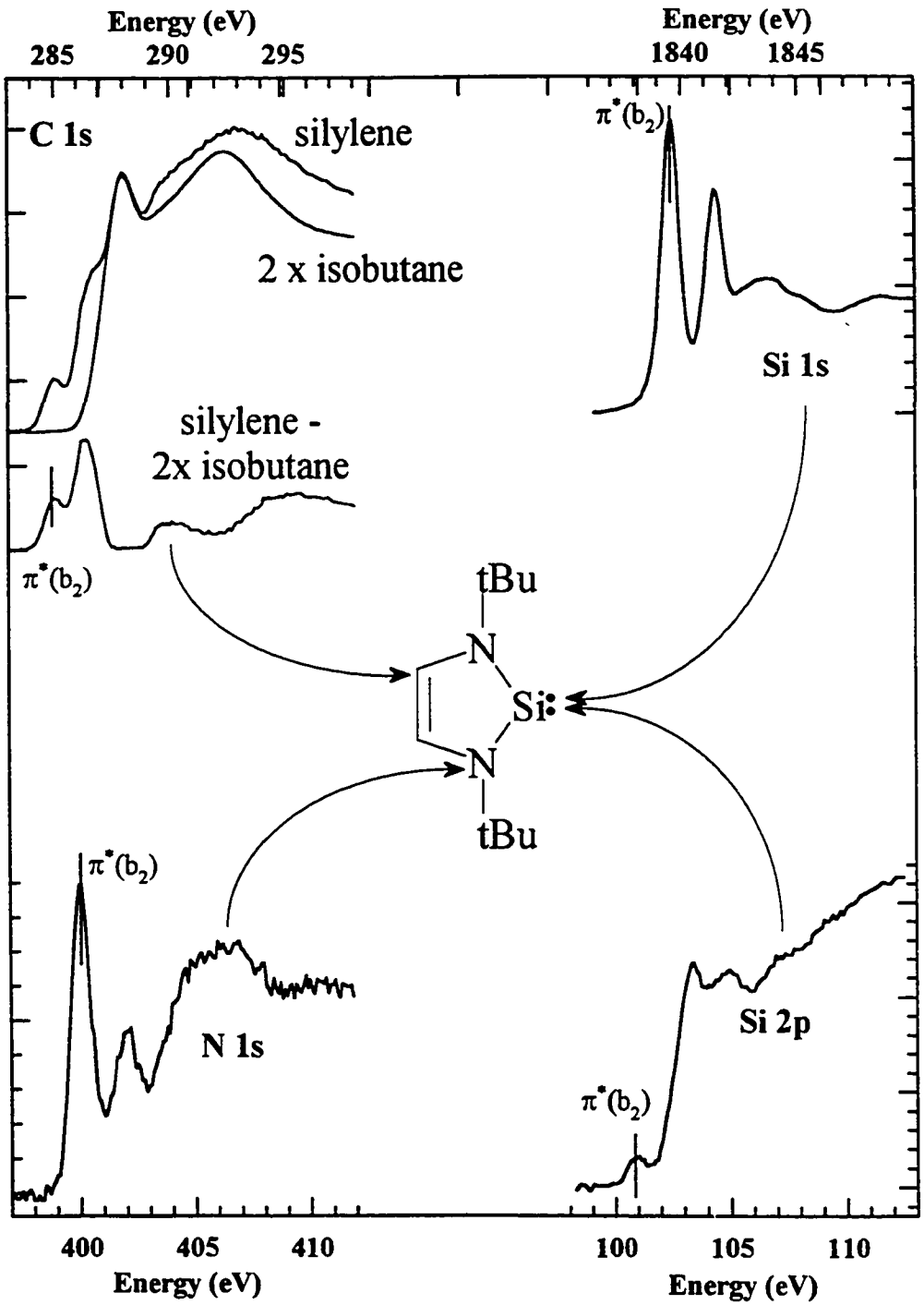

Figure 5.2.2 Si 1s NEXAFS and the Si 2p, C 1s and N 1s ISEELS spectra of silylene. A stoichiometrically weighted C 1s spectrum of isobutane has been subtracted from the C 1s spectrum of silylene to isolate the C=C contribution to the silylene spectrum.

spectrum of the saturated silylene (molecule **2** in Figure 6, Chapter 5B) does not show the low energy C 1s → π* transition. These results are consistent with the cyclic π-delocalization in silylene (**1**).

§5.3 Character of the Si-Si σ* Resonance

Materials containing Si-Si bonds have unusual electronic properties, notably a σ → σ* transition that is much lower in energy than in corresponding alkanes, and extensive σ-delocalization along Si-Si-Si chains. A core → $\sigma^*_{Si\text{-}Si}$ resonance was first identified in Si core edge spectra by A. T. Wen [W92]. The core excitation spectroscopy of molecules that contain Si-Si bonds has been further explored in this thesis, in collaboration with Dr. Wen and others (see Chapters 5C and 5D). The character of the core → $\sigma^*_{Si\text{-}Si}$ resonance has been explored at Si core edges for a wide range of organosilane molecules.

The Si 1s NEXAFS spectra of four molecules containing Si-Si bonds and tetramethylsilane is contained in Figure 3 of Chapter 5C. In each molecule that contains a Si-Si bond, a low energy Si 1s → $\sigma^*_{Si\text{-}Si}$ resonance is observed. The clearest example is hexamethyldisilane ($Me_3SiSiMe_3$) in which there are two low energy features (Si 1s → $\sigma^*_{Si\text{-}Si}$ at 1841.7 eV; Si 1s → $\sigma^*_{Si\text{-}C}$ at 1842.8 eV). In comparison, in tetramethylsilane there is a single Si 1s → $\sigma^*_{Si\text{-}C}$ transition (at 1842.6 eV). Some of the other molecules presented in this figure have a more complex Si 1s → $\sigma^*_{Si\text{-}Si}$ band because these molecules contain Si in multiple chemical environments (i.e. the central Si versus the outer Si in $Si(SiMe_3)_4$).

The low energy $\sigma^*_{Si\text{-}Si}$ resonance was also observed in the Si 2p spectra of molecules containing Si-Si bonds. The Si 2p NEXAFS and ISEELS spectra of four

molecules containing Si-Si bonds and tetramethylsilane is presented in Figure 2 in Chapter 5C. Once again, the simplest example is hexamethyldisilane ($Me_3SiSiMe_3$) where the presence of an "extra" transition can be observed by comparing the Si 2p spectrum of tetremethylsilane to hexamethyldisilane. This features is assigned as the Si 2p → $\sigma^*_{Si\text{-}Si}$ transition.

Multiple scattering calculations were employed by our collaborators (J. Z. Xiong) to examine this low energy resonance in hexmethyldisilane ($Me_3SiSiMe_3$) [XJ&96]. These calculations show that the first intense feature is a Si-Si σ^* orbital containing mostly Si 3p orbital character.

The core excitation spectra of the molecule hexaphenyldisilane ($Ph_3SiSiPh_3$) was also examined in this thesis. The unique nature of the spectrum of this molecule, notably the interaction of the $\sigma^*_{Si\text{-}Si}$ and π^*_{phenyl} density is discussed below in Chapter 5D.

§5.4 Phenyl-Si π-delocalization

In this thesis, the core excitation spectra of a series of phenyl and methyl substituted silanes is discussed. When silicon is coordinated by phenyl groups instead of methyl groups, an unusual low energy feature is observed in the Si core spectra. The Si 1s and Si 2p core excitation spectra of a series of phenyl and methyl substituted silanes is presented in Figures 1 and 3 in Chapter 5D. If we compare the Si 1s spectra of Me_3SiOH, Me_3SiOMe, and $Me_3SiOSiMe_3$ to the phenyl-substituted molecules Ph_3SiOH and $Ph_3SiOSiPh_3$, a low energy feature (~1841.8 eV) is clearly observed only in the phenylsilane molecular spectra. A similar low energy feature is observed in the Si 2p

spectra of these phenyl-substituted species (Fig. 3, Chapter 5D).

The empirical evidence clearly shows that there is a unique spectral feature present when a phenyl group is bonded to a silicon atom in phenyl silane molecules. However, the assignment of this feature is not immediately clear. Chemically, we should not expect π-bonding between Si and the phenyl ring when Si is fully saturated (i.e. tetracoordinate). EHMO and *ab initio* MO calculations were employed to investigate this feature (see Figure 2, Chapter 5D). On the basis of these calculations, this unusual low energy feature is assigned as a Si core → $\pi^*_{Si\text{-}Ph}$ transition, where the $\pi^*_{Si\text{-}Ph}$ MO is an *antibonding* π* MO in the phenyl ring (derived from the e_{2u} π* MO of benzene) but is *bonding* (i.e. has an in-phase π-overlap) between the Si atom and the phenyl ring. This result does not imply the existence of a Si-Ph π-bond. This is an unusual instance of Si-phenyl π-delocalization that occurs despite the saturation of the silicon atom.

CHAPTER 5B

Probing Delocalization in Stable Silylenes: Core Excitation Spectra of Si(NRCHCHNR), Si(NRCH$_2$CH$_2$NR), H$_2$Si(NRCHCHNR) and H$_2$Si(NRCH$_2$CH$_2$NR) (R= ^{t}bu)

The following work documents the Si 1s, Si 2p, Si 2s, C 1s and N 1s core excitation spectra of two stable silylenes and two analogous dihydrosilane molecules, and the use of ab initio calculations for interpreting these spectra. This work is an article in preparation and is presented here in present form. Authorization to reprint this article has been obtained from the coauthors.

The author of this thesis identified the subject of this investigation through independent contact with Dr M. Denk, performed all of the experimental work, carried out all of the calculations presented in this paper, and prepared the bulk of the paper in collaboration with Prof. A. P. Hitchcock and Prof. M. Denk.

Probing Delocalization in Stable Silylenes: Core Excitation Spectra of Si(NRCH=CHNR), Si(NRCH$_2$CH$_2$NR), H$_2$Si(NRCH=CHNR) and H$_2$Si(NRCH$_2$CH$_2$NR) (R = ^{t}Bu).

S.G. Urquhart[a], A.P. Hitchcock[a] and M. Denk[b]

a. Department of Chemistry, McMaster University, Hamilton, Canada, L8S 4M1
b. Department of Chemistry, University of Toronto, Mississauga, Canada, L5L 1C6

Abstract

The silicon 1s, 2p, and 2s; carbon 1s and nitrogen 1s gas phase core excitation spectra are reported for two stable silylenes: Si(NRCH=CHNR) and Si(NRCH$_2$CH$_2$NR) (R = ^{t}Bu); and for the two analogous dihydridosilane molecules: H$_2$Si(NRCH=CHNR) and H$_2$Si(NRCH$_2$CH$_2$NR) (R = ^{t}Bu). The nature of the π^* and σ^* core excited states at different sites on the silylene ring are examined by relating the changes in the spectra of these compounds to differences in their molecular structure. These spectra probe variations in the spatial extent of π^* delocalization and the nature of π stabilization in heterocycles containing divalent silicon. Low lying transitions to a π^*(Si-N) level observed in all core edge spectra strongly support the existence of π^* delocalization in the C=C unsaturated silylene.

Introduction

The two silylene compounds: Si(NRCH=CHNR) (**1**, *unsaturated silylene*) and Si(NRCH$_2$CH$_2$NR) (**2**, *saturated silylene*) (R = ^{t}Bu, see scheme 1), are remarkable examples of molecules containing a stable divalent and dicoordinate silicon. [1] In particular, the exceptional stability of the unsaturated silylene (**1**) has been attributed to cyclic (4n+2)-π

delocalization [2]. The high stability of these compounds and especially their volatility allows experimental investigation of divalent Si at a fairly sophisticated level. The electronic structures of unsaturated silylene (**1**), saturated silylene (**2**), and the dihydridosilane analogues $H_2Si(NRCH{=}CHNR)$ (**3**) and $H_2Si(NRCH_2CH_2NR)$ (**4**) have been examined previously by He(I) and He(II) photoelectron spectroscopy (PES) and *ab initio* MO calculations [2]. For (**1**), this PES study demonstrated that the Si 3p orbital contributes to and stabilizes the π HOMO through significant Si-N π bonding. However, comparison of the PES spectrum of the C=C unsaturated silylene (**1**) with that of the C-C saturated silylene (**2**) and the unsaturated dihydridosilane analogue (**3**) demonstrated that the energy of the lone pair on Si was not greatly affected by the saturation of carbon and that the π HOMO ($2b_2$) of (**1**) is stabilized by the C=C π bond. [2]

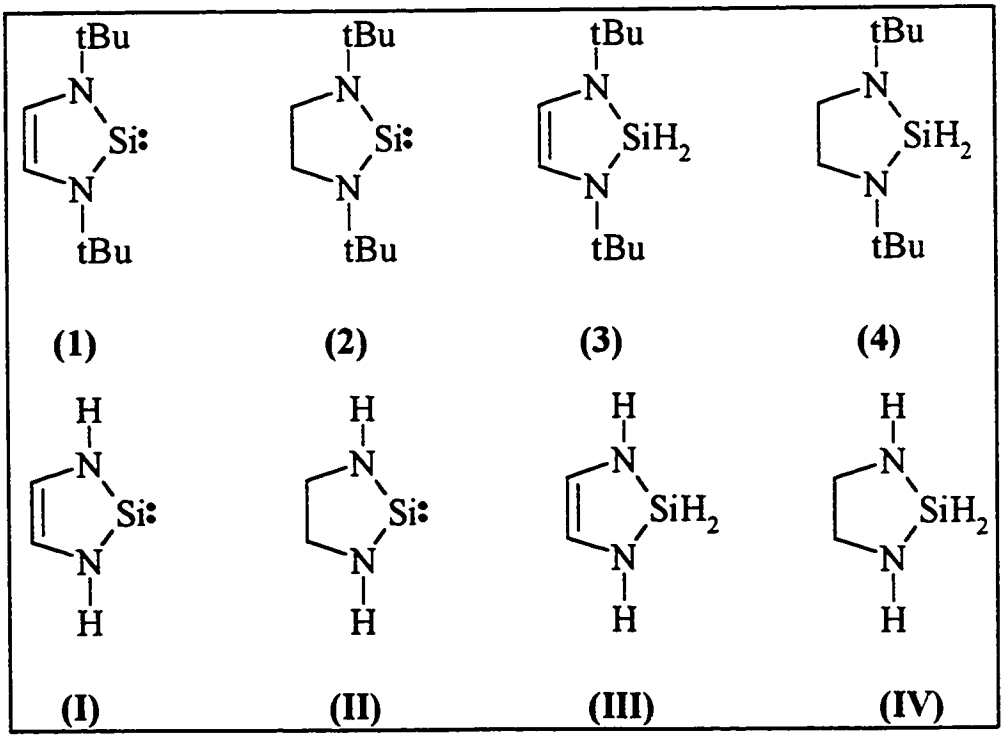

Scheme 1.

Core excitation spectroscopy [3-5] is a technique complementary to PES for electronic studies of molecules. While PES probes the energy and character of *bound* electronic levels, core excitation spectroscopy probes the *unoccupied* electronic structure. In addition, and unlike PES, core excitation spectroscopy is a *site* and *symmetry* sensitive probe of the electronic structure. The core excitation spectrum is the sum of contributions from each atomic site in the molecule. Site sensitivity arises because the spectrum of each atomic site is sensitive to both the charge on the atom (core level shift) and the influence of the chemical environment on the unoccupied electronic structure at the site. Symmetry sensitivity arises from the atomic electric dipole propensity model for core excitation transitions. The intensity of a feature identified as a one electron core excitation to a particular molecular orbital can be related to the contribution of atomic orbitals of appropriate symmetry to that MO. For example, Si 1s excitation in silylene samples the Si 3p density of the unoccupied MOs. Thus, comparison of electric-dipole core excitation from core edges of different symmetry and from different atomic sites allows a mapping of the spatial distribution and symmetry of the unoccupied electronic levels. The silylene molecules investigated here are exceptional examples in this regard. Each inequivalent site in the heterocycle ring of **(1-4)** is occupied by a different element and therefore each corresponding atomic core edge represents a discrete electronic environment.

With the exception of the Si 1s spectrum of SiO [6] and the Si 2p spectrum of Si^{+2} [7], gas phase core excitation spectroscopy has only been applied to tetracoordinate silicon. [5] Six coordinate silicon has been investigated in the solid phase: Si 1s and Si 2p spectra of α-quartz, stishkovite [8] and silicon diphosphate [9] clearly demonstrate that core excitation

spectra are quite sensitive to a change in the coordination number of silicon from four to six. Since the silylene unit represents two coordination of Si, similarly dramatic effects are expected.

This paper presents the silicon (1s, 2s, 2p), carbon 1s and nitrogen 1s core excitation spectra of the silylenes (**1**,**2**) and the dihydridosilanes (**3**,**4**) (see scheme 1). These spectra serve to identify core excited states that are specific to the silylene unit, as well as the general character of the unoccupied π^* and σ^* core excited states of these molecules. The character of the core excited states is determined by comparing spectra from different core edges, and by comparisons of the core edge spectra of molecules with different structures, illustrating empirically the spectral contribution of the differing structural components. Calculations are employed to support our spectral assignments of (**1-4**). *Ab initio* (MP2/HF/6-31G*) calculations have been performed on model compounds (**I-IV**) which differ from (**1-4**) in that the ^{t}Bu group is replaced by hydrogen. (See scheme 1.) These calculations are used to establish the energy ordering and spatial character of the unoccupied molecular orbitals of the ground states of (**1-4**). "Z+1" calculations of (**I**) at the same level of basis quality are used to examine the effect of electronic relaxation caused by the core hole on the unoccupied molecular orbitals.

2. Experimental Section

2.1. Compounds

The amides (**1**) [1,2] and (**2-4**) [2] were synthesized according to literature methods. The silylenes (**1**) and (**2**) are solids which were purified by sublimation. The dihydridosilanes

(**3**) and (**4**) are liquids which were purified by vacuum distillation. All compounds were handled under argon (99.999%).

2.2. Synchrotron Radiation Total Ion Yield Spectroscopy

The Si 1s gas phase spectra of the silylenes (**1-2**) and the dihydridosilanes (**3-4**) were recorded using the Canadian Synchrotron Radiation Facility (CSRF) double crystal monochromator at the Aladdin Synchrotron of the University of Wisconsin at Madison [10]. The monochromator energy scale was calibrated by setting the inflection point of the Si 1s spectrum of crystalline Si to 1839.2 eV [11]. The gas phase spectra were recorded in total ionization yield. The signal from the ~10 cm long chamber was recorded simultaneously with that of the incident photon flux, I_o (monitored using a N_2-filled ionization chamber separated from the sample by a polypropylene window), and the sample pressure (measured with a baratron gauge). After normalization to correct for the I_o and pressure variations, the total ion yield spectra were converted to an absolute oscillator strength scale by setting the Si 1s intensity to the atomic value of 0.16 10^{-2} eV^{-1} at 1860 eV [12-13].

2.3. Electron Energy Loss Spectroscopy

The inner-shell electron energy loss spectrometer and operating procedures have been described previously [3]. The spectra were obtained using inelastic scattering conditions where dipole transitions dominate (2.5 keV final electron energy, 2^{o} scattering angle) with an energy resolution of 0.7 eV full width at half maximum (FWHM). Heating the solid samples (**1,2**) to ~60°C was sufficient to generate adequate vapour pressure in the gas cell.

The vapour of the dihydridosilanes (**3**,**4**) was introduced into the gas cell through a leak valve after degassing the liquid by several freeze-pump-thaw cycles. Absolute energy scales were established by recording the spectrum of a stable mixture of the compound and CO, N_2 or CO_2 (standard calibrant species) as documented in the tables of spectral assignments. The as-recorded spectra in the Si 2p and Si 2s region were converted to absolute oscillator strengths by normalizing to the absolute Si 2p oscillator strength of SiH_4 in the featureless, atomic-like 145-151 eV region [14]. The C 1s and N 1s spectra were normalized to atomic oscillator strengths using procedures discussed elsewhere [5].

2.4. Theoretical Calculations

In order to discuss the core excitation spectra of the silylenes (**1-2**) and the dihydridosilanes (**3-4**), it is necessary to have a clear picture of the relative energies and spatial character of the final electronic states. Previously we have used Extended Hückel Molecular Orbital (EHMO) calculations for calculating core excitation spectra [15]. However, EHMO results for the ground state of (**1**) (carried out with and without Si 3d orbitals; results not shown) did not correctly reproduce the energy sequence of the occupied π MOs as observed by PES and as calculated at an *ab initio* (MP4/HF/6-31G*) level [2]. If EHMO is inadequate for occupied MOs, it may not be not appropriate for examining unoccupied MOs of silylene molecules.

In this study, we have employed ground state *ab initio* calculations to give a simple view of the unoccupied electronic structure of (**1-4**). For economy, calculations were performed on the model compounds (**I-IV**) where the ^{t}Bu groups are replaced by hydrogen.

The program SPARTAN [17] was used to provide geometry optimized structures at the HF/6-31G* level. Harmonic vibrational frequencies were calculated at this level to verify that optimized structures represent the minima in the potential energy surface. Electronic energies were obtained from single point calculations at the MP2 level (6-31G* basis set) with the optimized geometries.

Table 1 presents the energies and symmetries of the low energy unoccupied molecular orbitals of (**I-IV**) from the MP2/HF/6-31G* calculation. The geometry optimized structures of (**I**) and (**III**) are C_{2v} symmetry while (**II**) and (**IV**) are C_2 symmetry due to out-of-plane puckering of the C-C segment of the ring. For convenience, C_{2v} labels will be used uniformly to discuss the *experimental* core excited states of molecules (**1-4**). The total energies and

Table 1 Calculated[a] Energies of the Unoccupied Orbitals of ground state (**I-IV**).

(I)		(II)		(III)		(IV)	
Energy[b] (eV)	Sym. C_{2v}[c]	Energy[b] (eV)	Sym. C_2 (C_{2v})[d]	Energy[b] (eV)	Sym. C_{2v}[c]	Energy[b] (eV)	Sym. C_2 (C_{2v})[d]
2.91	b_2	2.84	b (b_2)				
4.04	b_1	4.28	b (b_1)	3.93	b_1	4.11	b (b_1)
5.90	a_1	5.70	a (a_1)	5.36	a_1	5.34	a (a_1)
6.16	a_2	7.10	a (a_1)	6.26	a_1	6.34	a (a_1)
6.40	a_1	7.50	a (a_1)	6.42	a_2	7.05	b (b_2)

a. Calculations performed on geometry optimized structures (HF-6-31G*), energies from single point calculations at MP2/6-31G* level.

b. Total energies (au): (**1**) E(HF)=-475.891, E(MP2) = -476.549
(**2**) E(HF)=-477.059, E(MP2) = -477.717
(**3**) E(HF)=-477.049, E(MP2) = -477.702
(**4**) E(HF)=-478.232, E(MP2) = -478.892

c. Symmetries defined for molecules lying in the xz plane.

d. The bracketted symbol indicates the symmetry of the MO if the molecule is forced into C_{2v} symmetry.

geometries of (**I-IV**) are in reasonable agreement with those published previously [2,18]. Figure 1 presents the energies of the low energy unoccupied molecular orbitals of (**I-IV**).

Caution must be exercised when comparing ground state MO calculations to spectra of core excited states. In principle one must account for the influence of the core hole on the unoccupied molecular orbitals. This is often done using the Equivalent Ionic Core Virtual Orbital Model (EICVOM) [15-16]. In this model, the effect of electronic relaxation in the presence of a core hole is approximated by replacing the core excited atom (atomic number Z) with its "Z+1" counterpart (e.g. by replacing Si by P), and putting a charge of +1 on the molecule to preserve the correct number of electrons. For simple semi-empirical MO methods, such as extended Hückel, the calculation of the "Z+1" equivalent species for a number of different sites is a fast and trivial matter. However for calculations at an *ab initio* level, a significant amount of computation time is required. For this study, EICVOM calculations were only carried out for (**I**) in order to investigate the effects of core hole relaxation. We assume similar trends occur in the other three species. Calculations were carried out using the "Z+1" approximation for core excited Si, N and C, using the optimized geometry from the (HF/6-31G*) ground state results. Table 2 presents the energies and symmetries of the unoccupied molecular orbitals of Si, N and C core excited (**I**), derived from single point Z+1 calculations at the MP2/HF/6-31G* level. Figure 2 presents these energy levels in comparison with the unoccupied molecular orbital energies of (**I**) calculated in the ground state. The ordering of some features, particularly the relative ordering of the $\pi^*(a_2)$ MO, varies considerably depending on the position of the core hole.

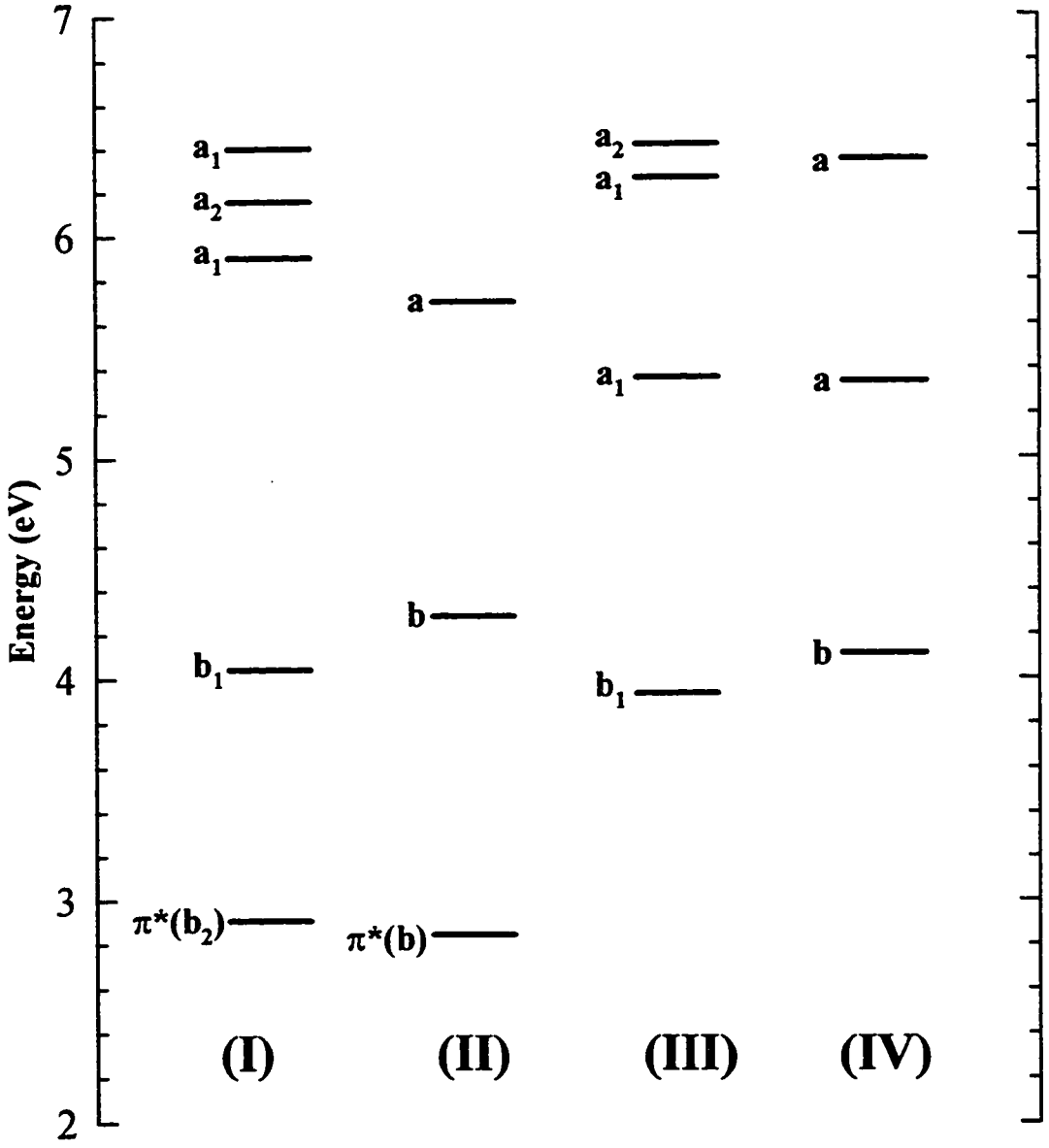

Figure 1. Orbital correlation diagram for the unoccupied molecular orbitals of the ground states of (I - IV) (see scheme 1) based on ab initio calculations at the MP2/HF/6-31G* level.

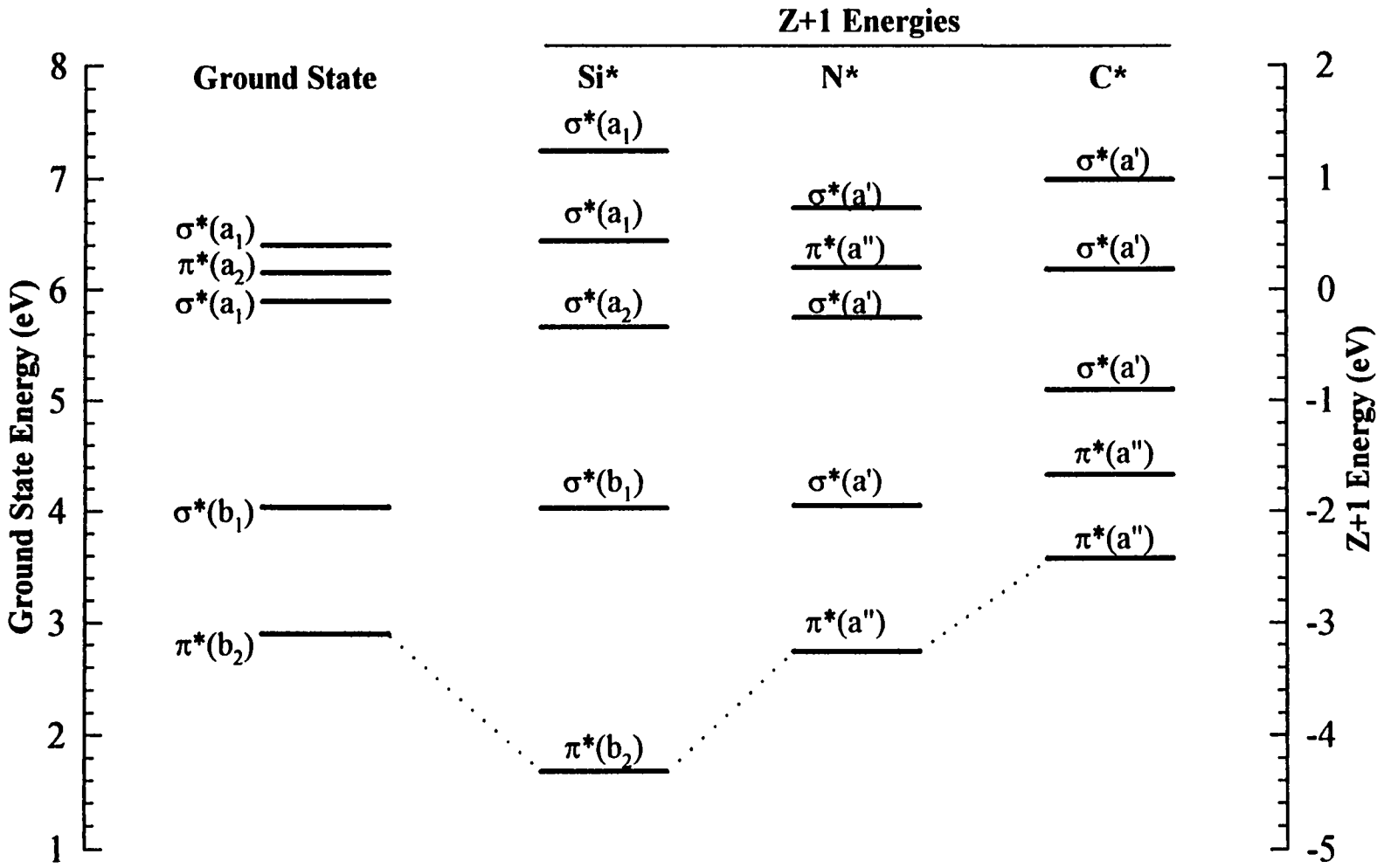

Figure 2. Orbital correlation diagram for the unoccupied molecular orbitals of the ground state of (**I**) compared to those for the unoccupied orbitals of the Si 1s, N 1s and C 1s core excited states of (**I**) computed (MP2/HF/6-31G*) using the equivalent ionic core virtual orbital model ("Z+1" approximation).

Table 2 Calculated Energies for Si 1s, N 1s and C 1s Excitation of (**I**)

Si 1s		N 1s		C 1s	
Energy (eV)	Symmetry C_{2v}	Energy (eV)	Symmetry C_s[a] (C_{2v})[a]	Energy (eV)	Symmetry C_s[a] (C_{2v})
-4.31	b_2	-3.26	a" (b_2)	-2.42	a" (b_2)
-1.97	b_1	-1.95	a' (b_1)	-1.67	a" (a_2)
-0.33	a_2	-0.25	a' (a_1)	-0.90	a' (b_1)
0.44	a_1	0.20	a" (a_2)	0.18	a' (a_1)
1.24	a_1	0.73	a' (a_1)	0.99	a' (a_1)

a. In "Z+1" calculations for N 1s or C 1s excitation, the symmetry of the molecule is reduced to C_s from C_{2v}. In this representation, the a_2 and b_2 irreducible representations in C_{2v} become the a" representation in C_s. [28] The symmetry of the parent, ground state MO is bracketed.

3. Results and Discussion:

3.1 Si 1s Spectra

The silicon 1s total ion yield core excitation spectra of the silylenes (**1**,**2**) and the dihydridosilanes (**3**,**4**) are presented in Figure 3. Energies and proposed assignments of the spectral features are presented in Table 3.

There are two, remarkably sharp, low lying transitions in the Si 1s spectra of the silylene compounds (**1**,**2**). The previous PES study of (**1**) and (**2**) [2] indicated strong Si-N π-bonding. Low lying Si 1s → π* transitions were therefore expected in the Si 1s core spectrum. A symmetry analysis for (**1**) (point group: C_{2v}, molecule in xz plane) indicates that π* (i.e., p_y) electronic states will be of a_2 or b_2 symmetry. However, as the Si atom is on the C_2 molecular symmetry axis of this molecule, the Si $3p_y$ orbitals cannot contribute to the a_2 symmetry π-MOs. Thus only Si 1s → π*(b_2) transitions will contribute to an electric dipole

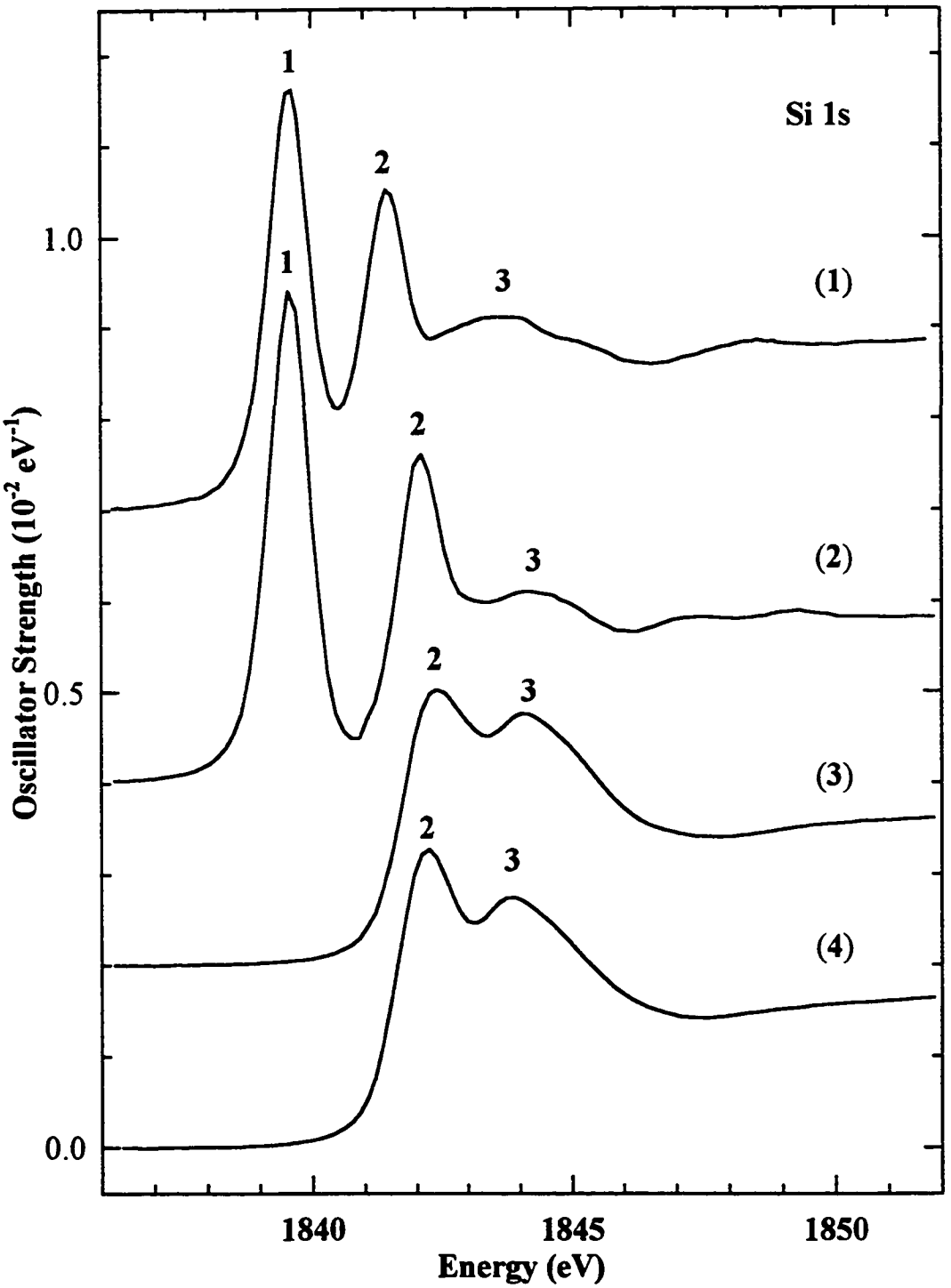

Figure 3. Background subtracted Si 1s oscillator strength spectra of (1), (2), (3) and (4), derived from total ion yield x-ray absorption spectra. Offsets of 0.7, 0.4 and 0.2 (10^{-2} eV^{-1}) have been used for clarity in the spectra of (1), (2) and (3), respectively.

Table 3 Energies (eV) and Assignments of Features in the Si 1s and 2s Spectra of Silylenes (R_2Si:) and Dihydridosilanes (R_2SiH_2)

	(1)		(2)		(3)		(4)		
#	Si 1s[a]	Si 2s	Si 1s	Si 2s	Si 1s	Si 2s	Si 1s	Si 2s	Assignments[b]
1	1839.56	151.9	1839.57	151.7					π^*(Si-N, b_2)
2	1841.48	153.9	1842.13	154.3	1842.5	154.4	1842.25	154.2	σ^*(Si-N, b_1)
3	1843.7		1844.2		1844.1	156	1843.9	156	σ^*(Si-N, a_1)

a. Calibration: Monochromator energy scale calibrated by setting the edge inflection of the Si 1s spectrum of crystalline Si to 1839.2 eV. [11]
b. C_{2v} symmetry labels are used for convenience in the case of the C_2 symmetry molecules (**2**) and (**4**).

excitation spectrum, although transitions to both $\pi^*(b_2)$ and $\pi^*(a_2)$ final states are possible from all other atomic sites in the molecule.

Ab initio calculations performed on the ground state of (**I**) predict a $\pi^*(b_2)$ LUMO, with $\sigma^*(b_1)$ and $\sigma^*(a_1)$ levels at higher energy (see Fig. 1, Table 1). The first peak in the Si 1s spectrum of (**1**) is assigned as the Si 1s → π^* (Si-N, b_2) transition. The second sharp peak is associated with the Si 1s → σ^*(Si-N, b_1) transition. The (Si^{-1}1s) Z+1 calculation (Fig. 2, Table 2) supports these assignments. Only the relative ordering of the optically silent $\pi^*(a_2)$ level is changed when core hole relaxation is considered in the calculation. This suggests that the ground state *ab initio* calculations of (**I-IV**) should be adequate to explain the Si 1s core excitation spectra.

For (**2**), the Si 1s →π^*(Si-N, b_2) transition occurs at approximately the same energy as for (**1**) but the Si 1s → σ^*(Si-N, b_1) transition is shifted to higher energy (by +0.65 eV). (For convenience, C_{2v} labels are used for assigning transitions in the spectra of (**2**) and (**4**)).

The calculated energy of the b_1 molecular orbital in (II) relative to that in (I) shifts in the same manner. Broad transitions are observed at 1843.7 eV and 1844.2 eV in (1) and (2) respectively. These are attributed to Si 1s → σ *(Si-N, a_1) transitions, in accordance with the calculated results.

Strong support for our Si 1s → π* assignments in (1,2) is provided by the Si 1s spectra of the dihydridosilanes (3,4). Consistent with the tetravalent coordination there is no signal below 1841 eV in (3,4), the region where the sharp Si 1s → π*(Si-N, b_2) transitions are observed in (1,2). The Si 1s → σ*(Si-N, b_1) transitions around 1842 eV are broader in (3,4) than in (1,2). Even though the Si in (3,4) is tetravalent, the calculations suggest that there is still some change in electronic structure at Si when the carbon segment of the heterocycle is changed from a single to a double bond.

The dihydridosilanes (3,4) show a second strong peak at ~1844 eV. This feature is assigned to the Si 1s → σ*(Si-N, a_1) transition. Similar but much weaker features are seen in the Si 1s spectra of (1) and (2). The difference in the intensity of this feature between (1,2) versus (3,4) is interesting. The atomic propensity model suggests that the A_1 state contains considerably more 3p density centred at Si in the tetrahedral dihydridosilanes (3,4) than in the dicoordinate silylenes (1,2).

The +0.65 eV difference in the Si 1s → σ*(Si-N, b_1) transition energy between (1) and (2) is a surprising effect. Two explanations that are not mutually exclusive can be offered. This shift may be related to the change in the Si-N bond length. Within the bond length correlation model, shorter/stronger bonds have associated σ* resonances at higher term values than longer/weaker bonds [19-21] (term value = ionization potential - transition

energy). Si-N bond lengths are available from gas phase electron diffraction for (**1**) and solid state X-ray diffraction for (**2**) [2]. The Si-N bond is 0.034 Å *shorter* in (**2**) than in (**1**). However, peak positions in core excitation spectra of *third row* element core edges (e.g. Si, P, S) are generally less dependent on bond lengths [22] than in the core spectra of second row elements where strong variations with bond length are observed [19].

The other explanation of the difference in the Si 1s → σ*(Si-N, b_1) transition energy may be a change in the effective atomic charge on Si. Previous *ab initio* calculations [2] predict that Si in (**2**) has 0.051 higher positive charge than in (**1**), suggesting that (**1**) will have a slightly smaller Si 1s core binding energy than (**2**). However, calculated core electron binding energies (from the *ab initio* calculations, not shown) predict the opposite: the Si 1s level of (**1**) is 0.074 eV more tightly bound than (**2**). As these calculated factors are small and contradictory and experimental core electron binding energies have not been measured, it seems unlikely that a Si 1s core binding energy shift, associated with a different charge on Si, is the origin of the shift in the Si 1s → σ*(b_1) transition between (**1**) and (**2**).

3.2 Si 2s Spectra

Since the core orbital symmetry is the same, the Si 2s spectra are expected to be similar to the Si 1s spectra. The background subtracted silicon 2s electron energy loss spectra of (**1-4**), are presented in Figure 4. The top panel of figure 4 presents the raw Si 2p and Si 2s spectra of (**1**) together with the fitted power-law background function subtracted to isolate the core edge signals. Energies and proposed assignments of the spectral features are presented in Table 3.

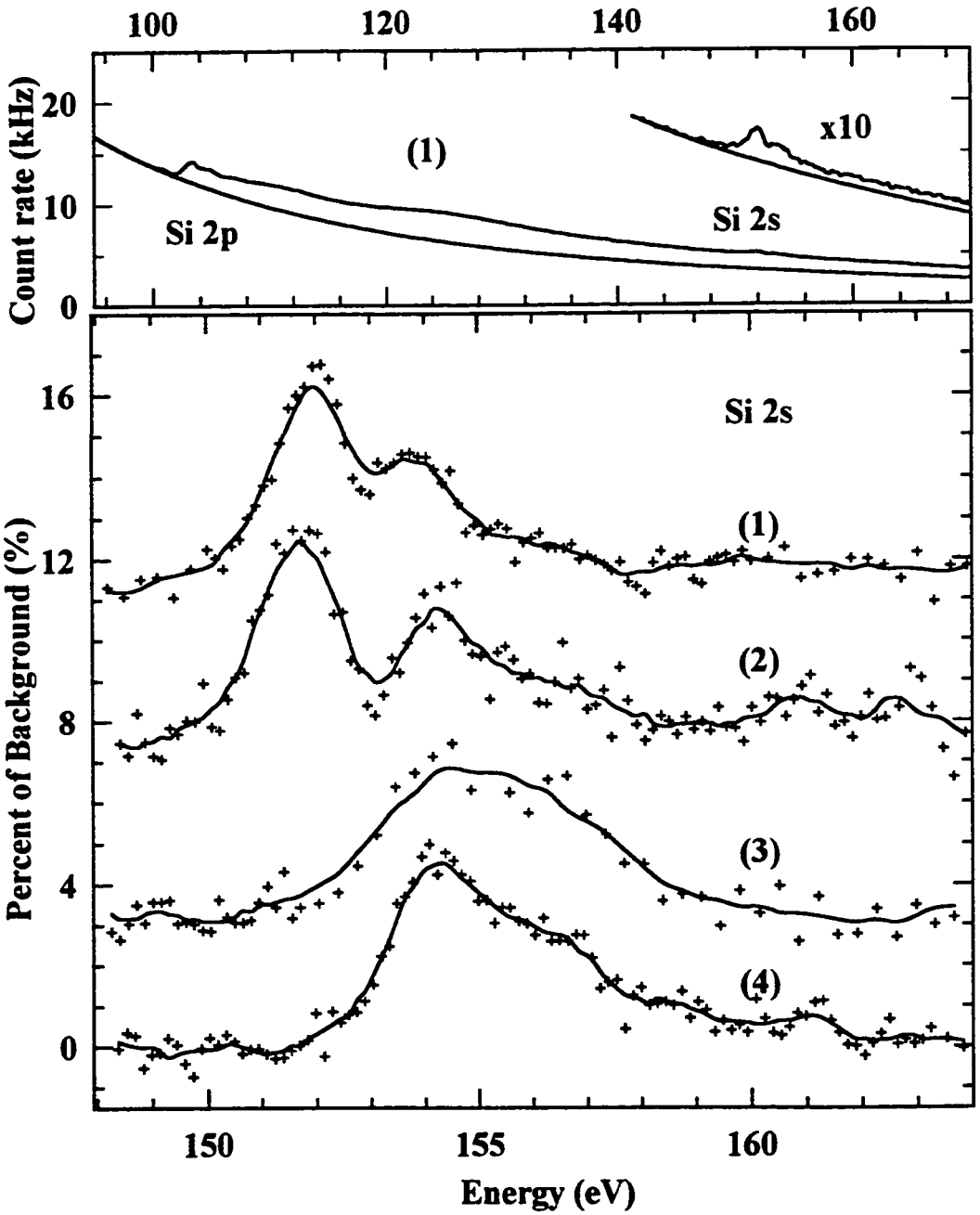

Figure 4. (top) The as-recorded Si 2p and Si 2s inner shell electron energy loss spectra of (1), measured using 2.5 keV final electron energy, 2° scattering angle and 0.7 eV fwhm resolution, presented with the fitted background functions used used to isolate the Si 2p and Si 2s signals. (bottom) Background-subtracted Si 2s spectra of (1), (2), (3) and (4). The spectral intensity is expressed as percent of the background signal. Offsets of 11, 7 and 3 (%) have been used for clarity in the spectra of (1), (2) and (3), respectively. The solid line is a smoothed version of the data included as a guide to the eye.

The Si 2s core edge is a relatively weak feature superimposed on a much larger Si 2p ionization signal. This large background makes it difficult to accurately isolate the Si 2s signal. Notwithstanding these difficulties, the Si 2s spectra are qualitatively similar to the Si 1s spectra. For (**1**) and (**2**), the Si 2s → π^*(Si-N,b_2) and Si 2s → σ^*(Si-N, b_1) transitions are clearly resolved, and the energy shift between them is similar to that observed in the Si 1s spectra. In particular the constancy of the energy of the $\pi^*(b_2)$ and the shift in the $\sigma^*(b_1)$ features closely follows that of the corresponding Si 1s features. The two σ^* features expected in the Si 2s spectra of (**3**) and (**4**) are not clearly resolved, although it should be noted that the σ^* features in the Si 1s spectra of (**3,4**) are broader than the corresponding peaks in the Si 1s of (**1,2**). These spectra demonstrate that Si 2s and Si 1s core excitation provide similar information. This is expected and is a useful confirmation of the "atomic propensity" model - core levels of the same atomic symmetry (1s, 2s) couple to the same final states with similar relative intensities.

3.3. Si 2p Spectra

The Si 2p spectra (Figure 5, Table 4) of the silylenes (**1,2**) and the dihydridosilanes (**3,4**) are quite different from the Si 1s and 2s spectra. This is consistent with the atomic propensity model, which favours excitations from p-symmetry core levels to unoccupied levels with large Si 3s or Si 3d character. Thus a Si 2p → $\pi^*(b_2)$ transition in (**1**) and (**2**) is expected to be absent or very weak, since Si $3p_y$ atomic orbitals are expected to be the main contribution to π^* molecular orbitals. In fact there is a weak low energy feature at 100.9 eV in the Si 2p spectrum of both (**1**) and (**2**) which we attribute to a Si 2p → $\pi^*(b_2)$ transition.

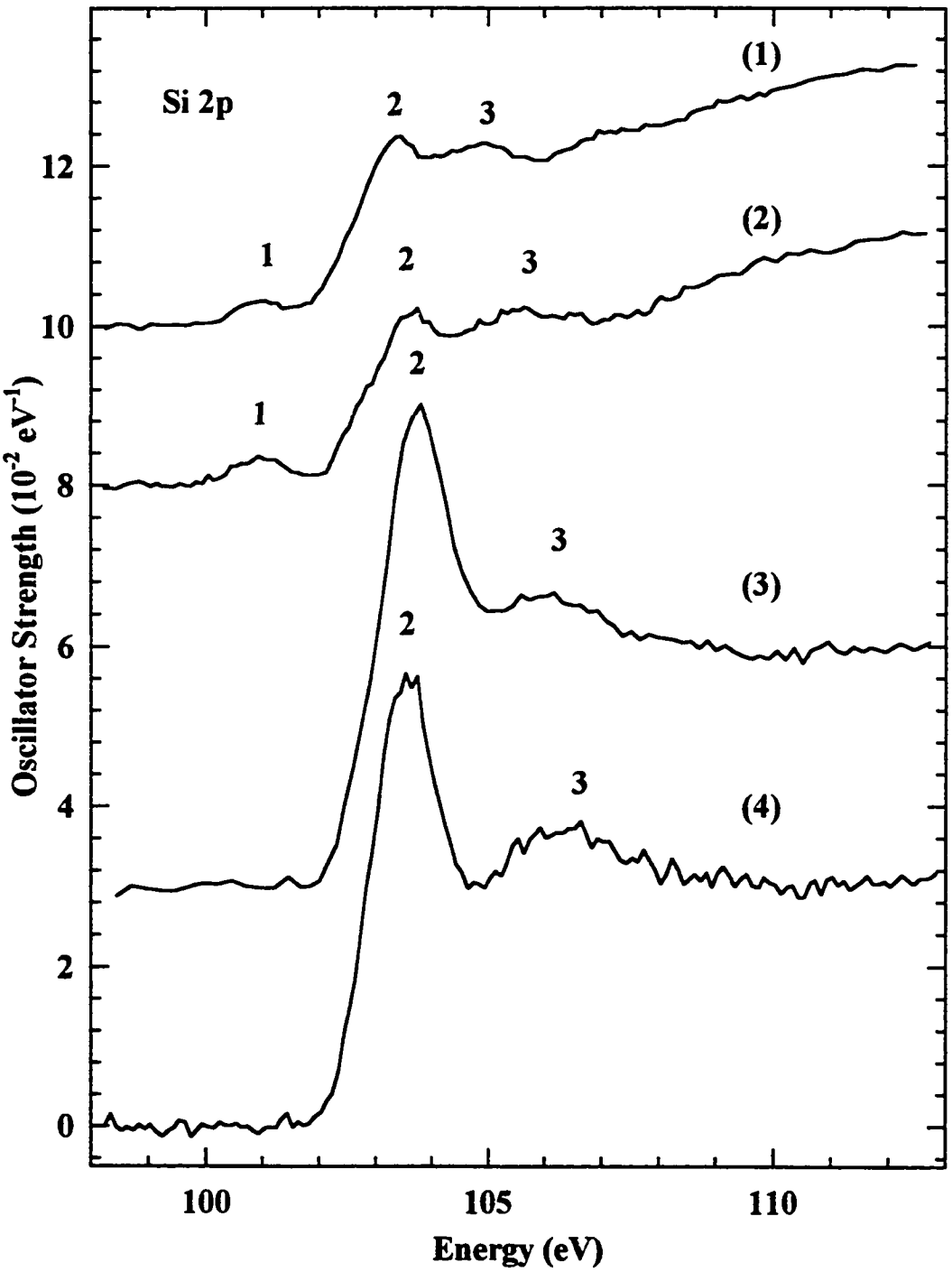

Figure 5. Background subtracted Si 2p oscillator strength spectra of (1), (2), (3) and (4), recorded using 2.5 keV final electron energy, 2° scattering angle and 0.7 eV fwhm resolution. Offsets of 10, 8 and 3 (10^{-2} eV^{-1}) have been used for clairity in the spectra of (1), (2) and (3), respectively.

Table 4 Energies (eV) and Assignments of Features in the Si 2p Spectra of Silylenes (R_2Si:) and Dihydridosilanes (R_2SiH_2)

#	(1)	(2)	(3)	(4)	Assignment[e]
1	101.0	101.0			π^*(Si-N, b_2)
2	103.4[a]	103.7[b]	103.8[c]	103.6[d]	σ^*(Si-N, b_1)
3	104.9	106.0	106.3	106.5	σ^*(Si-N, a_1)
4 br	112	112	113	113	ϵd
5 br	130	130	128	128	ϵd

a. Calibration relative to the C 1s → π^* transition of CO (287.40 eV) [27] E = -184.0 eV.
b. Calibration relative to the N 1s → π^* transition of N_2 (401.1 eV) [27] E = -297.4(1) eV.
c. Calibration relative to the C 1s → π^* transition of CO_2 (290.74 eV) [27] E = -186.82(6) eV.
d. Calibration relative to the C 1s → π^* transition of CO_2 [27] E = -187.16(5) eV.
e. C_{2V} symmetry labels are used for convenience in the case of the C_2 symmetry molecules (**2**) and (**4**).

Although the transition is disfavoured by the atomic propensity model, in a molecular picture, Si 2p → b_2 transitions are symmetry allowed. As well, in C_{2v} symmetry, final states of b_2 symmetry can contain a mixture of $3p_y$ and $3d_{yz}$ atomic contributions, thus permitting an "atomic propensity"-allowed Si 2p → $\pi^*(b_2)$ transition (e.g., Si 2p → Si 3d at the Si atom). The second, intense feature at 103.4 eV is attributed to a Si 2p → σ^*(Si-N, b_1) transition. At higher energy (104.9 eV) there is a broad feature that is only weakly observed in the corresponding Si ns spectra. This transition is assigned as a Si 2p → σ^*(Si-N, a_1) transition. There are also strong signals in the Si 2p continuum at 113 and 127 eV (See Fig. 4 for (**1**); not shown for (**2-4**)). These are characteristic of all Si 2p spectra, and have been attributed previously to delayed onset of the Si 2p → ϵd transitions [25].

The absence of a low energy Si 2p → π^* transition in the spectra of the

dihydridosilanes (**3**,**4**) supports our assignment of π^*(Si-N) to the first peak in the Si 2p spectra of (**1**) and (**2**). Furthermore, the intensity of the near edge features in the Si 2p spectra of (**3**) and (**4**) is much stronger than in (**1**) and (**2**). Application of the atomic propensity model suggests that the low energy unoccupied states in (**1**,**2**) are predominantly of p character - weak and formally forbidden in the Si 2p edge spectra - while the low energy core excited states (**3**,**4**) have much more s and/or d character. The character of the unoccupied orbitals of (**I-IV**) are consistent with this. The first and second transitions in the Si 2p spectra of (**3**,**4**) are assigned as Si 2p → σ^*(Si-N, b_1) and Si 2p → σ^*(Si-N, a_1) transitions, respectively, in analogy to the Si 1s spectra.

3.4 C 1s Spectra

The C 1s oscillator strength spectra (Figure 6, Table 5) of the silylenes (**1**,**2**) and the dihydridosilanes (**3**,**4**) are the sum of contributions from two distinct carbon sites: that from the two ring carbons and that from the eight ligand t-butyl carbons. For (**1-4**), the t-butyl related features are essentially identical to those of isobutane [26] (see Table 5). Comparison of the two unsaturated species (**1**,**3**) with the two saturated species (**2**,**4**) demonstrates characteristic peaks (~286.5 eV) for the ethylene carbon in (**1**) and (**3**). The unsaturated silylene (**1**) has an additional peak at 285.0 eV, arising from the mixing of the ethylene b_2 π^* states with the b_2 3pπ^* states on the dicoordinate Si. The ~286.5 eV π^* feature is attributed to a C 1s → π^*(C=C, a_2) transition. The energy and intensity of this feature does not vary substantially between the C 1s spectra of (**1**) and (**3**), consistent with the lack of symmetry allowed overlap with the Si 3p π density.

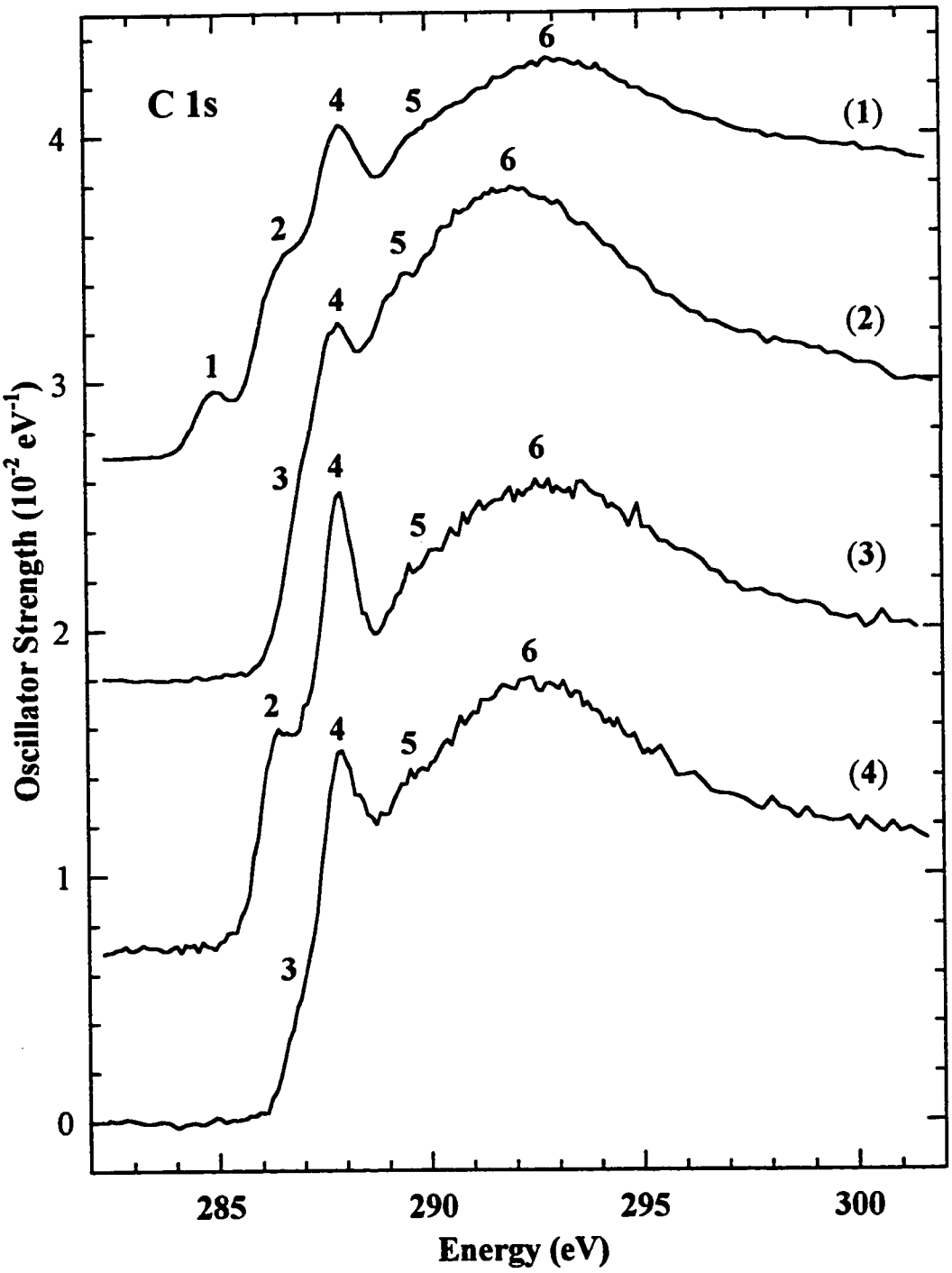

Figure 6. Background subtracted C 1s oscillator strength spectra of (1), (2), (3) and (4). See the caption of figure 5 for details of spectral acquisition. Offsets of 2.7, 1.8 and 0.7 (10^{-2} eV^{-1}) have been used for clarity in the spectra of (1), (2) and (4), respectively.

Table 5 Energies (eV) and Assignment of Features in the C 1s Spectra of Silylenes (R_2Si:) and Dihydridosilanes (R_2SiH_2)

#	(1)	(2)	(3)	(4)	Isobutane[a]	Assignment[f]
1	285.01[b]					π^*(C=C, b_2)
2	286.6	286.4				π^*(C=C, a_2)
3	-	287.0		286.9	287.0	3s Ryd. (^{t}Bu)
4	288.0	287.93(6)[c]	287.92(2)[d]	287.92[e]	287.8	π^*(CH_3)/3p (^{t}Bu)
5	289.6	289.6	289.6	289.6	288.6	4s Ryd. (^{t}Bu)
6 br	293	292	293	292	292.4	σ^*(C-C)
7 br	302				301	σ^*(C-C), σ^*(C-H)

a. Isobutane energies and term values from published C 1s spectrum. [26]
b. Calibration relative to the C 1s → π^* transition of CO : E = -2.32 eV.
c. Calibration relative to the N 1s → π^* transition of N_2 : E= -113.17(6) eV.
d. Calibration relative to the C 1s → π^* transition of CO_2 : E = -2.82(2) eV.
e. Calibration relative to the C 1s → π^* transition of CO_2 : E = -2.82 eV.
f. C_{2V} symmetry labels are used for convenience in the case of the C_2 symmetry molecules (**2**) and (**4**).

According to the ground state calculations of (**I**) and (**III**) (Fig. 1), the a_2 orbital is not the second lowest MO in (**I**) or the lowest energy MO in (**III**). This appears to be a discrepancy with our empirical assignment of the ~286.5 eV feature as the C 1s → $\pi^*(a_2)$ transition. However, core hole relaxation (Fig. 2, Table 2) must be considered. There is a strong C 1s core hole relaxation effect which dramatically stabilizes the a_2 MO such that the (C $1s^{-1}$,$\pi^*(a_2)$) state is indeed the penultimate C 1s excited state of (**I**). For higher energy features, the results of the calculations are not as useful, as the molecular structures used (**I-IV**) do not include the t-butyl group which dominates the C 1s spectrum above ~287 eV.

The similarity of the C 1s spectra of the two C-C saturated species (**2**,**4**) demonstrates that there is little interaction between the carbon atoms of the alkyl bridge and the silylene electronic density. This is in sharp contrast to the C=C unsaturated species where $\pi^*(b_2)$

ethylene-Si interactions generate a large difference between the spectra of (**1**) and (**3**). In the ground state of (II), the LUMO is a π^*(b) level (Fig. 1). A feature corresponding to a C 1s → LUMO excitation is not observed in the C 1s spectrum of (**2**) as this π^*(b) level does not have any density on the fully saturated carbon component of the ring.

As expected, the C 1s → σ^* region (289-295 eV) in the spectra of all four compounds is dominated by the C 1s($-CH_3$) → σ^*(C-C) and C 1s($-CH_3$) → σ^*(C-H) transitions associated with the t-butyl groups. C 1s(t-Bu) → σ^*(C-N) and C 1s(C=C) → σ^*(C-N) transitions are expected to contribute in this region but are unlikely to give well defined structure since they are masked by the large C 1s(t-Bu) → $\sigma^*(CH_3)$/3p Rydberg intensity.

3.5 N 1s Spectra

As with the other core edge spectra, the N 1s oscillator strength spectra (Figure 7, Table 6) are strongly influenced by the molecular structure. The lowest energy N 1s feature of the silylenes (**1**,**2**) is assigned to N 1s → $\pi^*(b_2)$ transitions, while the second feature is assigned to N 1s → $\pi^*(a_2$, Si-N) transitions. The strong N 1s → $\pi^*(b_2)$ transition dominates the spectrum of (**1**). The observation of an intense transition to this B_2 state in the Si, C and N core edge spectra of (**1**) indicates that there is strong mixing of ring p orbitals at all ring sites: Si 3p, C 2p and N 2p. The π^*(Si-N,b_2) orbital is thus completely delocalized. In (**2**), where C 2p$\pi(b_2)$ density is not present, saturation at the ring carbons weakens the N 1s → $\pi^*(b_2)$ transition intensity and shifts it to lower energy.

In the N 1s spectra of the dihydridosilanes (**3**,**4**), the $\pi^*(b_2)$ feature is entirely absent. In the ground state calculations for (**I-IV**) (Fig. 1., Table 1) the $\pi^*(b_2)$ level is the LUMO in

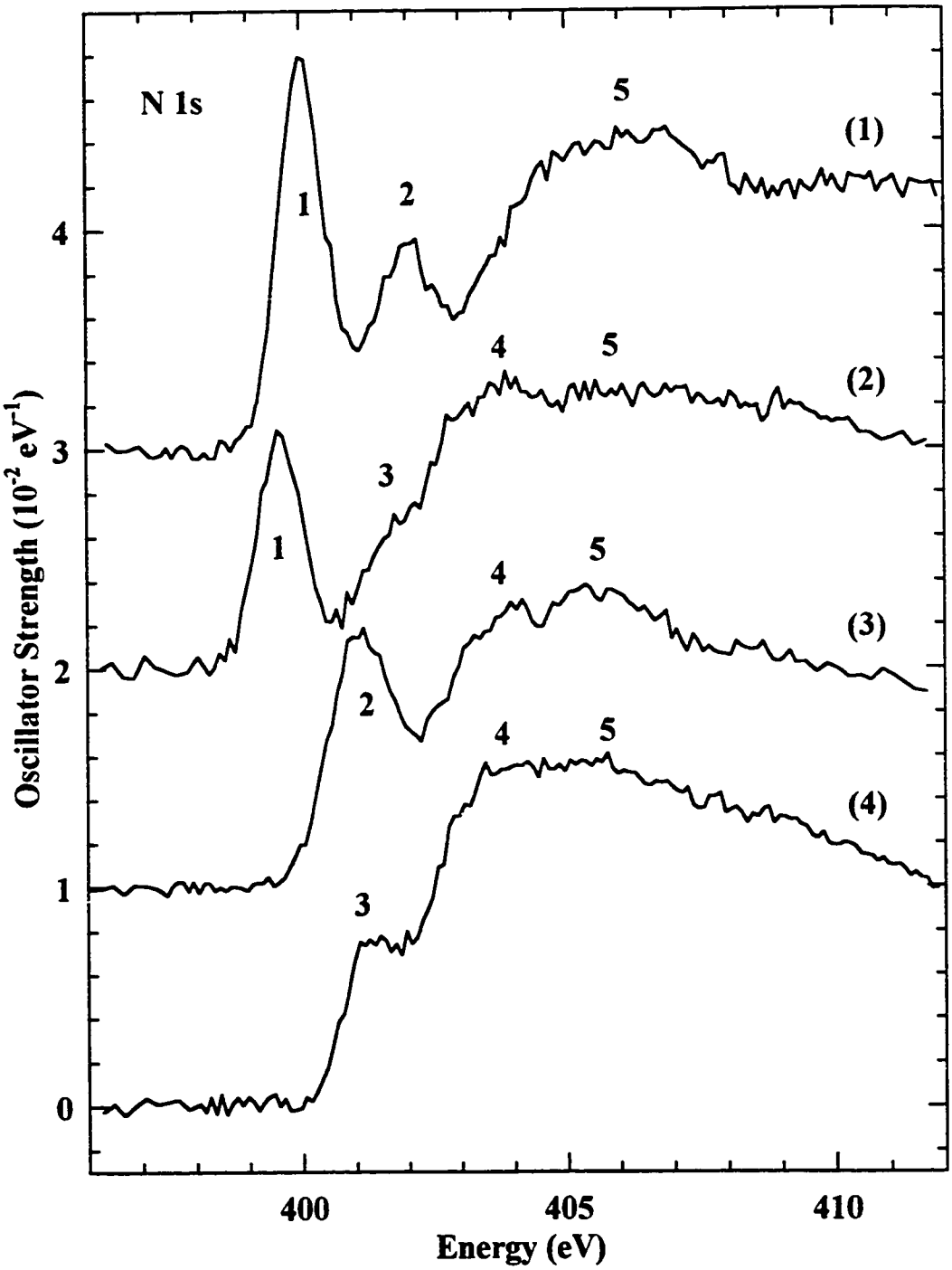

Figure 7. Background subtracted N 1s oscillator strength spectra of (**1**), (**2**), (**3**) and (**4**). See the caption to figure 5 for details of spectral acquisition. Offsets of 3, 2, and 1 (10^{-2} eV^{-1}) have been used for clarity in the spectra of (**1**), (**2**) and (**3**), respectively.

(**I-II**), and is absent in (**III-IV**), supporting this assignment. The N 1s "Z+1" calculation of (**I**) is not expected to be as applicable as the Si 1s and C 1s "Z+1" calculations to spectral interpretation of (**1**) because the replacement of the directly connected t-butyl group by hydrogen is expected to have a significant effect on the electronic environment of nitrogen.

Table 6 Energies (eV) and Assignments of Features in the N 1s Spectra of Silylenes (R_2Si:) and Dihydridosilanes (R_2SiH_2)

#	(1)	(2)	(3)	(4)	Assignment[e]
1	400.0[a]	399.6[b]			$\pi^*(b_2)$
2	402.0		401.2[c]		$\pi^*(a_2)$
3		401.8		401.3[d]	$\sigma^*(b_1)$
4 br		404	404	404	$\sigma^*(a_1)$
5 br	406	406	406	406	

a. Calibration relative to the C 1s → π* transition of CO : E = 109.25(6) eV.
b. Calibration relative to the N 1s → π* transition of N_2 : E = -1.51(3) eV.
c. Calibration relative to the C 1s → π* transition of CO_2 : E = +110.46(5) eV.
d. Calibration relative to the C 1s → π* transition of (**4**) : E = +113.4(1) eV.
e. C_{2V} symmetry labels are used for convenience in the case of the C_2 symmetry molecules (**2**) and (**4**).

The second feature at ~402 eV in the N 1s spectrum of (**1**) and (**3**) is attributed to N 1s → $\pi^*(a_2)$ transitions. A weak shoulder is observed in the spectra of (**2**) and (**4**), which is attributed to N 1s → $\sigma^*(b_1)$ transitions. The corresponding N 1s → $\sigma^*(b_1)$ transition in (**1**) and (**3**) is likely obscured by the N 1s → $\pi^*(a_2)$ transition.

Since nitrogen is coordinated by groups other than H in (**1-4**) (e.g., Si, the ring carbons and the t-butyl group) Rydberg transitions are very unlikely in the N 1s spectra. This observation is based on the N 1s spectra of variably substituted ureas and carbamates, in which the N 1s → Rydberg transitions in $-NH_2$ groups were strongly attenuated when the

hydrogen atoms were replaced by bulky phenyl groups [15].

4. Discussion

The presence of a low-energy core → π^* transition in each core excitation spectrum (Si ns, Si 2p, N 1s, C 1s) of the unsaturated silylene (**1**) illustrates that the lowest $\pi^*(b_2)$ orbital is delocalized over all of the atomic sites on the silylene ring. This is consistent with the model of (4n+2)-π delocalization as an important mechanism stabilizing (**1**) [2]. Saturation of the C=C double bond in (**2**) strongly perturbs the electronic and geometric structure relative to (**1**). The silylene unit may be characterized by the presence of an intense, low energy Si 1s → π^* resonance. Additionally, the lowest Si 1s → σ^* transition varies strongly with the molecular structure of the heterocycle ring containing the silylene unit. The dramatic spectral variations through this series of molecules demonstrates the capabilities of core excitation spectroscopy as a probe for delocalization, especially in highly symmetric aromatic systems. Inorganic heterocycles with their multitude of core levels of different symmetries, are a particularly fruitful area of application of this spectroscopy.

Acknowledgments

This research has been sponsored financially by NSERC (Canada). S.G.U. acknowledges the support of an Ontario Graduate Fellowship. This work is based in part on research conducted at the Synchrotron Radiation Center, Univ. of Wisconsin-Madison, which is supported by the NSF under award DMR-9212658. We thank Dr. X.H. Feng for his assistance with operation of the CSRF DCM at SRC. Computing facilities (SPARTAN, IBM RS-6000) were provided by the Department of Chemistry (McMaster). We thank M.A. Brook for reviewing the manuscript and for helpful comments, and M. Malott for assistance with the calculations.

References

1. M. Denk, R. K. Hayashi and R. West, *Chem. Commun.* **1994**, 33; M. Denk, R. Lennon, R. Hayashi, R. West, A. V. Belakov, H. P. Verne, A. Haaland, M. Wagner and N. Metzler, *J. Am. Chem. Soc.* **1994**, 116, 2691.
2. M. Denk, J. C. Green, N. Metzler and M. Wagner, *J. Chem. Soc. Dalton Trans.* **1994**, 1004, 2405.
3. A. P. Hitchcock, *Physica Scripta* **1990**, T31, 159.
4. J. Stöhr, NEXAFS Spectroscopy; Springer Trans. in Surface Science **1992**, 25.
5. A. P. Hitchcock and D. C. Mancini, J. Electro. Spectry. **1994**, 67, 1.
6. A. M. Flank, R. C. Karnatak, C. Blancard, J. M. Esteva, P. Lagarde and J. P. Connerade, *Z. Phys. D*, **1991**, 21, 357.; E. Bouisset, J. M. Esteva, R. C. Karnatak, J. P. Connerade, A. M. Flank and P. Lagarde, *J. Phys. B: At. Mol. Opt. Phys.* **1991**, 24, 1609.
7. M. H. Sayyad, E. T. Kennedy, L. Kiernan, J-P Mosnier and J. T. Costello, *J. Phys. B: At. Mol. Opt. Phys.* **1995**, 28, 1715.
8. D. Li, G. M. Bancroft, M. Kasrai, M. E. Fleet, X. H. Feng, K. H. Tan and B. X. Yang, *Solid State Comm.* **1993**, 87, 613.

9. D. Li, G. M. Bancroft, M. Kasrai, M. E. Fleet, X. H. Feng, K. H. Tan, *Amer. Minerol.* **1994**, 79, 785.

10. B. X. Yang, F. H. Middleton, B. G. Olsson, G. M. Bancroft, J. M. Chen, T. K. Sham, K. Tan and D. J. Wallace, *Nucl. Instr. and Methods in Phys. Res.* **1992**, A316, 422.

11. A. P. Hitchcock, T. Tyliszczak, P. Aebi, J. Z. Xiong, T. K. Sham, K. M. Baines, K. A. Mueller. X. H. Feng, J. M. Chen, B. X. Yang, Z. H. Lu, J.-M. Baribeau and T. E. Jackman, *Surf. Sci.* **1993**, 291, 349.

12. M. M. Thomas, J. C. Davis, C. J. Jacobsen and R. C. C. Perera, *Nucl. Instrum. and Meth. in Phys. Res.* **1990**, A291, 107.

13. B. L. Henke, P. Lee, T. J. Tanaka, R. L. Shimabukuro and B. J. Fujikawa, *Atom. Data Nucl. Data Tables* **1982**, 27, 1.

14. G. Cooper, T. Ibuli and C. E. Brion, *Chem. Phys.* **1990**, 140, 133.

15. S. G. Urquhart, A. P. Hitchcock, R. D. Priester and E. G. Rightor, *J. Polym. Sci: Part B: Polym Physics.* **1995**, 33, 1603.

16. W. H. E. Schwartz, *Chem. Phys.* **1975**, 11, 217.

17. Spartan version 4.0, Wavefunction Inc., 18401 Von Karman Ave., #370, Irvine, CA., 92715, U.S.A., All molecular orbital symmetries reported were verified by examining the molecular orbital output.

18. P. Blakeman, B. Gehrhus, J. C. Green, J. Heinicke, M. F. Lappert, M. Kindermann and T. Veszprémi, **1995**, private communication.

19. F. Sette, J. Stöhr and A. P. Hitchcock, *J. Chem. Phys.* **1984**, 81, 4906.

20. E. Lindholm, L. Asbrink and S. Ljunggren, *J. Phys. Chem.* **1991**, 95, 3923.

21. J. A. Sheehy, T. J. Gil, C. L. Winstead, R. E. Farren and P. W. Langhoff, *J. Chem. Phys.* **1989**, 91, 1796.

22. A. P. Hitchcock, S. Bodeur and M. Tronc, *Physica B* **1989**, 158, 257.

23. W. L. Jolly, K. D. Bomben and C. J. Eyermann, *At. Data Nucl. Data Tables* **1984**, 31, 109.

24. P. L. Hansen, R. Brydson and D. W. McComb, *Microsc. Microanal. Microstruct.* **1992**, 3, 213.

25. J. D. Bozek, G. M. Bancroft and K. H. Tan, *Chem. Phys.* **1990**, 145, 131.

26. A. P. Hitchcock and I. Ishii, *J. Electron Spectry.* **1987**, 42, 11.

27. R. N. S. Sodhi and C. E. Brion, *J. Electron Spectry.* **1984**, 34, 363.

28. G. Herzberg, Molecular Spectra of Polyatomic Molecules, D. Van Nostrand Co., **1966**.

CHAPTER 5C

Inner Shell Spectroscopy of Compounds Containing Si-Si Bonds: Is There a Localized, Low Energy Si-Si Resonance?

The following work documents the Si 1s, Si 2p, Si 2s, and C 1s core excitation spectra of a series of organosilane molecules containing Si-Si bonds. This work has been published in the journal Chemical Physics (*Chem. Phys.* **189**, 757, 1994) and is presented here in published form. The right to reprint this article was retained by the author and authorization has been obtained from the coauthors.

The author of this thesis acquired the spectra of dodecamethylcyclohexasilane (with G. G. B. de Souza) and wrote the bulk of the paper in collaboration with the coauthors. The other spectra were acquired by A. T. Wen (electron energy loss spectra) and J. Z. Xiong (X-ray absorption spectra). This paper is an extension of the work of A. T. Wen [W92], performed in collaboration with Dr. Wen.

ELSEVIER

Chemical Physics 189 (1994) 757–768

Chemical Physics

Inner-shell spectroscopy of compounds containing Si–Si bonds: is there a localised, low-energy Si–Si resonance?

S.G. Urquhart [a], J.Z. Xiong [b], A.T. Wen [a,1], T.K. Sham [b], K.M. Baines [b], G.G.B. de Souza [c], A.P. Hitchcock [a]

[a] *Department of Chemistry, McMaster University, Hamilton, Ontario, Canada L8S 4M1*
[b] *Department of Chemistry, University of Western Ontario, London, Ontario, Canada*
[c] *Instituto de Quimica, UFRJ, Rio de Janeiro, RJ, Brazil 21910-900*

Received 10 August 1994

Abstract

Oscillator strengths for the Si 2p, Si 2s, and C 1s excitation of tetramethylsilane, hexamethyldisilane, tetrakis-(trimethylsilyl)silane, and dodecamethylcyclohexasilane have been derived from electron energy loss spectra recorded in the dipole-regime. These results are compared to the Si 1s and Si 2p photoabsorption spectra of tetramethylsilane, hexamethyldisilane, tris(trimethylsilyl)silane, and tetrakis(trimethylsilyl)silane, recorded using synchrotron radiation. The spectra support the existence of a localised, low-lying state of large Si–Si character in species which contain Si–Si bonds.

1. Introduction

A notable property of alkylpolysilanes is that they exhibit a $\sigma \rightarrow \sigma^*$ electronic transition in the near UV, much lower in energy than that of the corresponding alkanes [1]. This observation, along with the chemistry of cyclic and linear polysilanes, has led to analogies between these saturated species and unsaturated hydrocarbons such as aromatic rings [2] and polyenes [3]. In this description, the HOMO of σ and the LUMO of σ^* character are considered to be *delocalised* over the Si–Si–Si framework of the polysilanes, and analogy is made to π and π^* delocalisation of unsaturated organic molecules. Photoelectron spectroscopy has been used to characterize the low-lying σ_{Si-Si} HOMO in polysilanes and organosilanes [4]. At the outset, we note that the designation "σ" (or "π") is not strictly correct for non-planar molecules and often inappropriate for large complex molecules. Indeed, the orbitals under discussion in these molecules have components both along and perpendicular to Si–Si (or Si–C) bonds, depending on the molecular structure and orbital symmetry. Of course the correct way to treat the molecular electronic structure and spectroscopy is to use a group theory based description of the unoccupied levels and states. However for the lower symmetry species this is not overly informative and even for the higher symmetry species, we believe it is reasonable to identify a "dominant" character of the upper level of any given transition in terms of where charge is located and whether the orbital is bonding, antibonding, or nonbonding with respect to a specific pair of atoms. Since much of the previous discussion in the literature has used the label "σ^*" for the low-lying states involved

[1] Present address: Département de Médécine Nucléaire et Radiobiologie, MRC Research Group, CHUS, Université de Sherbrooke, Sherbrooke, QU, Canada.

SSDI 0301-0104(94)00291-6

in electronic spectra of organosilanes, we will also use this as a convenient notation.

A complementary viewpoint of the electronic structure of Si–Si containing compounds is suggested by the "weak bond" model [5] which was proposed as a simple means to rationalize the relative energies of core excitation transitions in terms of bond strengths. In this picture, low-lying valence and core excited states in polysilanes are interpreted as evidence for a small σ–σ^* splitting associated with a relatively low Si–Si bond energy. McCray et al. [6] have used this model to interpret the lowest energy state in the Si 1s spectrum of poly(di-*n*-hexylsilane) as a *localised* σ^*_{Si-Si} feature. Higher energy states were attributed to Si 1s$\rightarrow\sigma^*_{Si-C}$ transitions. Polarisation dependent measurements on aligned solid samples [6] support assignment of the lowest energy band to a state aligned along the polysilane backbone and the higher energy features to states aligned perpendicular to the chain. In notable contrast, Kubiak et al. [7] have used ab initio small basis set calculations of the ground states of disilane and dimethyldisilane to assign Si 2p$\rightarrow\sigma^*_{Si-C}$ transitions *below* Si 2p$\rightarrow\sigma^*_{Si-Si}$ transitions in the Si 2p spectrum of several polysilane species. The lack of agreement among these descriptions indicates there are outstanding questions concerning the interpretation of the core excitation spectra and the electronic structure of Si–Si systems.

In this study we have investigated the core excitation spectra of a number of molecules which contain one or more Si–Si bonds. Dipole-regime electron energy loss spectroscopy (EELS) was used to record the Si 2p, Si 2s and C 1s spectra of tetramethylsilane (1), hexamethyldisilane (2), tetrakis(trimethylsilyl)silane (4) and dodecamethylcyclohexasilane (5). Synchrotron radiation was used to record the Si 2p and Si 1s photoabsorption spectra of (1), (2), tris(trimethylsilyl)silane (3) and (4), as well as the Si 1s spectrum of (5). Spectral comparisons are used to justify spectral assignments and to facilitate identification of features related to the presence or absence of a Si–Si bond in a given compound.

Most previous gas phase core excitation spectroscopic studies of silicon molecules have focused on simple halogenated or organo-substituted silicon molecules, typically those containing one silicon atom (see Ref. [8] for a bibliography of gas phase core excitation studies). Among the species we have studied, the Si 2p spectra of (1) [9,10] and (2) [11–13] and the Si 1s spectra of (1) and (4) [14] have been reported previously. The lowest energy feature in the Si 1s spectra of $Si(SiMe_3)_4$, $Ge(SiMe_3)_4$ and $Si(GeMe_3)_4$ ($Me=CH_3$) has been interpreted as a Si 1s$\rightarrow\sigma^*_{Si-Si}$ or σ^*_{Si-Ge} transition [14]. MS-Xα calculations [12] for the Si 1s, 2s and 2p spectra of $Me_3SiSiMe_3$ have attributed the lowest energy signal in all three Si core edges (2p, 2s, 1s) to a resonance of large σ^*_{Si-Si} character. However, the calculations also indicated a partial Si–C character to the lowest state and they predicted that there should be a relatively large number of transitions to discrete core excited states in which the upper level has mainly valence character.

For complex molecular systems high quality ab initio quantum chemical calculations using large basis sets are a major challenge. In the absence of such results, the spectra of series of related molecules provide a useful means for determining structure-spectral relationships. For example, the core excitation spectroscopy of molecules containing second row atoms (B ... F) has been used to establish a relationship between σ^* resonance energy and bond-length [15]. Studies of the S 1s spectra of series of sulphur compounds [16–18] have shown that there are features at well defined energies which have an intensity proportional to the number of S–X bonds (X=C, O, F). These features are attributed to localised S 1s $\rightarrow\sigma^*$(S–X) transitions [16–18].

Compounds containing silicon–silicon bonds are potentially useful as spectral models for silicon clusters and solid silicon materials. Core excitation spectroscopy is sensitive to the local unoccupied electronic structure at the core excited atom. In some cases the core spectra can be interpreted by considering only local bonding. In other cases delocalisation of the upper level of the transition must be taken into account. If a local picture applies, a "building block" model can be used to interpret the spectra of complex molecules, such as organic polymers, in terms of the spectra of simple molecular models [19,20]. Unlike organic species, there is relatively poor understanding of how core excitation spectra reflect the nature of electronic delocalisation in organosilanes. This study attempts to address this situation by using chemical systematics to determine whether or not a low-lying σ^*_{Si-Si} resonance is a general characteristic of compounds containing Si–Si bonds.

2. Experimental

2.1. Samples

Samples (1) and (2) were obtained commercially from Strem Chemical (stated purity of 97%). Published methods were used to synthesize (3) [41], (4) [42] and (5) [43]. The purity of the synthesized compounds estimated by gas chromatography is 86% (3), 98% (4) and 99% (5).

2.2. Electron energy loss spectroscopy

The inner-shell electron energy loss spectrometer and operating procedures have been described previously [21]. The spectra were obtained by inelastic scattering of a high energy electron beam (2.5 keV final energy) through a small scattering angle ($<2°$) with an energy resolution of 0.7 eV fwhm. All compounds were run without further purification, except for (1) and (2) which were subjected to multiple freeze pump thaw cycles. Species (4) and (5) are relatively involatile solids which were recorded by directly attaching the sample to the collision cell inside the vacuum chamber. Water cooling above and below the gas cell was used to trap the vaporised sample and thus prevent deposition on the sensitive electron optics. Multiple spectra were recorded to confirm reproducibility. Absolute energy scales were established by recording the spectrum with a stable mixture of the compound and CO_2, a standard calibrant species, as documented in the tables of spectral assignments.

The as-recorded spectra were converted to absolute oscillator strengths by normalizing to the absolute Si 2p oscillator strength of SiH_4 in the region of 145–151 eV [22]. This featureless, atomic-like region is higher in energy than the prominent Si 2p → ed transitions and before the onset of the Si 2s edge. C 1s spectra were normalized using procedures discussed elsewhere [8].

2.3. Synchrotron radiation photoabsorption

The total ion yield (TIY) spectra of the Si 2p edges were recorded in the gas phase with sample pressures of 20–65 mTorr, using the Canadian Synchrotron Radiation Facility (CSRF) Mark IV Grasshopper monochromator at the Aladdin synchrotron of the University of Wisconsin at Madison [23]. The slit size for these Si 2p measurements was 40 μm, which gave an energy resolution of 0.1 eV. The total ion signal is frequently used as an approximation to the true photoabsorption signal even though there may be some distortion in the intensity below the core edge relative to that above the core edge [17]. The TIY spectra presented in this paper were background subtracted and normalized to the Si 2p oscillator strength spectrum of (2) obtained as described in Section 2.2. The energy scale was calibrated using accepted values for the Si 2p spectral features of SiF_4 [10].

The Si 1s TIY spectra were recorded using the CSRF double crystal monochromator at the Aladdin facility. The energy scale was set by prior recording of the total electron yield spectrum of crystalline Si (edge inflection set at 1839.2 eV). The sample pressures were 0.1–0.3 Torr in a path length of 12 cm. The spectra were background subtracted to isolate the Si 1s signal which was then converted to an absolute oscillator strength scale by normalization to the atomic value of $0.16\,eV^{-1}$ at 1860 eV.

3. Results and discussion

3.1.1. Si 2p spectra: general features

The oscillator strength spectra in the Si 2p and 2s region of tetramethylsilane (1), hexamethyldisilane (2), tetrakis(trimethylsilyl)silane (4) and dodecamethylcyclohexasilane (5), derived from inner shell electron energy loss spectra are presented in Fig. 1. An expanded presentation of the Si 2p near edge region of these spectra is given in Fig. 2, in comparison to the optical data for (1), (2), (4) and (5). Energies, ionization potentials [24], term values and proposed assignments are presented in Table 1.

The Si 2p spectra of (2), (4) and (5) each exhibit a low energy peak or shoulder at ~ 102–103 eV, which is absent in the spectrum of (1). The 102 eV feature appears to be characteristic of the presence of a Si–Si bond, and thus we attribute it to Si 2p → σ^*_{Si-Si} transitions. Clearly the experimental chemical series approach supports the conclusion, deduced from the multiple scattering Xα calculations of (2) [12], that the lowest state in molecules containing Si–Si bonds is of dominant σ^*_{Si-Si} character.

In all of the organosilicon species there is a strong, broad feature peaking around 105 eV. This feature is

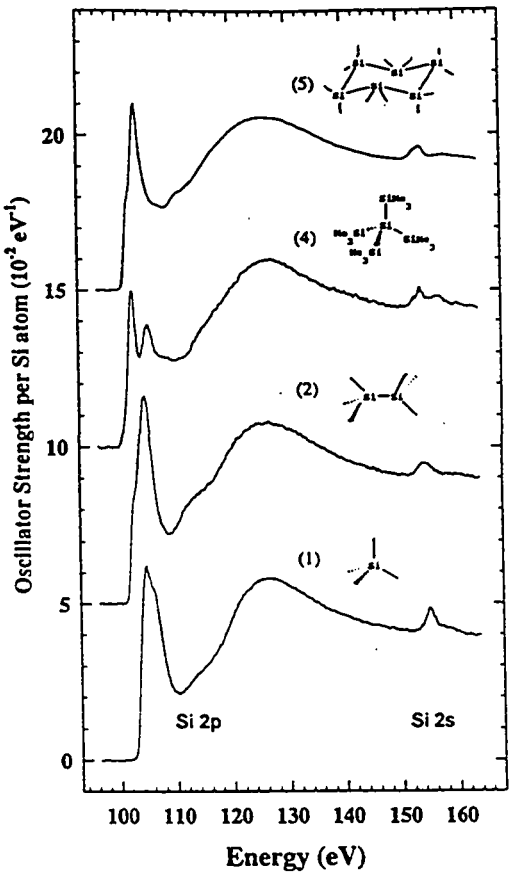

Fig. 1. Oscillator strength spectra in the region of Si 2p and 2s excitation of tetramethylsilane (1), hexamethyldisilane (2), tetrakis(trimethylsilyl)silane (4) and dodecamethylcyclohexasilane (5) derived from inner shell electron energy loss spectra recorded using 2.5 keV final electron energy, 2° scattering angle and 0.7 eV fwhm resolution. Successive spectra have been offset by 0.05 eV^{-1}. Unless otherwise indicated, the Me symbol has been omitted from the molecular diagram for clarity.

attributed to core → valence type transitions where the upper orbital of the transition is believed to be delocalised but to have a significant σ^*_{Si-C} character. The MS-Xα calculations of (2) indicate there are a number of orbitals of large valence character which are delocalised over the Si–C bonds [12]. The features attributed to Si 2p→σ^*_{Si-Si} and σ^*_{Si-C} transitions are broad (1–3 eV fwhm), such that the characteristic 0.6 eV Si 2p spin–orbit splitting cannot be detected. This is consistent with these (Si 2p^{-1}, σ^*) excited states having a highly dissociative character. Photoionization mass spectrometry studies of (2) have shown extensive fragmentation with both Si–Si and Si–C bond breaking occurring at the 102 and 105 eV resonances [11,13]. The Si 2p spectrum of (5) is somewhat different from that of the other four species in that both the first and

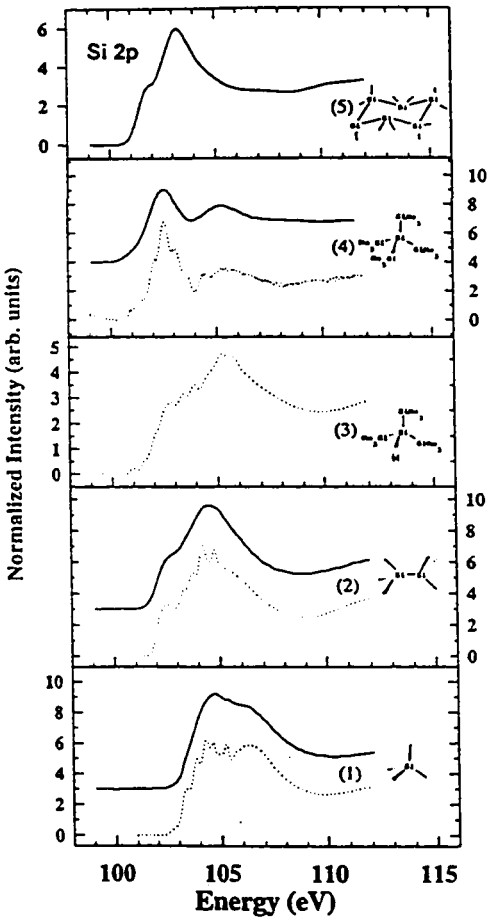

Fig. 2. Si 2p oscillator strength spectra (solid line, 0.7 eV fwhm) of tetramethylsilane (1), hexamethyldisilane (2), tetrakis-(trimethylsilyl)silane (4), and dodecamethylcyclohexasilane (5), derived from electron energy loss spectra; compared to the normalized Si 2p photoabsorption spectra (dotted line, 0.1 eV fwhm) of tetramethylsilane (1), hexamethyldisilane (2), tris-(trimethylsilyl)silane (3) and tetrakis(trimethylsilyl)silane (4). Offsets have been used for clarity.

Table 1
Energies, term values and proposed assignments for features in the Si 2p EEL spectra of tetramethylsilane (1), hexamethyldisilane (2), tetrakis(trimethylsilyl)silane (4), and dodecamethylcyclohexasilane (5)

$SiMe_4$ (1)		$Me_3SiSiMe_3$ (2)		$Si(SiMe_3)_4$ (4)			$c\text{-}Si_6Me_{12}$ (5)		Assignment	
E (eV)	T [a]	E (eV)	T [a]	E (eV)	T_{Si-C} [b]	T_{Si-TMS} [b]	E (eV)	T [a]	Si-C [b]	Si-TMS [b]
				101.1(sh)	3.5	–			σ^*_{Si-Si}	
		102.6	3.2	102.5 [c]	–	3.3	101.8	3.4		σ^*_{Si-Si}
							103.2 [c]	2.0		σ^*_{Si-Si}, σ^*_{Si-C}
104.6 [c]	1.7	104.5 [c]	1.3	105.2	–	0.6				σ^*_{Si-C}
				104.3 [d]					$IP(2p_{3/2})$	
				104.9 [d]					$IP(2p_{3/2})$	
106.0 [d]		105.5 [d]		105.5 [d]			104.9 [d]			$IP(2p_{1/2})$
106.6 [d]		106.1 [d]		106.1 [d]			105.5 [d]			$IP(2p_{1/2})$
106.1	0.2						107	−2	σ^*_{Si-C}	
114(sh)	−8	112	−6	112	−7		111	−6	σ^*_{Si-C}	
126(br)	−20	125	−19	125	−20		125	−20	Si 2p → εd	

[a] Term values (E-IP) are given relative to the average Si 2p IP since the 0.6 eV spin–orbit splitting is not resolved.
[b] Si-c refers to the central Si; Si-TMS refers to the pendant $SiMe_3$ group.
[c] Calibration relative to C 1s → π* in CO_2(290.74 eV) [38]; $\Delta E = -186.1(1)$, $-186.28(8)$, $-186.20(6)$ and $-187.54(8)$ eV for (1), (2), (4) and (5) respectively.
[d] Vertical Si $2p_{3/2}$ IPs from X-ray photoelectron spectroscopy (XPS). Si $2p_{1/2}$ IPs are 0.61 eV higher [24].

second peak occur at considerably lower energy than in (2), (3) or (4). This shift suggests both the upper levels for both the first and second transitions have a large Si–Si character and that there is appreciably more σ^*_{Si-Si} and σ^*_{Si-C} mixing in this cyclic compound.

Tossell et al. [14] have used the results of ab initio, equivalent core calculations of $(SiH_2)_n$, $n=2$–6 to attribute the main feature at 103.2 eV in the Si 2p spectrum of (5) to excitations to an MO of large Si $3p\pi$ character, which is Si–Si antibonding and mixed with σ^*_{Si-C} components. Aside from the use of a different label (see note on nomenclature in the introduction), this is in agreement with our assignment. The use of the π label reinforces the analogy with unsaturated and small saturated cyclic hydrocarbons [2,3].

In addition to the σ^*_{Si-Si} and σ^*_{Si-C} features discussed above, there are features at 112 eV and 125 eV in the Si 2p spectral continuum of (1), (2), (4), and (5). The 112 eV feature is a weak shoulder or peak which is assigned as a σ^*_{Si-C} shape resonance, in common with previous studies of organosilanes [10]. Double excitations could also contribute in this energy region. The higher energy feature, a broad intense resonance observed in the Si 2p spectra of essentially all Si compounds, is attributed to the intrinsic shape of the Si 2p ionization continuum [25,26] which is characterized by a delayed onset of 2p core ionization caused by the angular momentum barrier in the dominant 2p → εd channel. In contrast to our interpretation, Tossell et al. [14] have attributed the broad maximum at ~125 eV in (5) to excitations to high-lying σ^*_{Si-C} orbitals.

3.1.2. High resolution Si 2p photoabsorption spectra

Fig. 2 presents the normalized high resolution Si 2p photoabsorption spectra (dotted line) of tetramethylsilane (1), hexamethyldisilane (2), tris(trimethylsilyl)silane (3), and tetrakis(trimethylsilyl)silane (4) in comparison to the Si 2p oscillator strength spectra derived from the energy loss spectra (solid line). Energies, ionization potentials [24], term values and tentative assignments are presented in Tables 2 and 3.

The higher energy resolution photoabsorption spectra (0.1 versus 0.7 eV fwhm for EELS) exhibit a number of sharp peaks superimposed on the same broad Si 2p → σ* bands which dominate the EELS spectra. Aside from the absence of the sharp peaks, the shapes of the EEL spectra of (1), (2), and (4) agree well with those of the corresponding photoabsorption spectra. This supports our assumption that the energy loss spectra are dominated by the same electric dipole transitions as the optical spectra even though the momentum transfer is 1 $Å^{-1}$, a value which is sufficiently large that higher terms in the Bethe-Born expansion would contribute if the non-dipole matrix elements

Table 2
Energies, term values and proposed assignments for features in the Si 2p photoabsorption spectra of tetramethylsilane (1) and hexamethyldisilane (2)

$SiMe_4$ (1)			$Me_3SiSiMe_3$ (2)			Assignments	
E (eV)	$T_{3/2}$	$T_{1/2}$	E (eV)	$T_{3/2}$	$T_{1/2}$	3/2	1/2
102.7(sh)	3.3					4s	
			102.5	---3.2 [a]---		---σ^*_{Si-Si}---	
103.35		3.30					4s
103.84	2.20		103.36	2.08		3d	
104.29		2.36	103.74		2.31		3d
104.58	1.46		104.22	1.22		4d	
104.8(3)(br)	---1.5 [a]---		104.7	---1.0 [a]---		---σ^*_{Si-C}---	
105.2		1.45					
106.3(br)	---0---		105.1	---6---		---σ^*_{Si-C}---	
106.04 [b]			105.44 [b]			IP($2p_{3/2}$)	
106.65 [b]			106.05 [b]				IP($2p_{1/2}$)

[a] The term values for broad features are referenced to the average Si 2p IP.
[b] Vertical Si $2p_{3/2}$ IPs from XPS. Si $2p_{1/2}$ IPs are 0.61 eV higher [24].

were large [27]. The sharp peaks in the photoabsorption spectra are tentatively attributed to Si 2p → 4s and Si 2p → nd (n = 3, 4) Rydberg transitions. The specific assignments are based on the term values which are characteristic of the 4s and nd Rydberg states [28]. The MS-Xα calculations for $Me_3SiSiMe_3$ (2) predict that the intensity for Si 2p → Rydberg transitions is very small [12]. These calculations predict eleven closely spaced states, of mostly valence character, with term values between 5.1 and 1.5 eV. When spin–orbit coupling is included it is possible to attribute all of the sharp spectral features to these states. However we also

Table 3
Energies, term values and proposed assignments for features in the Si 2p photoabsorption spectra of tris(trimethylsilyl)silane (3) and tetrakis(trimethylsilyl)silane (4)

$HSi(SiMe_3)_3$ (3)					$Si(SiMe_3)_4$ (4)					Assignments			
E (eV)	T_{Si-C}		T_{TMS}		E (eV)	T_{Si-C}		T_{TMS}		Si-c		Si-TMS	
	3/2	1/2	3/2	1/2		3/2	1/2	3/2	1/2	3/2	1/2	3/2	1/2
101.0	3.6				101.1	3.2				4s			
101.5(sh)		3.7			102.1		2.8				4s		
102.0(sh)			3.5		102.5			3.0				4s	
102.8				3.3	103.1				3.0				4s
103.0(3)(br)	----------2.3 [a]----------				102.5(3)(br)	----------2.7 [a]----------				---σ^*_{Si-Si}---		---σ^*_{Si-Si}---	
103.4	1.2		2.1					2.0				3d	
103.9		1.3		2.2	103.5								3d
105.4(br)	----------0 [a]----------				104.4(br)	----------1 [a]----------				---σ^*_{Si-C}---		---σ^*_{Si-C}---	
104.61 [b]					104.30 [b]								
105.22 [b]					104.90 [b]					IP			
105.46 [b]					105.45 [b]						IP		
106.07 [b]					106.06 [b]							IP	
													IP
					105.7(br)	----------1----------				---σ^*_{Si-C}---		---σ^*_{Si-C}---	

[a] The term values for broad features are referenced to the average Si 2p IP.
[b] Vertical Si $2p_{3/2}$ IPs from XPS. Si $2p_{1/2}$ IPs are 0.61 eV higher [24].

note that a Rydberg interpretation has been given for sharp peaks at similar term values in the Si 2p spectra of other species [29]. It is likely that Rydberg-valence mixing plays an important role in these systems. The term value and apparent lack of vibrational excitation are typical of Rydberg states, whereas the transition intensity likely derives from the compact, valence-like character of the upper MO of the transition.

The Si 2p spectra of (3) and (4) need to be considered somewhat differently from those of the other Si–Si containing molecules since these two species contain Si in two different chemical environments. Photoelectron measurements [24] indicate that the IP (ionization potential) of the central Si atom (Si-c) lies at lower energy (104.6 eV for (3) and 104.3 eV for (4), versus 105.5 eV for the $Si(CH_3)_3$ site). The additional low energy peaks around 101–102 eV in the photoabsorption spectra of (3) and (4) are attributed to the Si 2p(Si-c) $\rightarrow \sigma^*_{Si-Si}$ transition, which lies about 1 eV below the more intense Si 2p($SiMe_3$) $\rightarrow \sigma^*_{Si-Si}$ transition.

3.2. Si 2s and Si 1s spectra

The Si 2s regions of the energy loss spectra of (1), (2), (4) and (5) are compared to the Si 1s photoabsorption spectra of (1)–(5) in Fig. 3. The energy scales are chosen such that the main features are aligned in the Si 1s and 2s spectra. The Si 2s spectra are of lower statistical quality because of the very weak cross section. A high resolution (0.15 eV fwhm) Si 2s spectrum of (2) collected using synchrotron radiation photoabsorption spectroscopy is in good agreement with the present EELS result [12]. Energies, term values and tentative assignments are presented in Tables 4 and 5.

As expected, the Si 2s and Si 1s spectra of the same compound are very similar. In each of the species containing Si–Si bonds there is a low-energy structure which is not present in the spectrum of (1). As for Si 2p excitation, the lowest energy peak is attributed to Si *ns* excitation to σ^*_{Si-Si}, the LUMO of large Si–Si antibonding character. In species (3) and (4) the Si 1s spectra exhibit a shoulder on the low-energy side of the first peak. This is attributed to Si 1s(Si-c) $\rightarrow \sigma^*_{Si-Si}$ transitions which are shifted lower in energy because of the shift of the Si 1s IP of the central Si (Si-c) relative to that of the methylated Si (Si-TMS). The lowest energy band in the Si 1s and Si 2s spectra of (5) is structured

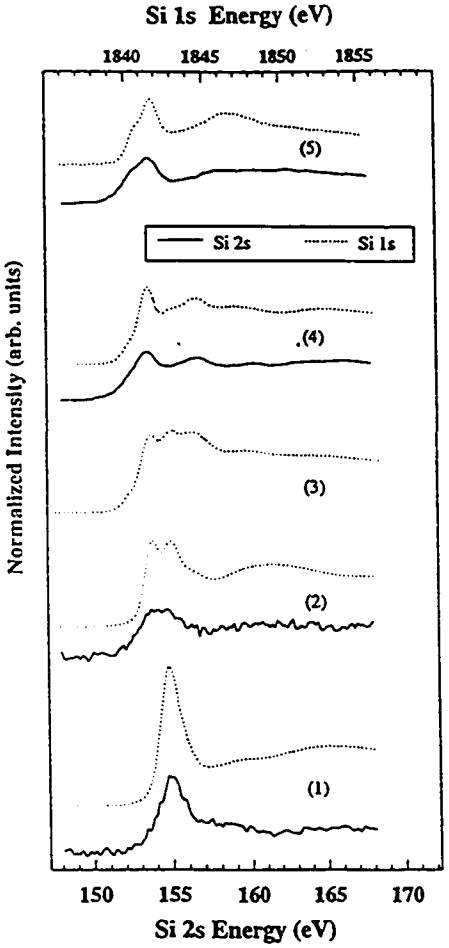

Fig. 3. Si 2s EELS spectra (solid line, 0.7 eV fwhm) and Si 1s photoabsorption spectra (dotted line, 0.8 eV fwhm) of tetramethylsilane (1), hexamethyldisilane (2), tris(trimethylsilyl)silane (3), tetrakis(trimethylsilyl)silane (4), and dodecamethylcyclohexasilane (5). The Si 2p and Si 1s energy scales are shifted relative to each other by 1687.8(1) eV, which is the average difference of the main spectral features in (1), (2), (4) and (5).

and somewhat lower in energy than the features attributed to σ^*_{Si-Si} in (2), (3) and (4). This pattern is similar to that already noted in the Si 2p spectrum of (5) and supports the occurrence of a greater amount of orbital mixing and delocalisation in this species relative to the non-cyclic species.

Table 4
Energies, term values and proposed assignments for features in the Si 1s photoabsorption spectra of tetramethylsilane (1), hexamethyldisilane (2), tris(trimethylsilyl)silane (3), tetrakis(trimethylsilyl)silane (4), and dodecamethylcyclohexasilane (5)

$SiMe_4$ (1)		$Me_3SiSiMe_3$ (2)		$HSi(SiMe_3)_4$ (3)			$Si(SiMe_3)_4$ (4)			c-Si_6Me_{12} (5)		Assignment	
E (eV)	T	E (eV)	T	E (eV)	T_{Si-C}	T_{TMS}	E (eV)	T_{Si-C}	T_{TMS}	E (eV)	T	Si-c	Si_{TMS}
				1840(sh)	4.6		1840(sh)	4.3				σ^*_{Si-Si}	
										1840.6	4.6		σ^*_{Si-Si}
		1841.7	3.8	1841.7		3.8	1841.5		3.7	1841.7	3.5		σ^*_{Si-Si}
1842.6	3.3	1842.8	2.7	1843		2.5	1842.8		2.4				σ^*_{Si-C}
		1844.4	1.1	1844.3		1.2	1844.5		0.7				σ^*_{Si-C}
				1844.6 [a]			1844.3 [a]					IP	
1845.9 [a]		1845.5 [a]		1845.5 [a]			1845.2 [a]			1845.2 [a]			IP
1847.2	−1.3	1849	−3	1848	−3		1848	−3		1846.7	−1.5		σ^*_{Si-C}

[a] Si 1s IPs were estimated by assuming the Si 2p–Si 1s splitting is the same as in tetramethylsilane (1740 eV) [39].

Table 5
Energies, term values and proposed assignments for features in the Si 2s EEL spectra of tetramethylsilane (1), hexamethyldisilane (2), tetrakis(trimethylsilyl)silane (4) and dodecamethylcyclohexasilane (5)

$SiMe_4$ (1)		$Me_3SiSiMe_3$ (2)		$Si(SiMe_3)_4$ (4)			c-Si_6Me_{12} (5)		Assignment	
E (eV)	T	E (eV)	T	E (eV)	T_{Si-C}	T_{Si-TMS}	E (eV)	T	Si-c	Si-TMS
		153.8	2.6	152.4	2.8		153.1	2.7	σ^*_{Si-Si}	
				153.8		2.6	154.1	1.7	σ^*_{Si-Si}	σ^*_{Si-Si}
155	2.1	154.9	1.5						σ^*_{Si-C}	σ^*_{Si-C}
				155.2 [a]					IP	
157.1 [a]		156.4 [a]		156.4 [a]			155.8 [a]			IP
159	−2	162	−6	157	−1.8	−0.6	158	−2	σ^*_{Si-C}	σ^*_{Si-C}

[a] Si 2s IPs were estimated by assuming the same Si 2p–Si 2s splitting as in tetramethylsilane (51.2 eV) [40].

The higher lying band in (2)–(5) and the single resonance in (1) are attributed to Si *ns* excitations to a relatively delocalised "σ^*_{Si-C}" orbital. The Si $ns \rightarrow \sigma^*_{Si-Si}$ transition is more intense relative to these features and the ionization continuum, than is the case for the Si $2p \rightarrow \sigma^*_{Si-Si}$ feature. This is consistent with a large Si 3p character to the σ^*_{Si-Si} LUMO. Because of the higher photon energy and thus greater penetrating ability and lower surface contribution, Si 1s X-ray absorption spectra measured on solid materials such as polysilanes can be obtained in a wider range of samples than the Si 2p or Si 2s spectra. This, along with the prominence of the Si $1s \rightarrow \sigma^*_{Si-Si}$ transition, makes Si 1s spectra more useful than the Si 2p or Si 2s spectra for general analytical characterization of Si–Si bonding in organosilicon clusters and polymers.

3.3. C 1s spectra

The C 1s spectra of (1), (2), (4) and (5) are presented in Fig. 4. Energies, ionization potentials [30], term values and tentative assignments are presented in Table 6. The C 1s spectrum of each species is characteristic of the methyl functional group bonded to silicon. Overall, the spectra are similar, although there are some differences, particularly around 290 eV. The main spectral feature at 290 eV is assigned to C $1s \rightarrow \sigma^*_{Si-C}$ transitions. Again we remind the reader that the upper orbitals in these transitions are likely delocalised over the whole molecule [12]. The most remarkable feature of these C 1s spectra is the very close similarity among all four spectra in the pre-edge region. In particular the introduction of a Si–Si bond into an organosilane molecule does not introduce any additional low-lying feature in the C 1s spectrum, in contrast to the situation in the Si core spectra. This

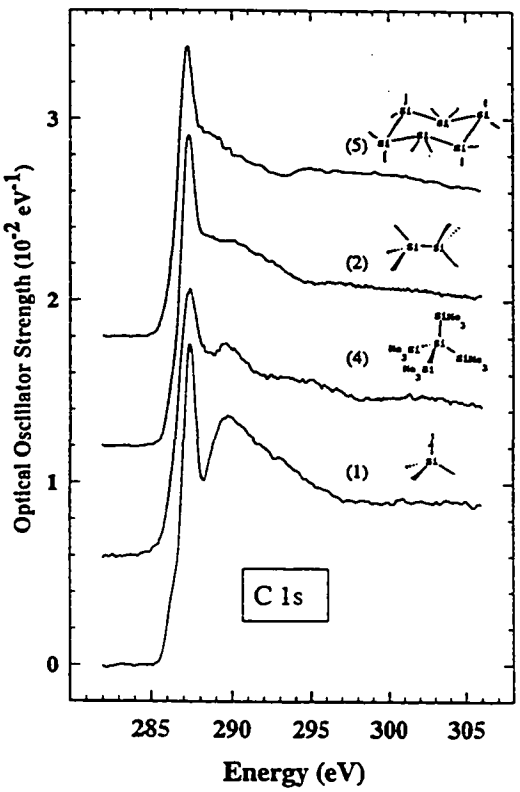

Fig. 4. C 1s oscillator strength spectra derived from dipole-regime EELS of tetramethylsilane (1), hexamethyldisilane (2), tetrakis-(trimethylsilyl)silane (4) and dodecamethylcyclohexasilane (5).

strongly suggests that C 1s→LUMO ("σ^*_{Si-Si}") excitations in the Si–Si containing species are of negligible intensity. One might consider attributing the shoulder at 286 eV (TV = 3.7 eV) to C 1s→σ^*_{Si-Si} transitions; however, this is inconsistent with the fact that this feature is most intense in $SiMe_4$. The C 1s spectra provide indirect support for our contention that the LUMO in the species containing Si–Si bonds is relatively strongly localised on the Si atoms and has relatively little Si–C character.

Since the carbon atoms in (1), (2), and (4) are all in a trimethylsilyl group, it is surprising there should be as large a difference as is observed in the 288–292 eV region. The C 1s spectrum of (1), and to a lesser extent (4), exhibits a dip at ~288 eV, whereas the C 1s spectra of (2) and (5) have little or no structure in this region. These changes may reflect different degrees of delocalisation of the "σ^*_{Si-C}" states which in turn may be associated with different orbital mixing.

4. Discussion

The spectra presented in this work strongly support the idea that organosilicon compounds which contain Si–Si bonds have a low-energy orbital of relatively localised Si–Si antibonding character which gives rise to a characteristic low-lying "σ^*_{Si-Si}" resonance in the Si 1s, 2s and 2p core excitation spectra. If the σ^*_{Si-Si} feature is very localised, its intensity should be proportional to the number of Si–Si bonds present in a molecule, and thus one could use the intensity of the core →σ^*_{Si-Si} resonance to provide semiquantitative infor-

Table 6
Energies, term values, and proposed assignments for features in the C 1s EEL spectra of tetramethylsilane (1), hexamethyldisilane (2), tetrakis(trimethylsilyl)silane (4) and dodecamethylcyclohexasilane (5)

$SiMe_4$ (1)		$Me_3SiSiMe_3$ (2)		$Si(SiMe_3)_4$ (4)		c-Si_6Me_{12} (5)		Assignment
E (eV)	T	E (eV)	T	E (eV)	T	E (eV)	T	
286.1(sh)	3.7	286(sh)	3.7	286(sh)	3.7	286	3.7	3s
287.4	2.5	287.31 [a]	2.4	287.37 [a]	2.3	287.19 [a]	2.5	σ^*_{C-H}, σ^*_{Si-C}
289.78 [b]		289.7 [b]		289.7 [b]		289.7 [b]		IP
289.8	0	290	−0.3	289.5	0.2	289.2	0.5	σ^*_{Si-C}
				294	−4	295	−5	exafs, 2e−(?)
				303	−13	300	−10	exafs

[a] Calibration relative to C 1s→π^* in CO_2 (290.74 eV) [39]: ΔE = −3.40(3), −3.43(5), −3.37(3) and −3.55(4) eV for (1), (2), (4), and (5), respectively.
[b] IP estimated from $Si(Me)_4$ (289.78) [30].

Table 7
Oscillator strengths of the Si 2p → σ^*_{Si-Si} transition of (2), (4), and (5) and the Si 1s → σ^*_{Si-Si} transition of (2), (3), (4), and (5)

Species	No. of Si–Si bonds	No. of transitions	Si 2p		Si 1s	
			$f(\times 10^{-2})$ [a]	$f(\sigma^*_{Si-Si})$/trans.	$f(\times 10^{-2})$ [a]	$f(\sigma^*_{Si-Si})$/trans.
(2) $Me_3SiSiMe_3$	1	2	6.8(6) [b]	3.4(3)	0.62(6)	0.31(5)
(3) $HSi(SiMe_3)_3$	3	6	–	–	1.12(15)	0.18(3)
(4) $Si(SiMe_3)_4$	4	8	39(2)	4.8(4)	1.7(2)	0.21(3)
(5) c-Si_6Me_{12}	6	12	36(3)	3.0(2)	3.6(3)	0.30(3)

[a] Area of the Si–Si signal in the TOTAL oscillator strength spectrum (per atom oscillator strength × number of Si atoms), as determined by a non-linear least squares fit to Gaussian line shapes. For (5) the areas of the two lowest energy features (both assigned to σ^*_{Si-Si}) are included.
[b] Errors were estimated from the variability of fits starting from different initial parameters.

mation about the structure of unknown molecules. Our data has been used to test this concept. Table 7 lists the intensity of the Si 2p → σ^*_{Si-Si} and Si 1s → σ^*_{Si-Si} features, obtained from fits of Gaussian lines to the energy loss and photoabsorption spectra. The intensity per Si core edge → σ^* transition is then evaluated by dividing the total intensity by the sum of the number of Si*–Si contributors in each molecule (Si* is the core excited atom). For Si 2p excitation, the per transition oscillator strength is relatively similar (within 25%) for all three species. We note that the value for (5) includes both the 101.8 and 103.2 eV features which are considered to have a large Si–Si character. For Si 1s excitation, the per transition oscillator strength is similar for all species. As for the Si 2p value, the per transition oscillator strength for (5) may be somewhat overestimated since it includes the intensity of both discrete spectral features which we have attributed to states of large Si–Si character. We conclude that the peak intensity per transition of the characteristic low-lying Si–Si resonance signal is similar in all species (±20%), even though the variation in spectral shape suggests that the extent of localisation varies with the molecular structure.

Compound (2) has been identified previously as a potential candidate to display the weak bond effect [31]. Molecules with weak (M–M) bonds are expected to have σ^*_{M-M} resonances at lower energy than the Rydberg transitions [5]. Since the Rydberg and valence transitions overlap in (2) and the other organosilanes of this study, they are not the archetypical "weak bond" molecules. A simplistic interpretation of the "weak bond" model would suggest σ^*_{C-C} resonances in alkanes and σ^*_{Si-Si} resonances in silanes might occur at similar term values since the Si–Si and C–C (alkane) bond strengths are quite similar [32–34]. In fact the characteristic σ^*_{Si-Si} resonances occur at term values of −3.5 eV, about 5 eV below the position of σ^*_{C-C} resonances in alkanes which occur around +2 eV. As concluded in the initial presentation [5], the "weak bond" model is not globally applicable and simple comparisons of second and third row elements are not generally valid. Basically the relative term values are dictated as much by the energetics and orbital mixing characteristics of the constituent atomic orbitals as by the bond length/strength.

In their study of the valence and core excitation spectra poly(di-*n*-hexylsilane), McCrary et al. [6] argued that the lowest energy $\sigma \rightarrow \sigma^*$ valence shell transition was aligned along the Si–Si backbone but extensively delocalised, consistent with the theoretical results of Bigelow on short-chain polysilanes [35]. In contrast the lowest energy Si 1s → σ^*_{Si-Si} transition at 1843 eV was interpreted as a highly localised state on account of the influence of the localised Si 1s core hole. Based on their relative Si 2p and Si 1s spectral shapes, the strongly localised picture may be appropriate for linear poly(Si–Si) systems but it is less suitable for cyclic species. This point has been deduced in previous comparative studies of linear and cyclic polysilanes [2].

We disagree with the interpretation of the Si 2p spectra of polysilanes given by Kubiak et al. [7], in particular their conclusion that σ^*_{Si-C} lies below σ^*_{Si-Si}. This was reached by comparison of experimental spectra with the results of small basis set calculations on the ground states of a few model species. The fact that the core hole was not explicitly considered may be a factor, although most other theoretical treatments of the ground state electronic structure of oligomeric or polymeric $(SiR_2)_n$ chains indicate the lowest energy orbital/band has large σ^*_{Si-Si} character [12,36].

The present results indicate that the lowest core excited state in species with Si–Si bonds has a large σ^*_{Si-Si} character. Of course the density of the excited electron in the core excited state will be distributed over many parts of the molecule. In addition much of the localised character of the upper level may be associated with core hole relaxation. Quantum calculations for a number of molecules have indicated that the core hole can convert a delocalised ground state orbital into a highly localised orbital in the core excited state [37]. Even so, the spectral trend is observed for a range of Si–Si containing species so that there is reason to believe the presence of a low-lying feature at ~ 102 eV in Si 2p and ~ 1840 eV in Si 1s may be taken as evidence of the presence of Si–Si bonds in a sample of unknown structure.

Certainly this concept has its limitations and needs to be used with caution, since there are other Si–X structures which undoubtedly give rise to features at similar energies. However, core excitation to a low-lying Si–Si resonance is a simple, chemically attractive concept which might be useful in analytical applications. This type of generalisation is very similar to the concept of group frequencies in vibrational spectroscopy. In any low symmetry molecule the normal modes of vibration involve motion of many atoms. However, there is a general and useful consensus that signals seen at particular energies in the IR or Raman spectra can be "more-or-less" associated with specific functional groups or bonds. A strict normal-mode analysis is inconsistent with this oversimplification but that has not stopped chemists from finding the "group frequency" concept extremely useful in practical analysis. The observation reported in this paper is one step in developing "working concepts" in the core spectroscopy of Si compounds.

5. Summary

The Si 2p, Si 2s and C 1s spectra of tetramethylsilane (1), hexamethyldisilane (2), tetrakis(trimethylsilyl)silane (4) and dodecamethylcyclohexasilane (5) have been recorded by EELS and the Si 2p and Si 1s spectra of tetramethylsilane (1), hexamethyldisilane (2), tris(trimethylsilyl)silane (3), tetrakis(trimethylsilyl)silane (4) and dodecamethylcyclohexasilane (5) have been recorded by synchroton radiation photoabsorption spectroscopy. While there are visible differences between the photoabsorption and EEL spectra, essentially all of these are associated with the difference in energy resolution. Based on chemical systematics the lowest energy feature in the Si 2p, Si 2s and Si 1s spectra of molecules containing Si–Si bonds has been assigned to core excitation to an orbital of dominant Si–Si antibonding character.

Acknowledgement

This research has been sponsored financially by the Ontario Centre for Materials Research and NSERC (Canada). We thank Cássia Turci for assistance with recording the spectrum of (1). This work is based in part on research conducted at the Synchrotron Radiation Center, Univ. of Wisconsin-Madison, which is supported by the NSF under award DMR-9212658. We thank the staff of SRC for their expert operation of Aladdin, as well as CSRF and Drs. X.H. Feng and K.H. Tan for their support of the beam lines.

References

[1] C.G. Pitt, M.M. Bursey and P.F. Rogerson, J. Am. Chem. Soc. 92 (1970) 519;
F.M. Schellenberg, R.L. Byer, R.H. French and R.D. Miller, Phys. Rev. B 43 (1991) 1008.
[2] R. West and E. Carberry, Science 189 (1975) 179.
[3] R.D. Miller and J. Michl, Chem. Rev. 89 (1989) 1359.
[4] H. Bock and W. Ensslin, Angew. Chem. Intern. Ed. Engl. 10 (1971) 404.
[5] R. McClaren, I. Ishii, A.P. Hitchcock and M.B. Robin, J. Chem. Phys. 87 (1987) 4344.
[6] V.R. McCray, F. Sette, C.T. Chen, A.J. Lovinger, M.B. Robin, J. Stöhr and J.M. Zeigler, J. Chem. Phys. 88 (1988) 5925.
[7] G.D. Kubiak, D.A. Outka, C.M. Rohlfing, J.M. Zieler, D.L. Windt and W.K. Waskiewicz, J. Vacuum Sci. Technol. B 8 (1990) 1643.
[8] A.P. Hitchcock and D.C. Mancini, J. Electron Spectry. 67 (1994) 1.
[9] V.I. Baranovskii, M.S. Nakhmanson and Yu.M. Zaitsev, Zh. Strukt. Khim. 13 (1972) 848.
[10] J.D. Bozek, G.M. Bancroft and K.H. Tan, Chem. Phys. 145 (1990) 131.
[11] S. Nagaoka, J. Ohshita, M. Ishikawa, T. Masuoka and I. Koyano, J. Phys. Chem. 97 (1993) 1488.
[12] J.Z. Xiong, D.T. Jiang, Z.F. Liu, K.M. Baines, T.K. Sham, S.G. Urquhart, A.T. Wen and A.P. Hitchcock, in preparation.

[13] M. Simon, T. Lebrun, R. Martins, G.G.B. de Souza, I. Nenner, M. Lavollee and P. Morin, J. Phys. Chem. 97 (1993) 5228.
[14] J.A. Tossell, D.C. Winkler and J.H. Moore, Chem. Phys. 185 (1994) 297.
[15] A.P. Hitchcock, T. Tyliszczak, P. Aebi, J.Z. Xiong, T.K. Sham, K.M. Baines, K.A. Mueller, X.H. Feng, B.X. Yang, Z.H. Lu, J.M. Baribeau and T.E. Jackman, Surface Sci. 291 (1993) 349.
[16] F. Sette, J. Stöhr and A.P. Hitchcock, Chem. Phys. Letters 110 (1984) 517; J. Chem. Phys. 81 (1984) 4096.
[17] A.P. Hitchcock and M. Tronc, Chem. Phys. 121 (1988) 265.
[18] C. Dezarnaud, M. Tronc and A.P. Hitchcock, Chem. Phys. 142 (1990) 455;
C. Dezarnaud, M. Tronc and A. Modelli, Chem. Phys. 156 (1991) 129.
[19] A.P. Hitchcock, S.G. Urquhart and E.G. Rightor, J. Phys. Chem. 96 (1992) 8736.
[20] J. Stöhr, Springer series in surface science, Vol. 25. NEXAFS spectroscopy (Springer, Berlin, 1992).
[21] A.P. Hitchcock, Physica Scripta T31 (1990) 159.
[22] G. Cooper, T. Ibuki and C.E. Brion, Chem. Phys. 140 (1990) 133.
[23] K.H. Tan, G.M. Bancroft, L.L. Coatsworth and B.W. Yates, Can. J. Phys. 60 (1982) 131.
[24] D.G.J. Sutherland, G.M. Bancroft and K.H. Tan, J. Chem. Phys. 97 (1992) 7918.
[25] D.G.J. Sutherland, M. Kasrai, G.M. Bancroft, Z.F. Liu and K.H. Tan, Phys. Rev. B. 48 (1993) 14989.
[26] E.O. Filatova, A.S. Vinogradov and T.M. Zimkina, Soviet Phys. Solid State 27 (1985) 606.
[27] M. Inokuti, Rev. Mod. Phys. 43 (1971) 297.
[28] M.B. Robin, Higher excited states of polyatomic molecules, Vols. 1–3 (Academic Press, New York, 1974, 1975, 1985).
[29] D.G.J. Sutherland, G.M. Bancroft, J.D. Bozek and K.H. Tan, Chem. Phys. Letters 199 (1992) 341.
[30] W.L. Jolly, K.D. Bomben and C.J. Eyermann, At. Data Nucl. Data Tables 31 (1984) 109.
[31] A.T. Wen, Ph.D. Thesis, McMaster University (1992).
[32] J.M. Gaidis, P.R. Briggs and T.W. Shannon, J. Phys. Chem. 75 (1971) 974.
[33] R. Walsh, Thermochemistry, in: The chemistry of organic silicon compounds, eds. S. Patai and Z. Rappoport (1989).
[34] R. Walsh, Accounts Chem. Res. 14 (1981) 246.
[35] R.W. Bigelow, Organometallics 5 (1986) 1502; Chem. Phys. Letters 126 (1986) 63.
[36] K. Takeda, H. Teramae and N. Matsumoto, J. Am. Chem. Soc. 108 (1986) 8186.
[37] A.T. Wen, E. Rühl and A.P. Hitchcock, Organometallics 11 (1992) 2559.
[38] R.N.S. Sodhi and C.E. Brion, J. Electron Spectry. 34 (1984) 363.
[39] D. Li, G.M. Bancroft, M. Kasrai, M.E. Fleet, X.H. Feng, K.H. Tan and B.X. Yang, Solid State Commun. 87 (1993) 613.
[40] R.N.S. Sodhi, S. Davel, C.E. Brion and G.G.B. de Souza, J. Electron Spectry. 35 (1985) 45.
[41] H.H. Gilman and C.L. Smith, J. Organomet. Chem. 14 (1968) 91.
[42] H.H. Gilman and C.L. Smith, J. Organomet. Chem. 8 (1967) 245.
[43] R. West, L. Brough and W. Wojnowski, Inorg. Synth. 19 (1979) 265.

CHAPTER 5D

Core Excitation Spectroscopy of Phenyl and Methyl-substituted Silanol, Disiloxane and Disilane Compounds: Evidence for Delocalization Across the Si-C_{phenyl} Bond

The following work documents the Si 1s, Si 2p, Si 2s, C 1s and N 1s core excitation spectra of a series of methyl and phenyl-substituted silanol, disiloxane and disilane compounds, and employs Extended Hückel and *ab initio* calculations to aid interpretation of the spectra. This work has been published in the journal Organometallics (*Organometallics*. **16**, 2080, 1997) and is presented here in published form. The right to reprint this article was retained by the author and authorization has been obtained from the coauthors.

The author of this thesis performed the experimental work and Extended Hückel calculations in cooperation with C. C Turci, performed the *ab initio* calculations and was a major contributor in the writing of this paper, in collaboration with Prof. C. C. Turci, Prof. A. P. Hitchcock and Prof. M. A. Brook.

Organometallics 1997, *16*, 2080–2088

Core Excitation Spectroscopy of Phenyl- and Methyl-Substituted Silanol, Disiloxane, and Disilane Compounds: Evidence for π-Delocalization across the Si–C_{phenyl} Bond

Stephen G. Urquhart,[†] Cássia C. Turci,[†,‡] Tolek Tyliszczak,[†] Michael A. Brook,[†] and Adam P. Hitchcock*,[†]

Department of Chemistry, McMaster University, Hamilton, Ontario, Canada L8S 4M1, and Instituto de Química, Universidade Federal do Rio de Janeiro, Rio de Janeiro, Brazil 21910-900

Received December 6, 1996[⊗]

The Si 1s and 2p solid state photoabsorption (total electron yield) spectra of triphenylsilanol, hexaphenyldisiloxane, and hexaphenyldisilane and the Si 1s spectra (total ion yield) of gaseous trimethylsilanol, hexamethyldisiloxane, hexamethyldisilane, and trimethylmethoxysilane have been recorded using synchrotron radiation. These spectra are compared to inner shell electron energy loss spectra of gaseous triphenylsilanol, hexaphenyldisilane, trimethylmethoxysilane, hexamethyldisiloxane, and hexamethyldisilane in the Si 2p and C 1s regions, measured under scattering conditions where electric dipole transitions dominate (2.5 keV residual energy, $\theta \leq 2°$). Comparison of the Si 1s and Si 2p spectra of the $Ph_3Si–X$ and $Me_3Si–X$ species shows there are low-lying transitions at Si which occur exclusively in the $Ph_3Si–X$ species. These transitions are attributed to (Si $1s^{-1},\pi^*_{Si-Ph}$) and (Si $2p^{-1},\pi^*_{Si-Ph}$) states in which the core excited electron is delocalized across the Si–C(phenyl) bond into the π^* levels of the phenyl ring. Extended Hückel and *ab initio* molecular orbital calculations of the core excitation spectra support this interpretation. Transitions characteristic of Si–Si and Si–O bonds are also identified.

1. Introduction

During the past five decades, the unique properties and industrial potential of organosilicon compounds, including silicone polymers, elastomers, and resins, have been recognized and these materials have become major industrial products.[1–3] Silicones have desirable thermal and oxidative stability, flexibility, inertness and radiation resistance. Polymethylphenylsilicones and polydiphenylsilicones, in particular, are more stable to oxidation, high temperature decomposition, and radiation damage than methylsilicones,[4] with the rupture of methyl groups occurring preferentially over phenyl groups at high temperatures.[5] Aromatic stabilization by the phenyl group has been postulated as the origin of this increased stability.[4,6] This work continues our study of the sensitivity of core excitation spectroscopy to chemical properties and bonding in organosilanes. We examine the effects of π^* and σ^* delocalization associated with Si–phenyl (Si–Ph), Si–Si, and Si–O bonding, focusing in particular on the nature of π^* delocalization across the Si–phenyl bond.

A study of the electronic spectroscopy of organosilanes must be considered in the context of organosilane bonding models. In Si–Ph and Si–O containing species, hyperconjugation and (d–p)π bonding[7] models have been invoked to explain spectral and physical characteristics. In the hyperconjugation model, phenyl 2pπ electrons (or the oxygen lone pair electrons in the case of Si–O bonding) are delocalized into vacant σ^* levels on silicon. In the (d–p)π bonding model, the 2pπ electrons are delocalized into unoccupied Si 3d orbitals[7] although recent studies are critical of the (d–p)π bonding model for silicon.[8] While the large Si–O–Si bond angles and bond flexibility in oxo-bridged organosilanes have been rationalized in terms of hyperconjugation and (d–p)π bonding, it has also been argued that the dominant ionic character of the Si–O bond, and the resulting weak localization of electron pair domains on oxygen, is the origin of this effect.[9,10] Through comparison of the core excitation spectra, we have explored the covalent versus ionic character of Si–O bonding.

Core excitation spectroscopy is a site-specific spectroscopic technique offering detailed information concerning the unoccupied electronic structure of molecules or extended systems. Core excitation can be studied by

[†] McMaster University.
[‡] Universidad de Federal do Rio de Janeiro.
[⊗] Abstract published in *Advance ACS Abstracts*, April 15, 1997.

(1) Greenwood, N. N; Earnshaw, A. *Chemistry of the Elements*; Pergamon Press: Cambridge, 1984.
(2) *The Chemistry of Organic Silicon Compounds*; Patai S., Rappoport, Z., Eds.; Wiley: New York, 1989.
(3) Walsh, R. Thermochemistry. In *The Chemistry of Organic Silicon Compounds*; Patai, S., Rappoport, Z., Eds.; Wiley: New York, 1989.
(4) Noll, W. *Chemistry and Technology of Silicones*; Academic Press: New York, 1968. Kennan, J. J. In *Siloxane Polymers*; Clarson, S. J., Semlyen, J. A., Eds.; PTR Prentice Hall: Englewood Cliffs, NJ, 1993; Chapter 2, pp 72–134.
(5) Murphy, C. M.; Saunders, C. E.; Smith, D. C. *Ind. Eng. Chem.* 1950, *42*, 2462.
(6) Miller, A. A. *I&EC Prod. Res. Dev.* 1964, *3*, 1964.
(7) Kwart, H.; King, K. G. *d-Orbitals in the Chemistry of Silicon, Phosphorus and Sulfur*; Springer: Berlin, 1977. Reed, A. E.; von Ragué Schleyer, P. *J. Am. Chem. Soc.* 1990, *112*, 1434.
(8) Shambayati, S.; Blake, J. F.; Wierschke, S. G.; Jorgensen, W. L.; Schreiber, S. L. *J. Am. Chem. Soc.* 1990, *112*, 697.
(9) Bader, R. F. W. *Atoms in Molecules: A Quantum Theory*; Oxford: New York, 1990.
(10) Gillespie, R. J.; Johnson, S. A. *Inorg. Chem.*, submitted for publication.

S0276-7333(96)01028-X CCC: $14.00

X-ray photoabsorption[11] or electron energy loss spectroscopy.[12] A bibliography and data base of gas phase core excitation studies has been published recently.[13] Several recent studies[14-18] have investigated the relationship between Si and ligand near edge spectral features and the local structure around Si in organosilicon compounds. In some cases, these studies have combined synchrotron radiation and electron energy loss results of the same species in the solid and/or gas phase (where volatility permits) with quantum chemical calculations.[17,18] The combination of multiple edge spectra with calculations makes core excitation spectroscopy a powerful probe of the molecular electronic structure.

In this work, we have used core excitation spectroscopy to study delocalization across the Si−phenyl bond and oxygen lone pair delocalization in Me_3SiO-X and Ph_3SiO-X species. We have also extended our earlier studies of low-lying σ^*_{Si-Si} features in disilanes (Si−Si).[16,17] In particular, we present inner shell electron energy loss spectra (ISEELS) in the Si 2p and C 1s region of *gas* phase triphenylsilanol (Ph_3SiOH), hexaphenyldisilane ($Ph_3SiSiPh_3$), hexamethyldisiloxane ($Me_3SiOSiMe_3$), hexamethyldisilane ($Me_3SiSiMe_3$), and trimethylmethoxysilane (Me_3SiOMe), recorded under experimental conditions dominated by electric dipole transitions. We also present total electron yield (TEY) spectra in the Si 1s and Si 2p region of *solid* phase triphenylsilanol (Ph_3SiOH), hexaphenyldisiloxane ($Ph_3SiOSiPh_3$), and hexaphenyldisilane ($Ph_3SiSiPh_3$), as well as total ion yield (TIY) spectra in the Si 1s region of *gas* phase trimethylsilanol (Me_3SiOH), hexamethyldisiloxane ($Me_3SiOSiMe_3$), trimethylmethoxysilane (Me_3SiOMe), and hexamethyldisilane ($Me_3SiSiMe_3$). Comparison of the spectra for the methyl- and phenyl-series has identified features related to Si−C, Si−Si, or Si−O bonds in a given compound and identified delocalization of phenyl π^* density across the Si−C(Ph) bond in Ph_3Si-X molecules.

2. Experimental Section

2.1. Samples. Triphenylsilanol (Ph_3SiOH), trimethylmethoxysilane (Me_3SiOMe), and hexamethyldisiloxane ($Me_3SiOSiMe_3$) (purchased from Aldrich, ≥98% purity), hexaphenyldisilane ($Ph_3SiSiPh_3$), hexamethyldisilane ($Me_3SiSiMe_3$), and hexaphenyldisiloxane ($Ph_3SiOSiPh_3$) (purchased from Hüls America, ≥98% purity) were used without further purification. Trimethylsilanol (Me_3SiOH) was prepared according to a literature method.[19] Spectra of trimethylsilanol were acquired within 6 h of synthesis, before any significant dimerization had occurred. All compounds were handled in a glovebag flushed with dry nitrogen in order to minimize hydrolysis. Liquid samples were loaded in dried glass vacuum flasks and were subjected to several freeze−pump−thaw cycles to remove dissolved gases. For Si 1s and 2p photoabsorption, the solid samples were mounted by pressing the sample powder into a copper surface that was previously pitted with strong nitric acid.

2.2. Electron Energy Loss Spectroscopy. The gas phase ISEELS spectrometer employed in these experiments has been described in detail previously.[12] The spectrometer is operated under conditions of small momentum transfer (2.5 keV impact energy, small (<2°) scattering angle) where the electronic excitations are dominated by electric-dipole-allowed transitions. The overall energy resolution, which is typically 0.6−0.7 eV full width at half maximum (fwhm), is determined by the convolution of the energy width of the unmonochromatized incident electron beam (~0.4 eV) and the analyzer acceptance (~0.4 eV).

The volatile samples (Me_3SiOH, $Me_3SiOSiMe_3$, Me_3SiOMe, $Me_3SiSiMe_3$) were introduced into the collision cell through a leak valve. The involatile Ph_3SiOH and $Ph_3SiSiPh_3$ samples were placed directly inside the spectrometer in a heatable glass tube attached to the collision cell. Spectra of Ph_3SiOH were obtained at a number of different heating conditions in order to confirm reproducibility and to check if sample heating might lead to thermal decomposition. The same procedure was not possible for $Ph_3SiSiPh_3$ due to the difficulty in maintaining an adequate sample pressure in the gas cell. For this reason, the ISEEL spectra of this compound are of lower statistical quality. The stability on heating was also checked for both compounds by electron impact mass spectrometry. The mass spectrum of Ph_3SiOH did not change until the sample was heated above 200 °C while that of $Ph_3SiSiPh_3$ was only observed to change when the temperature was above 550 °C.

The energy loss scale was established by simultaneously recording the spectrum of the sample with that of two reference compounds: CO_2, using the C 1s → π^* (290.74(4) eV) transition,[20,21] and SF_6, using the S $2p_{1/2} \rightarrow t_{2g}$ (184.54(5) eV) transition.[20] The signal associated with a particular core edge was isolated from the underlying valence shell and core ionization continua by subtracting a smooth curve determined from a curve fit of the function $a(E - b)^c$ to the pre-edge experimental signal. The C 1s background-subtracted spectra were converted to absolute oscillator strength scales by using a method described and tested previously.[13] The Si 2p background-subtracted spectra were converted to absolute oscillator strengths by normalizing to the absolute Si 2p oscillator strength of SiH_4 in the region of 145−151 eV.[22] This featureless, atomic-like region is higher in energy than the prominent Si 2p → ϵd transitions in the continuum and before the onset of the Si 2s edge.

2.3. Synchrotron Radiation Studies. 2.3.1. Si 1s Spectra. The Si 1s spectra of the solid Ph_3SiOH, $Ph_3SiOSiPh_3$, and $Ph_3SiSiPh_3$ samples were measured by total electron yield (TEY) detection, and the gas Me_3SiOH, $Me_3SiOSiMe_3$, Me_3SiOMe, and $Me_3SiSiMe_3$ samples were measured by total ion yield (TIY) detection, using the double-crystal monochromator[23] of the Canadian Synchrotron Radiation Facility (CSRF) located at the Synchrotron Radiation Center (SRC) in Wisconsin. This monochromator is equipped with InSb crystals and has an energy resolution of 0.8 eV at 1840 eV. The absolute energy scale was set by prior recording of the total electron yield spectrum of crystalline silicon (c-Si).

(11) Stöhr, J. *NEXAFS Spectroscopy*; Springer-Verlag: Berlin, 1992.
(12) Hitchcock, A. P. *Phys. Scr.* **1990**, *T31*, 159.
(13) Hitchcock, A. P.; Mancini, D. C. *J. Electron Spectrosc. Relat. Phenom.* **1994**, *67*, 1.
(14) Hitchcock, A. P.; Tyliszczak, T.; Aebi, P.; Xiong, J. Z.; Sham, T. K.; Baines, K. M.; Mueller, K. A.; Feng, X. H.; Chen, J. M.; Yang, B. X.; Lu, Z. H.; Baribeau, J. M.; Jackman, T. E. *Surface Sci.* **1993**, *291*, 350.
(15) Sutherland, D. G. J.; Kasrai, M.; Bancroft, G. M.; Liu, Z. F.; Tan, K. H. *Phys. Rev. B.* **1993**, *48*, 15089.
(16) Urquhart, S. G.; Xiong, J. Z.; Wen, A. T.; Sham, T. K.; Baines, K. M.; de Souza, G. G. B.; Hitchcock, A. P. *Chem. Phys.* **1994**, *189*, 757.
(17) Xiong, J. Z.; Jiang, D. T.; Liu, Z. F.; Baines, K. M.; Sham, T. K.; Urquhart, S. G.; Wen, A. T.; Tyliszczak, T.; Hitchcock, A. P. *Chem. Phys.* **1996**, *203*, 81.
(18) Urquhart, S. G.; Hitchcock, A. P.; Denk, M. *J. Am. Chem. Soc.*, submitted for publication.
(19) Sommer, L. H.; Pietrusza, E. W.; Whitmore, F. C. *J. Am. Chem. Soc.* **1946**, *68*, 2282.
(20) Sodhi, R. N. S.; Brion, C. E. *J. Electron Spectrosc. Relat. Phenom.* **1984**, *34*, 363.
(21) Brion, C. E.; Daviel, S.; Sodhi, R.; Hitchcock, A. P. *AIP Conf. Proc.* **1982**, *94*, 429.
(22) Cooper, G.; Ibuki, T.; Brion, C. E. *Chem. Phys.* **1990**, *140*, 147. Cooper, G.; Burton, G. R.; Chan, W. F.; Brion, C. E. *Chem. Phys.* **1995**, *196*, 293.
(23) Yang, B. X.; Middleton, F. H.; Olsson, B. G.; Bancroft, G. M.; Chen, J. M.; Sham, T. K.; Tan, K.; Wallace, D. J. *Nucl. Instrum. Methods* **1992**, *A316*, 422.; *Ibid. Rev. Sci. Instrum.* **1992**, *63*, 1355.

The inflection point of the absorption edge of c-Si (determined by the peak in the first derivative) was set to 1839.2 eV.[14,24]

The TEY spectra of the solid samples were obtained by measuring the sample current associated with all electrons emitted from the sample after the absorption of an X-ray photon (elastic, Auger, photoelectrons, and inelastically scattered electrons). The TIY spectra of gases were obtained by measuring the photoion current, using a 10 cm long parallel plate ionization chamber. The sample pressure was measured with a baratron gauge, and this signal was used to correct for (minor) pressure variations during acquisition. In addition, the gas phase spectra were scaled by $1/E$ to correct for the intrinsic bolometric effect of ionization current detection.[25] The incident photon flux (I_0) at the Si 1s edge was monitored using an inline gas ionization chamber equipped with thin Be windows. The I_0 signal was used to normalize the TEY and TIY spectra. Normalized and calibrated TEY and TIY spectra were background-subtracted to isolate the Si 1s core edge signal, and the results were converted to absolute oscillator strength intensity scale by normalization to the atomic value of 1.6×10^{-3} eV^{-1} at 1860 eV.[26]

2.3.2. Si 2p Spectra. The Si 2p spectra of the solid Ph_3SiOH, $Ph_3SiOSiPh_3$, and $Ph_3SiSiPh_3$ samples were measured by TEY detection using the Mark IV Grasshopper monochromator[27] of the Canadian Synchrotron Radiation Facility at SRC. For these experiments, the monochromator was run with 30 μm slits for an energy resolution of ~0.15 eV fwhm. The energy scale of this monochromator was calibrated by setting the energy of the first peak of the derivative of the Si 2p spectrum of c-Si to 99.804 eV. This value for the first inflection point in the Si 2p spectrum of c-Si is based on a careful calibration of its energy with respect to the Si $2p_{3/2} \rightarrow a_1^*$ transition of SiF_4.[28] The absolute energy scales are estimated to be accurate to within 0.1 eV in the region between 100 and 200 eV. For most of the pre-edge absorption features, the monochromator resolution is the limiting factor in determining the positions of the sharp discrete resonances. In the continuum regions, resonances are much broader and the estimated error in their position is 0.5 eV. The incident photon flux (I_0) was measured simultaneously using the photocurrent from a clean Ni mesh placed in the photon beam before the sample. The I_0 signal is used to normalize the TEY spectra. The spectra were background-subtracted and normalized to the Si 2p oscillator strength spectrum of SiH_4, as described in section 2.2.

2.4. Calculations. The core excitation spectra of phenylsilanes have been interpreted with the aid of extended Hückel molecular orbital (EHMO) as well as *ab initio* calculations of simple model molecules. EHMO calculations of the Si 1s spectra of Ph_3SiH and $PhSiH_3$ were carried out with the CACAO program[29] using the default Hückel parameters[30] calculated without d orbitals. Predictions of the Si 1s core excitation spectra were generated by EHMO calculations using the equivalent ionic core virtual orbital model (EICVOM),[31] with procedures described previously.[32,33] In this model, core hole relaxation is approximated by replacing the core excited atom by its "$Z + 1$" equivalent (e.g., silicon by phosphorus) and setting the molecular charge to +1.

Ab initio calculations of the Si 1s core excitation spectrum of $PhSiH_3$ and $PhSiMe_3$ were carried out with the program GSCF3.[34] This program treats core hole relaxation by explicit inclusion of the core hole.[35] The basis set used for this calculation is the extended basis set taken from (533/53) and (63/5) contracted Gaussian-type functions for Si and C and (5) for H of Huzinaga et al.,[36] where the contraction scheme was (311111111/31111/1*) for the core excited silicon, (621/41) for the carbon atoms, and (41) for H. The core excited states were obtained with the improved virtual orbital (IVO) method.[37] The relaxed Hartree–Fock (HF) potential is essential in accurately considering large electronic reorganization upon inner shell hole creation; therefore, the IVO method based on the relaxed HF potential is superior to the method using the ground state orbitals. This method has been shown to be quite accurate in predicting term values and intensities of core excitations.[38–40]

The program SPARTAN[41] was used to provide the geometry-optimized structures of Ph_3SiH, Ph_3SiH, and $PhSiMe_3$ at the *ab initio* HF/3-21G* level. These geometries were used for both the EHMO and *ab initio* core excitation calculations. Gaussian line widths used in generating the predicted spectra from both the EHMO and *ab initio* results were 4 eV fwhm for orbitals of eigenvalue (ϵ) above 3 eV 2 eV for $0 < \epsilon < 3$, and 0.6 eV for $-15 < \epsilon < 0$ eV. The energy scales of the EHMO-predicted spectra were set by matching the first calculated transition to the first experimental transition of Ph_3SiOH. Relative to aligning the zero of the Hückel eigenvalue scale to the *estimated* ionization potential (IP), alignment at the first experimental transition requires energy shifts of +3.0 eV for $PhSiH_3$ and Ph_3SiH. The energy scales of the *ab initio* calculated spectra were set by setting the zero of the term value scale to the ionization potentials calculated by GSCF3 (1843.11 eV for $PhSiH_3$; 1842.41 eV for $PhSiMe_3$).

3. Results and Discussion

3.1. Si 1s Spectra. Figure 1 presents the Si 1s oscillator strength spectra for three $Ph_3Si–X$ molecules (X = $SiPh_3$, $OSiPh_3$, and OH) and four $Me_3Si–X$ species (X = $SiMe_3$, $OSiMe_3$, OMe, and OH). Energies, term values, and tentative assignments for the Si 1s spectra are presented in Table 1. The energy scale for presenting the disilane spectra ($Me_3SiSiMe_3$ and $Ph_3SiSiPh_3$; top scale) is shifted by 1.3 eV relative to that for the triphenyl and trimethyl Si–O species ($Ph_3SiOSiPh_3$, Ph_3SiOH, $Me_3SiOSiMe_3$, Me_3SiOMe, and Me_3SiOH; bottom scale). This shift is introduced to account for the ~1 eV difference in the ionization potentials of the disilane (Si–Si)- and the Si–O-bonded species, since states of a similar final orbital character usually have similar core excitation term values (TV = IP − E).

The most dramatic difference in the Si 1s spectra is the dominant low-lying peak around 1842 eV in the spectrum of each $Ph_3Si–X$ species (X = OH, $OSiPh_3$, $SiPh_3$). We attribute this feature to Si 1s $\rightarrow \pi^*_{Si-Ph}$ excitations, where π^*_{Si-Ph} refers to an orbital involving

(24) McGrath, R.; McGovern, I. T.; Warburton, D. R.; Purdie, D.; Muryn, C. A.; Prakash, N. S.; Wincott, P. L.; Thornton, G.; Law, D. S. L.; Norman, D. *Phys. Rev. B* **1992**, *45*, 9327.
(25) Hitchcock, A. P.; Tronc, M. *Chem. Phys.* **1988**, *121*, 265.
(26) Henke, B. L.; Lee, P.; Tanaka, T. L.; Shimabukuro, R. L.; Fujikawa, B. K. *At. Data Nucl. Data Tables* **1982**, *27*, 1.
(27) Tan, K. H.; Bancroft, G. M.; Coatsworth, L. L.; Yates, B. W. *Can. J. Phys.* **1982**, *60*, 131.
(28) Bozek, J. D.; Bancroft, G. M.; Tan, K. H. *Chem. Phys.* **1990**, *145*, 131.
(29) Meali, C.; Proserpio, D. M. *J. Chem. Educ.* **1990**, *67*, 399.
(30) Howell, J.; Rossi, A.; Wallace, D.; Haraki, K.; Hoffmann, R. *FORTICON8 Program QCMP011 from Quantum Chemical Program Exchange*; Indiana University: Bloomington, IN, 1982.
(31) Schwarz, W. H. E. *Chem. Phys.* **1975**, *11*, 217.
(32) Francis, J. T.; Hitchcock, A. P. *J. Phys. Chem.* **1992**, *96*, 6598.
(33) Urquhart, S. G.; Hitchcock, A. P.; Priester, R. D.; Rightor, E. G. *J. Polym. Sci., Part B: Polym. Phys.* **1995**, *33*, 1603.
(34) Kosugi, N. *Theor. Chim. Acta* **1987**, *72*, 150.
(35) Kosugi, N.; Kuroda, H. *Chem. Phys. Lett.* **1980**, *74*, 500.
(36) Huzinaga, S.; Andzelm, J.; Klobukowski, M.; Radzio-Andzelm, E.; Sasaki, Y.; Tatewaki, H. *Gaussian Basis Sets for Molecular Calculations*; Elsevier: Amsterdam, 1984.
(37) Hunt, W. J.; Goddard, W. A., III *Chem. Phys. Lett.* **1969**, *3*, 414.
(38) Kosugi, N.; Shigemasa, E.; Yagishita, A. *Chem. Phys. Lett.* **1992**, *190*, 481.
(39) Kosugi, N.; Adachi, J.; Shigemasa, E.; Yagishita, A. *J. Chem. Phys.* **1992**, *97*, 8842.
(40) Iwata, S.; Kosugi, N.; Nomura, O. *Jpn. J. Appl. Phys.* **1978**, *17-S2*, 109.
(41) *Spartan*, version 4.0; Wavefunction Inc.: Irvine, CA, 1994.

Table 1. Energies, Term Values, and Proposed Assignments for Features in the Si 1s Photoabsorption Spectra of (A) Triphenylsilanol, Hexaphenyldisiloxane, and Hexaphenyldisilane and (B) Trimethylsilanol, Hexamethydisiloxane, Trimethylmethoxylsilane, and Hexamethyldisilane

A. Ph_3Si-X

Ph_3-SiOH[a]		$Ph_3Si-O-SiPh_3$[a]		$Ph_3Si-SiPh_3$[a]		
E (eV)	T	E (eV)	T	E (eV)	T	assignment
1841.8	5.1	1841.9	5.0	1840.8	4.9	$1\pi^*_{Si-Ph}$
				1842.7	3.0	σ^*_{Si-Si}
				1844.1	1.6	σ^*_{Si-C}, $2\pi^*_{Si-Ph}$
1844.8	2.1	1844.7	2.2			σ^*_{Si-C}, σ^*_{Si-O}, $2\pi^*_{Si-Ph}$
1846.9[b]		1846.9[b]		1845.7[b]		IP
		1849.4	−2.5			$2e^-$
1852.9	−6.0	1852.7	−5.8	1850.1	−4.4	$1\sigma^*_{C-C}$
1863	−16	1862	−15	1862	−16	$2\sigma^*_{C-C}$, EXAFS

B. Me_3Si-X

Me_3-SiOH[a]		$Me_3Si-O-SiMe_3$[a]		$Me_3Si-OMe$[a]		$Me_3Si-SiMe_3$[a]		
E (eV)	T	E (eV)	T	E (eV)	T	E (eV)	T	assignment
						1841.5	4.2	σ^*_{Si-Si}
1843.6	3.3	1843.8	3.1	1843.7	3.2	1842.6	3.1	σ^*_{Si-C}
						1844.2	1.5	σ^*_{Si-C}
1844.6	2.3	1844.5	2.4	1844.5	2.4			σ^*_{Si-O}, σ^*_{Si-C}
1846.9[b]		1846.9[b]		1846.9[b]		1845.7[b]		IP
1849	−2.1	1848.6	−1.7	1847.7	−0.8	1849	−3.3	σ^*_{Si-C}
1856	−9	1856	−9	1856	−9	1855	−9	EXAFS

[a] Monochromator energy scale was set by previous recording of the Si 1s spectrum of crystalline Si (edge inflection set at 1839.2 eV).[14,24] [b] Si 1s IPs were estimated from the Si 2p IPs by assuming the Si 2p−Si 1s splitting is the same as the Si Kα X-ray energy (1740 eV).[49] IP of Me_3SiOH estimated from the IP of Me_3SiOMe.

mixing of Si atomic orbitals (AOs) and the π* orbitals of the phenyl ring. The absence of a feature at this energy in the Si 1s spectra of the corresponding Me_3Si-X species is support for our attribution of the ~1842 eV peak in the Ph_3Si-X species to Si 1s excitation to a π^*_{Si-Ph} level. Our detailed rationalization for this assignment is postponed to the following section. First, we will discuss the other Si 1s spectral features.

As expected from previous work on $Me_3SiSiMe_3$,[16,17] $Ph_3SiSiPh_3$ also exhibits a low-energy peak at 1842.7 eV. There is no counterpart in the spectra of any of the nondisilane species. This feature is attributed to S 1s → σ^*_{Si-Si} excitations, where σ^*_{Si-Si} is the LUMO, which has a large Si−Si antibonding character. The somewhat higher energy of this feature in $Ph_3SiSiPh_3$ is likely a consequence of the interaction of the low-lying σ^*_{Si-Si} and π^*_{Si-Ph} levels. An analogous effect, namely strong π(phenyl) and σ(Si−Si) mixing, has been reported in the valence photoelectron spectra of phenyl-substituted disilanes.[42]

The Si 1s spectra of the two Ph_3Si-X molecules (X = OH, $OSiPh_3$), which have an identical next-neighbor chemical environment of Si, are very similar. The Si 1s spectra of Me_3SiOH, Me_3SiOMe, and $Me_3SiOSiMe_3$ are also quite similar, but different from the spectra of the corresponding Ph_3Si-X species. The similarity of the pair (Ph_3Si-OH, $Ph_3Si-O-SiPh_3$) and the triplet (Me_3SiOH, $Me_3SiOSiMe_3$, Me_3SiOMe) indicates that Si 1s excitation is not greatly affected by the nature of the Y group in these $Me_3Si-O-Y$/$Ph_3Si-O-Y$ species. We were somewhat surprised by this observation because the Si−O bond strength differs by 10% among the molecules $Me_3Si-O-Y$, Y = H, Me, $SiMe_3$.[3] If this bond strength difference was caused by differences in a covalent bonding interaction, such as hyperconjugation, then we would expect to see changes in excitations involving σ^*_{Si-O} levels. However if Si−O bonding is predominantly (but not entirely) ionic as some have argued,[10] then there should be very little dependence of the Si 1s spectrum on the nature of the Y group. The absence of any spectral dependence on the nature of the Y group in either the $Me_3Si-O-Y$ or $Ph_3Si-O-Y$ series supports interpretations which stress large ionic contributions to the Si−O−Y bond.

At somewhat higher energy (~1845 eV), a strong, broad peak is seen in the two $Ph_3Si-O-Y$ species. A similar but less symmetric feature is seen in the corresponding $Me_3Si-O-Y$ species. We attribute these peaks to an overlap of excitations to orbitals of σ^*_{Si-O} and σ^*_{Si-C} character, with $2\pi^*_{Si-Ph}$ contribution in the Ph_3Si-X species (see section 3.2). In the hexaphenyldisilane species, the ~1845 eV feature is relatively weak, since it lacks the σ^*_{Si-O} contribution. At higher energy (>1850 eV), the Si 1s continua of all three Ph_3Si-X compounds are relatively similar, each exhibiting a two peak pattern which is remarkably similar to that found in the C 1s spectrum of benzene (at 294 and 300 eV in Figure 4). The Si 1s continua for the Me_3Si-X species are distinctly different. These observations suggest interpretation of the 1850 and 1862 eV peaks in the Ph_3Si-X species as Si 1s → $1\sigma^*_{C-C}$ and Si 1s → $2\sigma^*_{C-C}$ transitions, respectively. This is a rather surprising suggestion since one normally would expect poor spatial overlap. However, previous studies have found that delocalization often occurs simultaneously in both the π* and σ* manifolds.[32] Thus, the π^*_{Si-Ph} features at ~1842 and 1844.5 eV and these two continuum features ascribed to σ^*_{C-C} provide a consistent picture of extensive delocalization from the phenyl ring to the Si atom, which does not occur in the corresponding Me_3Si species. Note that this picture of extensive delocalization and mixing of Si and phenyl ring orbitals (both π* and σ*) is further supported by the Si 2p spectra (see section 3.3).

3.2. π Delocalization across the Si−C_{Phenyl} Bond. Figure 2 compares the experimental Si 1s spectrum of

(42) Pitt, C. G.; Bock, H. *J. Chem. Soc., Chem. Commun.* **1972**, 28.

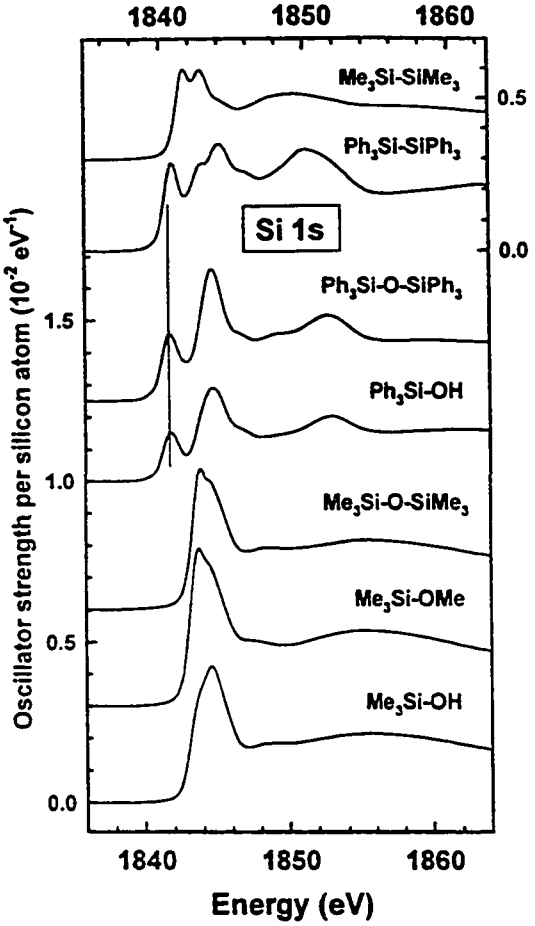

Figure 1. Oscillator strength spectra in the region of Si 1s excitation of hexaphenyldisilane (s), hexamethyldisilane (g), hexaphenyldisiloxane (s), triphenylsilanol (s), hexamethyldisiloxane (g), trimethylmethoxysilane (g), and trimethylsilanol (g). The solid state spectra were recorded with sample current detection, while the gas phase spectra were recorded using total ionization yield detection. The energy scales of the two disilane spectra (top scale) are shifted by 1.3 eV relative to the energy scales of the five triphenyl and trimethyl Si–O species (bottom scale) to account for the ionization potential difference between the disilane (Si–Si) and Si–O bonded species.

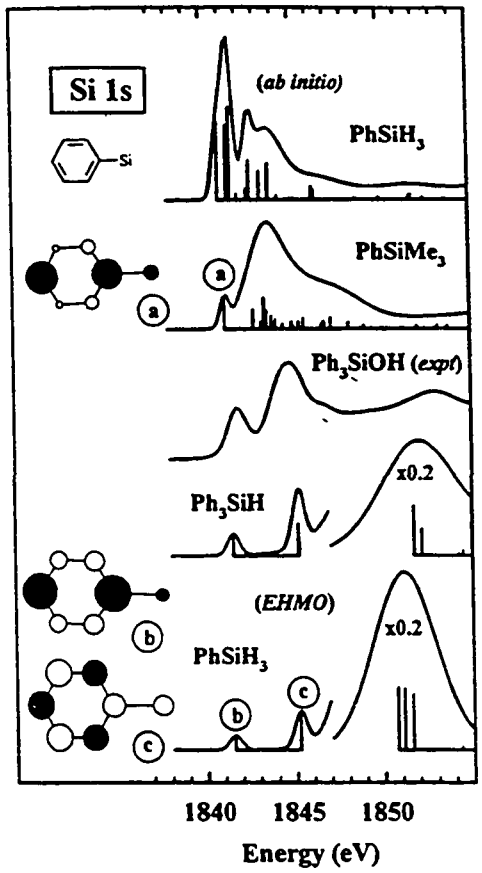

Figure 2. Comparison of the experimental Si 1s spectrum of Ph_3SiOH to the spectra of $PhSiH_3$ and Ph_3SiH, predicted by EHMO calculations carried out using the EICVOM ($Z + 1$) approach, and the spectra of $PhSiH_3$ and $PhSiMe_3$, predicted by *ab initio* calculations. See text for further details of the calculation and spectral generation. The MO sketches indicate the np_z contributions to selected low energy unoccupied molecular orbitals of core excited $PhSiMe_3$: (a) calculated by *ab initio* methods and $PhSiH_3$ (b,c) calculated by EHMO methods. The area of each circle is proportional to the C $2p-\pi$ or Si $3p-\pi$ density. For the EHMO MOs, the orbital contribution on silicon is multiplied by three for better visualization.

Ph_3SiOH to the EHMO-predicted Si 1s spectra of $PhSiH_3$ and Ph_3SiH and the *ab-initio*-predicted Si 1s spectra of $PhSiH_3$ and $PhSiMe_3$. The high-energy portion of the EHMO-calculated spectra are reduced in intensity by a factor of five in order to compensate for an artificially strong σ^*_{Si-H} contribution. The molecule $PhSiH_3$ was chosen as a simple model for examining Si 1s excitation in phenylsilanes. The EHMO spectrum of $PhSiH_3$ predicts two weak, low-energy Si 1s $\rightarrow \pi^*$ transitions. Sketches of the π-contribution to the molecular orbitals associated with the two low-lying features in $PhSiH_3$ (b,c) are used to examine the character of the core excited states. The area of each circle is proportional to the π-orbital density on the atom. Peak b corresponds to Si 1s excitation into the lowest unoccupied MO (LUMO) in $PhSiH_3$, an orbital in which the LUMO phenyl $1\pi^*$ level (e_{2u} in benzene) is delocalized onto Si; the second transition, peak c, involves a Si 1s state in which there is delocalization of the second lowest phenyl $2\pi^*$ level (b_{2g} in benzene) onto Si. In both cases, the orbital has π-overlap (in phase) between Si and the C–R carbon of the phenyl ring but it is clearly of π^* character on the phenyl group. We refer to such states as having π^*_{Si-Ph} character in view of the orbital character on the phenyl ring, even though this labeling is formally incorrect because there is no orbital node at the Si–Ph bond. The nature of this orbital suggests there may *not* be a corresponding occupied Si–C π-bonding molecular orbital (i.e., one involving an in-phase mix of a Si 3p orbital with a π orbital on the phenyl ring). On the basis of the position of the second peak in the EHMO spectrum, the feature at ~1844.5 eV in the Ph_3-

SiOH spectrum likely contains contributions from the Si 1s → $2\pi^*_{C-C}$ transitions.

The large difference in intensity between the EHMO-calculated and the experimental Si 1s → π^*_{Si-Ph} transition (relative to the higher energy Si 1s → σ^* features) led us to question the validity of the EHMO calculations in this context. One might rationalize the low Si 1s → π^*_{Si-Ph} intensity in terms of the single phenyl coordination in $PhSiH_3$, relative to the triphenyl coordination of Ph_3SiOH. This possibility was examined by comparing the EHMO calculation of the Si 1s spectrum of $PhSiH_3$ to that of Ph_3SiH. While the π^* features are slightly more intense in the triphenylsilane molecule (and the higher energy σ^*_{Si-H} features are diminished), the weakness of the π^* features remains.

In order to provide further confirmation of the identity and assignment of the EHMO π^* features, *ab initio* calculations were performed for $PhSiH_3$. These are also presented in Figure 2. Unlike the EHMO spectrum of $PhSiH_3$, there is no clearly separated π^* transition(s) at low energy, but rather many closely spaced transitions. Examination of the MO character of the calculated core excited states shows that the lowest feature is in fact the Si 1s → $1\pi^*$ transition and the next two intense features are of mixed σ^*_{Si-H}–Rydberg character. The presence of low-lying Si 1s → σ^*_{Si-H}–Rydberg transitions in $PhSiH_3$ is consistent with literature assignments of the Si 1s spectrum of silane.[43] In order to remove the "interference" associated with the Si–H bonds, we wanted to compare our experimental results with an *ab initio* calculation of the triphenyl species (Ph_3SiH; $C_{18}H_{16}Si$). However, this is presently beyond our computational resources at this level of theory. Instead, we have carried out an *ab initio* calculation for Si 1s excitation of $PhSiMe_3$. Replacement of the hydrogen atoms with methyl groups eliminates the strong Si 1s → σ^*_{Si-H}–Rydberg transitions. While $PhSiMe_3$ is substantially different from Ph_3SiOH, it allows visualization of the low-lying Si 1s → π^* feature(s) without interference from the (accurate) prediction of the Si 1s → σ^*_{Si-H} transitions. The calculated spectrum of $PhSiMe_3$ has a single low-energy feature at approximately the same energy as the feature we assign as Si 1s → π^*_{Si-Ph} in Ph_3SiOH. As shown in Figure 2 (sketch a), the π-$2p_z$ contribution to the lowest MO of $PhSiMe_3$ calculated by GSCF3 is very similar to that of the lowest π^* in the EHMO calculation of $PhSiH_3$. Detailed examination of the higher lying MOs reveals the Si 1s → π^* transition at ~1843 eV hiding in a forest of Si 1s → σ^*_{Si-C} transitions.

At first glance, the existence of a LUMO of π^*_{Si-Ph} character in Ph_3Si–X species is unusual because silicon is tetrahedrally coordinated in these species and, thus, one does not expect any formal Si–Ph π bonding. Si core → π^* features have been observed for several undercoordinated silicon species, including silylenes[18] with cyclic π delocalization, and SiO,[44] which has a formal Si=X π bond. The observation of π interactions with tetrahedral silicon is not necessarily surprising, as other experiments have shown phenomena which can be explained in a similar manner. For example, in *tert*-butyl- and trimethylsilyl-substituted polyacetylenes (Me_3X–$(CC)_n$–XMe_3, X = C, Si), a stabilization in the HOMO binding energy (acetylene π) is seen when carbon is replaced by silicon. This largely arises from the inductive effect of the silicon group.[45] However, the $\pi \rightarrow \pi^*$ transition of these systems shows a *decrease* in transition energy when carbon (*tert*-butyl) is replaced by silicon (trimethylsilyl).[45] This suggests that there must be a strong Si–phenyl π^* interaction that lowers the energy of the LUMO π^* level. However, π and π^*

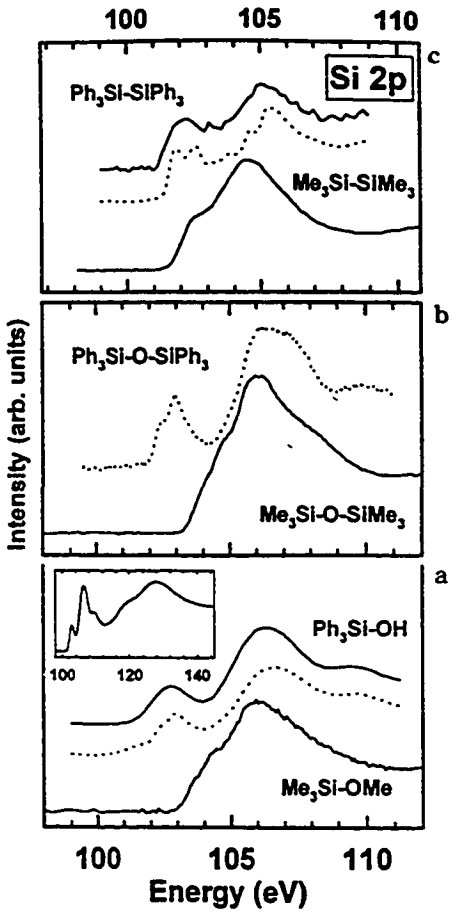

Figure 3. Si 2p gas phase energy loss spectra (solid line) and Si 2p solid state photoabsorption spectra (dotted line) of (a) triphenylsilanol (g,s) and trimethylmethoxysilane (g) (b) hexaphenyldisiloxane (s) and hexamethyldisiloxane (g) and (c) hexamethyldisilane (g) and hexaphenyldisilane (g,s). The energy scale of the upper panel (RSi–SiR) is shifted +1.2 eV relative to that of the lower two panels to take into account IP differences. A background generated by extrapolation of the pre-edge signal has been subtracted from each spectrum. The insert is the Si 2p gas phase EELS spectrum of triphenylsilanol acquired over a larger energy loss range. The energy loss spectra were recorded using a 2.5 keV final electron energy, ~2° scattering angle, and 0.7 eV fwhm resolution. A background generated by extrapolation of the pre-edge signal has been subtracted from each spectrum.

(43) Bodeur, S.; Millié, P.; Nenner, I. *Phys. Rev. A* **1990**, *41*, 252.
(44) Flank, A. M.; Karnatak, R. C.; Blancard, C.; Esteva, J. M.; Lagarde, P.; Connerade, J. P. *Z. Phys. D* **1991**, *21*, 357. Bouisset, E.; Esteva, J. M.; Karnatak, R. C.; Connerade, J. P.; Flank, A. M.; Lagarde, P. *J. Phys. B: At., Mol. Opt. Phys.* **1991**, *24*, 1609.

(45) Bock, H.; Seidl, H. *J. Chem. Soc. B* **1968**, 1158. Eastmond, R.; Johnson, T. R.; Walton, D. R. M. *Tetrahedron* **1972**, *28*, 4601.

Table 2. Energies, Term Values, and Proposed Assignments for Features in the Si 2p Photoabsorption Spectra of (A) Triphenylsilanol, Hexaphenyldisiloxane, and Hexaphenyldisilane and (B) Trimethylmethoxysilane, Hexamethyldisiloxane, and Hexamethyldisilane

(A) Ph_3Si-X (Gas, EELS; Solid, Total Electron Yield Photoabsorption)

Ph_3Si-OH				$Ph_3Si-O-SiPh_3$			$Ph_3Si-SiPh_3$				assignments	
E (eV)		solid		*E* (eV)	solid		*E* (eV)		solid			
gas	solid	$T_{3/2}$	$T_{1/2}$	solid	$T_{3/2}$	$T_{1/2}$	gas	solid	$T_{3/2}$	$T_{1/2}$	3/2	1/2
102.8[a]	102.3	4.3		102.4	4.2		102.2	101.7	3.7		π^*_{Si-Ph}	
	102.9		4.3	102.9		4.3		102.5		3.5		π^*_{Si-Ph}
								103.9	1.5		σ^*_{Si-Si}	
							104.3 (sh)	104.6	0.8		σ^*_{Si-C}	
							105.2	105.3		0.7		σ^*_{Si-C}
106.3	106.7(3)	0.2[b]		106.3	0.6[b]						σ^*_{Si-O}	
106.6[c]				106.6[c]			105.4[c]				IP ($2p_{3/2}$)	
107.2[c]				107.2[c]			106.0[c]					IP ($2p_{1/2}$)
109.5	109.7	−2.8[b]		109.8	−2.9[b]						σ^*_{Si-C}	
120		−13									Si 2p → ϵd	
127.6		−21									Si 2p → ϵd	

(B) Me_3Si-X (Gas, EELS)

$Me_3Si-OMe$		$Me_3Si-O-SiMe_3$		$Me_3Si-SiMe_3$		
E (eV)	*T*[b]	*E* (eV)	*T*[b]	*E* (eV)	*T*[b]	assignment
				102.6	3.1	σ^*_{Si-Si}
104.3	2.6	104.4	2.5	104.5	1.2	σ^*_{Si-C}
106.0[a]	0.9	105.9[a]	1.0			σ^*_{Si-O}
106.6[d]		106.6[d]		105.4[d]		IP($2p_{3/2}$)
107.2[d]		107.2[d]		106.0[d]		IP($2p_{1/2}$)
108	−1.1	108	−1.1			σ^*_{Si-C}, EXAFS
114	−7.1	114	−7.1	112	−6	Si 2p → ϵd
128	−21	128	−21	125	−19	Si 2p → ϵd

[a] Calibration: triphenylsilanol, −81.7 eV relative to (S $2p^{-1}$,t_{2g}) of SF_6; hexaphenyldisilane, as for photoabsorption spectrum; trimethylmethoxysilane, −78.5(1) eV relative to SF_6; hexamethyldisiloxane, −184.9(2) relative to π^* of CO_2; hexamethyldisilane, −186.28(8) relative to CO_2. [b] Where only a single term value is listed, this refers to the average Si 2p IP. [c] Vertical Si $2p_{3/2}$ IPs for Ph_3SiX species estimated from XPS measurements for Me_3SiOMe,[50] $Me_3SiOSiMe_3$,[51] and $Me_3SiSiMe_3$[50,51] (Me = methyl). Si $2p_{1/2}$ IPs are 0.61 eV higher.[50,52] [d] XPS.[50,51]

interactions are not expected in nonplanar molecules, and thus, it is appropriate to characterize these effects when they are observed. Core excitation spectroscopy is clearly useful in this context.

3.3. Si 2p Spectra. The Si 2p electron energy loss spectra (solid lines) of gas phase $Ph_3SiSiPh_3$, $Me_3SiSiMe_3$, $Me_3SiOSiMe_3$, Ph_3SiOH, and Me_3SiOMe are presented in Figure 3, in comparison to the Si 2p TEY photoabsorption spectra (dotted lines) of $Ph_3SiSiPh_3$, $Ph_3SiOSiPh_3$, and Ph_3Si-OH. The Si 2p spectrum of $Me_3SiSiMe_3$, recorded at medium resolution by ISEELS and high-resolution photoabsorption, has been reported and analyzed in detail elsewhere.[16,17] Energies, term values, and proposed assignments are presented in Table 2. The Si 2p spectrum of Me_3SiOMe is in good agreement with those reported earlier by Winkler et al.,[46] using ISEELS, and by Sutherland et al.,[15] using X-ray photoabsorption.

In the spectra of all three Ph_3Si-X species, there is a strong low-energy feature peaking around 102−103 eV, which is absent in the spectra of the three Me_3Si-X species. The same features are observed in the higher energy resolution photoabsorption spectra of the three Ph_3Si-X molecules, but with the characteristic 0.6 eV Si 2p spin−orbit splitting detected. We attribute the 102−103 eV peak in the Ph_3Si-X species to core → valence-type transitions where the upper orbital of the transition has significant π^*_{Si-Ph} character.

The spectra of the four molecules containing Si−O bonds exhibit an intense broad feature peaking around 106 eV. These are attributed to Si 2p → σ^*_{Si-O} excitations. At somewhat lower energy (~105 eV), there is a broad shoulder which we attribute to Si 2p → σ^*_{Si-C} transitions. We might expect a Si 2p → $2\pi^*_{Si-Ph}$ transition above the Si 2p → σ^*_{Si-O} transitions in the Ph_3Si-X species, in analogy to that observed in the Si 1s spectra. While a discrete transition is not resolved, the Si 2p → σ^*_{Si-O} transition in the Ph_3Si-X species is broader and is shifted to higher energy than the similar feature in the Me_3Si-X species. It is possible that the additional broadening is associated with a Si 2p → $2\pi^*_{Si-Ph}$ contribution.

In $Ph_3SiSiPh_3$, we expect to observe a Si 2p → σ^*_{Si-Si} transition, by analogy to its Si 1s spectrum and the observation of a Si 2p → σ^*_{Si-Si} transition in $Me_3SiSiMe_3$.[16,17] This transition is not resolved, but it is likely that it "fills in" the space between the π^*_{Si-Ph} feature (102 eV) and the σ^*_{Si-C} structure at 105 eV. Recently Gardelis et al.[54] have used S 2p spectral features at 102 and 106 eV, assigned to σ^*_{Si-Si} and σ^*_{Si-O} resonances, to characterize relative amounts of Si−Si and Si−O bonds in porous silicon samples.

The Si 2p spectra of all species exhibit further structure at higher energies (see the extended range energy loss spectrum of gas phase Ph_3SiOH in the insert to Figure 3). In addition to the features discussed above, there are a number of broad features, such as those occurring at 109.5, 120, and 127.6 eV in Ph_3SiOH. These higher energy features are attributed to a combination of higher order σ^* excitations and to the intrinsic shape of the Si 2p ionization continuum,[15,46] which is characterized by a delayed onset of 2p core

(46) Winkler, D. C.; Moore, J. H.; Tossell, J. A. *Chem.Phys. Lett.* 1994, *222*, 1.

Table 3. Energies, Term Values, and Proposed Assignments for Features in the C 1s EELS Spectra of (A) Benzene, Triphenylsilanol, and Hexaphenyldisilane and (B) Trimethylmethoxylsilane, Hexamethydisiloxane, and Hexamethyldisilane

(A) Ph_3Si-X

C_6H_6[a]		Ph_3Si-OH		$Ph_3Si-SiPh_3$		
E (eV)	T	E (eV)	T	E (eV)	T	assignment[c]
285.3	5.0	285.1[d]	5.2	285.1[d]	5.2	$1\pi^*(e_{2u})$
287.2	3.1	287.6	2.7	287.3	3.0	3p
288.9	1.4	289.0	1.3	288.8	1.5	$2\pi^*(b_{2g})$
290.3[b]		290.3[e]		290.3[e]		IP
293.5	−3.2	293.4	−3.1	293.4	−3.1	$1\sigma^*(e_{1u})$
300	−10	301	−11			$2\sigma^*(e_{2g} + a_{2g})$

(B) Me_3Si-X

$Me_3Si-OMe$		$Me_3Si-O-SiMe_3$		$Me_3Si-SiMe_3$[f]		
E (eV)	T	E (eV)	T	E (eV)	T	assignment[c]
286.3	3.5	286.0	3.7	286 (sh)	3.7	3s
287.3[d]	2.5	287.3[d]	2.4	287.4[d]	2.3	3p/C–H
290.2	−0.4					σ^*_{C-O}, σ^*_{C-Si}
		289.6	0.1	290	−0.3	σ^*_{C-Si}
289.8[e]		289.7[e]		289.7[e]		IP

[a] From ref 47. [b] From gas phase XPS, relative to vacuum level.[53] [c] Only the final orbital is listed. [d] Calibration relative to C 1s → π* in CO_2 (290.74 eV):[20,21] Ph_3Si-OH $E = -5.69(1)$ eV; $Ph_3Si-SiPh_3$ $E = -5.67(6)$; $Me_3Si-OMe$ $E = -3.39(4)$ eV; $Me_3Si-O-SiMe_3$ $E = -3.40(4)$ eV; $Me_3Si-SiMe_3$ $E = -3.43(5)$ eV. [e] IPs for Ph_3SiX species are estimated from C 1s IP of C_6H_6 (290.3 eV):[53] IPs for $Me_3SiSiMe_3$ and Me_3SiOMe estimated from C 1s IP of $Si(Me)_4$ (289.78 eV) and of $Me_3SiOSiMe_3$ (289.72 eV).[51] [f] Also reported in ref 16.

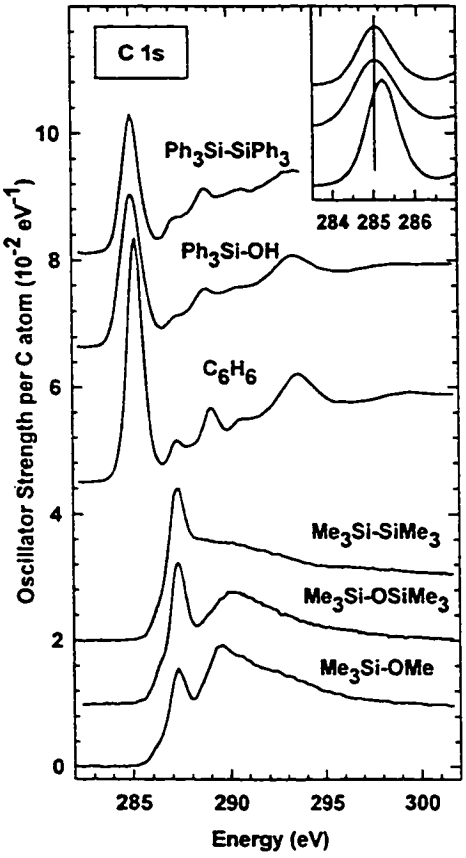

Figure 4. C 1s oscillator strength spectra of benzene,[47] triphenylsilanol, hexaphenyldisilane, trimethylmethoxysilane, hexamethyldisiloxane, and hexamethyldisilane[16] derived from dipole-regime EELS (see caption to Figure 3 for experimental details). The insert is an expanded presentation of the phenyl π* peak illustrating the changes in position and line shape between benzene and the phenylsilanes.

ionization caused by the angular momentum barrier in the dominant 2p → εd channel.

3.4. C 1s Spectra. Figure 4 compares the C 1s oscillator strength spectra derived from inner shell electron energy loss spectra of Ph_3SiOH, $Ph_3SiSiPh_3$, benzene,[47] Me_3SiOMe, $Me_3SiOSiMe_3$, and $Me_3SiSiMe_3$.[16] The energies, term values, and proposed assignments of the spectral features are presented in Table 3, along with the results for benzene from the literature.[47] Not surprisingly, the C 1s spectra of both phenylsilane species are essentially benzene-like, since the environment of most of the C atoms is approximately the same in all three molecules. The Si–Si bond in $Ph_3SiSiPh_3$ does not introduce any additional low-lying feature in the C 1s spectrum, in contrast to the situation in the Si core spectrum, suggesting that C 1s → LUMO (σ^*_{Si-Si}) excitation in this compound has negligible intensity. At first sight, the overall similarity of the C 1s spectra of the Ph_3SiX species to that of benzene appears inconsistent with our interpretation of the Si core level spectra as involving low-lying excitations to π^*_{Si-Ph} orbitals, since one might expect corresponding excitations in the C 1s spectra. However, the C–Si signal should only be 1/6 of the total C 1s signal, and thus, it will be overshadowed by that of the C–H carbons. There is little difference in electronegativity between the C–H and C–Si carbons, so there should not be any significant chemical shift of the C 1s energy. The greater breadth of the π^*_{C-C} (285 eV) transition and the shift of the centroid by 0.2 eV to lower energy may be the signature of π^*_{Si-Ph} contributions and delocalization across the Si–phenyl bond (see the insert to Figure 4). Higher energy resolution spectra would be of great interest as the $1\pi^*_{C-C}$ and π^*_{Si-Ph} features might be resolved.

The dominant lowest energy feature in the C 1s spectrum of each Ph_3SiX species corresponds to excitations to π* orbitals, which correlate with the $1\pi^*(e_{2u})$ orbital of benzene. The peaks at 287–288 eV are attributed to C 1s → Rydberg transitions. The feature

(47) Horsley, J. A.; Stöhr, J.; Hitchcock, A. P.; Newbury, D. C.; Johnson, A. L.; Sette, F. *J. Chem. Phys.* **1985**, *83*, 6099.

around 289 eV is assigned to one-electron C 1s $\rightarrow \pi^*$-(b_{2g}) transitions. Experimental and theoretical studies of benzene suggest this state is one in which the one-electron (C $1s^{-1}$, $\pi^*(b_{2g})$) configuration is heavily mixed with the (C $1s^{-1}$, π^{*-1}, π^{*2}) multielectron excited configuration.[48] Interestingly, the $2\pi^*$ (b_{2g} in benzene) feature for Ph_3Si-X is less prominent and apparently less intense than that for benzene. This may be a further manifestation of the Si–Ph delocalization. At higher energy, the C 1s continuum of Ph_3Si-OH exhibits a two peaked pattern very similar to that of benzene[47] and, thus, these features are attributed to C 1s $\rightarrow \sigma^*_{C-C}$ transitions.

The C 1s spectra of Me_3SiOMe, $Me_3SiOSiMe_3$, and $Me_3SiSiMe_3$ (Figure 4) are rather similar to the C 1s spectra of saturated hydrocarbons, such as ethane. The relatively sharp peak at 287 eV is attributed to excitation to a level of mixed valence–Rydberg character with σ^*_{C-H} valence and 3p Rydberg character. The shoulder around 286 eV is the 3s Rydberg level. The broad peak at 289.5–290 eV is mainly σ^*_{C-Si} in character. This C 1s $\rightarrow \sigma^*_{C-Si}$ feature is substantially stronger in $Me_3SiOSiMe_3$ than in $Me_3SiSiMe_3$, even though the next-neighbor environment of carbon is identical in both molecules. In Me_3SiOMe, this feature is stronger because it also contains the C 1s (MeO) $\rightarrow \sigma^*_{C-O}$ resonance.

4. Summary

Core excitation spectra at the Si 1s, Si 2p, and C 1s edges were recorded for a range of triphenylsilyl and trimethylsilyl species in the gas and/or solid state. There is excellent agreement between the gas and solid state spectra for the same edge of the same molecule, suggesting the spectra are dominated by valence-type excitations and that electronic interactions in the solid make little change to the molecular electronic structure in the region of the molecule sampled by core excitation. Assignments for all spectral features have been proposed. The Si 1s spectrum of each Ph_3Si-X species exhibits a low-lying feature (~1842 eV), which we interpret as Si 1s $\rightarrow 1\pi^*_{Si-Ph}$ transitions. This assignment is consistent with the absence of a π^* feature in the Si 1s spectra of all Me_3Si-X species and is supported by EHMO and *ab initio* calculations, both of which predict delocalization of phenyl π^* orbital density onto Si in Ph_3Si-X species. We note that both the low-level semi-empirical EHMO ($Z + 1$) calculation and the high-level *ab initio* calculation played important roles in developing our interpretation of these spectra. Calculations of large molecules are trivial with extended Hückel, but occasionally the results are not entirely convincing. While high-level *ab initio* calculations are limited to smaller molecules, their results are often more accurate. Simplified model systems can thus be examined by *ab initio* methods, but one must be careful that spectral features associated with inappropriate aspects of a simplified molecular model do not complicate the spectral interpretation, as was the case in the *ab initio* calculation for $PhSiH_3$.

Low-lying σ^*_{Si-Si} states are observed in the Si 1s and Si 2p spectra of $Ph_3Si-SiPh_3$ and $Me_3Si-SiMe_3$, further supporting the generality of a previously formulated hypothesis that molecules containing Si–Si bonds exhibit low-lying core excited states associated with excitations to an orbital with large σ^*_{Si-Si} character.[16,17] Comparison of the Si 1s spectra of $Ph_3Si-SiPh_3$ and $Me_3Si-SiMe_3$ indicates that the σ^*_{Si-Si} state in $Ph_3Si-SiPh_3$ is perturbed by interaction with the phenyl levels. Finally, silicon core excitation spectra are relatively unaffected by the nature of the Y group in $Ph_3Si-O-Y$ or $Me_3Si-O-Y$ compounds, indicating that the nature of the Y substituent does not affect the unoccupied electronic structure at Si. This result, which is rather surprising given the well-known dependence of Si–O bond strength on the nature of Y, may reflect an appreciable ionic character of the Si–O bond.

Acknowledgment. This work is based upon research conducted at the Chemistry Department, McMaster University and at the Synchrotron Radiation Center, University of Wisconsin–Madison. Mass spectra were recorded at the McMaster Regional Centre for Mass Spectrometry. We thank the staff of the SRC for their expert operation of Aladdin, which is supported by the NSF under award no. DMR-9212658. We also thank Professor West for the use of his laboratory in Madison for the Me_3SiOH synthesis. This work has been supported financially by NSERC (Canada). C.C.T. acknowledges CNPq (Brasil) for support of a fellowship, while S.G.U. acknowledges the support of an Ontario Graduate Fellowship.

OM961028F

(48) Schwarz, W. H. E.; Chang, T. C.; Seeger, U.; Hwang, K. H. *Chem. Phys.* **1987**, *117*, 73. Bader, M.; Haase, J.; Frank, K.-H.; Ocal, C.; Puschmann, A. *J. Phys. (Paris)* **1986**, *47*, C8-501. Ågren, H.; Vahtras, O.; Carravetta, V. *Chem. Phys.* **1995**, *196*, 47.

(49) Li, D.; Bancroft, G. M.; Kasrai, M.; Fleet, M. E.; Feng, X. H.; Tan, K. H.; Yang, B. X. *Solid State Commun.* **1993**, *87*, 613.

(50) Sutherland, D. G. J.; Bancroft, G. M.; Tan, K. H. *J. Chem. Phys.* **1992**, *97*, 7918.

(51) Jolly, W. L.; Bomben, K. D.; Eyermann, C. J. *At. Data Nucl. Data Tables* **1984**, *31*, 109.

(52) Kelfve, P.; Blomster, B.; Siegbahn, H.; Siegbahn, K.; Sanhueza, E.; Goscinski, O. *Phys. Scr.* **1980**, *21*, 75.

(53) Davis, D. W.; Shirley, D. A. *J. Electron Spectrosc. Relat. Phenom.* **1974**, *3*, 157.

(54) Gardelis, S.; Bangert, U.; Hamilton, B.; Pettifer, R. F.; Hill, D. A.; Keyse, R.; Teehan, D. *Appl. Surf. Sci.* **1996**, *102*, 408.

CHAPTER 6

CONCLUDING REMARKS

In this thesis, core excitation spectroscopy, performed using Inner Shell Electron Energy Loss Spectroscopy (ISEELS) and Near Edge X-ray Absorption Fine Structure (NEXAFS) has been applied to molecules that are structural analogues of polymers and to organosilane molecules. Molecular orbital calculations (extended Hückel and *ab initio*) were used to assist spectral interpretation and to examine structure-spectral relationships.

The core excitation spectra of molecules that are structural analogues of polymers has been demonstrated to be of great utility in modeling and interpreting the core excitation spectroscopy of polymers. Functional group "fingerprints", such as the $\pi^*_{C=O}$ feature in urea and carbamate linkages, the $\pi^*_{C=C}$ band in TDI and MDI polyurethanes, and the $\pi^*_{C=C}$ and $\pi^*_{C=O}$ bands in isomeric polyphthalate polymers have been identified. These fingerprints permit spectromicroscopic techniques, such as Scanning Transmission X-ray Microscopy (STXM) to chemically speciate microscopic polymer phases. The potential for multi-edge studies in polyureathane and polyphthalate polymers has been explored by molecular model investigations at the N 1s and O 1s core edges.

This thesis has examined the role of electronic delocalization in the application of molecular models to polymer spectral analysis. Through π-delocalization, unsaturated components introduce a non-local structure sensitivity to core excitation spectroscopy. While the spectroscopic probe is still "local", but the local electronic structure is perturbed by delocalization. This effect is illustrated by the structural isomerism sensitivity in the

core excitation spectroscopy of polyphthalates.

The molecular model - polymer study presented in this thesis is part of a rich collaboration between industrial and academic material scientists, spectroscopists and microscopists. The contribution of this thesis research to this collaboration has had a strong impact on the development of polymer STXM spectromicroscopy. For example, the spectral distinguishability of urea and carbamate linkages has been applied to the quantification of these linkages in polyurethane polymer samples [WP&97]. Strong collaborations such as this one function dynamically -the molecular model studies pushed the development of polymer spectromicroscopy and the high-resolution polymer spectral studies in turn pushed the interpretation of the molecular model spectra.

In the core excitation spectroscopy investigation of organosilane molecules, the ideas of functional group "fingerprinting" and π-delocalization have been extended to molecules that incorporate silicon. A bond specific $\sigma^*_{Si\text{-}Si}$ resonance was identified and characterized in molecules that contain Si-Si bonds, and the character of Si-O bonds was investigated in methylsilanes. π-delocalization has a significant role in determining the core excitation spectra of organosilanes. In a heterocyclic silylene, π-delocalization is observed, consistent with the role of cyclic delocalization in the stability of the silylene unit. In phenylsilanes, an unusual π-delocalization across a Si-phenyl bond is characterized.

APPENDIX 1

PROJECTS RELATED TO THIS THESIS

This appendix lists some of the research projects in which I have been involved other than that presented above in my thesis. This is organized into three sections: A.1) Published work; A.2) Progress reports or Major Projects and A.3) Short Term Projects.

A.1. Published Work

Articles Published, In-Press or Submitted to Peer-Reviewed Journals

12. S. G. Urquhart, C. C. Turci, T. Tyliszczak, M. A. Brook, A. P. Hitchcock, *Core Excitation Spectroscopy of phenyl- and methyl-substituted silanol, disiloxane and disilane compounds: Evidence for π-delocalization across the Si-C_{Phenyl} bond*, Organometallics 16, 2080-2088, 1997.

11. A. P. Hitchcock, S. G. Urquhart, A. T. Wen, A. L. D. Kilcoyne, T. Tyliszczak, E. Rühl, N. Kosugi, J. D. Bozek, J. T. Spencer, P. Dowben, *Inner-Shell Excitation Spectroscopy of closo-carboranes*, J. Phys. Chem. 101, 3483-3493, 1997.

10. S. G. Urquhart, A. P. Hitchcock, A. P. Smith, H. Ade, E. G. Rightor, *Inner-shell Excitation Spectroscopy of Polymer and Monomer Isomers of Dimethyl Phthalate*, J. Phys. Chem. B. **101**, 1997, 2267-2276.

9. E. G. Rightor, G. Mitchell, D. Fischer, A. P. Hitchcock, S. G. Urquhart, R. D. Leapman, A. P. Smith, H. Ade, H. J. Shin, T. Warwick, *Spectromicroscopy of*

Poly(ethylene terepthalate): Comparison of spectra and radiation damage rates in X-ray Absorption and Electron Energy Loss Spectroscopy, J. Phys. Chem. B. **101**, 1997, 1950-1960.

8. C. C. Turci, S. G. Urquhart, A. P. Hitchcock, *Inner Shell Energy Loss Spectroscopy of Aniline, Nitrobenzene and Nitroanilines*, Can. J. Chem. **74**, 1996, 851-869.

7. J. Z. Xiong, D. T. Jiang, Z. F. Liu, K. M. Baines, T. K. Sham, S. G. Urquhart, A. T. Wen, T. Tyliszczak, A. P. Hitchcock, *Si Core Level Excitation of Hexamethyldisilane Studied by Synchrotron Radiation and Multiple-scattering Xα Calculations*, Chem. Phys. **203**, 1996, 81-92.

6. S. G. Urquhart, A. P. Hitchcock, R. D. Priester, E. G. Rightor, *Analysis of Polyurethanes using Core Excitation Spectroscopy. Part II: Inner-shell Spectra of Ether, Urea and Carbamate Model Compounds*, J. Polymer Science B: Polymer Physics **33**, 1995, 1603-1620.

5. S. G. Urquhart, A. P. Hitchcock, R. D. Leapman, R. D. Priester, E. G. Rightor, *Analysis of Polyurethanes using Core Excitation Spectroscopy. Part I: Model Polyurethane Foam Polymers*, J. Polymer Science B: Polymer Physics **33**, 1995, 1593-1602.

4. S. G. Urquhart, J. Z. Xiong, A. T. Wen, T. K. Sham, K. M. Baines, G. G. B. de Souza, A. P. Hitchcock, *Inner Shell Spectroscopy of compounds containing Si-Si bonds: Is there a localized, low energy Si-Si resonance?*, J. Phys. Chem. **189**, 1994, 757-768.

3. A. P. Hitchcock, T. Tyliszczak, M. L. M. Rocco, J. T. Francis, S. G. Urquhart, Z. H. Lu, J. M. Baribeau, T. E. Jackman, *Polarization Dependence of the Si 1s X-ray Absorption Spectra of Single Crystal Si-Ge Atomic Layer Superlattices and Si-Ge Alloys,* J. Vac. Sci. Tech. A. **12**, 1994, 1142-1147.

2. A. P. Hitchcock, S. G. Urquhart, E. G. Rightor, *Inner-shell Excitation Studies of Poly(ethylene terephthalate) and Related Small Molecule Analogues by Electron Energy Loss Spectroscopy*, J. Phys. Chem. **96**, 1992, 8736-8750.

1. E. G. Rightor, G. P. Young, S. G. Urquhart, A. T. Wen, A. P. Hitchcock, *Correlation of polymer(PET) parallel-EELS spectra with spectra from related molecular analogues,* Microscopy: The Key Research Tool **22**, 1992, 67-72.

Refereed Conference Proceedings

C1. E. G. Rightor, A. P. Hitchcock, S. G. Urquhart, A. T. Wen, *Core Excitation Studies of poly(Ethylene Terephthalate) and Molecular Analogues by EELS*, (49th EMSA), Proceedings of 49th EMSA, (San Francisco Press, CA, 1991).

C2. S. G. Urquhart, A. P. Hitchcock, E. G. Rightor, A. P. Smith, H. Ade, *Chemical Speciation by NEXAFS Spectromicroscopy: Insights from Molecular Modelling of Polymers.*, in Applications of Synchrotron Radiation to Materials Science III, L. Terminello, S. Mini, D.L. Perry, H. Ade, Eds., Mater. Res. Soc. Proc. **437**, 1996, 243-248.

Conference Presentations (underlined indicates presenter: T=talk, P=poster)

T9 A. P. Hitchcock, S. G. Urquhart, E. G. Rightor, W. Lidy, H. Ade, A. P. Smith, T. Warwick, *Quantitative Chemical Analysis Of Sub-micron Phase Segregation In Polyurethane Polymers By Soft X-ray Spectromicroscopy*, Microscopy & Microanalysis '97, (Cleveland, August 1997).

P10. S. G. Urquhart, A. P. Hitchcock, M. A. Brook, C. C. Turci, M. Denk, *Delocalization in Organosilanes: A Core Excitation Spectroscopy Investigation*, CSC-97, Chemical Society of Canada, (Windsor, Jun 1-3, 1997).

T9. S. G. Urquhart, A. P. Hitchcock, E. G. Rightor, H. Ade, A. P. Smith, *Chemical Speciation by NEXAFS Spectro-microscopy: Insights from Molecular Modelling of Polymers*, CSC-97, Chemical Society of Canada, (Windsor, Jun 1-3, 1997).

P8. C. C. Turci, S. G. Urquhart, A. P. Hitchcock, *Inner shell excitation spectroscopy of aniline, nitrobenzene and nitroanilines*, SAIFEM 96 - Simposio Acerca da Interacao de Fotons e Eletrons com a Materia, (Universidade Federal de Sao Carlos - Sao Paulo, April 1996).

P7. C. C. Turci, S. G. Urquhart, T. Tyliszczak, M. A. Brook, A. P. Hitchcock, *Core excitation spectroscopy of triphenylsilanol, hexaphenyldisiloxane and hexaphenyldisilane*, VII Workshop anual de usuarios do Laboratorio Nacional de Luz Sincrotron (LNLS), (LNLS, Campinas, Sao Paulo, April 1996).

P6. S. G. Urquhart, A. P. Hitchcock, E. G. Rightor, A. P. Smith, H. Ade, *Chemical Speciation by NEXAFS Spectromicroscopy: Insights from Molecular Modelling of Polymers*, Materials Research Society Spring Meeting, (San Francisco, CA., April

1996).

P5. A. P. Hitchcock, S. G. Urquhart, M. Denk, *Inner Shell Excitation and Ionic Fragmentation of Si(N'BuCHCHN'Bu): Delocalization in a stable silylene*, International Chemical Congress of Pacific Basin Societies, (Honolulu, Hawaii, December 1995).

P4. S. G. Urquhart, A. P. Hitchcock, M. Denk, *Probing Delocalization in a Stable Silylenes by Core Excitation Spectroscopy,* Symposium on Chemical Physics, (University of Waterloo, Waterloo, Ontario, November 1995).

P3. S. G. Urquhart, M. Denk, A. P. Hitchcock, *Probing Delocalization in a Stable Silylene: Core Excitation Spectroscopy of Si(NBu'CHCHNBu'),* Canadian Society for Chemistry Conference, (Guelph, Ontario, May 1995).

T2. E. G. Rightor, G. Mitchell, R. D. Leapman, S. G. Urquhart, A. P. Hitchcock, D. Fischer, J. Hunt, J. Gland, *Polymer Characterization in the STEM by EELS and Comparison to Synchrotron and Gas Phase EELS Results*, Microscopic Analysis Society, (Los Angeles, CA., July 1993).

T1. S. G. Urquhart, A. P. Hitchcock, E. G. Rightor, R. D. Leapman, *Core Excitation Spectroscopy for Polymer Microanalysis,* Symposium on Chemical Physics, (University of Waterloo, Waterloo, Ontario, November 1992).

A.2) Progress reports or Major Projects

1.) XAS and TEM-EELS of Conducting SiCN Ceramics

This study was undertaken to determine if four-coordination of nitrogen is

responsible for the conductivity of SiCN ceramics, and was performed in collaboration with Prof. J. Harrod (McGill). X-ray Absorption Spectroscopy (XAS) experiments were performed at the Synchrotron Radiation Center, University of Wisconsin (Si 2p, N 1s, C 1s in April, 1995; Si 1s in May 1995) and Transmission Electron Microscopy- Electron Energy Loss Spectroscopy (TEM-EELS) experiments were performed at McMaster (with Dr. D. McComb). The results of these experiments were reported as:

I..) S.G. Urquhart, A.P. Hitchcock, J Harrod, *X-ray Absorption of Silicon Carbonitride Materials: Report on Studies Performed at SRC in April, 1995*, (May 1995).

ii.) S.G. Urquhart, T. Tyliszczak, A.P. Hitchcock, J. Harrod, *Si 1s X-ray Absorption of Silicon Carbonitride Materials: Report on Studies Performed at SRC in May, 1995.* (May 1995);

iii.) S. G. Urquhart, D. McComb, A. P. Hitchcock, J. Harrod, *TEM-EELS of Conducting Silicon Carbonitride Ceramics*, (November, 1995).

2.) XAS Study of SiO_xN_y Thin Films

This study was undertaken to structurally and chemically characterize SiO_xN_y thin film waveguides using X-ray Absorption Spectroscopy (XAS). This project was performed in collaboration with Prof. P. Mascher, M. Boudreau and J. Brown, and the results were reported as:

I.) S. G. Urquhart, *Report on Experiments at the Canadian Synchrotron Radiation Facility - Double Crystal Monochromator: Si 1s NEXAFS of SiO_xN_y films and silylene.* (July 1994)

ii.) S.G. Urquhart, *Report on Experiments at the Canadian Synchrotron Radiation Facility - Double Crystal Monochromator: Si 1s NEXAFS of Si-N, Si-O and Si-C Compounds and SiO_xN_y films*, (January 1994).

3.) Core Excitation Spectroscopy of Si-O and Si-N Bonded Molecules

The core excitation spectroscopy of a wide range of Si-O and Si-N bond containing molecules has been explored. Some of these results have been published (see publications 12, 13 above). Unpublished material includes the multi-edge core excitation spectra of $Me_3SiOSO_2CF_3$, Et_3SiOH, $Me_3SiON{=}CMe_2$, c-$[SiMe_2O]_3$, c-$[SiMe_2O]_4$, $Si[OEt]_4$, $HSi[NMe_2]$, $Si[NMe_2]_3$, $SiMe[NMe_2]_3$, $SiMe_2[NMe_2]_2$, $SiMe_3[NMe_2]$ and $Si[NMe_2]_4$. The spectra of these molecules was acquired in order to examine the character of Si-O bonds (in collaboration with M. A. Brook) or as models for SiO_xN_y thin films (in collaboration with P. Mascher). A study of the core excitation spectra of the series $SiMe_x(NMe_2)_{4-x}$ (x=0,4) is in preparation.

4.) Molecular Models of Polymer Spectra: Collaboration with DOW Chemical.

In this collaboration, I have examined the core excitation spectroscopy of a large series of molecular models of polymer structures, as well as performed molecular orbital calculations. A subset of this work is presented in Chapter 4 of this thesis.

A.3) Short Term Projects

1.) Photochemistry and Photodecomposition Products of IR Irradiated Poly(butylene terephthalate).

Core excitation spectra of the molecular model benzoic anhydride were used to examine hypothesized irradiation products in poly(butylene terephthalate). The results of this study were reported to Y. Ouchi (Nagoya Univ.) in "On the core excitation of benzoic anhydride", January 20, 1997.

2.) Core Excitation Spectroscopy of Phenol and Anisole

The C 1s spectra of anisole and phenol were examined to investigate the ability of core excitation spectroscopy to distinguish "anisole" and "phenol" chemical environments in coal samples, based on the C 1s(C-1) → $\pi^*_{C=C}$ transition intensity. The results were reported to Dr. G. Cody, "On the intensity of the C 1s(C-1) → 1π*(C=C) transition in phenol and anisole", December 4, 1996.

3.) Core Excitation Spectroscopy of Ortha, Para, Meta Xylene.

With Brian Huo and G. Eustatu, the isomeric xylenes was examined by core excitation spectroscopy to look for isomeric sensitivity (August 1996). This study is ongoing.

4.) Core Excitation Spectroscopy of Dimethyl Tetrafluorobenzeocyclobutene.

The spectra of dimethyl tetrafluorobenzeocyclobutene was examined to investigate the possibility of loss of phenyl aromaticity and electronic delocalization onto the CF_2 groups. The results were reported to Prof. R. Moore (Rensselaer Polytechnical Institute) "Report on the ISEELS Spectra of dimethyl tetrafluorobenzeo-cyclobutene", May 1996.

5.) Core Excitation Spectroscopy of DABCO

The core excitation spectra of DABCO (1,4-diazabicyclo[2,2,2]-octane) was examined as a model for x-ray photofragmentation studies. The results were reported to

Prof. E. Rühl, Feb. 1996.

6.) Absolute Si 2p Core Excitation Cross Sections of $SiCl_4$ and SiF_4.

Results reported to Dr Sean Frigo (Munich), Feb. 1995.

7.) Core Excitation Spectra of SiGe Atomic Layer Superlattices

I participated in a TEM-EELS study of SiGe atomic layer superlattices in collaboration with Dr. T. Jackman (NRC). This work was performed at McMaster (with Dr. M. Chadwick) and a XAS study at Cornel High Energy Synchrotron Source (with Dr. T. Tyliszczak). The XAS study has been published (publication 3, above); the TEM-EELS study was reported as:

M. M. Chadwick, F. Pearson, G. Weatherly, J-M Baribeau, T. E. Jackman, *Studies of the Si-K and Ge-L Near Edge Spectra of a $[(Si)_6(Ge)_2]_{48}$ Atomic Layer Superlattice Using Parallel EELS in a Transmission Electron Microscope*, December 16, 1992.

8.) Core Excitation Spectroscopy of Singlet Oxygen.

A core excitation study of singlet oxygen from polymer and molecular endoperoxide sources was undertaken at McMaster. These results were reported as:

A. P. Hitchcock, J. T. Francis, S. G. Urquhart, W. J. Leigh, E. Ruhl, N. Kosugi, *Oxygen 1s Excitation of Singlet Molecular Oxygen*, (1994).

REFERENCES

A96 J. Aubry, , M. Eng. Thesis, McMaster University, 1996.

AC&94 H. Ågren, V. Carravetta, O. Vahtras, L. G. M. Pettersson, *Chem. Phys. Lett.* **222**, 75, 1994.

AS&95 H. Ade, A. P. Smith, S. Cameron, R. Cieslinski, G. Mitchell, B. Hsiao, E. G. Rightor, *Polymer* **36**, 1843, 1995.

AS96 H. Ade, A. P. Smith, private communication, 1996.

AVC95 H. Ågren, O. Vahtras, V. Carravetta, *Chem. Phys.* **196**, 47, 1995.

B30 H. Bethe, *Ann. Phys. (Leipzig)* **5**, 325, 1930.

B92 P. Batson, *Electron Energy Loss Studies in Semiconductors*, in "Transmission Electron Energy Loss Spectroscopy in Materials Science", M. M. Disko, C. Ahn, B. Fultz, eds., The Minerals, Metals and Materials Society, Warrendale PA, 1992.

BB92 G. Beamson, D. Briggs, High Resolution XPS of Organic Polymers: The Scienta ESCA300 Database, Wiley, NY, 1992.

BBT90 J. D. Bozek, G. M. Bancroft, K. H. Tan, *Chem. Phys.* **145**, 131, 1990.

BH81 C. E. Brion, A. Hamnett, *Adv. Chem. Phys.* **45**, 1, 1981.

CA&95 V. Carravetta, H. Ågren, L. G. M. Pettersson, O. Vahtras, *J. Phys. Chem.* **102**, 5589, 1995.

CH&86 C. P. Christenson, M. A. Harthcock, M. D. Meadows, H. L. Spell, W. L. Howard, M. W. Creswick, R. E. Guerra, R. B. Turner, *J. Polym. Sci. B: Polym. Phys.* **24**, 1401, 1986.

CMS89 C. T. Chen, Y. Ma, F. Sette, *Phys. Rev. A.* **40**, 6737, 1989.

C96 Canadian Light Source (CLS) Proposal, 1996.

DDP85 J. L. Dehmer, D. Dill, A. C. Parr, in "Photophysics and Photochemistry in the Vacuum Ultraviolet", eds. S. P. McGlynn, G. L. Findley, R. H. Huebner,

Reidel, Dordrecht, 1985.

DG&94 M. Denk, J. C. Green, N. Metzler, M. Wagner, *J. Chem. Soc. Dalton Trans.* 1004, 2405, 1994.

DHR94 M. Denk, K. Hayashi, R. West, *Chem. Commun.* 33, 1994.

DL&94 M. Denk, R. Lennon, R. Hayasho, R. West, A. V. Belakov, H. P. Verne, A. Haaland, M. Wagner, N. Metzler, *J. Am. Chem. Soc.* **116**, 2691, 1994.

DPS86 J. L. Dehmer, A. C. Parr, S. H. Southworth, "Resonances in Molecular Photoionization", North-Holland, Amsterdam, 1986.

E86 R. F. Egerton, *Electron Energy-Loss Spectroscopy in the Electron Microscope*, Plenum, New York NY, 1986.

EK&96 K. Endo, Y. Kaneda, H. Okada, D. P. Chong, P. Duffy, *J. Phys. Chem.* **100**, 19455, 1996.

F95 J. T. Francis, "Non-Dipole and Dipole Electric Energy Loss Spectroscopy", Ph.D. Thesis, McMaster University, 1995.

FH92 J. T. Francis, A. P. Hitchcock, *J. Chem. Phys.* **96**, 6598, 1992.

FH94 J. T. Francis, A. P. Hitchcock, *J. Chem. Phys.* **98**, 3650, 1994.

FKH94 J. T. Francis, N. Kosugi, A. P. Hitchcock, *J. Phys. Chem.*, **101**, 10429, 1994.

G97 Gatan Model 766 DigiPEELS Parallel Detection Electron Energy Loss Spectrometer Technical Specifications, Gatan Inc. (Warrendale, PA) 1997.

GA95 F. Gelmukhanov, H. Ågren, *J. Phys. B: At. Mol. Opt. Phys.* **28**, 3699, 1995.

GJ96 R. J. Gillespie, S. A. Johnson, *Inorg. Chem.*, submitted, 1996.

H63 R. Hoffmann, *J. Chem. Phys.* **39**, 1397, 1963; **40**, 2745, 2474, 2480, 1963; *Tetrahedron*, **22**, 521, 539, 1966.

H88 S. M. Heald, *EXAFS with Synchrotron Radiation*, in "X-ray Absorption: Principles, Applications, Techniques of EXAFS, SEXAFS and XANES", D.C. Koningsberger, R. Prins, eds, Wiley, New York, 1988.

H90 A. P. Hitchcock, *Physica Scripta* **T31**, 159, 1990.

H91 A. P. Hitchcock, Program *Simile*, 1991, with updates by S. G. Urquhart, A. P. Hitchcock, and B. Huo, 1991-1997.

HA&84 S. Huzinaga, J. Andzelm, M. Klobukowski, E. Radzio-Andzelm, Y. Sasaki, H. Tatewaki, *Gaussian Basis Sets for Molecular Calculations* (Elsevier, Amsterdam, 1984).

HB77 A. P. Hitchcock, C. E. Brion, *J. El. Spectrosc.* **10**, 317, 1977.

HBT89 A. P. Hitchcock, S. Bodeur, M. Tronc, *Physica B.* **158**, 257, 1989.

HC&97 W. S. Ha, Y. K. Chun, S. S. Jang, D. M. Rhee, C. R. Park, *J. Polym. Sci B: Polym Phys.* **35**, 309, 1997.

HG68 W. J. Hunt, W. A. Goddard, *Chem. Phys. Lett.* **3**, 414, 1968.

HI87 I. Ishii, A. P. Hitchcock, *J. Chem. Phys.* **87**, 830, 1987.

HM94 A. P. Hitchcock, D. C. Mancini, *J. Electron Spectrosc.* **67**, 1, 1994.

HRA96 A. P. Hitchcock, E. G. Rightor, H. Ade, private communication, 1996.

HS87 A. P. Hitchcock, J. Stöhr, *J. Phys. Chem.* **87**, 3253, 1987.

HT88 A. P. Hitchcock, M. Tronc, *Chem. Phys.* **121**, 265, 1988.

HT95 A. P. Hitchcock, T. Tyliszczak, *Surf. Rev. Lett* **2**, 43, 1995.

HT&93 A. P. Hitchcock, T. Tyliszczak, P. Aebi, J. Z. Xiong, T. K. Sham, K. M. Baines, K. A. Mueller, X. H. Feng, J. M. Chen, B. X. Yang, Z. H. Lu, J. -M. Baribeau, T. E. Jackman, *Surf. Sci.* **241**, 349, 1993.

HU&97 A. P. Hitchcock, S. G. Urquhart, A. T. Wen, A. L. D. Kilcoyne, T. Tyliszczak, E. Rühl, N. Kosugi, J. D. Bozek, J. T. Spencer, P. Dowben, *J. Chem. Phys.*, in press, 1997.

HUR92 A. P. Hitchcock, S. G. Urquhart, E. G. Rightor, *J. Phys. Chem.* **96**, 8736, 1992.

HW&93 A. P. Hitchcock, A. T. Wen, S. Lee, J. A. Glass, Jr., J. T. Spencer, P. A. Dowben, *J. Phys. Chem.* **97**, 8171, 1993.

I71 M. Inokuti, *Rev. Mod. Phys.* **43**, 297, 1971.

IH87 I. Ishii, A. P. Hitchcock, *J. Electron. Spectro. and Rel. Phen.* **42**, 11, 1987.

IH88 I. Ishii, A. P. Hitchcock, *J. Electron Spectrosc. and Rel. Phen.* **46**, 55, 1988.

IIT71 M. Inokuti, Y. Itikawa, J. Turner, *J. Rev. Mod. Phys.* **43**, 176, 1971.

IKN78 S. Iwata, N. Kosugi, O. Nomura, *Jpn. J. Appl. Phys.* **17**, 109, 1978.

IM&87 I. Ishii, R. McLaren, A. P. Hitchcock, M. B. Robin, *J. Phys. Chem.* **87**, 4344, 1987.

JC91 C. Jacobsen, S. Williams, E. Anderson, M. T. Browne, C. J. Buckley, D. Kern, J. Kirz, M. Rivers, X. Zhang, *Optics Comm.* **86**, 351, 1991.

K72 Y.-K. Kim, *Phys. Rev.* **A6**, 666, 1972.

K79 M. O. Krause, *J. Phys. Chem. Ref. Data.* **8**, 307, 1979; M. O. Krause, J. H. Oliver *J. Phys. Chem. Ref. Data.* **8**, 329, 1979.

K86 K-J. Kim, *X-ray Sources*, in "X-ray Data Booklet", D. Vaughan, Ed., Center for X-ray Optics, Berkeley CA, 1986.

K88 D. C. Koningsberger, *Laboratory EXAFS Facilities*, in "X-ray Absorption: Principles, Applications, Techniques of EXAFS, SEXAFS and XANES", D.C. Koningsberger, R. Prins, eds, Wiley, New York, 1988.

KA&92 N. Kosugi, J. Adachi, E. Shigemasa, A. Yagishita, *J. Chem. Phys.* **97**, 8842, 1992.

KJH95 J. Kirz, C. Jacobsen, M. Howells, *Quarterly Rev. Biophysics* **28**, 33, 1995.

KK80 N. Kosugi, H. Kuroda, *Chem. Phys. Lett.* **74**, 490, 1980.

KSY92 N. Kosugi, E. Shigemasa, A. Yagishita, *Chem. Phys. Lett.* **190**, 481, 1992.

KT&77 G. C. King, M. Tronc, F. H. Read, R. C. Bradford, *J. Phys. B.* **10**, 2479, 1977.

L91 I. N. Levine, *Quantum Chemistry*, 4th edition, 1991, Prentice Hall, NJ.

LAL91 E. Lindholm, L. Asbrink, S. Ljunggren, *J. Phys. Chem.* **95**, 3923, 1991.

MC&87 R. McLaren, S. A. C. Clark, I. Ishii, A. P. Hitchcock, *Phys. Rev. A.* **36**, 1683, 1987.

MP90 C. Mealli, D. M. Proserpio, *J. Chem. Ed.* **67**, 339, 1990.

N86 D.C. Newbury, M.Sc. Thesis, McMaster University, 1986.

NIH86 D. C. Newbury, I. Ishii, A. P. Hitchcock, *Can. J. Chem.* **64**, 1145, 1996.

PL&87a M. N. Piancastelli, D. W. Lindle, T. A. Ferrett, D. A. Shirley, *J. Phys. Chem.* **86**, 2765, 1987.

PL&87b M. N. Piancastelli, D. W. Lindle, T. A. Ferrett, D. A. Shirley, *J. Phys. Chem.* **87**, 3255, 1987.

R74 M. Robin, *Higher Excited States of Polyatomic Molecules,* Vol. 1, Academic, NY, 1974.

RH89 E. Rühl, A. P. Hitchcock, *J. Am. Chem. Soc.* **111**, 5069, 1989.

RH&93 E. Rühl, C. Heinzel, A. P. Hitchcock, H. Baumgärtel, *J. Chem. Phys.* **98**, 2653, 1993.

RH&97 E. G. Rightor, A. P. Hitchcock, H. Ade, R. D. Leapman, S. G. Urquhart, A. P. Smith, G. Mitchell, D. Fischer, H. J.Shin, T. Warwick, *J. Phys. Chem.* 1997.

RI&88 M. B. Robin, I. Ishii, R. McLaren, A. P. Hitchcock, *J. Electron Spectrosc.* **47**, 53, 1988.

S75 W. H. E. Schwarz, *Chem. Phys.* **11**, 217, 1975.

S82 T. Steel, B.Sc. Thesis, McMaster University, 1982

S85 J. J. Sakurai, Modern Quantum Mechanics (Addison-Wesley, 1985).

S88 E. A. Stern, *Theory of EXAFS,* in "X-ray Absorption: Principles, Applications, Techniques of EXAFS, SEXAFS and XANES", D.C. Koningsberger, R. Prins, eds, Wiley, New York, 1988.

S92 J. Stöhr, NEXAFS Spectroscopy, Spr. Ser. Surf. Sci. Vol. 25 (Heidelberg, 1992).

SB84 R. N. Sohdi, C. E. Brion, *J. Electron Spectrosc.* **13**, 193, 1984.

SG&89 J. A. Sheehy, T. J. Gil, C. L. Winstead, R. E. Farren, P. W. Langhoff, *J. Phys. Chem.* **91**, 1796, 1989.

SKR80 D. A. Shaw, G. C. King, F. H. Read, *J. Phys. B.* **13**, L723, 1980.

SO&87 J. Stöhr, D. A. Outka, K. Baberschke, D. Arvanitis, J. A. Horseley, *Phys. Rev. B.* **36**, 2976, 1987.

SSH84 F. Sette, J. Stöhr, A. P. Hitchcock, *Chem. Phys. Lett.* **110**, 517, 1984.; F. Sette, J. Stöhr, A. P. Hitchcock, *J. Chem. Phys.* **81**, 4906, 1984.

T83 W. Thiel, *J. Electron Spectrosc.* **31**, 151, 1983.

TB&82 K. H. Tan, G. M. Bancroft, L. L. Coatsworth, B. W. Yates, *Can. J. Phys.* **60**, 131, 1982.

TK94 T. Tyliszczak, M. Kiela, Tolmar Instruments, Hamilton, ON., L8S 4M1, tolek@mcmaster.ca, kiela@mcmaster.ca.

TKR79 M. Tronc, G. C. King, F. H. Read, *J. Phys. B.* **12**, 137, 1979.

UH&96 S. G. Urquhart, A. P. Hitchcock, E. G. Rightor, A. P. Smith, H. Ade, *Chemical Speciation by NEXAFS Spectromicroscopy: Insights from Molecular Modelling of Polymers.*, in Applications of Synchrotron Radiation to Materials Science III, L. Terminello, S. Mini, D.L. Perry and H. Ade, eds., Mater. Res. Soc. Proc. (1996).

UH&97 S. G. Urquhart, A. P. Hitchcock, A. P. Smith, H. Ade, E. G. Rightor, *J. Phys. Chem.* 1997.

V92 D. D. Vvedenski, *Theory of X-ray Absorption Fine Structure*, in "Unoccupied Electronic States", J. C. Fuggle, J. E. Inglesfield, eds., Springer-Verlag, Berlin, 1992.

W80 M. J. van der Wiel, in "Electronic and Atomic Collisions", ed. N. Oda and K. Takayanagi, North-Holland, Amsterdam, 1980, p209.

W89 R. Walsh, *Thermochemistry*, in "The Chemistry of Organic Silicon Compounds", S. Patai, Z. Rappoport, eds., Wiley, 1989.

W92 A.T. Wen, "Core Excitation of Some Organometallic and Organosilicon Molecules", Ph.D. Thesis, McMaster University, 1992.

WB74 G. R. Wight, C. E. Brion, *J. Electron Spectrosc.* **4**, 313, 1974.

WBW72 G.R. Wight, C.E. Brion, M.J. van der Wiel, J. Electron Spectrosc. **1**, 457,

1972/3

WP&97 T. Warwick, H. Padmore, H. Ade, A. P. Hitchcock, E. G. Rightor, B. P. Tonner, *J. Electron Spectrosc. and Rel. Phen.*, submitted, **1997**.

XJ&96 J. Z. Xiong, D. T. Jiang, Z. F. Liu, K. M. Baines, T. K. Sham, S. G. Urquhart, A. T. Wen, T. Tylisczak, A. P. Hitchcock, *Chem. Phys.* **203**, 81, 1996.

YM&92 B. X. Yang, F. H. Middleton, B. G. Olsson, G. M. Bancroft, J. M. Chen, T. K. Sham, K. Tan, D. J. Wallace, *Nucl. Instr. and Meth.* **A316**, 422, 1992.

ZS&94 C. Ziegler, T. Schedel-Niedrig, G. Beamson, D. T. Clark, W. R. Salaneck, H. Sotobayashi, A. M. Bradshaw, *Langmuir* **10**, 4399, 1994.